THEORY AND OBSERVATIONS OF X–RAY PULSARS IN BINARY SYSTEMS

Thesis submitted for the degree of

"Magister Philosophiae"

Astrophysics Sector

Candidate:

Mauro Orlandini

Supervisors:

Prof. Massimo Calvani

Prof. Filippo Frontera

October 1988

To Daniela

Index

List of Figures

List of Figures

List of Tables

Chapter 1

INTRODUCTION

The discovery of X–ray emission by celestial objects further extended the knowledge of our Universe, which resulted very different from the quiet and unchanging Universe that since the last century the astronomers described. It was just at the beginning of the 1960's [3] that, by the advent of the first rockets, was possible to launch outside our atmosphere some Geiger counters, by which the existence of discrete X–ray source in our Galaxy was discovered (in this work we will deal only with objects which belong to our Galaxy).

In 1966 it was discovered the first optical counterpart in the position of the brighter X–ray source, Sco X-1 [6], which resulted to be an old 12^{th}–13^{th} magnitude star. In the following years, a theoretical model was developed, which is more or less the same which we use today, according to which in the galactic X–ray sources which are in close binary systems, the X–ray emission is due to high–temperature gas flowing onto a compact object from the companion star [9].

In these same years it was understood that the spherical accretion could become non symmetric, with the formation of a disk around the compact object, if the infalling matter has enough angular momentum [5].

It was re-discovered a very old theory, elaborated by a french mathematician of the 19^{th} century, Edouard Roche, who studied in the context of the classical mechanics the interactions between two objects which orbit each other in a close orbit.

But the decisive step towards the understanding of these objects occurred with the discovery of pulsed emission from some X–ray source [10]. In fact, the variability on short timescale —for example Her X-1 pulses at $1^s.24$— implies a little emitting region. Further, because the system not be destroyed by the centrifugal force, it is necessary that at the surface of the object the gravitational force is greater than the centrifugal one, i.e. [8]

$$G\frac{M_\star}{R_\star^2} > \Omega_p^2 R_\star \quad \Longrightarrow \quad \Omega_p \leq \sqrt{G\langle\rho\rangle} \tag{1.1}$$

where $\langle\rho\rangle$ is the mean density of the object and Ω_p is the pulse frequency. The observed values imply that $\langle\rho\rangle \geq 10^6$ g/cm^3 and therefore the compact

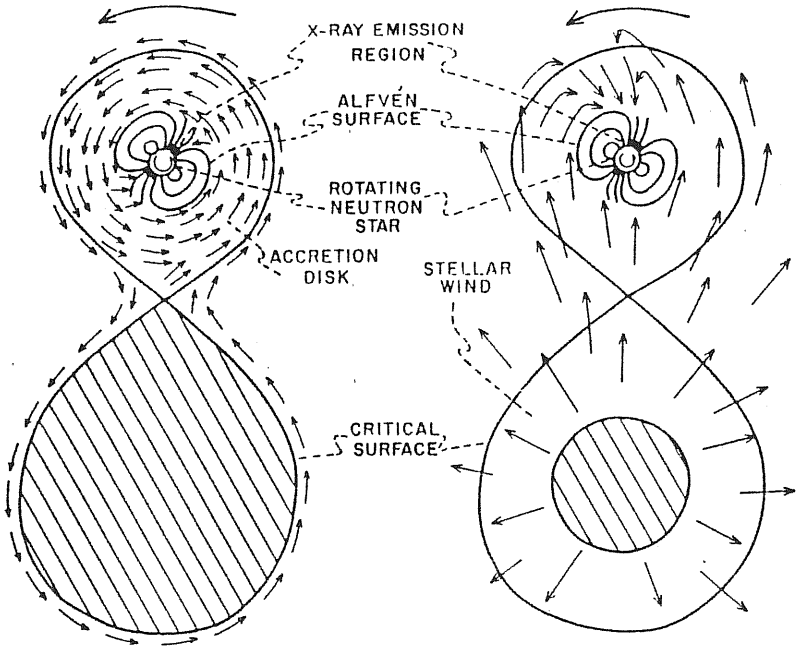

Figure 1.1: Schematic representation of the rotating neutron star for pulsating X–ray binary systems. Both disk-fed and wind-fed systems are shown.

nature of the object responsible of the pulsed X–ray emission was established.

Black holes are not expected to give pulsed emission (unless we consider non steady, non axisymmetric black holes [8], which is unlikely), so the compact objects which give X–ray pulsar phenomena will be white dwarf and neutron star. While white dwarfs are not able to explain the observed range of X–ray luminosity, neutron star are; therefore the standard model of X–ray binary pulsars consider them as close binary systems in which the (optically) invisible star is a neutron star (see Fig. 1.1 [1]). The pulsed emission is due to a misalignment between the rotation axis and the magnetic dipole axis, at the caps of which matter is driven by the field lines (light house effect).

In Table 1.1 we show the X–ray pulsar known, to date, with the respective optical counterparts.

The binary nature of the X–ray pulsars was also demonstrated by the observation of eclipses and Doppler delays in the pulse arrival times [7]: these gave the possibility to obtain the values of the masses, which all agrees with the assumed values for neutron stars.

The presence of intense magnetic fields (given by the observation of cyclotron lines in the energy spectra of Her X-1 [11] and 4U 0115+63 [12]) and our absolute ignorance how to manage them, renders very difficult the

Name	Optical counterpart	Spectral type
A0538-66	Johnston's star	$B2\,III - V$e
SMC X-1	Sk 160	$B\,0\,I$
Her X-1	HZ Her	$A\,5\,V$
4U 0115+63	V 635 Cas	$B\,III$e
V0332+53		$B2\,III$e
Cen X-3	V 779 Cen	$O7\,III$
1E 2259+586	SNR G109.1-1.0	
4U 1626-67	Kz TrA	
2S 1553-54		Be
LMC X-4		$O8\,III - V$
2S 1417-62		$B0\,Ia - Ib$e
OAO 1653-40		
EXO 2030+375		Be
4U 1700-37	HD 153919	$O6\,f$
A0535+26	HDE 245770	$B0\,III$e
GX 1+4	V 2116 Oph	$M6\,III$
4U 1320-61[a]		
GX 304-1	MMV	$B2\,V\,ne$
VELA X-1	HD 77581	$B0.5\,I\,ab$
4U 1145-61	HEN 715	$B0.5\,III - V$e
1E 1145.1-6141		$B2\,Ia$
A1118-61	He 3-640	$O9.5\,V$e
4U 1907+09		$B2\,III - V$e
4U 1538-52	QV Nor	$B0.2\,Ia$
GX 301-2	Wray 977	$B1.5\,Ia$
4U 0352+30	X Per	$O9.5\,III - Vc$

Table 1.1: X–ray binary pulsars with corresponding optical counterparts.

[a]This source has been seen only in 1977. It is also called A1239-59.

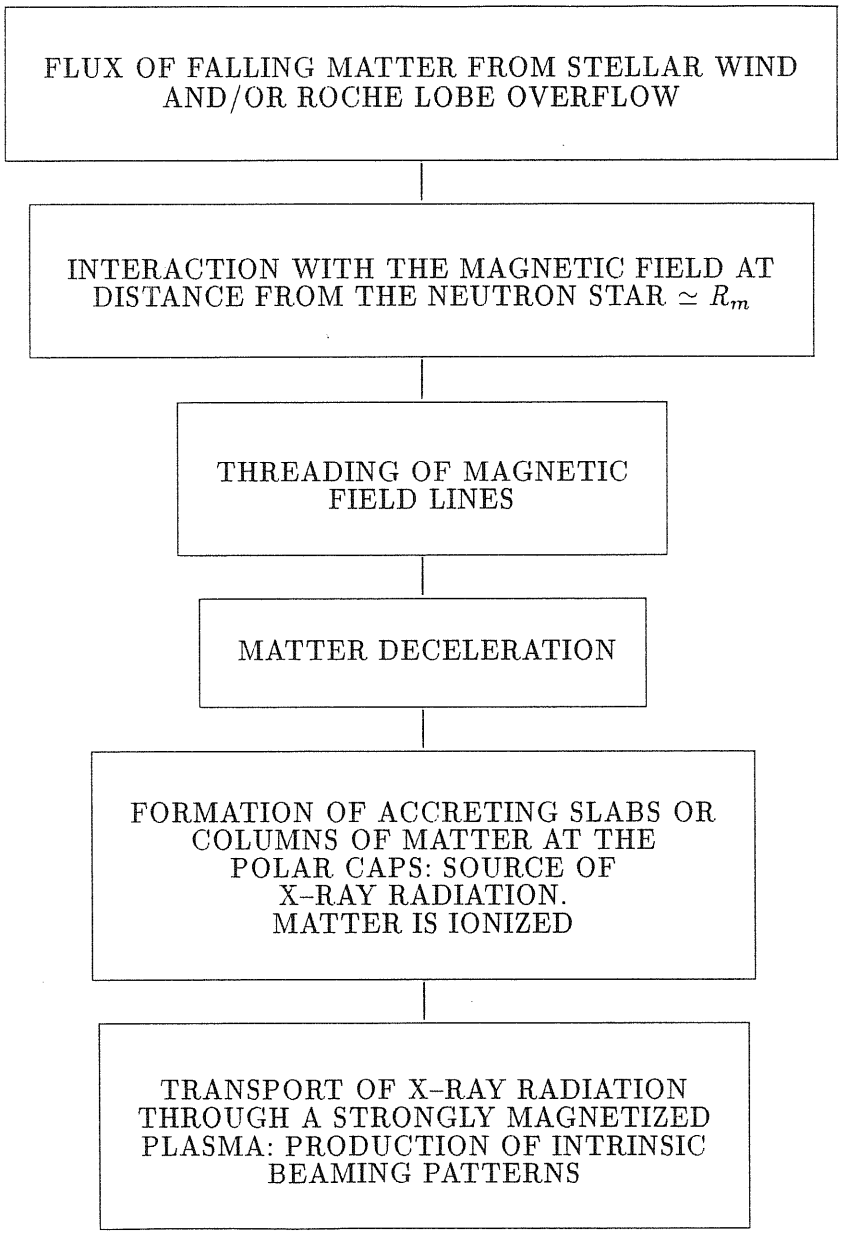

Figure 1.2: Block diagram of the physical processes of production and emission of the X–ray flux in X–ray binary pulsars.

construction of a theory of emission which is able to explain all the observed features. In Fig. 1.2 is shown a sort of block diagram which shows the basic processes of X–ray emission production in X–ray binary pulsars. Until now, what we are able to do is to build very simplified non parametric models, in which all the variables but one are maintained constant [4]. A first step towards the solution of this problem is given in [2].

In this thesis we will give a review on theories and observations regarding X–ray pulsars. In Chapter 2 we will give a simple classification of X–ray binary systems according to the mass of the systems. In this way several (but not all) observed properties can be well understood.

In Chapter 3 a brief panorama will be given on models of formation of these systems, from which we will see that often the evolutionary models are adapted only to particular sources which are included in the general scheme (as A0538-66 and 1E 2259+586).

Chapter 4 is a brief review about the main accretion phenomena which occur in these systems and the interactions with the magnetosphere.

After a brief discussion, in Chapter 5, about the basic radiative processes of X–ray emission, in Chapter 6 we will show some general observational data about X–ray pulsars, together with theories which describe them.

In Chapter 7 we will treat into details some peculiar X–ray pulsars, which clearly show all the difficulties of interpretation and analysis of the observations.

Finally, in Chapter 8 we will take everything into account about this little trip in the universe of X–ray pulsed sources, while in Chapter 9 we will give an ordered bibliography for each source.

Bibliography

[1] BLUMENTHAL G.R. - TUCKER W.H. 1974. *Annual Review of Astronomy and Astrophysics*, **12 p.23**.

[2] DAL FIUME D. - FRONTERA F. - MORELLI E. 1988. *Astrophysical Journal*, **331 p.313**.

[3] GIACCONI R. - GURSKY H. - PAOLINI F.R. - ROSSI B.B. 1962. *Physical Review Letters*, **9 p.439**.

[4] HARDING A.K. - MESZAROS P. - KIRK J.K. - GALLOWAY D.J. 1984. *Astrophysical Journal*, **278 p.369**.

[5] PRENDERGAST K.H. - BURBIDGE G.R. 1968. *Astrophysical Journal*, **151 p.L83**.

[6] SANDAGE A. *et al.* 1966. *Astrophysical Journal*, **146 p.316**.

[7] SCHREIRER E. - LEVINSON R. - GURSKY H. - KELLOGG E. - TANANBAUM H. - GIACCONI R. 1972. *Astrophysical Journal*, **172 p.L79**.

[8] SHAPIRO S.L. - TEUKOLSKY S.A. 1983. *Black Holes, White Dwarfs and Neutron Stars. The Physics of Compact Objects.* John Wiley & Sons, Inc.

[9] SHKLOVSKII I.S. 1967. *Soviet Astronomy*, **11 p.749**.

[10] TANANBAUM H. - GURSKY H. - KELLOGG E.M. - LEVINSON R. - SCHREIRER E. - GIACCONI R. 1972. *Astrophysical Journal*, **174 p.L143**.

[11] TRUEMPER J. - PIETSCH W. - REPPIN C. - VOGES W. - STAUBERT R. - KENDZIORRA E. 1978. *Astrophysical Journal*, **219 p.L105**.

[12] WHITE N.E. - SWANK J.H. - HOLT S.S. 1983. *Astrophysical Journal*, **270 p.711**.

Chapter 2

CLASSIFICATION OF X–RAY BINARY SYSTEMS

X–ray astronomy has had an incredible development in the last ten years, because of the launching of numerous satellites which explored the X–ray sky with higher sensitivity than the previous missions that, in the pioneeristic era of the X–ray exploration of the Heavens, were able to study only the most intense sources.

The increase of the number of detected sources was followed by the attempt to describe the wide range of observed properties in terms of a small number of models and to classify the sources in a more general scheme.

The study of the optical counterparts of the galactic X–ray sources, when possible, lead to interpret most of them as the compact members of binary systems and to understand the physical mechanisms for their X–ray emission.

Severals are the criteria which may be at the basis of a classification. The most general one, which is suitable to explain the observed properties of the compact galactic X–ray sources, considers the mass of the system as the key parameter. On the basis to this criterion, the galactic X–ray sources can be classified in two classes [4]: high–mass X–ray binary systems (thereafter HMXRBs) —also called Class I systems—and low–mass X–ray binary systems (thereafter LMXRBs)—also called Class II systems.

These names imply that the companion star is more (less) massive than about two solar masses; if the companion is a main–sequence star the luminosity is greater (less) than about ten solar luminosity and the spectral type is earlier (later) than type A.

We do not observe significant differences in the X–ray luminosity of the objects belonging the two classes. In fact there are sources which are classified as LMXRBS but have high X–ray luminosity, as is the case of Her X-1.

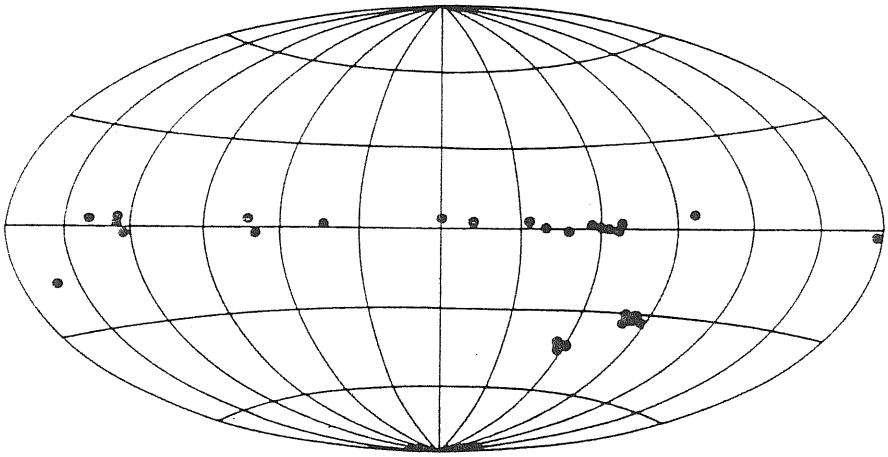

Figure 2.1: Spatial distribution, in galactic coordinates, of HMXRBs.

2.1 Class I: High–Mass X–ray Binaries

In HMXRBs the companion star is a massive star ($M_* \geq 10\ M_\odot$) of early spectral type which transfers matter to the compact object by stellar wind or incipient Roche-lobe overflow. Most of the HMXRBs show pulsed emission, because the accretion occurs onto a neutron star with a strong magnetic field not aligned with the rotation axis of the star, and along which the matter is driven towards the magnetic polar caps.

The binary character of many of these systems is apparent from the observation of periodic eclipses of the X–ray source by the companion star and from the Doppler shifts of the X–ray pulse arrival times, which vary in phase with the X–ray eclipses.

Further, the analysis of the orbital parameters of the HMXRBs gave very important informations about the neutron star masses.

The X–ray spectra of the HMXRBs are generally "hard", i.e. with values of kT in exponential fit greater than 15 keV [5].

The total luminosity of the HMXRBs is dominated by the optical companion. The values of the ratio between X–ray luminosity (in the range 2–10 keV) and optical luminosity (in the range 3.000–7.000 Å) for these systems is less than 0.1 [1].

Among the 26 HMXRBs with pulsed X–ray emission [1], 11 show strong emission lines in the optical spectrum, typical of Be sources. These lines suggest the presence of a large envelope surrounding the optical star. Among them, a lot are very variable and are called "hard transients"; they show relative flat spectra up to 10 keV. Some others, instead, show periodic increases in the X–ray luminosity and are called "recurrent transients", as for example A0535+26.

As we can see from Fig. 2.1 [4], the HMXRBs are distributed on all the galactic plane, and seven of the eight X–ray sources in the Magellanic Clouds are HMXRBs . The sources show a narrow galactic latitude distribution ($\langle|b^{II}|\rangle = 2°.4$). This fact, together with the association of early spectral type stars, shows that the HMXRBs belong to stellar Population I, which consists of stars with ages less than $\sim 10^8$ years.

2.2 Class II: Low–Mass X–ray Binaries

These systems are composed of a neutron star or a white dwarf and a low–mass star (in general $M_\star \leq 1\ M_\odot$), which transfer matter by Roche-lobe overflow.

The X–ray emission by these objects is generally complex, with more than one component (values of kT in exponential fits less than 10 keV [3]).

Only in three sources (i.e. Her X-1, 1E 2259+586 and 4U 1626-67) we observe pulsed emission[1] and this suggests that the absence of pulsation is due to the decay or the alignment of the magnetic field of the neutron star with the rotation axis.

The optical counterparts of the LMXRBs are intrinsically faint objects [1]. The optical spectra show characteristic emission lines (for example HeII) superposed to a practically flat continuum, which shows a ultraviolet excess. This indicates the presence of a disk, in which occurs the reprocessing of a fraction of the X–rays in optical photons. In some cases it is also possible to distinguish the contribution of the companion star.

Normally we do not observe eclipses in LMXRBs—the exception being Her X-1— and this may be due to the thickness of the accretion disk, which shields the companion star from the X–ray emission.

About one third of the LMXRBs are concentrated in the galactic center, although there are sources which are more than 10° away, see Fig. 2.2 [4], and show a wider galactic latitude distribution ($\langle|b^{II}|\rangle = 9°.2$).

The spatial distribution and the association with globular clusters (together with the fact that a lot of LMXRBs are composed by white dwarfs) had brought to suspect that the LMXRBs belong to stellar Population II. But to this class belong stars which are of spectral type earlier than G and are on the galactic plane (Her X-1 and Cyg X-2 for example) so the LMXRBs are a mixture of Population I and Population II objects.

In Table 2.1 we show the main differences between the two classes [2].

[1] The compact object is a neutron star.

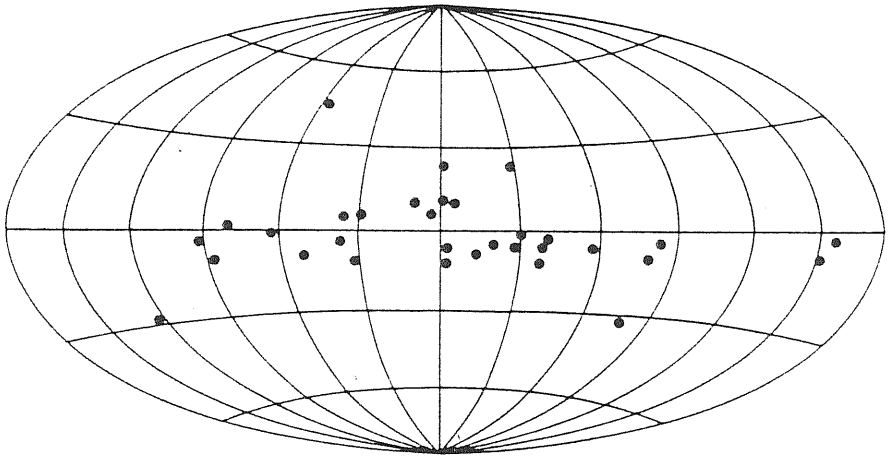

Figure 2.2: Spatial distribution, in galactic coordinates, of LMXRBs.

Class	I. Massive systems	II. Low–mass systems
Optical star	early type	late type
L_{opt}/L_x	≥ 0.1	≤ 0.1
X–ray spectrum	hard	soft
X–ray eclipse	yes	no[a]
Binary separation	$\geq 10^{12}$ cm	$\leq 10^{12}$ cm
Spatial distribution	all b^{II}	concentrated towards the galactic center
Age	$\leq 10^8$ yr	$\geq 10^9$ yr
Population	extreme I	old I and II

Table 2.1: Main properties of X–ray binary systems.

[a]But the most typical X–ray binary pulsar, Her X-1, *does* !

Bibliography

[1] BRADT H.V.D. - McCLINTOCK J.E. 1983. *Annual Review of Astronomy and Astrophysics*, **21 p.13**.

[2] HA AKAWA S. 1985. *Physics Reports*, **121 p.318**.

[3] SCHULZ N.S. - HASINGER G. - TRUEMPER J. 1988. *Max–Planck Preprint*, **111**.

[4] VAN PARADIJS J. 1983. In *Accretion–Driven Stellar X–ray Sources*, Accretion–Driven Stellar X–ray Sources, Cambridge Un. Press.

[5] WHITE N.E. - SWANK J.H. - HOLT S.S. 1983. *Astrophysical Journal*, **270 p.711**.

Chapter 3

EVOLUTIONARY MODELS FOR X–RAY BINARY PULSARS

As we have seen in the previous chapter the X-ray binary sources with a neutron star as a companion can be subdivided in two classes; this subdivision can be understood by considering the mass exchange between the two components, the mass loss from the system and the evolution of the components.

Many progresses have been made about the evolution of compact binary systems introducing the conditions [22,15]:

1. the total mass of the system $M = M_c + M_x$ is conserved;
2. the total angular momentum of the system is conserved;
3. the stars rotate synchronously with the revolutionary motion;
4. the orbit is circular.

This is the so called *conservative* evolution.

Of course, it is evident that conservative evolution can occur only for very restrictive conditions and that, generally, there are mass and angular momentum losses during several phases of the evolution. But the amount of these losses is not known and so it is not possible to compute all the stages of the evolution.

In any case it is possible to build plausible scenarios for the evolution of close binary systems (with the term "close" we intend that during some stages of the evolution the components the system interact between them) with the smallest number of *ad hoc* assumptions and trying to compute rigorously the smallest possible number of evolutionary stages.

For HMXRBs we can see that the amount of matter and angular momentum lost during their formation is moderately small and so this systems can be described by *quasi*-conservative models.

On the other hand, it is more difficult to describe LMXRBs, because they lost more than 90% of the original mass and angular momentum.

Now we will try to give a more complete evolutionary scenario for all the classes of X-ray binary systems (thereafter XRBSs), taking into account the recent theories about the formation of the "common envelope" phase.

3.1 The three basic cases of mass exchange in close binary systems

In binary systems with orbital periods up to ten years [22] the envelope of the primary star may, in some stages of the evolution, overflow a critical surface (Roche-lobe) and matter can be transferred to the companion star or lost from the system.

It is important to point out here about the terms 'primary' and 'secondary'. In X–ray binary systems we normally assume that the primary star is the visible, more massive, optical star, while the secondary is the X–ray star, i.e. the neutron star. But during the evolution of the system may occur that what we call primary is, on the contrary, the star which will become the neutron star (see LMXRBs). For this reason, some authors call the two components a close binary system "gainer" and "looser" star, referring to the fact that, in some evolutionary stage, they are gaining or loosing matter.

The way in which the two component interact between them depends on the evolutionary stage of the core of the primary at the beginning of the mass transfer, on the structure of the envelope and on the masses of the components (we define the mass ratio as $q \equiv M_c/M_x$, where thereafter M_c is the mass of the optical companion and M_x is the mass of the neutron star).

The aim of each theoretical model is to determine the final stage of the binary system by starting from a given initial configuration. We will not take care about the possibility that the system may be disrupted by the supernova explosion of the primary.

The beginning of mass exchange in terms of the evolutionary stage of the core of the primary allows to determine the final stage of the primary, and therefore the kind of remnant which is left [9].

Three cases of mass exchange are generally considered and are called case A, B and C. Let us consider, for example, a binary system with a mass of the primary of 9 $M_\odot$ and a mass of the secondary of 4.5 $M_\odot$[9]. If the orbital period is less than 0.652^d the primary already overflows its Roche-lobe when it is on the zero-age main sequence; to fill its Roche-lobe before the end of the hydrogen-burning phase, the orbital period should be $P_{orb} \leq 1.9^d$. We say that this binary is in the *case A* mass transfer when the primary fills its Roche-lobe.

If the orbital period is greater than 1.9^d but less than 394^a the primary will fill its Roche-lobe after the end of the burning in the hydrogen-core but before the helium-burning phase. In this case we have a *case B* mass transfer.

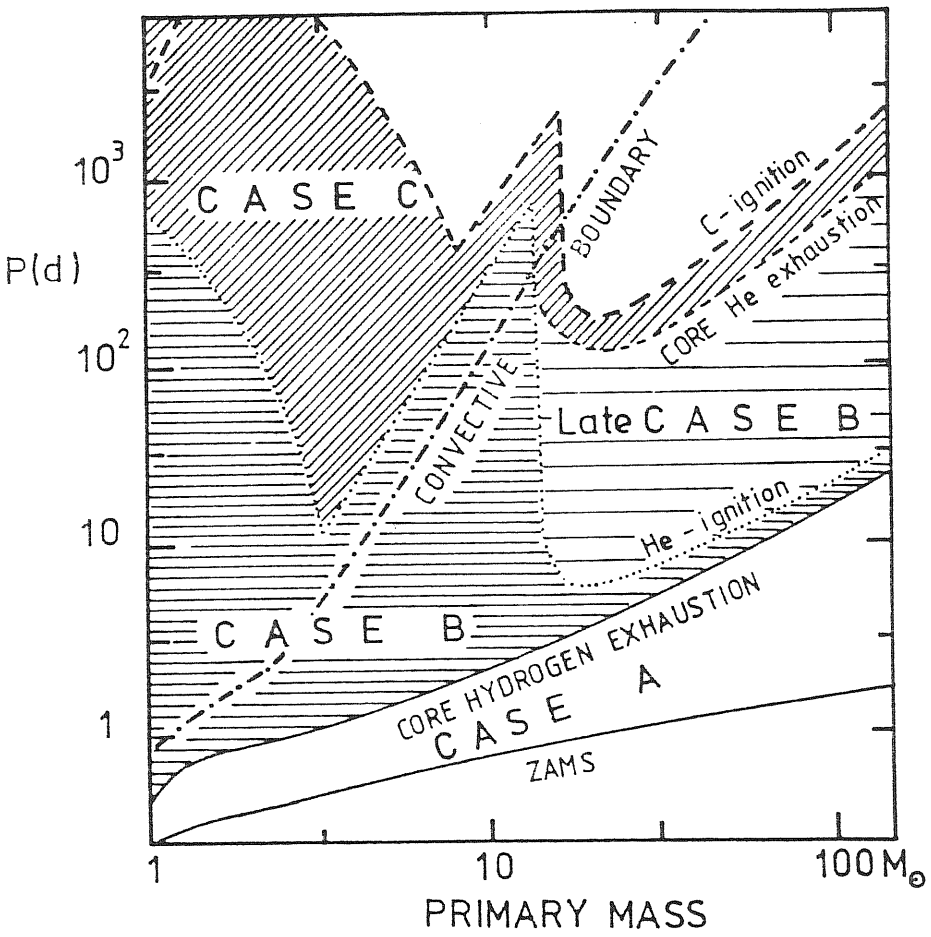

Figure 3.1: Types of close binary evolution as a function of primary mass and orbital period.

If the orbital period is greater than 394^d but less than 800^d the primary will fill its Roche-lobe after the helium-burning but before the carbon-burning; this is a *case C* mass transfer.

The precise values of the critical periods mainly depend on the mass of the primary and comparatively less on mass ratio q and chemical composition of the primary. In Fig. 3.1 [12] we can see the critical periods as a function of the mass of the primary for $q = 0.5, X = 0.7$ and $Z = 0.02$ where X and Z are the mass fractions of Hydrogen and metals, respectively. For $q = 1$ the critical periods are greater by a factor 1.0334 [22].

In mass transfer cases B and C the assumption of the conservative evolution is not important and since almost all of the observed periods are in this range we will treat only these two cases.

The final stage which we expect from the evolution of a helium-star may be described as follows [22]:

1. $M_{He} \leq 2\ M_\odot$: the CO core degenerate during the helium-shell burning and the outer layers expand rapidly. This matter is transferred to the companion, leaving a CO white dwarf.

2. $2\,M_\odot \leq M_{He} \leq 2.8 - 3.0\,M_\odot$: the CO core left by the helium burning is not very degenerate so the carbon burning begins, producing a degenerate O-Ne-Mg core with mass of the order of 1.2-1.4 $M_\odot$. The helium-shell burning around this nucleus causes its mass to grow and the envelope to expand. This envelope will overflow the primary Roche-lobe and will be lost. Finally, we have a O-Ne-Mg white dwarf of about 1.2-1.4 $M_\odot$.

3. $M_{He} \geq 2.8 - 3.0\,M_\odot$: in this case the star can loose a consistent part of its envelope, by mass transfer, before the collapse occurs. This stars, with mass close to the photo-disintegration limit, can be reduced to a *bare* core of about a Chandrasekhar mass at the moment of the collapse due to photo-disintegration. In this case the matter expelled via supernova will be negligible.

3.2 The formation of HMXRBs

3.2.1 The (quasi) conservative evolution

Let us consider primaries which evolve directly towards the core collapse and therefore $M_{He} \geq 2.8 - 3.0\,M_\odot$. In binary systems which evolve conservatively the remnant of the primary at the moment of its collapse will become the less massive star, i.e. the mass ratio q will pass from being less than one to be greater than one.

Generally, the orbital angular momentum J_{orb} is

$$J_{orb} = M_c R_c v_c + M_x R_x v_x \tag{3.1}$$

where R_i are the orbital radii ($R_c + R_x \equiv R$), M_i the masses and v_i the orbital velocities of the two components ($i = c, x$, respectively), which are given by the Kepler's third law

$$v_i = \frac{2\pi}{P_{orb}} R_i \equiv \omega_{orb} R_i \tag{3.2}$$

so we have

$$J_{orb} = \frac{2\pi}{P_{orb}} (M_c R_c^2 + M_x R_x^2) \tag{3.3}$$

Because of, by definition, $R_{c,x} = R(M_{x,c}/M)$ we can write

$$J_{orb} = \frac{2\pi}{P_{orb}} \frac{M_c M_x}{M} R^2. \tag{3.4}$$

Using again the Kepler's third law

$$\omega_{orb}^2 = \left(\frac{2\pi}{P_{orb}}\right)^2 = \frac{GM}{R^3} \tag{3.5}$$

where G id the gravitational constant, we can eliminate the orbital period P_{orb} or the orbital separation R obtaining

$$\frac{R}{R_0} = \left(\frac{1+q}{1+q_0}\right)^4 \left(\frac{q_0}{q}\right)^2 \left(\frac{J_{orb}}{J_{orb,0}}\right)^2 \left(\frac{M_0}{M}\right)^3 \overset{\text{conserv.}}{=} \left(\frac{1+q}{1+q_0}\right)^4 \left(\frac{q_0}{q}\right)^2 \tag{3.6}$$

$$\frac{P}{P_0} = \left(\frac{1+q}{1+q_0}\right)^6 \left(\frac{q_0}{q}\right)^3 \left(\frac{J_{orb}}{J_{orb,0}}\right)^3 \left(\frac{M_0}{M}\right)^5 \overset{\text{conserv.}}{=} \left(\frac{1+q}{1+q_0}\right)^4 \left(\frac{q_0}{q}\right)^3 \quad (3.7)$$

where the suffix 0 means the initial situation.

Differentiating Eq. 3.6 with respect to time we obtain

$$\frac{dR}{R} = -2\left(\frac{1-q}{1+q}\right)\frac{dq}{q} = -2\left(1-\frac{M_c}{M_x}\right)\frac{\dot{M}_c}{M_c}. \quad (3.8)$$

Because the more massive star evolves earlier and eventually fills its Roche-lobe, until q is less than one, we have $dR < 0$, i.e. R decreases. When the two masses will be equal the process will continue but now $q > 1$, so $dq > 0$ and consequently $dR > 0$: the orbital separation will increases.

Because it is difficult that the explosion of the more evolved and therefore less massive component destroys the binary system, also if we consider impact and oblation effects [18,23,4], we can expect that the compact object formed after the explosion will be bound in a binary system. In fact this is the case of HMXRBs, because their orbital periods are so short that a mass transfer must be occurred during the evolution: in particular the mass transfer is a case B [8].

In Fig. 3.2 [22] and Fig. 3.3 [22] two examples of conservative evolution are shown, with initial masses of 25&10 $M_\odot$ and 16&9.6 $M_\odot$ respectively. The initial orbital periods are both $P_{orb} = 50^d$ and the initial chemical composition is $X = 0.6$ and $Z = 0.044$.

The system parameters are chosen in order to give a standard HMXRB and a system containing a Be star, respectively.

We can distinguish the following evolutionary phases (the parameters for the second system are shown in parenthesis):

(a)–(b) Initial condition: non evolved system.

(b)–(c) First stage of mass transfer: 4.71 (6.88) $\cdot 10^6$ yr after the birth of the system the primary overflows its Roche-lobe and transfers its hydrogen-rich envelope of about 16.5 (12.0) $M_\odot$ to its companion in about 10^4 ($3 \cdot 10^4$) yr.

(c)–(d) Helium-star binary: the system consists of a helium-star of 8.5 (4) $M_\odot$ and of a main sequence star of 26.5 (21.6) $M_\odot$. The orbital period has changed (see Eq. 3.7) to $6^d.84$ ($28^d.1$).

(d) Supernova explosion: $5 \cdot 10^5$ ($1.1 \cdot 10^6$) yrs after the mass transfer, the helium-star explodes by supernova photo-disintegration; here we assume that the remnant is a 1.4 $M_\odot$ neutron star. The orbital period has a sudden increase to $11^d.9$ ($35^d.6$) , the orbit acquires an eccentricity of 0.35 (0.10) and the system has a runaway velocity of 71 (18) Km/sec.

(e) Persistent X-ray binary (not shown in Fig. 3.2): 3.8 (3.6) $\cdot 10^8$ yrs after the supernova explosion, the secondary leaves the main sequence and

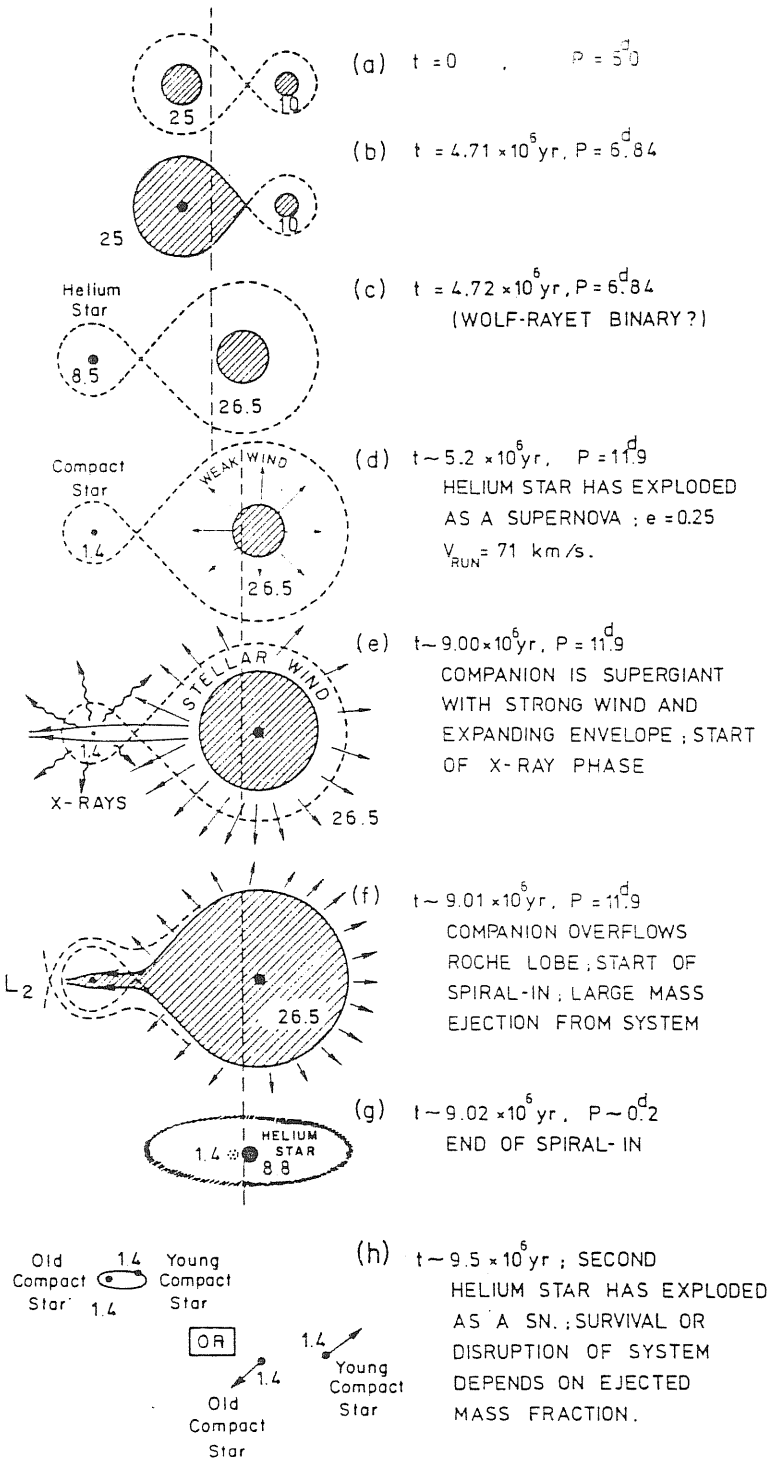

Figure 3.2: Conservative evolution of a close binary system with initial masses of 25 and 10 $M_\odot$. Each stage is labelled with the approximate age of the system and the orbital period in days. The numbers inside the representations of the stars indicate mass ($M_\odot$).

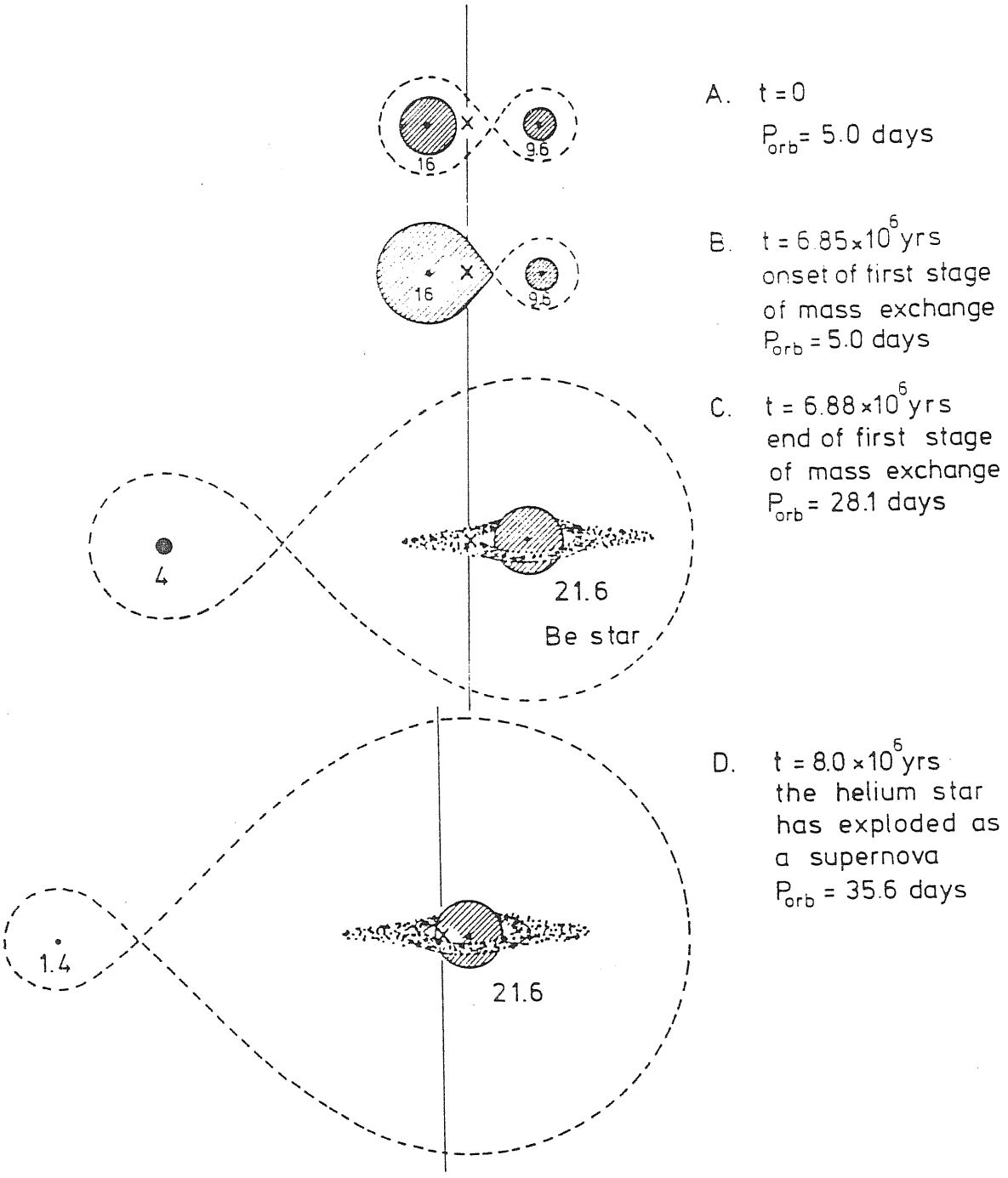

Figure 3.3: Conservative evolutionary scenario for the formation of a Be/X-ray binary system out of a close pair of early B stars with masses of 16 and 9.6 $M_\odot$. The numbers inside the representations of the stars indicate mass ($M_\odot$). After the end of the mass transfer, the Be star presumably has a circumstellar disk or a shell of matter associated with the rapid rotation (induced by the previous accretion of matter with high angular momentum).

becomes a giant or a blue supergiant. It will overflow its Roche-lobe up to $\sim 10^4$ yr. The mass accretion from the strong stellar wind or the beginning Roche-lobe overflow renders the neutron star a strong X-ray source for at least 10^4 yrs.

This evolutive scheme explains the existence of the HMXRBs, with relatively long orbital periods ($P_{orb} \geq 9^d$); further, the Be/X-ray binary systems are well explained in this theory because we expect that, after the mass transfer phase, in the (c) stage, the secondary becomes a very rapid rotator (in fact the exchanged matter has a large specific angular momentum and so will flow in through a disk [17]). When this matter arrives to the equatorial region of the star with Keplerian angular velocity, it will have spun-up the rotation of the star. Because the exchanged amount of matter is of the same order or greater than the original matter of the secondary, and because of the compression of the surrounding matter, the spin-up will be very close to the break-up velocity.

Once that a star of spectral type OB becomes a rapid rotator it will pass through emission line phases, expelling blobs of matter from the equatorial region [20]. During this phase the neutron star will become a transient X-ray source.

Since for $P_{orb} \geq 10^d - 15^d$ the tidal forces do not play an important role [2], we expect that the transient character will occur mainly in the (d) and (e) phases. Of course, before the neutron star becomes a pulsar it must slow-down for allowing matter to enter into its magnetosphere.

The fact that we do not observe Be systems with orbital periods less than 15^d is a demonstration of the fact that the tidal forces are more efficient in these closer systems [15]. In systems with $P_{orb} < 10^d - 15^d$ we expect that the neutron star becomes a X-ray source only whether the secondary becomes a supergiant with strong stellar wind nor when it becomes to overflow its Roche-lobe.

3.2.2 The non conservative evolution

The conservative evolution can explain the existence of Be/X-ray binaries with orbital periods greater than 9^d but if we look carefully at Eqs. 3.6 and 3.7 we can see that in order to obtain $P_{orb} < 2^d - 3^d$ with the hypothesis of conservative mass transfer we must assume $q \leq 0.3$. We can demonstrate that systems with low mass ratio and short period cannot form. In fact, for $M = 25\, M_\odot$ and $P_{orb} = 5^d.0$ we obtain that, if the secondary swells up by a factor two during the accretion, all the systems with $q < 0.4$ will become contact systems, surrounded by a common envelope. Therefore, only for $q \geq 0.4$ these systems can evolve separately; for $q = 0.3$, with the same conditions on the radius of the secondary, we find that only systems with $P_{orb} \geq 9^d$ may avoid the contact phase.

Thus we need a non conservative treatment of the mass transfer and to do this we assume that a fraction α of the transferred matter is lost from the system. In this case Eq. 3.8 becomes

$$\frac{\dot{R}}{R} = -2\left[1+(\alpha-1)\frac{M_c}{M_x}-\frac{1}{2}\alpha\left(\frac{M_c}{M}\right)\right]\frac{\dot{M}_c}{M_c}+2\frac{\dot{J}_{orb}}{J_{orb}}. \tag{3.9}$$

Of course, in the case of conservative evolution, i.e. $\dot{J}_{orb} = \alpha = 0$, we re-obtain Eq. 3.8.

If $\alpha > 0$, which occurs when M_c expels stellar wind, the orbital evolution depends on the specific angular momentum of the outflowing matter

$$l = \frac{1}{\alpha}\frac{\dot{J}_{orb}}{\dot{M}_c} \tag{3.10}$$

The evolution of the binary system may be non conservative also when $\alpha = 0$. For example tidal interactions may permit angular momentum to be exchanged between orbit and rotation of the components the system [23]. Because normally is $J_{orb} \gg J_{spin}$ we can ignore this case.

In close binary systems and with very short orbital periods (see Sec. 3.2.3) the components rotate so fast that they emit gravitational radiation, which take away angular momentum at a rate [10]

$$\frac{\dot{J}_{orb}}{J_{orb}} = -\frac{32}{5}\frac{G^3}{c^5}\frac{M_c M_x M}{R^4} \quad \sec^{-1}. \tag{3.11}$$

For R small we can see that Eq. 3.11 dominates in Eq. 3.9 and therefore can occur that $\dot{R}/R < 0$: we will have a *spiral-in* of the compact component towards the primary.

As we have seen, a non conservative evolution of a binary system with a Roche-lobe overflow leads to the formation of a common envelope star, a so called *double* star. When an envelope forms we expect that the mass loss occurs from the outer Lagrangian points L_2 and L_3. Because the specific angular momentum of matter lost in this way will be always greater than the average orbital angular momentum of the components [13], the system will tend to shrink rapidly. For example, for $M_c \approx M_x$ we have that the orbital angular momentum loss is [22]

$$\frac{dJ_{orb}}{dM} = 4\frac{J_{orb}}{M} \tag{3.12}$$

i.e. $J_{orb} \propto M^4$.

If we consider, as an example, the evolutionary history of a 30&10 $M_\odot$ with $P_{orb} \cong 5^d.0$, in which we assume that 5 $M_\odot$ of the 20 $M_\odot$ exchanged are lost during the mass transfer we find, by means of Eq. 3.12, that the system will have a post-mass-transfer configuration of 18&25 $M_\odot$ and a final orbital period of $P_{orb} \cong 2^d.27$.

If we assume that the helium star looses more than 3 $M_\odot$ via stellar wind before its explosion and that it leaves a 1.4 $M_\odot$ remnant, then we will have a post-supernova configuration with orbital period $P_{orb} = 3^d.5$ and an eccentricity $e = 0.2$.

As a conclusion, we can say that:

1. Systems with $q \leq 0.4$ will evolve through a common envelope phase in which the mass transfer is not conservative. This is the only way to explain the short orbital periods observed in some HMXRBs.

2. Systems with $q \geq 0.4$ may evolve more or less conservatively and will produce post-supernova binaries with orbital period of the order of or greater than $9^d - 10^d$.

3.2.3 Formation of highly-eccentric systems

There is a class of HMXRBs in which we observe very high eccentricity (e.g. the system A0538-66 has an eccentricity $e = 0.82$ [7]). Such high values can be explained either in terms of a conservative mass exchange but introducing an asymmetric supernova explosion [5,21] (due, for example, to asymmetry in the mass-ejection in the off-center explosion that gives a kick to the collapsing star) or in terms of a non conservative mass exchange but within a frame of symmetric supernova explosion [3].

In this latter case the initial orbital period is chosen in such a way that the mass transfer occurs during the hydrogen-shell burning.

As we have seen at the end of the last section, for $q \leq 0.4$ we have the formation of a common envelope system and a spiral-in of both the component due to the emission of gravitational waves. When the common envelope is lost, because of frictional heating [1], the binary system consists of a neutron star and an evolute core of a massive star. If the spiral-in is not stopped, the neutron star spirals towards the center of the primary [19].

In the stage (3) of Fig. 3.4 [6] the orbital period is constrained to be greater than $\sim 0^d.9$, which is the period that we expect in the case in which a 8 $M_\odot$ star fills its Roche-lobe. If the mass ratio is very close to unity at the moment of the supernova explosion, a symmetric explosion gives a very high eccentricity in the post-supernova explosion.

The tidal interactions will be very strong between the stages (3) and (4). Further we will have a spin-up from phases (4) to (5) because of the tidal interaction during the periastron passage. Probably in this phase the star becomes a Be, with mass of the order of 10 $M_\odot$, and the star emits X-rays (see chapter 7 for X–ray emission mechanisms in Be/X–ray binary systems).

This model is able to explain this subclass of HMXRBs which show very high eccentricity without introducing the *ad hoc* assumption of an asymmetric supernova explosion, which gives rise to many difficulties from a theoretical point of view. In this way we remain in the general evolutionary track for the formation of HMXRBs , making the smaller possible number of special assumption.

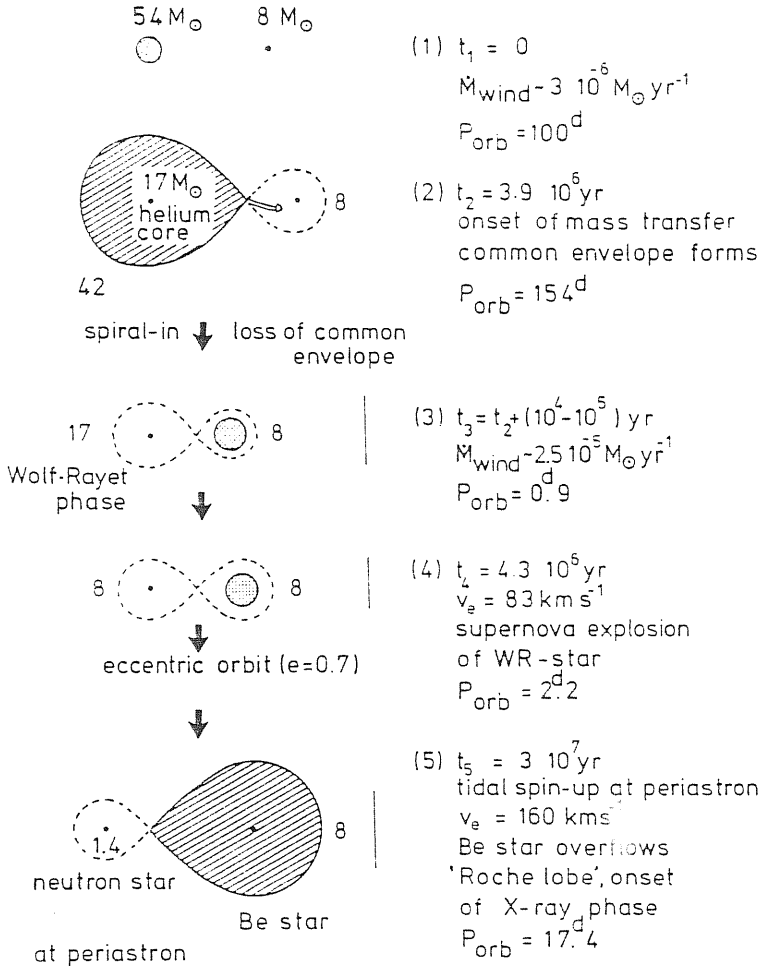

Figure 3.4: The evolutionary scenario for the formation of highly eccentric Be/X–ray binaries from very massive close binaries by a symmetric supernova explosion. The masses of the components in each state are indicated. The scale of state (3) is $\sim$ 20 times that of (1) and (2). Stellar wind mass loss occurs between (1) and (2) and between (3) and (4); the adopted mean mass loss rates in these phases are indicated. The supernova explosion occurs just after state (4). The equatorial velocity v_e of the synchronized 8 $M_\odot$ star is given in states (4) and (5). Bars on the right indicate a distance of $10_\odot$.

3.3 Formation of LMXRBs

3.3.1 Class I systems

As we have seen, in the class of LMXRBs there are both Population I and Population II stars. In this section we will discuss Class I (that is Population I) LMXRBs.

In the previous section we saw that HMXRBs with mass ratio less that 0.4 evolve through a common envelope stage. In this stage the secondary star spirals-in towards the core of the primary with a very short timescale, heating the envelope by frictional effects and therefore giving the possibility for it to leave the system. If $M_{core} \geq 2.8\, M_\odot$ the nucleus of the primary will explode as a supernova event and will leave a neutron star remnant. Normally the effect of this explosion is to destroy the system but *if* the system remains bound we will have a very eccentric orbit and a high space velocity.

Because the periastron separation is not modified by the explosion [18], the tidal forces will be very strong and will circularize very quickly the orbit. The result will be a LMXRBs in a circular orbit and a high space velocity.

In view of the high disruption probability of the post-spiral-in systems these systems have a low probability of formation. Their prototype is Her X-1.

3.3.2 Formation of ultra-compact Class I LMXRBs

The evolution of LMXRBs with orbital periods less that 10^h is mainly influenced by orbital angular momentum losses due to emission of gravitational waves, which cause an orbital decay which increases during the mass transfer.

Because we do not know the detailed hydrodynamics of tidal mass transfer in close binaries we will assume all the assumptions of conservative evolution except the point 2. for which $\dot{J}_{orb}$ is given by Eq. 3.11.

We have that Eq. 3.9, with the aid of Eq. 3.11, becomes

$$\frac{\dot{R}}{R} = -\,2\left(1-\frac{M_c}{M_x}\right) - \frac{64}{5}\frac{G^3}{c^5}\frac{M_c M_x M}{R^4}. \tag{3.13}$$

To derive a simple expression for the mass transfer rate in the system we assume a simplified mass-radius relation for the primary[1] [15,16]

$$\frac{R_c}{R_\odot} = \alpha\left(\frac{M_c}{M_\odot}\right)^\beta \tag{3.14}$$

where α and β are constant. Assuming that the radius remains exactly equal to the volume averaged radius of the Roche-lobe, the value of which is approximated by [14]

[1] We call this star "primary" but, from the standard evolutionary point of view, its name should be "secondary" because it will become the neutron star ,which we normally associate to the *less* massive star. In this case the neutron star will be the *more massive* component the system (this is a low-mass system !!).

$$R_{Rl} = \begin{cases} R\,[0.38 + 0.2 \log q] & \text{for } 0.3 \leq q \leq 20 \\ 0.426 R\,(M_c/M)^{1/3} & \text{for } q \leq 0.3 \end{cases} \tag{3.15}$$

we obtain, imposing $\dot{R}_c = \dot{R}_{Rl}$

$$\frac{\dot{R}}{R} = (\beta - \frac{1}{3})\,\frac{\dot{M}_c}{M}. \tag{3.16}$$

Eliminating $\dot{R}/R$ from Eqs. 3.13 and 3.16 we obtain an expression for the mass transfer rate

$$\dot{M}_c = \left(\frac{5}{6} + \frac{\beta}{2} - \frac{M_c}{M_x}\right)^{-1} \left(\frac{M_c}{\tau_g}\right) \tag{3.17}$$

where $\tau_g \equiv (\dot{J}_{orb}/J_{orb})^{-1}$ is the orbital decay timescale due to the emission of gravitational waves. From Eq. 3.16 we can see that the minimum value for the orbital separation is obtained for $\beta = 1/3$.

For smaller values of β the mass losing secondary can no longer be accommodated in a binary system with a decaying orbit. The mass transfer towards the more massive companion will then counteract the shrinking of the orbit due to gravitational radiation and it will become to expand.

To describe the system we will use three timescales [16]:

- *evolutionary timescale* τ_{ev} defined as the time that the system elapses up to the ignition of helium burning in the core of the primary;
- *thermal timescale* τ_{KH}[2] defined as the ratio between the total thermal energy and the rate of its lo

$$\tau_{KH} \equiv \frac{U}{(dU/dt)} \approx \frac{GM^2}{RL} \tag{3.18}$$

  where L is the luminosity. This timescale describes the time needed to the system for returning in the position of thermal equilibrium, which has been modified by thermal perturbations due to the mass transfer.

- *gravitational timescale* τ_g defined as the timescale for the orbital decay due to emission of gravitational waves, which can be expressed as

$$\tau_g \equiv \frac{J}{(dJ/dt)} \approx 1.2 \cdot 10^9\, \frac{R^4}{M_c M_x M} \quad \text{yr.} \tag{3.19}$$

These timescales are plotted in Fig. 3.5 [16] as a function of the mass of the primary.

The first phase of the evolution of the system is characterized by $\tau_{KH} < \tau_g < \tau_{ev}$. This implies that the orbit initially decays with a timescale τ_g

[2] KH means Kelvin-Helmholtz and it is referred to the type of instabilities.

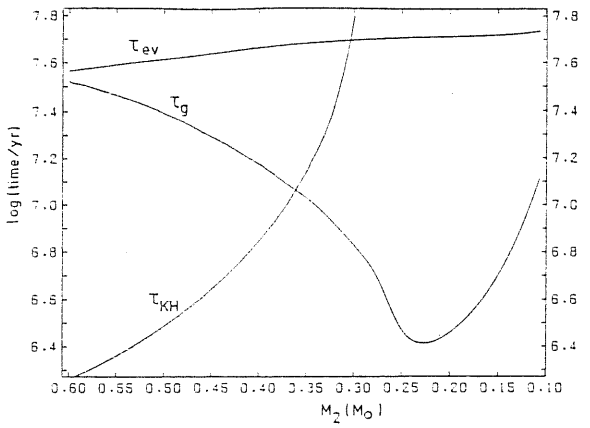

Figure 3.5: The three timescales which describe the evolution of an ultra-compact LMXRBs as a function of the primary star.

much greater than the timescale in which the secondary relaxes from the thermal perturbations due to the mass transfer.

Therefore the secondary remains in thermal equilibrium, although it loses mass at a high rate. Because $\tau_{ev} > \tau_g$, the nuclear evolution is not very important.

From Fig. 3.5 we can see that τ_g decreases rapidly because of the orbital decay due to emission of gravitational waves.

When the primary becomes less massive its luminosity decreases and consequently τ_{KH} increases. For $M_c \sim 0.36\, M_\odot$ τ_g is comparable to τ_{KH}. This occurs $1.2 \cdot 10^7$ years the onset of the mass transfer.

Just from this moment the mass transfer begins to drive the primary out from the thermal equilibrium, therefore, the evolutionary track for LMXRBs will be as follow:

We start from a binary system composed by a 5 $M_\odot$ and a 8 $M_\odot$ stars in a wide orbit ($\sim 100\, R_\odot$). The mass transfer starts when the 8 $M_\odot$ star is a giant or a supergiant; this mass transfer is unstable and a common envelope forms.

Because at this stage $q \sim 1$, the amount of matter in the envelope is not much more than that contained in the "inner binary" (consisting of the 5 $M_\odot$ and the core of the giant), it will not be necessary that the orbit drastically shrinks to expels the envelope.

After the expulsion of the envelope the system will be formed by a massive white dwarf with a O-Ne-Mg core and the 5 $M_\odot$ star. The white dwarf magnetic field will not vary significantly during the evolution and it will be of the order of $10^7 - 10^8$ G. When the gravitational emission dominated era is finished, the system is driven, as we have seen, by the matter accretion which increases considerably up to bring to collapse of the white dwarf which will become, after a supernova explosion, a neutron star. Of course, the primary will be an intermediate class star.

3.3.3 Class II systems

The non compact object which forms these systems is a Population II star.

In this class pulsed emission are not yet been observed so we will give here only an idea of the formation mechanisms for these objects, without enter into details.

The problem of the formation and evolution of the Class II LMXRBs is open but the model which seems to give better results [11] considers the formation of binary systems composed by a neutron star and an evolved star as due to accretion-induced collapse of a white dwarf in a cataclysmic binary system.

Bibliography

[1] BODENHEIMER P. - TAAM R.E. 1985. In *The Evolution of Galactic X-ray Binaries. NATO ASI Series Vol.167*, TRUEMPER J. - LEWIN W.H.G. - BRINKMAR W. Eds., Reidel Publ. Co.

[2] DE GREEVE J.P. - DE LOORE C. - SUTANTYO W. 1975. *Astrophysics and Space Science*, **38 p.301**.

[3] DE LOORE - BURGER M. - VAN DESSEL E.L. - MOUCHET M. 1982. In *Be Stars. IAU Symposium n.*92, JASHEK M. - GROTH H.G. Eds., Reidel Publ. Co.

[4] FRYXELL B.A. - ARNETT W.D. 1981. *Astrophysical Journal*, **243 p.994**.

[5] HABETS G.M.H.J. 1986. In *Physics of Be Stars. IAU Colloquium n.*92, SLETTEBAK A. - SNOW T.D. Eds., Cambridge Un. Press.

[6] HABETS G.M.H.J. 1987. *Astronomy & Astrophysics*, **184 p.209**.

[7] HUTCHINGS J.B. *et al.* 1985. *Pubbl. Astron. Soc. Pacific*, **97 p.418**.

[8] KIPPENHAHN R. 1969. *Astronomy & Astrophysics*, **3 p.83**.

[9] KIPPENHAHN R. - WEIGERT A. 1967. *Zeitschrift fur Astrophysik*, **65 p.251**.

[10] LANDAU L. - LIFSHITZ E. 1958. *FIELD THEORY*. Pergamon Press.

[11] LEWIN W.H.G. - VAN PARADIJS J. - VAN DER KLIS M. 1988. *EXOSAT Preprint*, **74**.

[12] MEYER F. - MEYER-HOFMEISTER E. 1979. *Astronomy & Astrophysics*, **78 p.167**.

[13] NARIAI K. 1975. *Astronomy & Astrophysics*, **43 p.309**.

[14] PACZYNSKI B. 1971. *Acta Astronomica*, **21 p.1**.

[15] SAVONIJE G.J. 1983. In *Accretion-Driven Stellar X-ray Sources*, LEWIN W.H.G. - VAN DEN HEUVEL E.P.J. Eds., Cambridge Un. Press.

[16] SAVONIJE G.J. - DE KOOL M. - VAN DEN HEUVEL E.P.J. 1986. *Astronomy & Astrophysics*, **155 p.51**.

[17] SHU F.H. - LUBOW S.H. 1981. *Annual Review of Astronomy and Astrophysics*, **19 p.277**.

[18] SUTANTYO W. 1975. *Astronomy & Astrophysics*, **41 p.47**.

[19] THORNE K.S. - ZYTKOW A.N. 1977. *Astrophysical Journal*, **212 p.832**.

[20] UNDERHILL A. - DOAZAN V. 1982. *B Stars with and without Emission Lines*. NASA SP-456.

[21] VAN DEN HEUVEL E.P.J. 1986. In *Physics of Be Stars. IAU Colloquium n.*92, SLETTEBAK A. - SNOW T.D. Eds., Cambridge Un. Press.

[22] VAN DEN HEUVEL E.P.J. 1983. In *Accretion–Driven Stellar X–ray Sources*, LEWIN W.H.G. - VAN DEN HEUVEL E.P.J. Eds., Cambridge Un. Press.

[23] WHEELER J.C. - LECAR M. - McKEE C.F. 1975. *Astrophysical Journal*, **200 p.145**.

Chapter 4

ACCRETION PROCESSES AND INTERACTIONS WITH THE MAGNETOSPHERE

If the companion star fills its Roche-lobe the accretion onto the compact object occurs overflow through the inner Lagrangian point [10]. The accreted matter has an angular momentum with respect to the compact object therefore a disk will form.

If, on the other hand, the companion does not fill its Roche-lobe , the matter expelled by the stellar wind will pass through the Roche-lobe and will be gravitationally captured by the compact object.

In this chapter we will examine into details these two accretion processes, because they are the energy sources which power the X–ray emission of pulsed X–ray sources.

4.1 Theory of wind accretion

A neutron star of mass M_x which is moving with velocity v_{rel} through a medium of sound velocity v_c, will gravitationally capture matter from a roughly cylindrical volume of radius R_a given by [5]

$$R_a = \frac{2GM_x}{v_{rel}^2 + c_s^2} \tag{4.1}$$

which is called *accretion radius*.

In every application we neglect the term c_s^2 because, normally, we have $v_{rel}^2/c_s^2 \ll 1$ [7] (it is therefore possible that X-ray heating may cause the increase of this ratio close to unity).

The relative velocity v_{rel} is given by

$$v_{rel}^2 = v_{orb}^2 + v_w^2 \tag{4.2}$$

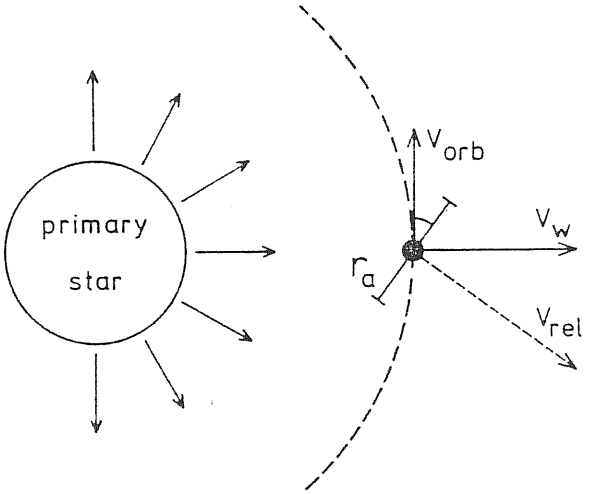

Figure 4.1: A neutron star that accretes from a stellar wind may capture angular momentum, depending on existing gradients across the target face R_a.

where v_{orb} is the orbital velocity and v_w is the velocity of the wind at the orbital radius (see Fig. 4.1 [15]).

The orbital velocity is given by (see Eqs. 3.2 and 3.5)

$$v_{orb}^2 = \frac{G(M_c + M_x)}{R_{orb}}. \tag{4.3}$$

From this expression we can see that, generally, R_{orb} is greater than the accretion radius

$$\frac{R_a}{R_{orb}} = \frac{2GM_x}{v_{orb}^2 + v_w^2} \frac{v_{orb}^2}{G(M_c + M_x)} = \frac{2}{1 + (v_w/v_{orb})^2} \frac{1}{1 + M_c/M_x} \ll 1. \tag{4.4}$$

The accretion rate onto the compact object will be [15]

$$\dot{M} = \pi R_a^2 \rho v_{rel} \tag{4.5}$$

where ρ is the mass density of the stellar wind near the accretion radius. This density may be estimated, assuming *symmetric* and *spherical accretion* and *steady mass loss*, using the continuity equation

$$\dot{M}_c = 4\pi\rho R_{orb}^2 v_w. \tag{4.6}$$

Combining Eqs. 4.5 and 4.6 we obtain

$$\frac{\dot{M}}{\dot{M}_c} = \frac{1}{(1 + M_c/M_x)^2} \left(\frac{v_{orb}}{v_w}\right)^4 \frac{1}{[1 + \alpha(v_{orb}/v_w)^2]^{3/2}} \tag{4.7}$$

where we include, for completeness, a correction factor α, which takes into account the effect of the rotation of the companion on the relative velocity [15]. The value of α is unity in the case of a non rotating primary star.

In the case of a rotating primary of radius R_c and of a steady stellar wind which conserves its angular momentum, we have [15]

$$\alpha = \left[1 - \lambda \left(\frac{R_c}{R_{orb}}\right)^2\right]^2 \tag{4.8}$$

where λ is the ratio between the angular velocities of the rotating primary and of the orbital motion of the compact object, $\lambda \equiv \omega_{rot,c}/\omega_{orb,x}$.

It is important, now, to remark that the hypothesis of spherical symmetry is essential in the derivation of Eq. 4.7, expecially in the case of a Be/X-ray binary system, in which, as we have seen, we have an envelope only in the equatorial plane of the primary and therefore this condition is not verified.

During the evolution of the massive star, $\dot{M}_c$ increases and the velocity of the wind decreases while the other parameters of Eq. 4.7 are in practice constant, so we have

$$\dot{M}(t) \propto \frac{\dot{M}_c(t)}{v_w^4(t)} \tag{4.9}$$

which is a stronger increasing function in time.

In case of accreted matter we calculate the net angular momentum with respect to the compact object of all the particles which enter in the cylinder-like volume of radius R_a and we assume that *all* the angular momentum is accreted [7,16,24].

A non rotating neutron star, even in orbital motion, will not be able to capture angular momentum from the accreted matter which forms a stellar wind in case of symmetric, spherical accretion [15].

On the contrary, we have capture in case of a orbiting neutron star and this is why, in accordance with Eq. 4.2, the target force for incoming wind particles is perpendicular to the relative velocity vector of the neutron star (see Fig. 4.1). This means that, if exists a density gradient in the stellar wind along the accretion cross section, the target force will capture different amount of matter on the two faces.

The same will occur if there is a velocity gradient, so the velocity of particles in the far and in the close surface will be different.

Of course, azimuthal velocity and/or density gradients may contribute to this asymmetry [26].

Taking into account only the radial density gradient in the stellar wind, we have that the captured specific angular momentum with respect to the neutron star is given by [24]

$$l = \frac{1}{2}\,\eta\,\omega_{orb} R_a^2 \tag{4.10}$$

where ω_{orb} is the orbital angular momentum and η is a parameter the value of which is not clear. In fact from the theory it is not sure if η is close [24]

or not [8] to unity and from numerical simulations it is found [26] that it may be much less than one, even it may be negative ! This remains an open question.

For taking into account the rotation of the primary we should have to include in the Eq. 4.10 the factor α, defined in Eq. 4.8.

Eq. 4.10 gives an estimate of the amount of specific angular momentum captured in the accretion cylinder but *what fraction* of this is transferred onto the neutron star is still an open question [8].

Before to go on, it is better to introduce two quantities, the corotation radius and the magnetospheric radius (also called Alfvèn radius) which, together with the already introduced accretion radius, characterize the accretion theory.

We define *magnetospheric radius* R_m [14] this distance from the neutron star surface within which the motion of the plasma is determinate by the magnetic field of the neutron star. To determine its expression in terms of physical quantities of the neutron star let us consider 'radial' capture of matter, with velocity $v_{in}(r)$ and density $\rho(r)$, onto a neutron star of mass M_x, radius R, dipole magnetic field of strength B_0 at the surface of the star and magnetic moment $\mu \equiv B_0 R^3$ (r is the distance measured from the neutron star).

Balance between magnetic pressure and ram pressure of the infalling matter at the magnetospheric boundaries demands that [7,18]

$$\frac{B^2(r)}{8\pi} = \rho(r)\, v_{ff}^2(r) \tag{4.11}$$

where v_{ff} is the free-fall velocity of the accreting matter and we use Gauss units. For a dipole magnetic field we have $B(r) = \mu/r^3$. The density is correlated to the accretion rate (assumed stationary) by the expression

$$\dot{M} = 4\pi\, r^2 \rho(r)\, v_{in}. \tag{4.12}$$

The infall velocity is a fraction $\xi(\leq 1)$ of the free-fall velocity

$$v_{in}(r) \equiv \xi v_{ff}(r) = \xi \sqrt{\frac{2GM_x}{r}} \tag{4.13}$$

therefore, solving for $r = R_m$, we obtain

$$R_m = \left(\frac{1}{2}\xi\right)^{2/7} \mu^{4/7} (2GM_x)^{-1/7} \dot{M}^{-2/7} \tag{4.14}$$

We can put $\xi \simeq 1$, because the poor dependence from ξ.
An estimate of R_m is given by [15,14]

$$R_m = \begin{cases} (2.7 \cdot 10^8 \mathrm{cm})\, \mu_{30}^{4/7} m^{-1/7} \dot{M}_{17}^{-2/7} \\ (3.8 \cdot 10^8 \mathrm{cm})\, \mu_{30}^{4/7} m^{-1/7} \varepsilon_{0.1}^{2/7} L_{37}^{-2/7} \\ (2.9 \cdot 10^8 \mathrm{cm})\, \mu_{30}^{4/7} m^{-1/7} R_6^{-2/7} L_{37}^{-2/7} \end{cases} \tag{4.15}$$

where we define $\mu_{30} \equiv \mu/10^{30}\ G \cdot \mathrm{cm}^3$; $R_6 \equiv R/10^6$ cm; $L_{37} \equiv L/10^{37}$ erg/sec; $m \equiv M_x/M_\odot$; $\varepsilon_{0.1} \equiv \varepsilon/0.1$ is defined as the efficiency of the conversion process $L = \varepsilon \dot{M} c^2$.

The expression in Eq. 4.15 that contains the term R_6 is valid only if *all* the accreted matter is converted in X-ray emission.

Note that $R_m \simeq 100\ R$ for a typical neutron star.

The assumptions which are implicit in Eq. 4.15 are:

1. spherical infall;
2. infall velocity equal to the free-fall velocity ($\xi = 1$);
3. we neglect the outgoing velocity;
4. we neglect the thermal pression of the infalling matter;
5. we neglect the plasma pressure within the magnetosphere with respect to the magnetic pressure.

The last quantity we introduce is the corotation radius.

The key question is: *What are the assumptions we need for the accretion to occur ?* Because we assume that the neutron star rotates, otherwise we have not pulsed emission, a condition is that the neutron star rotates not so fast that the plasma is expelled because of the centrifugal force.

The distance at which there is balance between the centrifugal force of the neutron star and the gravitational force is called *corotation radius* R_c, defined by the expression

$$R_c = \left(\frac{GM_x}{\Omega_p^2}\right)^{\frac{1}{3}} = \left(\frac{GM_x P_p^2}{4\pi^2}\right)^{\frac{1}{3}} \tag{4.16}$$

where $P_p \equiv 2\pi/\Omega_p$ is the pulse period.

Eq. 4.16 may be written as

$$R_c = (1.5 \cdot 10^8 \mathrm{cm})\ m^{1/3} P_p^{2/3}. \tag{4.17}$$

4.1.1 Interactions of the stellar wind with the magnetosphere

In this section we will study the interactions between the matter accreted by stellar wind and the magnetosphere, argument which is very far to be well understood. For the moment only very simplified theories exist, and they are not able to explain all the variety of observed phenomena.

The first topic to treat is the thermal structure of the accretion flux, which is mainly characterized by the interaction with the outgoing X-ray emission.

Ionization equilibrium results from the balance between ionization due to X-ray emission and recombination. Because the former is proportional to

the X-ray flux $\Phi_x \equiv \mathcal{L}_x/4\pi r^2$, while the latter is proportional to the electron density n_e, the ratio [14]

$$\mathcal{H} \equiv \frac{\mathcal{L}_x}{n_e r^2} \tag{4.18}$$

is the key parameter which determines the ion abundances and the temperature. For $\mathcal{H} > 10^4$ almost all the elements of interest are completely ionized and the Compton heating plays a very important role.

With the decreasing of $\mathcal{H}$ below the value of 10^4, the ions with higher ionization energies become to capture electrons. The partially ionized ions may absorb X-rays, but this effect is not so important to modify the X-ray spectrum, at least until when the more abundant ions, as helium, begin to recombine electrons.

We call r_I and r_{II} the distances from the neutron star at which the helium is neutral and ionized once, respectively (we recall that we assume spherical, symmetric accretion). We have that for $r > r_{II}$ $HeII$ becomes the more abundant ion among the helium ions and it is responsible of the absorption of X-rays with energy greater than 54.5 keV. The ions with higher ionization energies become to recombine electrons and an ionization front forms at $r = r_{II}$.

For r increasing, helium becomes neutral at $r = r_I$. For $r > r_I$ we are left only with ions with ionization energies less than 24.6 keV. Another ionization front will form at $r = r_I$.

For $r_{II} < r < r_I$, the majority of the Oxygen and Sulphur ions have the L-shell, while the iron ions have the M and N shells.

The ions of the outer shells are efficient in cooling mainly by ion excitation followed by lines emission; therefore the temperature of matter quickly decreases at the increase of r along the fronts [17].

Of course, the values of r_I and r_{II} depend on the X-ray spectrum and on $\mathcal{H}$.

The accretion flux is stopped by the magnetic field. The border between the magnetosphere and the infalling matter defines, as we have seen, the magnetospheric radius R_m (Eqs. 4.14 and 4.15).

The term ξ we introduced in Eq. 4.13 takes into account the shock formation and the fact that the magnetic field deviates from a perfect dipolar field.

We can rewrite the second expression of Eqs. 4.15 in terms of the magnetic latitude λ:

$$R_m(\lambda) = (2.7 \cdot 10^8 \mathrm{cm})\, \mu_{30}^{4/7} m^{-1/7} \varepsilon_{0.1}^{2/7} \dot{M}_{17}^{-2/7} H(\lambda) \tag{4.19}$$

where the function $H(\lambda)$ may be expressed as [3]

$$H(\lambda) = \begin{cases} (\cos\lambda)^{0.27} & \text{for } |\lambda| \le \lambda_0 \\ \\ H_c + S(1 - 2|\lambda|/\pi)^{2/3} & \text{for } |\lambda| > \lambda_0 \end{cases} \tag{4.20}$$

and the terms in the second expression are related to the geometry of the magnetic field as follows [3]

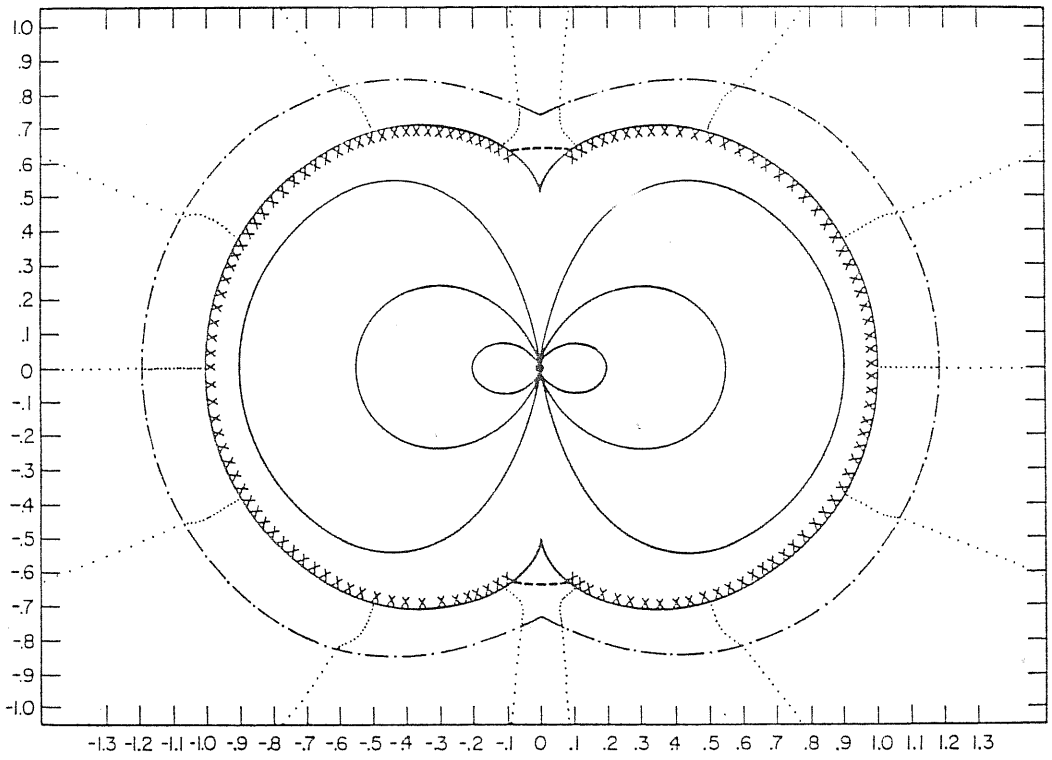

Figure 4.2: Magnetospheric structure for spherical accretion onto a neutron star of magnetic moment 10^{30} G cm^3 and the accretion rate of $3 \cdot 10^{17}$ g/sec.

$$H_c = r_{cusp}/R_m(0) \simeq 0.51; \quad S \cong 0.63; \quad \lambda_0 \cong 1.3 \ .$$

To understand the geometry of the accretion and the meaning of r_{cusp} see Fig. 4.2 [3], in which the distance scale is represented in units of 10^8 cm, whereas the stand-off distance of the shock front indicated by the dot-dashed curve is seven times the true value. The crosses represent an interchange unstable part of the magnetosphere, whereas dashed lines in the polar regions show tangential discontinuities. Dotted curves shows stream lines.

When the falling gas approaches the magnetosphere, there is a formation of a stand-off shock wave. Behind the shock wave the density and velocity decrease to $\rho_2(r_s) = 4\,\rho_{ff}(r_s)$ and $v_2(r_s) = v_{ff}/4$ [3], where r_s is the front shock radius and ρ_{ff} is given by the expression

$$\rho_{ff}(r_s) = \frac{\dot{M}}{4\pi r_s^2 v_{ff}(r_s)} \tag{4.21}$$

where $v_{ff}(r_s) = \sqrt{2GM_x/r_s}$.

The ion temperature increases to [14]

$$T_{i2} = \left(\frac{3}{16}\right) m_p \left(\frac{v_{ff}^2(r_s)}{k}\right) \cong (6.0 \cdot 10^9 \ ^\circ K\ )\ M_x\ r_{s8}^{-1} \tag{4.22}$$

where, again, r_{s8} is r_s in units of 10^8 cm and k is the Boltzmann constant.

The thermal energy of the ions is transferred to the electrons by Coulomb collisions, while the electrons are cooled by Compton collisions with X-rays. The electron temperature is determined by the balance between Coulomb heating and Compton cooling.

The two rates of transferring energy by these processes to the electrons are [14]:

$$\Gamma_{Cou} = (9.2 \cdot 10^{13}) \frac{3}{2} k(T_i - T_e) \left(\frac{\log \Lambda}{15}\right) \rho_2(r_s)\, T_e^{-3/2} \ \text{erg/sec} \tag{4.23}$$

where $\log \Lambda \simeq 15$ is the Coulomb logarithm and T_e is the electron temperature; and

$$\Gamma_{Com} = 4 \frac{k(T_e - T_x)}{m_e c^2} \sigma_T \frac{\mathcal{L}_x}{4\pi r^2} = 2.6 \cdot 10^2\ k(T_e - T_x) \frac{L_{37}}{r_8^2} \ \text{erg/sec} \tag{4.24}$$

where σ_T is the Thomson cross section and T_x is the effective X-ray temperature, in keV.

Imposing $\Gamma_{Cou} = \Gamma_{Com}$, we obtain the electron temperature for $T_x \ll T_e \ll T_i$

$$T_e = 31 \left(\frac{\log \Lambda}{15}\right)^{2/5} m^{1/15} r_8^{-1/5} \varepsilon_{0.1}^{-2/5} \quad \text{keV}. \tag{4.25}$$

The stand-off distance of the shock is given by [14]

$$l \cong v_2 \left(\frac{3}{2} k T_i\right) / \Gamma_{Cou} \cong 0.15\ r_s\ L_{37}^{-32/35} \mu_{30}^{-6/35} m^{47/35} \varepsilon_{0.1}^{11/35} \left(\frac{\log \Lambda}{15}\right)^{-1}. \tag{4.26}$$

The optical depth of the shock region by electron scattering is given by [14]

$$\tau_{es} = \kappa_{es}\, \rho_2\, l \simeq 5.5 \cdot 10^{-2}\ L_{37}^{6/5} \mu_{30}^{2/7} \varepsilon_{0.1}^{3/5} m^{6/5} \left(\frac{\log \Lambda}{15}\right)^{-2/5}. \tag{4.27}$$

where κ_{es} is the electron scattering opacity.

About other processes we have that Comptonization is too small to modify the X-ray spectrum in the underlying regions, because the Comptonization parameter y (see section 5.2 for the definition)

$$y \equiv \frac{4kT_e}{m_e c^2} \tau_{es} \simeq 1.0 \cdot 10^{-2}\ L_{37}^{-8/7} \varepsilon_{0.1}^{1/7} \mu_{30}^{6/35} m^{10/7} \tag{4.28}$$

is very small.

Thermal bremsstrahlung yields a smaller luminosity than the total luminosity, but gives an appreciable contribution at higher energies, because of the higher electron temperature—if the temperature of the X-rays emitted by the stellar surface is not very high.

At lower energies the shocked plasma is optically thick, because of the free-free absorption, and the Rayleigh-Jeans spectrum is attained in the infrared region.

4.1.2 Matter infall in the magnetosphere

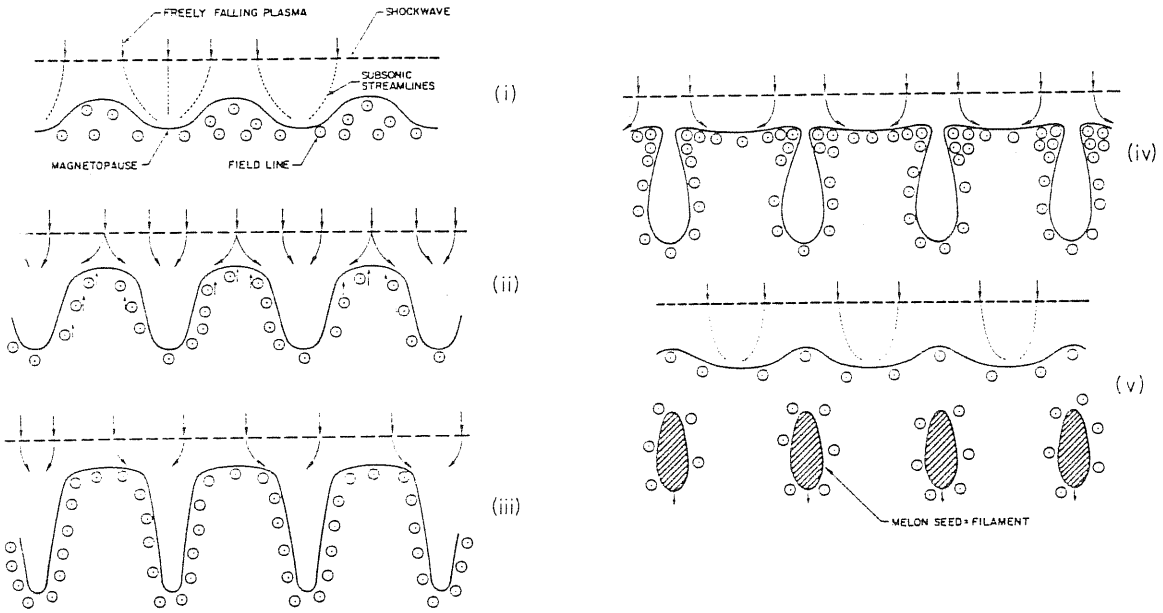

Figure 4.3: Development of interchange instability at the magnetopause of a neutron star.

At the magnetopause, defined as the region of the magnetosphere where the stellar wind is stopped by the magnetic pressure, the outer kinetic pressure P_m^+ is balanced by the magnetic pressure $B_M^{2\,-}/8\pi$ (the $\pm$ signs mean the direction of the force, assuming positive the infall radial direction).

Matter at the magnetopause is subject to the gravitational force normal to the magnetopause, $+\, g\,\rho_m$, and to the magnetic force $B_m^{2\,-}/4\pi r_{cur}$, where r_{cur} is the curvature radius of the lines of the magnetic field.

The marginal stability of matter is reached if

$$\frac{B_m^{2\,-}}{4\pi} = 2\,P_m^+ > g\,\rho_m r_{cur} \cong \frac{GM_x}{R_m^2} \cong \rho_m\,\frac{GM_x}{R_m}. \qquad (4.29)$$

The left hand side of Eq. 4.29 is proportional to the temperature, while the right hand side is not, therefore the equilibrium is lost as matter cools by Compton cooling and we have a Rayleigh-Taylor instability, along the azimuthal direction [29,26].

The plasma is absorbed in the magnetosphere and it splits in filaments [28,6,4] of mean radius $\pi R_m/n$ and length $\pi R_m/n^{1/2}$, where n is the mode

number of the perturbations, defined by the wave number

$$\mathcal{K} \equiv \frac{n}{R_m|\cos\lambda|} \tag{4.30}$$

with λ magnetic latitude.

The filaments further split in smaller pieces, because of the density perturbations in the latitude direction, so the infalling matter consists of blobs of radius $\sim \pi R_m/n$. While the blobs fall in the magnetosphere they reduce their dimensions, because of the increase of the magnetic pressure (see Fig. 4.3 [3]).

The temperature of the blobs, at the beginning, is constant and equal to the X-ray temperature because of the Compton scattering, therefore $\rho \propto r^{-6}$ and $R_b \propto r^{-2}$, where R_b is the radius of the blob.

As the blob falls further, the y parameter of Eq. 4.28 decreases as r^4 and the temperature drops abruptly at $\mathcal{H} = \mathcal{H}_{II} \sim 10^3$ by resonant recombination (see section 5.2) and the blobs become optically thick.

As the blobs fall in the magnetosphere they are subject to Kelvin-Helmholtz instabilities [29,26,6,28,4]. The motion of a blob with infall velocity $v_{b,i}$ excites an Alfvén wave of velocity v_A in the interblob plasma. This, again, excites another Alfvén wave of velocity $v_{A,b}$ on the blob surface and it yields a perturbation, which penetrates in the blob for a distance $(v_{b,i}/v_{A,b})R_b$. The perturbation amplitude increases at a rate $\mathcal{K}v_{A,b}$, where $\mathcal{K}$ is the wave number of the perturbation (see Eq. 4.30).

Therefore the rate of growing of the Kelvin-Helmholtz instabilities is given approximatively by

$$\Gamma_{KH} \cong \mathcal{K}v_{b.i}\left(\frac{v_{A,b}}{v_A}\right) = \mathcal{K}v_{b,i}\left(\frac{\rho_l}{\rho_b}\right)^{1/2} \tag{4.31}$$

where ρ_l and ρ_b are the interblob and blob densities, respectively.

The increase of the Kelvin-Helmholtz instabilities has as a result the disruption of the blobs in little pieces, which are then diffused by the magnetic field.

The plasma is then dragged along the lines of force of the magnetic field and slides along the force lines onto the star surface [4]. These force lines form a boundary layer, the plasmapause, behind which spherical accretion does not occur.

The position of the plasmapause depends, in a complicated way, on several parameters, but it is possible to show that the accretion along the force lines of the magnetic field occurs also in the case of spherical accretion if the magnetic field is strong and the luminosity is high [4].

For a X-ray source of given magnetic field strength, the flow pattern changes with luminosity variations. If the plasmapause radius is greater than the star radius, then plasma will fall onto the magnetic polar caps, of area $2\,A_{cap}$, with [14]

$$2\,A_{cap} = A_\star\left[1 - \sqrt{1 - \frac{R_\star}{R_p}}\right] \tag{4.32}$$

where $A_\star = 4\pi R_\star^2$ is the superficial area of the star and R_p is the plasmapause radius. If $R_p \gg R_\star$ then

$$A_{cap} \cong \pi \left(\frac{R_\star^3}{R_p} \right) \tag{4.33}$$

therefore the polar cap area depends on the luminosity, because R_p depends on it.

4.1.3 Non continuum stellar wind accretion: regimes of inhibition

After having introduced the three radii which characterize the wind accretion (see Eqs. 4.1, 4.14 and 4.16), i.e. the accretion radius R_a, the magnetospheric radius R_m and the corotation radius R_c, we will see what are the possible processes which may influence the accretion, according to the relative values of these radii [25].

Regime I: direct wind accretion

When $R_a > R_m$ and $R_c > R_m$, the captured wind matter goes from the accretion radius to the magnetospheric radius where, as we have seen, it is stopped by a collisionless shock. The accretion then occurs by wind, with penetration in the magnetosphere by means of Kelvin-Helmholtz or Rayleigh-Taylor instabilities [29,28,26,4,6].

Regime II: centrifugal inhibition of accretion

If $R_c < R_m < R_a$, then the wind matter which penetrates through the accretion radius is stopped at the magnetospheric radius and does not penetrate beyond, because of $R_m > R_c$ and so the magnetic force is greater than the gravitational force in that point.

Then matter assumes a prolate configuration, which strongly shocks the wind matter by supersonic rotation [16,27]. This mechanism, called *propeller mechanism* may throw matter beyond the accretion radius, giving therefore a torque to the neutron star , which suffers a spin-down.

But is is also possible that the ejection does not occur, so that material forms surrounding the magnetosphere; this occurs if the wind matter accumulates more quickly than the ejection rate [19].

Regime III: magnetic inhibition of accretion

If $R_m > R_a$, the stellar wind will flow around the obstacle presented by the magnetosphere of the neutron star, similar to the interaction of the solar wind with the terrestial magnetosphere.

4.2 Theory of disk accretion

A normal assumption which is made in case of Roche-lobe overflow is that all the matter leaves the Roche-lobe close to the inner lagrangian point. The specific angular momentum with respect to the orbiting compact object is [15]

$$l = \omega_{orb}(R - r_L)(R - \lambda r_L) \tag{4.34}$$

where R is the orbital separation, r_L is the distance of the inner lagrangian point and λ is the ratio between the rotation angular velocity of the compact object and orbital angular velocity.

From this expression we can see that the specific angular momentum transferred during a Roche-lobe overflow is a factor $(R/R_a)^2$ greater than that transferred by stellar wind (see Eq. 4.10).

If the companion star overflows its Roche-lobe, there is the probability that a disk forms around the compact object. In fact, if R_k is the radius at which a fluid element of specific angular momentum l rotates in Keplerian circular orbit around the compact object of mass M_x, then

$$R_k = \frac{l^2}{GM_x}. \tag{4.35}$$

If $R_k > R_a$ a disk will form, so using Eq. 4.34

$$R_k = R\left(1 + \frac{M_c}{M_x}\right)\left(1 - \frac{r_L}{R}\right)^2\left(1 - \lambda\frac{r_L}{R}\right)^2 > R_a \tag{4.36}$$

obtained by means of Kepler's third law.

Therefore, for the formation of a disk, the matter must be such that

1. the specific potential energy with respect to the compact object must be greater than the specific kinetic energy $\varepsilon_k = v_{rel}^2/2$, where v_{rel} is the relative velocity of the gas with respect to the object. In this way matter can be accreted.

2. the specific angular momentum of the captured gas must be greater enough to avoid the direct infall onto the object.

This is a general criterion useful to verify the formation of an accretion disk around a compact object; now we will construct a model of the disk which will be able to explain the observational data, assuming that the disk is formed.

The first step is to understand if it is possible to obtain informations about the structure of the disk starting from the formation conditions.

Because we deal with a real gas, the gas viscosity will tend to minimize the energy of the gas orbiting around the compact object, without modifying, of course, the total angular momentum [10]. Because of this, the random velocities in the 'vertical' direction (i.e. parallel to the average angular momentum vector of the gas at that radius) will be dissipated up to

reaching thermal values. The disk will become *thin*; this process is relatively fast because particles at the same radius can effectively communicate.

Other consequences, due to viscous forces, on the structure of the disk are:

1. the inner particle orbits are circular, because this is the lower energy configuration;
2. the disk is flat (we will treat later the case of a tilted, twisted disk);
3. the mass is transported radially in the disk

To describe the disk structure we will use the hydrodynamical equations for a viscous gas [20]:

1. *Conservation of mass*:

$$\frac{\partial \rho}{\partial t} + \nabla \cdot (\rho \vec{\mathbf{v}}) = 0 \tag{4.37}$$

where ρ is the mass density and $\vec{\mathbf{v}}$ is the fluid velocity.

2. *Conservation of angular momentum*:

$$\rho \left[\frac{\partial \vec{\mathbf{v}}}{\partial t} + (\vec{\mathbf{v}} \cdot \nabla)\vec{\mathbf{v}} \right] = \rho \left(\vec{\mathbf{F}} - \nabla \Phi \right) - \nabla p - \nabla \cdot \vec{\mathbf{T}} \tag{4.38}$$

with $\vec{\mathbf{F}}$ external torque, Φ gravitational potential given by

$$\Phi = - \frac{GM_c}{|\vec{\mathbf{r}} - \vec{\mathbf{r}}_c|} - \frac{GM_x}{|\vec{\mathbf{r}} - \vec{\mathbf{r}}_x|} \tag{4.39}$$

where $\vec{\mathbf{r}}_{c,x}$ are the distances of $M_{c,x}$ from the center of mass of the system; p is the pressure and $\vec{\mathbf{T}}$ is the viscous stress.

3. *Conservation of energy*:

$$\rho \left[\frac{\partial E}{\partial t} + (\vec{\mathbf{v}} \cdot \nabla) E \right] = - p \nabla \cdot \vec{\mathbf{v}} - (\vec{\mathbf{T}} \cdot \nabla) \cdot \vec{\mathbf{v}} - \nabla \cdot \vec{\mathbf{q}} \tag{4.40}$$

where E is the internal energy of the fluid element and $\vec{\mathbf{q}}$ is the heat generated by the viscous stress.

These five scalar equations are not enough to determine all the unknowns, among them the velocity field $\vec{\mathbf{v}}$ and the emitted spectrum: we need auxiliary equations which link among them E, p, ρ, $\vec{\mathbf{T}}$ and $\vec{\mathbf{q}}$.

The first step towards the solution of the problem of the structure of an accreting disk is to make some simplifying assumptions, to reduce at minimum the number of the parameters. They are:

1. *The disk is axisymmetric.*

   This implies that the gravitational influence of the mass-losing star is neglected. We will use an inertial frame and a cylindric coordinate system r, ϕ, z ($z = 0$ the orbital plane) to describe the disk.

2. *The disk is thin.*

   Its half-thickness h satisfies to the expression

$$\frac{h}{r} \ll 1 \tag{4.41}$$

   at any distance r. This implies that the pressure forces, in the disk, are much less than the gravitational ones, i.e. $p \ll \rho\, v^2$.

   This further implies that $v_z \ll v_r$, where $v_{z,r}$ are the components of the velocity in the z and r direction, respectively.

3. *The viscosity little influences the flux.*

   This implies that any the component of the stress-tensor is much greater than the pressure, i.e. $T_{ij} \leq p$. With the aid of point 2. we have that $T_{i,j} \ll \rho\, v^2$.

   Because the viscosity causes radial motion, we obtain $v_r \ll v_\phi$, where v_ϕ is the ϕ component of the velocity.

4. *The disk is stationary*

   All the variables and the parameters are time-independent, *included the mass flux* $\dot{M}$.

An approximation at the lowest level of the hydrodynamical equations, based on these approximations, gives rise to the following equations:

1. *Conservation of mass.*

$$\dot{M} = -\,4\pi\, r\, \rho\, v_r. \tag{4.42}$$

   The half-thickness is defined as

$$h = \frac{1}{\rho} \int_0^\infty \rho(z)\, dz. \tag{4.43}$$

2. *Conservation of angular momentum.*

$$v_\phi^2 = \frac{GM_x}{r} \qquad (r \text{ component}) \tag{4.44}$$

$$\frac{\dot{M}}{4\pi}\, r\, v_\phi = r^2\, T_{\phi r} + \frac{\dot{J}}{4\pi} \qquad (\phi \text{ component}) \tag{4.45}$$

$$p \sim \rho\, h^2 \frac{GM_x}{r^3} \qquad (z \text{ component}) \tag{4.46}$$

   where $\dot{J}$ represents the net rate at which the angular momentum is lost from the disk, at the inner radius r_i, by the interaction with the object. For an arbitrary torque we may use

$$\dot{J} = \beta_L \dot{M} (r\, v_\phi)_i \tag{4.47}$$

where β_L is a parameter of the order of unity.

Inside the interaction region β_L depends on r, while outside does not. Where β_L can be considered constant, Eq. 4.45 can be written as

$$\dot{M}\, r\, v_\phi \left[1 - \beta_L \sqrt{\frac{r_i}{r}}\right] = 4\pi\, r^2 T_{\phi r}. \tag{4.48}$$

3. *Conservation of energy.*

If we define Q^- the mass flux lost from the disk surface per unity of area as

$$Q^- = \int_0^\infty \frac{\partial q}{\partial z}\, dz = q(\infty) \tag{4.49}$$

we obtain

$$Q^- = -\, T_{\phi r} r\, \frac{\partial}{\partial r}\left(\frac{v_\phi}{r}\right) \tag{4.50}$$

which, by means of Eqs. 4.44, 4.45 and 4.48 gives

$$Q^- = \frac{3}{8\pi} \dot{M}\, \frac{G M_x}{r^3} \left[1 - \beta_L \sqrt{\frac{r_i}{r}}\right] \tag{4.51}$$

which shows that the emitted flux Q^- at a certain radius r is completely determined by M_x and $\dot{M}$. The absence of a dependence on any viscous mechanism and on heat transport is due to the assumption of stationarity.

Of course, for $r \gg r_i$ the term in square parenthesis becomes negligible: this is an inner-edge effect.

To complete the set of hydrodynamical equations, a sufficient set of equations is: the equation of state for matter, a viscosity law and an equation which specifies the cooling process transporting heat from the disk interior to the surface.

If we assume *a priori* that the mechanism which yields the radial motion of the particles is the viscosity (i.e. the product between a viscous coefficient and the velocity gradient),then, in our model, will be

$$T_{\phi r} \approx -\, \eta \left(\frac{\partial v_\phi}{\partial r} - \frac{v_\phi}{r}\right) \tag{4.52}$$

where η is dynamic viscosity coefficient.

By means of the Keplerian value of v_ϕ, putting Eq. 4.52 into Eq. 4.45 we obtain

$$\dot{M} \approx 3\pi\, h\, \eta. \tag{4.53}$$

Therefore, in a stationary, axisymmetric disk the value of $(h\,\eta)$ is univocally determinate by the accretion rate $\dot{M}$. At any radius in which the viscous mechanism does not give a sufficient value to η, matter will grow h until when Eq. 4.53 is satisfied.

From Eq. 4.53 we can obtain an estimate of η. Because of $h/r \ll 1$, we obtain $h \ll 10^{10}$ cm, and for a typical accretion rate of $\dot{M} \sim 10^{17}$ g/sec we obtain $\eta \geq 10^6$ g/cm·sec.

This value is several order of magnitude greater than the viscosity expected between particles, therefore the viscous mechanism in the disk must be much more effective than particle viscosity.

There are only few physical processes which may produce such high values for viscosity. Among them, the most probable, according to the physical conditions on a neutron star, is the action of small-scale magnetic field in the gas. This tends to reduce the velocity gradient such that the flux is driven towards uniform rotation.

While entering the disk with the transferred matter, the field may have been very small. Once it is in the disk, the Keplerian shear amplifies it at a rate

$$\frac{\partial B}{\partial t} = -\nabla \times (\vec{\mathbf{v}} \times \vec{\mathbf{B}}) \tag{4.54}$$

which does not modify the r component B_r, but stretches the ϕ component B_ϕ

$$\frac{\partial B_\phi}{\partial t} = r \frac{\partial \omega_k}{\partial r} B_r \tag{4.55}$$

where ω_k is the Keplerian angular velocity $\omega_k \equiv (GM_x/r^3)^{1/2}$.

The $T_{\phi r}$ component of the viscous-stress tensor, due to these magnetic fields, has a value of the order of

$$T_{\phi r} \approx \frac{B_r B_\phi}{4\pi}. \tag{4.56}$$

Because the shearing motions of the gas tends to string the fields out in the ϕ direction, we expect that $T_{\phi r}$ is less than the magnetic pressure $B^2/8\pi$. If this pressure is greater than the internal pressure of the disk, the force lines of the field form some coronal loops, as those seen in our Sun. Therefore we may put [20]

$$T_{\phi r} \approx \alpha p = \alpha \rho c_s^2 \tag{4.57}$$

where $\alpha \leq 1$ is an adimensional parameter and $c_s^2 = (p/\rho)$ is the sound velocity in the plane $z = 0$.[1]

As equation of state, we will simply consider the ordinary equation of state for a mixture of radiation and ideal gas

$$p = \frac{1}{3} a T^4 + \rho \frac{k}{\mu m_p} T \tag{4.58}$$

where a is the radiation constant, k is the Boltzmann constant, μ is the average molecular weight, of the order of $1/2$, and m_p is the proton mass.

A cooling equation which we can choose is that based on radiative transport, which occurs mainly in the z direction through a optically thick disk (in fact the optically depth $\tau > \kappa \rho h \gg 1$) [23]

$$q_z = -\frac{1}{\kappa \rho} \frac{\partial}{\partial z} \left(\frac{a}{3} T^4 \right). \tag{4.59}$$

[1] We can derive the same result of Eq. 4.57 considering turbolence as the cause of viscosity.

The integration in the z direction on half disk gives

$$Q^- = \frac{c\, a\, T^4}{\kappa\, \rho\, h} \tag{4.60}$$

where c is a constant and the values of T , ρ and the opacity κ are taken on the plane $z = 0$.

The superficial term of the integration , proportional to the superficial temperature to the fourth has been neglected, in the hypothesis that $T > T_s$.

The major contribute to the opacity κ is given by the Thomson and the free-free scattering, so [20]

$$\kappa \approx 0.4 + 6 \cdot 10^{22} (\rho\, T^{-7/2}) \quad \mathrm{cm}^2/\mathrm{g}. \tag{4.61}$$

By means of all these equations ,we are now able to determine all the quantities which characterize the structure of the disk by purely algebraic manipulations. The result is often called 'α-disk model' [23].

We will not write the resultant formulae, which are to be found in any textbook of astrophysics [10], but will give the most important features:

1. *The disk is concave.*

   It thickens outward as $h \sim r^\gamma$, with $\gamma > 1$, except for the closest regions to the compact object. For radius $r > 10^8$ cm we have that $\gamma \approx 9/8$.

2. *The disk is thin.*

   This is a check of the auto-consistency of the model.

3. *The disk extends radially towards the Roche-lobe.*

   This results from the necessity of the disk to remove the excess of angular momentum [11].

4. *The mass of the disk is negligible.*

   For $M_x \sim 1\, M_\odot$ and $\dot{M} \sim 10^{17}$ g/sec, we find the total mass of the disk is of the order of $10^{-9}\, M_\odot$. This involves that the disk self-gravity can be completely neglected.

5. *The disk is optically thick.*

   This implies that the disk can irradiate its energy only thermally.

6. *The disk has a $\nu^{1/3}$ spectrum.*

   If all the radiation coming from the disk is emitted thermally, the integration of the flux on all the range of radii gives a frequency dependence of the form $\nu^{1/3}$.

This is the simplest model and, of course, does not explain all the features which we observe in the disks; this is, however, the basic model for all the other more refined models.

A more realistic model takes into account the possibility that the disk is tilted (this may be due to the manner in which matter leaves the inner lagrangian point and arrives on the disk). Then we have that the tidal force of the companion will acquire a vertical component [21], which will cause the orbit to precess, with angular velocity ω_{pre}, which a dependence on its radius of the form $\omega_{pre} \sim r^{3/2}$. The accretion disk is not a rigid body, so the ring of matter at different radii will precede at different rates, each of them in accordance with its value of ω_{pre}. On the other hand, these rings are coupled, because of the viscosity which oppose to this phenomenon. The result may be a twisted disk with stationary slope, precessing with a single period, which is a sort of average on all the precession periods of the rings (see section 7.3).

4.2.1 Interactions of the accretion disk with the magnetosphere

As matter is accreted onto the neutron star, torques arise, which will tend to spin it up or down. In fact, a neutron star of moment of inertia I and angular velocity Ω_p will be influenced by the accretion of matter of specific angular momentum l in the sense that [22]:

$$\frac{d}{dt}(I\Omega_p) = \dot{M}l - H \tag{4.62}$$

where H represents the non-thermal torque, including torques arising from magnetic and/or viscous forces and torques arising from matter that leaves the system.

This same expression can be rewritten in terms of $P_p = 2\pi/\Omega_p$:

$$\frac{\dot{P}_p}{P_p} = \frac{\dot{M}}{M}\left(\frac{M}{I}\frac{dI}{dM} - \frac{l_M}{l_\star}\right) + \frac{H}{I\Omega_p} \tag{4.63}$$

where $l_M = R_m^2\Omega_K(R_m)$ is the component of the specific angular momentum, parallel to Ω_p, of matter which crosses the magnetopause; $\Omega_K(R_m) = \sqrt{(GM/R_m^3)}$ is the Keplerian angular velocity of the matter in the disk at $r = R_m$ and $l_\star$ is the specific angular momentum of the star of radius $R_\star$, equal to $I\Omega_p/M$.

If the accreted matter counter-rotates with respect to Ω_p, then $l_M < 0$ and the second term between parenthesis in Eq. 4.63 will tend to increase $\dot{P}_p/P_p$ (i.e. tends to spin-down the object). The first term between parenthesis is, in general, small with respect to the second, because, in our case, we have $R_m \gg R$.

The maximum spin-up or spin-down rate will occur when the external torques are small, and therefore we have

$$\frac{\dot{P}_p}{P_p} \propto \frac{\dot{M}}{M}\left(\frac{l_M}{l_\star}\right) \tag{4.64}$$

which may be expressed in terms of parameters of the compact object and of the luminosity as follows [22]

$$\frac{\dot{P}_p}{P_p} \approx -\,2\cdot 10^{-5}\, m^{-3/2} R_6 \left(\frac{R_g}{10^6\ \mathrm{cm}}\right)^{-2} \left(\frac{R_m}{10^8\ \mathrm{cm}}\right)^{1/2} L_{37} P_p \quad \mathrm{yr}^{-1} \tag{4.65}$$

where R_g is the gyration radius of the compact object and the other quantities are defined as above. By means of Eq. 4.14 we obtain [22]

$$\frac{\dot{P}_p}{P_p} \approx -\,3\cdot 10^{-5}\, f\, P_p L_{37}^{6/7} \quad \mathrm{yr}^{-1} \tag{4.66}$$

where the parameter f is of the order of unity for a standard neutron star of $M_x = 1.4\ M_\odot$, $R_x = 10^6$ cm and $I = 10^{45}$ g·cm^2.

An accretion disk around a neutron star is perturbed by the magnetic field, as the matter flux approaches the magnetosphere. The disk will stop when the disk pressure is equal to the magnetic pressure, i.e.

$$p = \frac{\mu^2}{8\pi r^6} \tag{4.67}$$

where we assume a dipolar magnetic field of momentum μ.

From the section 4.2 we have that the disk pressure is given by [14]

$$p = \frac{GM_x \rho\, h^2}{r^3} = \frac{GM_x \dot{M}\, h}{4\pi\, v_r r^4} \tag{4.68}$$

and therefore the inner radius r_i of the disk is situated at

$$r_i = 0.82 \left(\frac{r\, v_r}{v_{ff} h}\right)^{2/7} R_m \tag{4.69}$$

where $(v_r r / v_{ff} h) \simeq 0.25$ depends poorly on r.

The force lines of the magnetic field enter in the disk at $r > r_i$ and are deformed by the accretion flux [12,13]. Close to r_i the angular momentum of the accretion flux is transferred to the magnetosphere by spinning-up or spinning-down the neutron star. As the interactions of the accretion flux with the magnetosphere depend on the relative configurations, we will consider two limit cases:

a. The axis of the accretion disk is parallel to the magnetic axis.

In this case the magnetic field is dragged by the flux and it is amplified to possess a toroidal component. The toroidal field of the internal surfaces is antiparallel to that of the external surface, and they reconnect with each other. The amplification and the reconnection balance to maintain the equilibrium. The radial field pinches the magnetic field inside.

The poloidal configuration of the field is represented in Fig. 4.4 [12].

The radial flux of matter which crosses the poloidal magnetic field generates a toroidal current which shields the magnetic field. The screening radius is $r_s \sim 10^2 R_m$. The magnetic field is confined inside r_s. In the transition

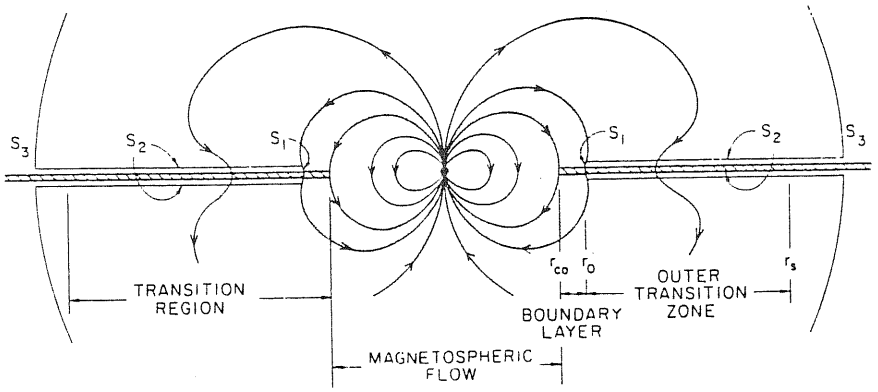

Figure 4.4: Cross-sectional view of the accretion disk in the parallel geometry.

zone between r_0 (defined as $R_c + \delta$, with R_c corotation radius (see Eq. 4.16) and δ thickness of the boundary layer) and r_s, the angular velocity of the accretion flux is Keplerian but the field lines are twisted by the flux.

Inside r_0, the magnetic field is so strong that the angular velocity is no more Keplerian, and reaches the corotation value at $r = R_c$.

If $R_c < r_0$, the angular velocity in the transition zone is less than that of the star, therefore the transfer of angular momentum decelerates the rotation of the star. The spin-up (or spin-down) rate will become (compare with Eq. 4.66) [13]

$$\frac{\dot{P}_p}{P_p} \approx 5.8 \cdot 10^{-5} f\, n(\omega_s)\, P_p\, L_{37}^{6/7} \tag{4.70}$$

where ω_s is the 'fastness parameter' [9], defined as the ratio between ω_* and the Keplerian angular velocity at $r = R_m$:

$$\omega_s = \frac{\omega_*}{\Omega_K(R_m)} = \left(\frac{R_m}{R_c}\right)^{3/2} \tag{4.71}$$

and $n(\omega_s)$ is an adimensional function, the behaviour of which is shown in Fig. 4.5 [15].

From Fig. 4.5 we can see that a critical fastness parameter ω_c exists, at which a rotating neutron star will suffer neither spin-up nor spin-down, although it accretes matter.

The equilibrium period P_{eq}, defined by imposing $\dot{P}_p = 0$, is given by the relation $\omega_s = \omega_c \cong 0.35$, i.e.

$$P_{eq} = (3.9 \text{ sec})\, f\, L_{37}^{-3/7} \tag{4.72}$$

therefore we will have a spin-up or a spin-down according to $P_p > P_{eq}$ or $P_p < P_{eq}$, respectively. If the period is close to P_{eq}, the sign of the spin change varies according to the accretion rate.

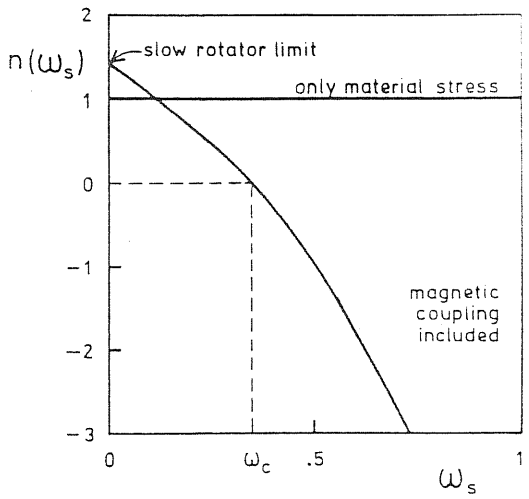

Figure 4.5: The dimensionless torque $n(\omega_s)$ as a function of the fastness parameter ω_s.

b. The axis of the accretion disk is perpendicular to the magnetic axis

In this case the accretion disk arrives close enough to the central object without distorting appreciably the magnetic field [1,2].

Again, the inner edge of the disk is determined by imposing the balance between the disk pressure and the magnetic pressure.

Matter, attacked to the force lines of the magnetic field, corotates with the star with angular velocity Ω_p, while the diamagnetic matter rotates with Keplerian angular velocity Ω_K. The difference between these two velocities

$$\Delta v = (\Omega_K - \Omega_p)\, r \tag{4.73}$$

may create Kelvin-Helmholtz instabilities; consequently the plasma in the disk is disrupted in pieces that are dragged by the force lines of the magnetic field and eventually fall onto the star [1].

Generally, a part of the matter of the disk is trapped by the magnetosphere and corotates, while the other is lost. Therefore, the rate of transfer of angular momentum is expressed by

$$\dot{J} = \nu \dot{M}\, \Omega_p R_c^2 \tag{4.74}$$

where ν is a parameter which may be both signs, according to the mass transfer process [14]. If ν does not depend on other parameters, we have [1]

$$\frac{\dot{P}_p}{P_p} = -\frac{P_p}{2\pi}\dot{M}\,\omega_s R_c = 1.7\cdot 10^{-13}\,\frac{\nu}{0.1}\, f\, L_{37} P_p^{4/3}. \tag{4.75}$$

The difference with Eq. 4.66 is due to the fact that the former has been obtained by imposing balance between the magnetic pressure and the ram pressure, while Eq. 4.75 has been obtained considering the magnetic and Keplerian pressures.

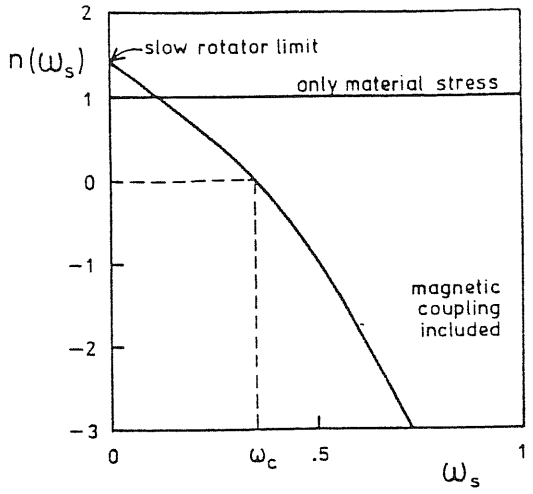

Figure 4.5: The dimensionless torque $n(\omega_s)$ as a function of the fastness parameter ω_s.

b. The axis of the accretion disk is perpendicular to the magnetic axis

In this case the accretion disk arrives close enough to the central object without distorting appreciably the magnetic field [1,2].

Again, the inner edge of the disk is determined by imposing the balance between the disk pressure and the magnetic pressure.

Matter, attacked to the force lines of the magnetic field, corotates with the star with angular velocity Ω_p, while the diamagnetic matter rotates with Keplerian angular velocity Ω_K. The difference between these two velocities

$$\Delta v = (\Omega_K - \Omega_p)\, r \tag{4.73}$$

may create Kelvin-Helmholtz instabilities; consequently the plasma in the disk is disrupted in pieces that are dragged by the force lines of the magnetic field and eventually fall onto the star [1].

Generally, a part of the matter of the disk is trapped by the magnetosphere and corotates, while the other is lost. Therefore, the rate of transfer of angular momentum is expressed by

$$\dot{J} = \nu \dot{M} \Omega_p R_c^2 \tag{4.74}$$

where ν is a parameter which may have both signs, according to the mass transfer process [14]. If ν does not depend on other parameters, we have [1]

$$\frac{\dot{P}_p}{P_p} = -\frac{P_p}{2\pi} \dot{M}\, \omega_s R_c = 1.7 \cdot 10^{-13} \frac{\nu}{0.1} f\, L_{37} P_p^{4/3}. \tag{4.75}$$

The difference with Eq. 4.66 is due to the fact that the former has been obtained by imposing balance between the magnetic pressure and the ram pressure, while Eq. 4.75 has been obtained considering the magnetic and Keplerian pressures.

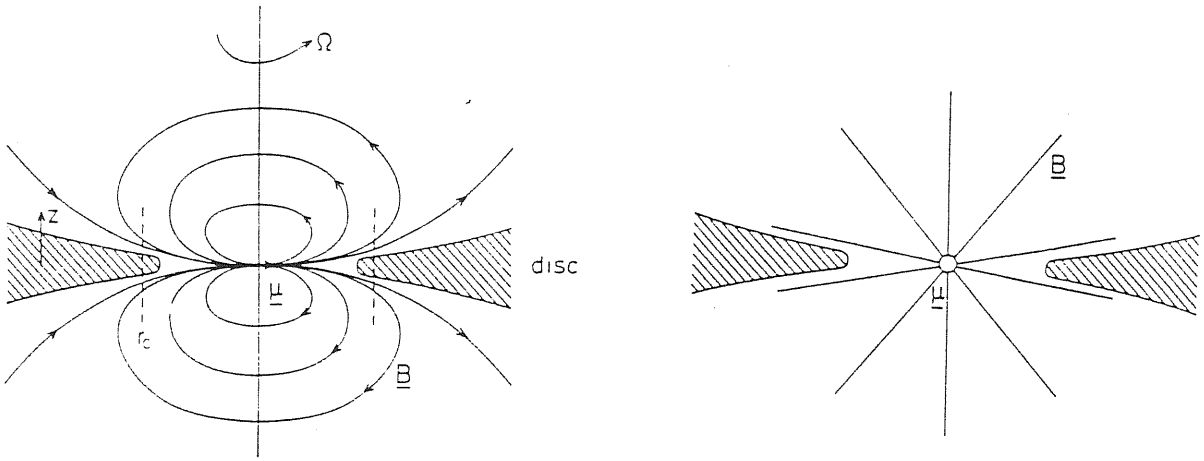

Figure 4.6: Two cross-sectional views of the accretion disk in the perpendicular geometry

Bibliography

[1] ANZER U. - BORNER G. 1980. *Astronomy & Astrophysics*, **83 p.133.**

[2] ANZER U. - BORNER G. - MEYER-HOFMEISTER E. 1987. *Astronomy & Astrophysics*, **188 p.85.**

[3] ARONS J. - LEA S.M. 1976. *Astrophysical Journal*, **207 p.914.**

[4] ARONS J. - LEA S.M. 1980. *Astrophysical Journal*, **235 p.1016.**

[5] BONDI H. - HOYLE F. 1944. *Montly Notices of R.a.S.*, **104 p.273.**

[6] BURNARD D.J. - LEA S.M. - ARONS J. 1983. *Astrophysical Journal*, **266 p.175.**

[7] DAVIDSON K. - OSTRIKER J.P. 1973. *Astrophysical Journal*, **179 p.585.**

[8] DAVIES R.E. - PRINGLE J.E. 1980. *Montly Notices of R.a.S.*, **191 p.599.**

[9] ELSNER R.F. - LAMB F.K. 1977. *Astrophysical Journal*, **215 p.897.**

[10] FRANK J. - KING A.R. - RAINE D.J. 1985. *Accretion Processes in Astrophysics.* Cambridge Un. Press.

[11] GEREND D. - BOYNTON P.E. 1976. *Astrophysical Journal*, **209 p.562.**

[12] GHOSH P. - LAMB F.K. 1979. *Astrophysical Journal*, **232 p.259.**

[13] GHOSH P. - LAMB F.K. 1979. *Astrophysical Journal*, **234 p.296.**

[14] HAYAKAWA S. 1985. *Physics Reports*, **121 p.318.**

[15] HENRICHS H.F. 1983. In *Accretion–Driven Stellar X–ray Sources*, LEWIN W.H.G. - VAN DEN HEUVEL E.P.J. Eds., Cambridge Un. Press.

[16] ILLARIONOV A.F. - SUNYAEV R.A. 1975. *Astronomy & Astrophysics*, **39 p.185**.

[17] KALLMAN T.R. - McGRAY R. 1982. *Astrophysical Journal Suppl.*, **50 p.263**.

[18] LAMB F.K. - PETHICK C.J. - PINES D. 1973. *Astrophysical Journal*, **184 p.271**.

[19] MARASCHI L. - TRAVERSINI R. - TREVES A. 1983. *Montly Notices of R.a.S.*, **204 p.1179**.

[20] PETTERSON J.A. 1983. In *Accretion–Driven Stellar X–ray Sources*, LEWIN W.H.G. - VAN DEN HEUVEL E.P.J. Eds., Cambridge Un. Press.

[21] PETTERSON J.A. 1977. *Astrophysical Journal*, **218 p.783**.

[22] RAPPAPORT S. - JOSS P.C. 1977. *Nature*, **266 p.683**.

[23] SHAKURA N.I. - SUNYAEV R.A. 1973. *Astronomy & Astrophysics*, **24 p.337**.

[24] SHAPIRO S.L - LIGTHMAN A.P. 1976. *Astrophysical Journal*, **204 p.555**.

[25] STELLA L. - WHITE N.E. - ROSNER R. 1986. *Astrophysical Journal*, **308 p.669**.

[26] WANG Y.N. 1981. *Astronomy & Astrophysics*, **102 p.36**.

[27] WANG Y.M. - ROBERTSON J.A. 1984. *Max–Planck Preprint*, **146**.

[28] WANG Y.N. - WELTER G.L. 1980. *Astronomy & Astrophysics*, **113 p.113**.

[29] WHITE N.E. - SWANK J.H. 1984. *Astrophysical Journal*, **287 p.856**.

Chapter 5

RADIATION PROCESSES IN PRESENCE OF STRONG MAGNETIC FIELDS

The radiation we observe in XRBSs comes from a plasma plunged in a strong magnetic field. To interpret the observational data and build models it is necessary to solve the problem of radiative transport in strong magnetic fields [31,8,19].

We can divide the models in roughly two categories. In the first category the aim of the models is to understand the features of the accretion flux. For doing this it is necessary to introduce some simplifying assumption concerning the geometry of the so-called "accretion funnel".

The second class of models tries to treat the radiative processes in a more consistent manner, but ignoring the details of the accretion flux and specifying only the density and temperature profiles in the atmosphere.

Only recently [21] the problem has been attacked in its globality.

Now we will describe briefly how radiation interacts with a magnetic field.

5.1 Physical processes in a strongly magnetized plasma

An electron plasma, at the temperature T_e, and plunged in a strong magnetic field of value B emits cyclotron radiation of harmonic order n at a rate of [7]

$$Q_n = \frac{2e^2}{c}\omega_c^2 \left(\frac{3kT_e}{m_e c^2}\right)^n \frac{n+1}{(2n+1)!} \tag{5.1}$$

where e is the electron charge, c is the speed of light, k is the Boltzmann constant, m_e is the electron mass and $\omega_c \equiv eB/m_e c^2 = 11.6\, B_{12}$ keV$/\hbar$ is the cyclotron frequency ($B_{12} \equiv B/10^{12}\ G$). The levels n are said "Landau

levels" and the spectrum presents lines, which are called cyclotron lines. In a strong magnetic field we have that Q_n is greater that the free-free emission rate.

The most important consequence of the fact that the electrons are quantized in the transverse direction to B is that the electromagnetic waves which propagate in such a plasma have well-defined polarization normal modes (i.e. the medium is birifringent) [6].

Choosing two orthogonal linearly polarized basis states (in a coordinate system with the magnetic field in the z-direction and the wave vector in the x-z plane), the polarization vectors have the form [23,19]

$$\mathbf{e}_n = (e_+,\ e_-,\ e_x)_n \tag{5.2}$$

where $e_\pm = (e_x \pm \imath e_y)/2$, with e_x and e_y the polarization vectors in the x and y direction, respectively, and $n = 1$: for extraordinary wave, $n = 2$: for ordinary wave.

For a cold electron plasma[1], i.e. for $\omega \gg (m_e/m_p)\,\omega_c$, where ω is the photon frequency and m_p is the proton mass, these components has the form [19,6]

$$(e_\pm)_n = \frac{1}{\sqrt{2(1+K_n^2)}}\, e^{\mp\phi}\,(K_n \cos\theta \pm 1) \tag{5.3}$$

$$(e_x)_n = \frac{1}{1+K_n^2}\, K_n \sin\theta \tag{5.4}$$

where $\cos\theta = \mathbf{K}\cdot\mathbf{B}$ and ϕ is a cylindrical coordinate.

The ellipticity parameter $K_n(\omega,\theta)$ is the ratio between the axes of the polarization ellipse (see Fig. 5.1 [23])

$$K_n \equiv \left(\frac{E_x}{E_y}\right) = b_0[1+(-1)^n(1+b_0^{-2})^{1/2}] \tag{5.5}$$

which is determined by the parameter b_0, given by [24,23]

$$b_0 \approx u^{1/2}\frac{1}{1-v}\,\frac{\sin^2\theta}{\cos\theta} \tag{5.6}$$

with

$$u \equiv \left(\frac{\omega_c}{\omega}\right)^2 \qquad v \equiv \left(\frac{\omega_p}{\omega}\right)^2 \tag{5.7}$$

where ω_p is the plasma frequency, defined as [6]

$$\omega_p \equiv \left(\frac{4\,\pi\, n_e e^2}{m_e}\right)^2 = 3.7\cdot 10^{-4}\, n_{20}^{1/2}\ \ \text{keV} \tag{5.8}$$

where $n_{20} \equiv (n_e/10^{20}\ \text{cm}^{-3})$ is the electron number density.

On the y-z plane both modes describe orthogonal ellipses, the sign of K_n determining the sense of rotation.

[1] For an hot electron plasma see [11].

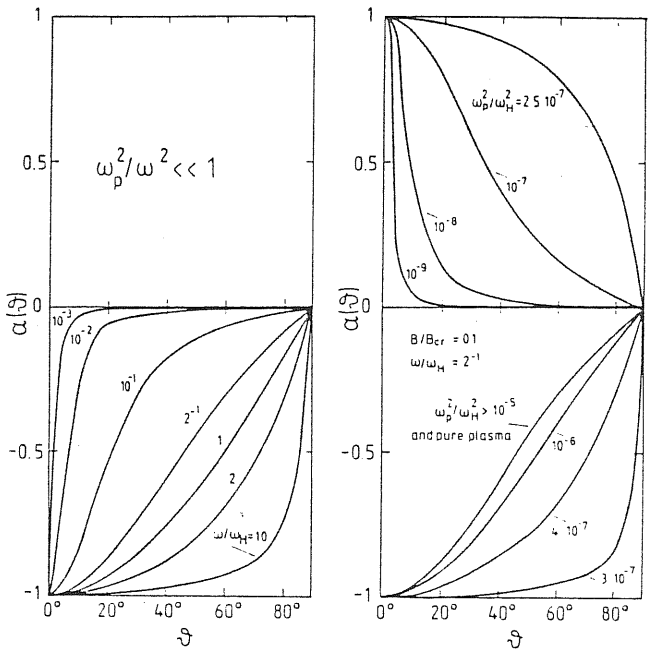

Figure 5.1: The ellipticity parameter $K_n(\theta)$, characterizing the propagation of normal modes of *(a)* the cold plasma at various frequencies, without taking into account vacuum polarization; *(b)* the same but with vacuum polarization, at $\omega = 0.5\,\omega_c$ and various values of the electron density, parametrized with ω_p/ω_c.

For $|b_0| \gg 1$ the polarization is almost linear, for $|b_0| \ll 1$ the polarization is almost circular.

An important role is played by the virtual electron-positron pairs (vacuum polarization), which occurs for magnetic fields not far below the critical value $B_c \equiv (m_e^2 c^3)/\hbar e = 1.414 \cdot 10^{13}$G [23,24,11].

These virtual photons, created by the annihilation of the e^+e^- pairs, dominate the polarization properties of the medium and modify the ellipticity parameter K_n. Therefore b_0 has to be substituted by [23,24]

$$b_0 \rightarrow b = b_0 \left[1 + \frac{3\xi(1-u)}{uv}\right] \tag{5.9}$$

with

$$\xi = \frac{1}{45\,\pi} \left(\frac{e^2}{\hbar\, c}\right) \left(\frac{B}{B_c}\right)^2 . \tag{5.10}$$

The correction factor, for $B \geq 10^{12}$G, $n_e \leq 10^{24}$ cm^{-3} and $\omega \sim 10^{19}$ Hz by far exceeds the contribution of the plasma electrons. This tends to make the modes more linearly polarized (see Fig. 5.1 [23]) because b increases for frequencies between ω_{v1} and ω_{v2}, where $\omega_{v1(2)}$ is the first (second) vacuum frequency, defined as [32,28]

$$\omega_{v1} \simeq 3\sqrt{n_{22}} \left(\frac{0.1\,B_c}{B}\right) \quad \text{keV} \tag{5.11}$$

$$\omega_{v2} \simeq \omega_c . \tag{5.12}$$

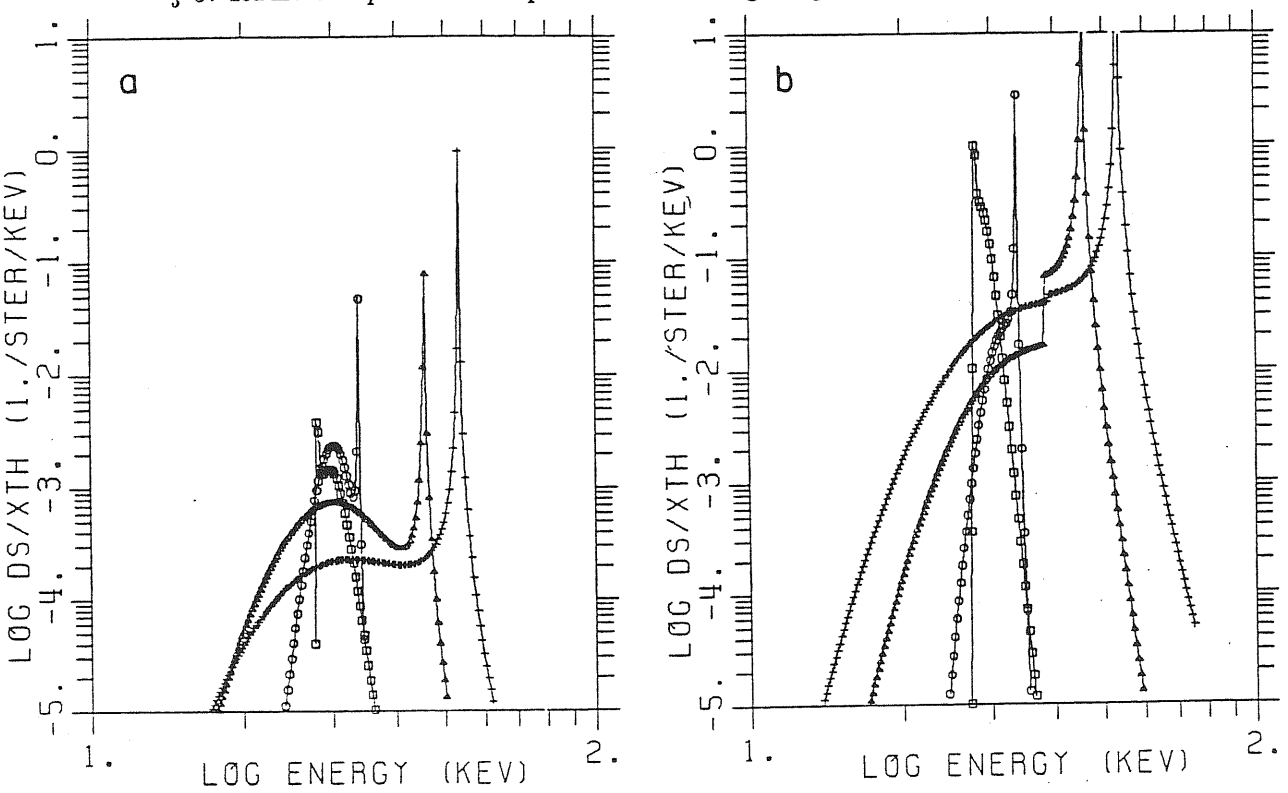

Figure 5.2: The differential scattering cross section from ordinary into extraordinary polarizations for photons of 30 keV energy in a magnetized plasma of temperature 10 keV, with cyclotron frequency at 38 keV (normalized to the Thomson value). Incoming photon angle is $\theta_i = 45°$, outgoing angles $\theta_o = 20°$, 70°, 120° and 120° from left to right. *(a)* Without polarization; *(b)* with vacuum polarization.

Above and below these frequencies the real plasma dominates, while between these two frequencies the plasma is vacuum-dominated.

The importance of the medium polarization resides in the fact that the radiative opacities depend on the normal modes, because the cross sections are given by [31]

$$d\sigma = r_0^2 \, |\langle e'|\Pi|e\rangle|^2 \tag{5.13}$$

where Π is an operator (scattering amplitude), r_0 is the classical electron radius and e' and e are the polarization vectors after and before the scattering. This implies that the dielectric tensor [6] greatly affects the radiative processes [24], because of the dependence on e.

The differential scattering cross section in a strong magnetic field is given by [26]

$$\frac{d^2\sigma}{d\omega' \, d\Omega'}(\omega'\theta' \leftarrow \omega\theta) = r_0^2 \, \frac{\omega'}{\omega} \int dp \, f(p) \, |\langle e'|\Pi|e\rangle|^2 \, \delta(\omega + \Delta\omega - \omega'). \tag{5.14}$$

Here the primes refers to quantities evaluated after the scattering and $f(p)$ is the electron momentum distribution, which is normally assumed one-dimensional Maxwellian for electrons in the lowest Landau level. Energy and

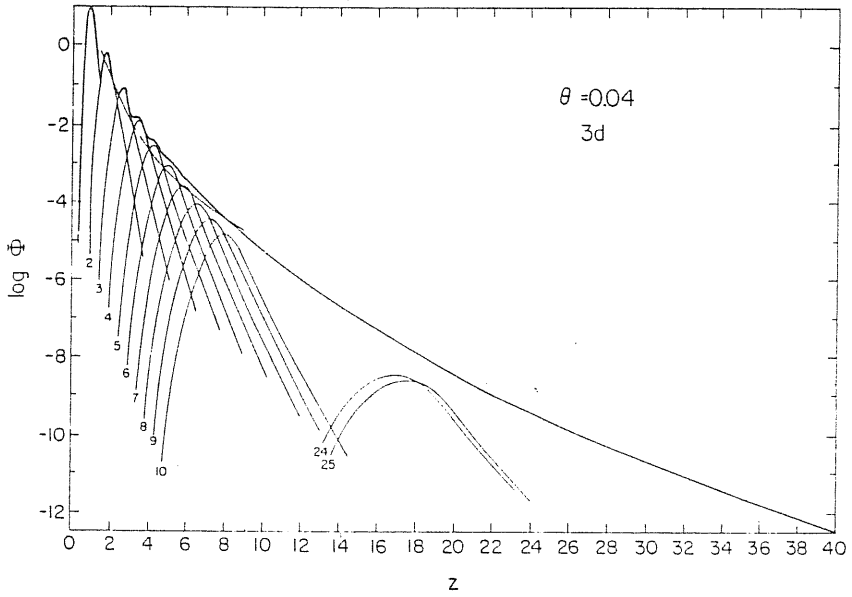

Figure 5.3: Dimensionless spectral flux Φ from a three-dimensional distribution of electrons with $\theta = 0.04$ (see text). The heavy curve is the total flux; the light curves are the individual harmonics. Note that the peak of the nth harmonic lies increasingly farther below nz as n becomes large.

(z-)momentum conservation laws give $\Delta\omega = p^2/2 - p'^2/2 = p\Delta k - \Delta k^2/2$, $\Delta k = k' - k = \omega' \cos\theta' - \omega \cos\theta$. Here k is the photon momentum along the magnetic field, δ is the Dirac delta function and $\hbar = c = m_e = 1$.

A plot of the scattering cross section is given in Fig. 5.2 [21], where we compare the values with and without vacuum polarization.

5.2 Formation of cyclotron lines

In an accretion column of a neutron star, cooling by cyclotron emission is so rapid that the electron temperature would become less than the ion temperature. The spontaneous transition of an electron from the Landau level with $n = 1$ to that with $n = 0$ is an extremely fast process; in fact the lifetime of the state $n = 1$ is $\tau = 2.4 \cdot 10^{-16} B_{12}^2$ sec [15], which is much less than the collisional excitation time at $T_e = 10^4 \rho^{2/3}$ °K.

Thus in most practical cases the plasma is optically thick for low harmonics of cyclotron lines and so cooling occurs at a lower rate for the emission of higher harmonics: the plasma is an hot plasma [6]. It is therefore necessary to consider, for the radiation in a strong magnetic field, radiative transfer and higher harmonics.

As we have seen, only for energies greater than some E^* the emitted cyclotron flux is optically thin (this may occur for $n \sim 50$). Below E^* the source is heavily self-absorbed and the emitted flux is limited by the Rayleigh-Jeans tail of a blackbody spectrum having a temperature equal to the electron temperature T_e [16].

Therefore neither the optically thin cyclotron spectrum nor the blackbody spectrum give an adequate representation of the emitted spectrum,

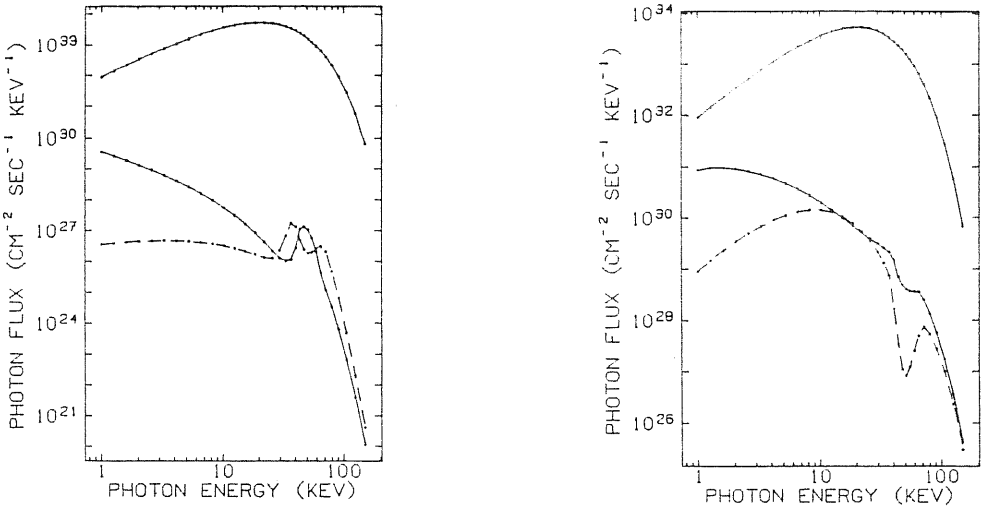

Figure 5.4: *(a)* The photon flux from a slab of hot, strongly magnetized plasma of density 10^{-2} g/cm^3, temperature 10 keV and cyclotron frequency of 50 keV. The slab has a thickness of 25 cm, corresponding to a Thomson depth $\tau_T \sim 0.1$. The uppermost curve represents the Wien spectrum. *Solid line*: ordinary photons; *dashed line*: extraordinary photons. *(b)* Same as *(a)* for $\tau_T \sim 10$.

and therefore of the cyclotron cooling rate [16].

In Fig. 5.3 [16,7] the dimensionless flux $\Phi(z,\theta)$, relative to a Rayleigh-Jeans spectrum, at $T_e = 20$ keV, is shown. It is only function of $\theta \equiv kT_e/m_ec^2$ and $z \equiv \omega/\omega_c$. The heavy curve shows the total spectral flux, while the light curves show the contributions of individual harmonics. From the figure we can see three important features of the cyclotron emissivity [16]:

1. Most of the emission occurs above the fundamental, if the temperature is moderate or high (and this is our case);

2. The emissivity falls steeply with frequency;

3. Thermal broadening of the individual harmonics produces a smooth continuum at higher frequencies.

Therefore we have that, since the optical depth is greater at the center of the line, the line profile is broadened in such a way that the emissivity in the center of the line is bounded by the blackbody values and that the wings show a profile in the optically thin case. Because of the increase of the optical depth when we observe at lower energies, we have a Rayleigh-Jeans spectrum at lower energies, also if the cyclotron emission rate is high.

Because of their large scattering cross section [26], extraordinary photons are trapped in the cyclotron line. They might escape after that few incoherent scatterings have taken them into the wings of the line. This leads to the self-reversed emission line of extraordinary photons which is shown in Fig. 5.4a [26].

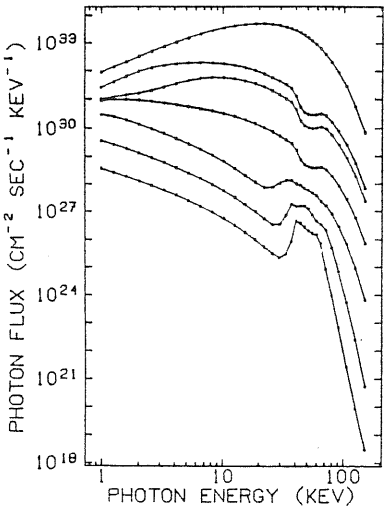

Figure 5.5: Comptonized spectra for a uniform plasma slab of density 10^{-2} g/cm^3, temperature of 10 keV and $\hbar\omega_c = 50$ keV. This curve represents the spectra for the electron scattering optical depths 10^{-2} and 10^3 and the Wien spectrum.

The asymmetry of the line is due to the multiplication by the Wien spectrum [26], which drops steeply, or, in other words, to the quantum recoil [33]: when the cyclotron energy is higher than the electron plasma temperature, then the photon energy decreases with increasing optical depth because of scattering, thus the low part of the line must be stronger.

Another way the cyclotron photons have to escape is scattering into the ordinary mode. Ordinary photons have a larger free mean path [26] and therefore can easily escape. Although the cross section from the extraordinary to the ordinary mode is quite small (see Fig. 5.4a [26]), the large amount of trapped extraordinary photons leads to a significant flux of ordinary photons in the cyclotron line. In the case shown in Fig. 5.4a, the flux of the ordinary photons is so strong that completely fills the self-reversal dip of the extraordinary photons.

Increasing the optical depth, the continuum flux rises more rapidly than the line flux, until only an absorption line is left (see Fig. 5.4b [26]). The majority of photons which escape in the energy range 30–80 keV are of the ordinary polarization.

The variation of the spectrum with the optical depth is shown in Fig. 5.5 [25,26].

In computing the spectra in Fig. 5.5 radiative transfer was taken into account [26]. In fact the propagation of photons depends on the mean free path per scattering, Λ_i, and on the mean free path by absorption, L_i, where $i = 1, 2$ is for the extraordinary and the ordinary wave, respectively.

The mean path that the photon travels before being absorbed is $z_i \simeq (\Lambda_i L_i)^{1/2}$ [6]. Λ_i is related to the immaginary part of the refraction index n_i [10]

$$\Im(n_i) = \frac{C}{2\omega\Lambda_i} \tag{5.15}$$

which depends on the angular frequency ω of the photon and on the wave vector $\vec{\mathbf{k}} = \hat{\mathbf{k}}k$. The intensities of the two components, in the case of free propagation, are [9]:

$$I_i = \frac{1}{2\pi z_i}\left[\left(\int(\vec{\mathbf{n}}\cdot\vec{\mathbf{k}}')\,\Lambda_i(\omega,\vec{\mathbf{k}}')\,d\Omega_{\vec{\mathbf{k}}'}\right) + (\vec{\mathbf{n}}\cdot\hat{\mathbf{k}})\,\Lambda_i(\omega,\vec{\mathbf{k}})\right] \tag{5.16}$$

where $\vec{\mathbf{n}}$ is the unit vector in the direction of the magnetic field. The sum of the two component gives the intensity without considering the polarization, the difference gives the polarization index.

For $\omega \gg \omega_c$ the effect of the magnetic field is negligible so Λ_i does not depend on the direction and therefore all the dependence on the direction is in $(\vec{\mathbf{n}}\cdot\vec{\mathbf{k}})$, which produce smooth maxima while the star rotates. For $\omega < \omega_c$, Λ_i depends in a complex manner on the directions of $\vec{\mathbf{n}}$ and $\vec{\mathbf{k}}$ with respect to the spin axis.

5.3 Formation of the continuum spectrum

As we will see, most of the X-ray pulsar spectra follow an almost homogeneous pattern [34]: they are almost flat (in intensity) in the energy range 2–20 keV and show a sharp cut-off toward higher frequencies (and so higher energies). Unfortunately, this pattern is not reproduced by the most part of the theoretical models.

In fact, the fundamental problem associated to the radiative transfer in accretion columns in X–ray pulsars regards the presence of a very strong magnetic field: the assumption of local thermodynamical equilibrium cannot be valid [2] since, because of the very rapid spontaneous decay rate of the excited Landau levels, their population is not controlled by collisions in the plasma, but is directly related to the radiation field itself.

This problem is usually solved by omitting the source term corresponding to cyclotron emission, and arguing that this process should be included only as a part of a resonant scattering [33].

For electrons in the ground state the (Thomson) scattering cross section formally has a divergence at the cyclotron frequency $\omega = \omega_c$, and this resonance is treated by replacing the resonant denominator $\omega - \omega_c$ by $\omega - \omega_c - \imath(\Gamma/2)$, where Γ is the decay rate of the first excited state due to cyclotron emission [31]. There is also a resonance in the cross section for bremsstrahlung, and this has been treated in the same way [14].

This implies that the source of photons is the bremsstrahlung process, and all the treatment of radiative transport in strong magnetic field have been used these two ingredients: Compton scattering plus bremsstrahlung [20,21,22,25].

But since the bremsstrahlung is a process quadratic in the particle density [30], it is not an adequate source of photons in relatively thin plasmas (i.e. $n_e \leq 10^{22}$ cm^{-3}). Consequently, the photon transport is dominated by scattering, and the energy flux lies well below that corresponding to the blackbody spectrum at all the frequencies of interest [5].

This is why the possibility that higher order processes, linear in the density, may compete with bremsstrahlung as a source of photons was investigated, although they have a much smaller cross sections than does ordinary Compton scattering [4].

While for unmagnetized plasmas this does not occur [17], for strongly magnetized plasmas the scattering can be resonant [12] and it can be expected to be the dominant source of photons in the continuum of X–ray pulsars [18,13].

This model [12] for continuum spectrum formation[2] is able to fit the experimental data but contains a bug: it is valid only for low frequencies and so it does not explain the observed cut-off at high frequencies.

Now we start to analyze the model into details: we can expect that Compton scattering influences the radiation spectrum of an X-ray pulsar because of the observed range of temperatures on these objects [29].

In general Comptonization tends to lead the photon spectrum toward a Bose-Einstein distribution [27], which is the equilibrium distribution of bosons when the particle number is conserved. As the photon density is such that we can neglect the stimulated processes, the photons will have a Bose-Einstein distribution with chemical potential, rather than a Planck distribution since photons cannot be created or destroyed by scattering [27]. Whether or not this distribution is achieved depends on the Comptonization parameter y, equal to the number of scatters suffered before escape multiplied by the average fractional energy change per scattering[3].

The first term in y is given by

$$\frac{\Delta\omega}{\omega} = \frac{4kT_e}{m_e c^2} \tag{5.19}$$

where T_e is the electron temperature. The average number of scatters is rough either the optical depth to Thomson scattering τ (for $\tau < 1$) or τ^2 (for $\tau > 1$).

In a strong magnetic field the scattering coefficients are modified, giving a reduction of the parameter y [1,26,21].

---

[2] For the mathematical formalism see [3,18].

[3] We will obtain the value of y in the non-relativistic case, as it is our case, and we will assume thermal distribution of the electrons.

To evaluate the average number of scatters we consider that the net displacement of the photon after N free paths is

$$\mathbf{R} = \mathbf{r}_1 + \mathbf{r}_2 + \cdots + \mathbf{r}_N \tag{5.17}$$

To find a rough estimate of the distance $|\mathbf{R}|$ crossed by a photon we square Eq. 5.17 and then average (averaging directly Eq. 5.17 we will obtain zero !). All the terms as $< \mathbf{r}_i \cdot \mathbf{r}_j >$, for isotropic scattering, are zero so

$$|\mathbf{R}^2| \equiv l_\star^2 = Nl^2 \tag{5.18}$$

where l is the free path of the photon. So we have

$$l_\star = \sqrt{N} l$$

which is the root mean square *net* displacement of the photon, which increases with $\sqrt{N}$.

If we introduce the spatial transport (i.e. convective motions), the number of scattering which are suffered by the electrons before escaping may be reduced, if the photon lies in a thin layer close to the plasma boundary, with a upper limit for N of $\tau^2(\sigma_{res}/\sigma_T)$, which is relevant only for $\tau < (\sigma_T/\sigma_{res})$, where σ_{res} and σ_T are the average resonant scattering cross-section and the Thomson cross-section, respectively, and σ_{res} has the form [33]

$$\sigma_{res} = \frac{\pi}{2}\frac{\sigma_T}{\alpha}\frac{m_e c^2}{\hbar\omega_c}\left(\frac{m_e c^2}{2kT}\right)^{1/2} \tag{5.20}$$

where α is the fine-structure constant.

Questioned about *when* photons may suffer Compton scattering remains to understand *how* it happens.

The trick consists in the fact that a *double* Compton scattering occurs [12], which can be seen as a sequence of two events:

1. A resonant process which produce soft photons is the absorption of a photon of frequency close to the cyclotron frequency ω_c, coupled with the transition of the electron from its fundamental state to the first excited Landau level, followed by the decay of this state by emission

---

For region of great optical depth the number of scatters required for the photon escape completely is obtained roughly putting $l_\star = L$, where L is the medium length scale. Thus we can write, by means of Eq. 5.18, that $N \approx L^2/l^2$. But, because of $L/l \sim \tau_{es}$, the optical depth of the medium for electron scattering, we have that

$$N \approx \tau_{es}^2 \quad (\tau \gg 1)$$

For regions of lower optical depth the average number of scatters becomes

$$N \sim 1 - e^{-\tau} \approx \tau_{es} \quad (\tau \ll 1)$$

The second term in the definition of y, i.e. the average fractional energy change per scattering, is obtained starting from

$$\frac{\Delta E}{E} = -\frac{E}{m_e c^2} + \frac{\alpha k T_e}{m_e c^2}$$

where E is the photon energy, α a parameter to determine and the equation was obtained averaging over the angles the Compton scattering equation.

Using the expression of the thermal distribution for the electrons we obtain

$$< E >= \frac{\int E(dN/dE)\,dE}{\int (dN/dE)\,dE} = 3kT$$

$$< E^2 >= 12(kT)^2$$

Because of $< \Delta E >= 0$ we obtain

$$\frac{\alpha kT}{m_e c^2} < E > - \frac{< E^2 >}{m_e c^2} =< \Delta E >= 0$$

$$\frac{3kT}{m_e c^2}(\alpha - 4)kT = 0$$

So we have $\alpha = 4$ and

$$\frac{\Delta E}{E} = \frac{4kT - E}{m_e c^2}.$$

of *two* photons: a photon of frequency ω and a photon of frequency $\omega - \omega_c$.

This process is important for the production of all photons of frequency less than ω_c.

2. The process consisting in an anelastic scattering of an incoming photon of frequency $\omega_c + \omega$ to an outgoing photon of frequency ω, followed by the transition of the electron from the fundamental state to the first excited state. This is then followed by the radiative decay of the excited state, with the emission of a photon of frequency ω_c.

The kinetic equation which governs the production of soft photons is very much simplified if we assume that the photon occupation number with frequency range from $\omega_c - \omega$ to $\omega_c + \omega$ is given by a Bose-Einstein distribution.

As discussed before, this happens when the plasma thickness is greater than τ_{res}, the optical depth to Compton scattering, defined as

$$\tau_{res} \approx \frac{\sigma_T}{\sigma_{res}} \sqrt{\frac{\omega_c}{\Gamma}} \approx 4 \cdot 10^{-4} B_{12}^{1/2} \, T_{keV}^{1/2} \tag{5.21}$$

with Γ the cyclotron line width and ω such that $\omega_c + \omega$ and $\omega_c - \omega$ lies in the cyclotron line.

Just this last constrain prevents us from applying this flat optically thin spectrum to frequencies greater than 20 keV, because of Eq. 5.21 is not more valid.

Bibliography

[1] BASKO M.M. - SUNYAEV R.A. 1975. *Astronomy & Astrophysics*, **42 p.311**.

[2] BONAZZOLA S. - HEYVAERTS J. - PUGET J.L. 1979. *Astronomy & Astrophysics*, **78 p.53**.

[3] BURNARD D.J. - KLEIN R.I. - ARONS J. 1988. *Astrophysical Journal*, **324 p.1001**.

[4] BUSSARD R.W. - MESZAROS P. - ALEXANDER S. 1985. *Astrophysical Journal*, **297 p.L21**.

[5] FELTEN J.E. - REES M. 1972. *Astronomy & Astrophysics*, **17 p.226**.

[6] GINZBURG V.L. 1970. *The Propagation of Electromagnetic Waves in Plasmas*. Pergamon Press.

[7] HAYAKAWA S. 1985. *Physics Reports*, **121 p.318**.

[8] KAMINKER A.D. - PAVLOV G.G. - SHIBANOV YU.A. 1982. *Astrophysics and Space Science*, **86 p.249**.

[9] KANNO S. 1980. *Pubbl. Astron. Soc. Japan*, 32 p.105.

[10] KANNO S. - HAMADA T. 1975. *Pubbl. Astron. Soc. Japan*, **27 p.545.**

[11] KIRK J.G. 1980. *Plasma Phys.*, **22 p.639.**

[12] KIRK J.G. 1986. *Astronomy & Astrophysics*, **158 p.305.**

[13] KIRK J.G. - MELROSE D.B. 1986. *Astronomy & Astrophysics*, **156 p.277.**

[14] KIRK J.G. - MESZAROS P. 1980. *Astrophysical Journal*, **241 p.1153.**

[15] KIRK J.G. - TRUMPER J.E. 1983. In *Accretion-Driven Stellar X-ray Sources*, LEWIN W.H.G. - VAN DEN HEUVEL E.P.J. Eds., Cambridge Un. Press.

[16] LAMB D.Q. - MASTER A.R. 1979. *Astrophysical Journal*, **234 p.L117.**

[17] LIGHTMAN A.P. 1981. *Astrophysical Journal*, **244 p.392.**

[18] MELROSE D.B. - KIRK J.G. 1986. *Astronomy & Astrophysics*, **156 p.268.**

[19] MESZAROS P. 1984. *Space Science Review*, **38 p.325.**

[20] MESZAROS P. - HARDING A.K. - KIRK J.G. - GALLOWAY D.J. 1983. *Astrophysical Journal*, **266 p.L33.**

[21] MESZAROS P. - NAGEL W. 1985. *Astrophysical Journal*, **298 p.147.**

[22] MESZAROS P. - NAGEL W. 1985. *Astrophysical Journal*, **299 p.138.**

[23] MESZAROS P. - VENTURA J. 1979. *Physical Review*, **D19 p.3565.**

[24] MESZAROS P. - VENTURA J. 1978. *Physical Review Letters*, **41 p.1544.**

[25] NAGEL W. 1981. *Astrophysical Journal*, **251 p.278.**

[26] NAGEL W. 1981. *Astrophysical Journal*, **251 p.288.**

[27] RYBICKI G.B. - LIGHTMAN A.P. 1975. *Radiative Processes in Astrophysics.* John Wiley & Sons.

[28] SOFFEL M. *et al.* 1983. *Astronomy & Astrophysics*, **126 p.251.**

[29] SUNYAEV R.A. - TITARCHUK L.G. 1980. *Astronomy & Astrophysics*, **86 p.121.**

[30] TUCKER W.H. 1977. *Radiation Processes in Astrophysics.* The MIT Press.

[31] VENTURA J. 1979. *Physical Review*, **D19 p.1684.**

[32] VENTURA J. - NAGEL W. - MESZAROS P. 1979. *Astrophysical Journal*, **233 p.L125**.

[33] WASSERMAN I. - SALPETER E. 1980. *Astrophysical Journal*, **241 p.1107**.

[34] WHITE N.E. - SWANK J.H. - HOLT S.S. 1983. *Astrophysical Journal*, **270 p.711**.

Chapter 6

OBSERVATIONAL DATA ON X–RAY BINARY PULSARS

6.1 X–ray binary system parameters

To determine the orbital parameters of X-ray pulsars we use the Doppler delays of X-ray pulse arrival times [35], which is the analogous to the classical optical measurements of Doppler shifts in spectral lines.

In case of a perfect clock which emits pulses at uniform intervals and which is moving at constant velocity, a plot of the pulse arrival times as a function of pulse number will reveal a simple, linear relation (see Fig. 6.1 [31]). If the intrinsic clock rate increases in time (as is the case of a spinning up neutron star), then the same type of plot gives a curved line.

If the clock is in a Keplerian orbit, then the periodic Doppler delays in arrival times, due to the flight-time of the pulses through the orbit, will be superposed.

If the curvature due to the orbital motion is much greater than that due to the variation in the intrinsic pulse period, the orbit can be determined by subtracting a polynomial, function of time, from the arrival time plot [35].

The polynomial representative of the *emission* time of the pulse N, which takes into account the intrinsic variation of the pulse period, i.e. t'_N, will have the form [35]

$$t'_N = t_0 + Nt_p + \frac{1}{2}N^2 P_p \dot{P}_p + \frac{1}{6}N^3 P_p^2 \ddot{P}_p + \cdots \tag{6.1}$$

where P_p, $\dot{P}_p$, $\ddot{P}_p$ are the pulse period and its first and second derivative at time t_0, respectively. The corresponding *arrival* times t_N, obtained introducing the orbital time delay, are

$$t_N = t'_N + f_{orb}(t'_N) \tag{6.2}$$

where $f_{orb}(t'_N)$ contains the orbital elements as parameters (we suppose to

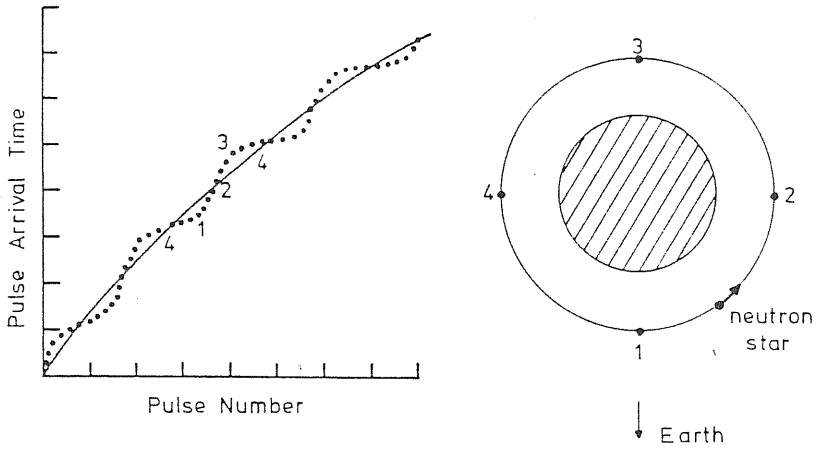

Figure 6.1: Schematic sketch of the Doppler delays in X-ray pulse arrival times. The numbered points on the Doppler delay curve *(left)* correspond to the indicated points on the orbit.

have already subtracted the effects due to the orbital motion of the Earth—the so-called Earth-to-barycenter reduction [10]).

It is sufficient to stop at the first, or at most at the second order in the interpolating polynomial. The function $f_{orb}(t'_N)$ is written as

$$f_{orb}(t'_N) = \frac{a_x \sin i}{c} F(\theta,\, e,\, \omega) \tag{6.3}$$

where $a_x \sin i$ is the projected semimajor axis of the orbit of the compact object, i is the inclination angle of the orbit, $F(\theta,\, e,\, \omega)$ is a function representing an orbit of eccentricity e, periastron longitude ω and mean anomaly θ, defined as $\theta = 2\pi(t_N - \tau)/P_{orb}$, where τ is time of orbital phase zero.[1]

The arrival times are then compared to an ephemeris based on an initial estimate of t_0, P_p, P_{orb}, $(a_x \sin i)/c \equiv x$ and τ to obtain residual time differences δt_N. These residuals contain small terms due to differential corrections to the initial parameter estimates.

If it is possible to stop to the first order, the expression for each residual is simple enough [10]:

$$\begin{aligned}\delta t_n \;=\; & \delta t_0 + N\,\delta P_p + \frac{1}{2} N^2 P_p \dot{P}_p + \delta x \,\sin l_N - \\ & - \frac{2\pi\, x}{P_{orb}} \delta\tau \,\cos\theta_N + \frac{2\pi\, x}{P_{orb}^2} \delta P_{orb}(t'_N - \tau) \,\cos\theta_N - \\ & - \frac{3}{2}\, x\, e \,\sin\omega + \frac{1}{2}\, x\, e \,\cos\omega \,\sin(2\theta_N) -\end{aligned}$$

[1] Normally assumed as the periastron passage, corresponding to the maximum distance of the X-ray star from the Earth.

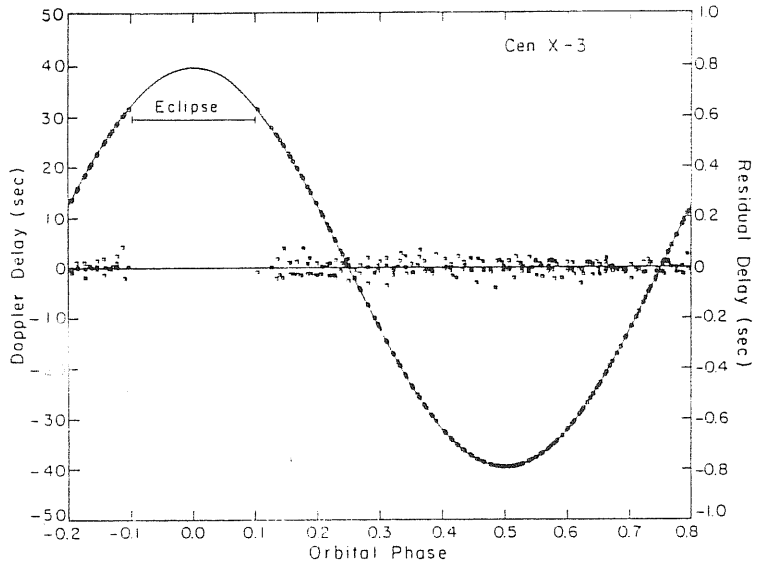

Figure 6.2: Doppler delay data for Cen X-3 from SAS 3 observations in 1978 December–1979 January. Solid curve represents the best-fit circular orbit[2] while points clustered around zero Doppler delay, shown as small squares, are the residuals of the data points from the best-fit orbit. Note that the scale for the residuals (right-hand ordinate) is 50 times less than that of the Doppler delays.

$$-\frac{1}{2}\,x\,e\,\sin\omega\,\cos(2\theta_N) \tag{6.4}$$

where

$$\theta_N = \frac{2\pi}{P_{orb}}(t'_N - \tau) + \frac{\pi}{2}. \tag{6.5}$$

Fig. 6.2 shows an orbit determination based on Doppler delays of X-ray pulses [16]. The projected semi-major axis can be read directly from the figure, because it is given by the wave amplitude. Once this is known, it is possible to obtain the mass function of the system:

$$f(M) = \frac{4\pi^2(a_x \sin i)^3}{GP_{orb}^2} = \frac{M_c \sin^3 i}{(1+q)^2} \tag{6.6}$$

where, again, M_c is the mass of the companion and $q \equiv M_x/M_c$ is the mass ratio which, in turn, may be computed by the ratio between the velocities of the two components the system (obtained by optical measurement)

$$q = \frac{a_c \sin i}{a_x \sin i} = \frac{K_c P_{orb}\sqrt{1-e^2}}{2\pi\, a_x \sin i} \tag{6.7}$$

[2] In case of an eccentric orbit, the curve is no more a sinusoidal but becomes a deformed curve.

where $a_c \sin i$ is the projected semimajor axis of the orbit of the companion and K_c is the semi-amplitude of the optical Doppler velocity curve.

The last ingredient to evaluate the orbital parameters of X-ray pulsars is the inclination angle i. This can be computed approximately by means of a simple model.

We approximate the companion star with a sphere of radius R, the volume of which is equal to the volume of the star, obtaining

$$R_{co} \approx a\,[\cos^2 i + \sin^2 i \,\sin^2 \theta_e]^{1/2} \tag{6.8}$$

where $a \equiv a_c + a_x$ is the separation between the centers of mass of the two components and θ_e is the eclipse semi-angle, defined as π times the fraction of the orbital period which the star spends in eclipse (note that in absence of eclipse $R_{co} \approx a \cos i$).

From the mass ratio and from the rotation rate of the companion it is possible to compute the size and slope of the Roche-lobe, the radius R_{Rl} of which is given by[3] [29,3]

$$R_{Rl} \approx a\,[A + B \log q + C \log^2 q] \tag{6.9}$$

where A, B and C are constant which depends on the ratio λ between the rotational frequency of the companion and the orbital frequency, and the value of which is given by [31]

$$\begin{aligned} A &\approx +0.398 - 0.026\,\lambda^2 + 0.004\,\lambda^3 \\ B &\approx -0.264 + 0.052\,\lambda^2 - 0.015\,\lambda^3 \\ C &\approx -0.023 - 0.005\,\lambda^2. \end{aligned} \tag{6.10}$$

These expressions give R_{Rl} with an accuracy of 2% in the range $0 \leq \lambda \leq 2$ and $0 \leq q \leq 1$.

Since we have $R_{co} = \beta R_{Rl}$ with $\beta < 1$, we can combine Eq. 6.8 and Eq. 6.9 to obtain [31]

$$\sin i \approx \frac{1}{\cos \theta_e} \sqrt{1 - \beta^2 \left(\frac{R_{Rl}}{a}\right)^2} \tag{6.11}$$

In Table 6.1 there is a summary of the binary parameters of the known X-ray binary pulsars, where T_e is the duration of the X–ray eclipse.

6.2 Pulse profiles

If we assume an isotropic emission pattern, the pulse profiles reveal the X-ray beam patter with respect to the rotation axis and the line of sight. For simplicity, we will assume that the beam pattern is symmetric with respect to the magnetic axis.

[3] We assume that *all* the volume of the Roche-lobe is contained in a sphere of radius R_{Rl}.

Name	P_{orb} (days)	$a_x \sin i$ (lt-s)	Masses ($M_\odot$)		T_e (days)
			M_x	M_c	
A0538-66	16.6	-	1.7	9.0	-
SMC X-1	3.89	53.4	1.02	16.2	0.6
Her X-1	1.7	13.1	1.3	2.18	0.24
4U 0115+63	24.3	140.1	-	>5	-
V0332+53	34.25	50	-	>0.1	-
Cen X-3	2.09	39.8	1.0	17	0.45
1E 2259+586	0.0266?	-	-	-	-
4U 1626-67	0.0289	<0.04	1.8	<0.5	-
2S 1553-54	30.6	170	-	>5	-
LMC X-4	1.41	30	1.6	17	0.23
2S 1417-62	>15	>25	-	-	-
OAO 1653-40	-	-	-	-	-
EXO 2030+375	47.8	-	-	>9	-
4U 1700-37	3.41	-	2	20	0.61-1.10
A0535+26	111	1000	1–2	10–20	-
GX 1+4	>50	>60	-	-	-
4U 1320-61[a]	-	-	-	-	-
GX 304-1	132.5	-	-	-	-
VELA X-1	8.96	113	1.85	23	1.8
4U 1145-61	186.5	>100	1	15	-
1E 1145.1-6141	10.75	>50	-	-	-
A1118-61	>5000	-	-	-	-
4U 1907+09	8.38	80	1.4	12	-
4U 1538-52	3.73	55.2	1.8	16	0.51
GX 301-2	41.5	367	-	>30	-
4U 0352+30	580?	-	2	20	-

Table 6.1: Orbital parameters of X–ray binary pulsars

[a]This source has been observed only during 1977. It is also known as A1239-59.

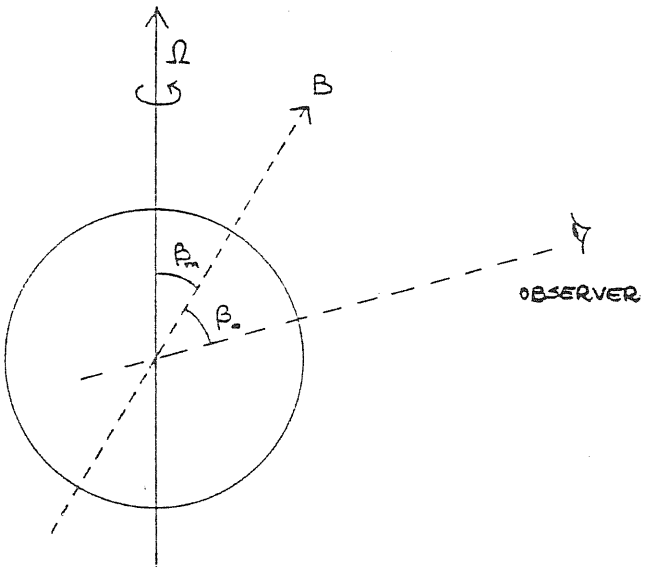

Figure 6.3: Definition of the aspect angles β_m and β_o.

Let β_m and β_o be the angles between the magnetic axis and the rotation axis, and between the line of sight and the rotation axis, respectively (see Fig. 6.3) [14]. According to $\beta_m + \beta_o$ being greater or less than $\pi/2$, we will see both or only one magnetic pole, therefore we will observe a double or a single peak in the impulse, respectively.

According to the fact that the beam has a maximum in the direction parallel to the magnetic field (the so called 'pencil beam') or in the direction perpendicular to the magnetic field (the so called 'fan beam') [41], at the same phase angle we find a maximum intensity or a minimum intensity, respectively. In case we observe two peaks in the pulse profile (i.e. $\beta_m + \beta_o > \pi/2$), the intensities of the two maxima/minima are equal for the fan/pencil beam.

In Fig. 6.4 [41] examples are given of pulse profiles for the assumed beam patterns [41]

$$F_p(\theta) = \begin{cases} \cos\theta & \text{for } \theta \leq \pi/2 \\ 0 & \text{for } \theta > \pi/2 \end{cases} \tag{6.12}$$

$$F_f(\theta) = \begin{cases} \sin\theta & \text{for } \theta \leq \pi/2 \\ 0 & \text{for } \theta > \pi/2 \end{cases} \tag{6.13}$$

where the suffixes p and f stand for the pencil and fan beam, respectively and θ is the polar angle. This, in principle, should permit to obtain the beam pattern from the observations.

In Fig. 6.5 [24] is shown the physical interpretation of the two different beam geometries. In (a) pillbox shape, arising when matter is decelerated by radiation or collisionless shock. This gives a fan pattern, radiation being

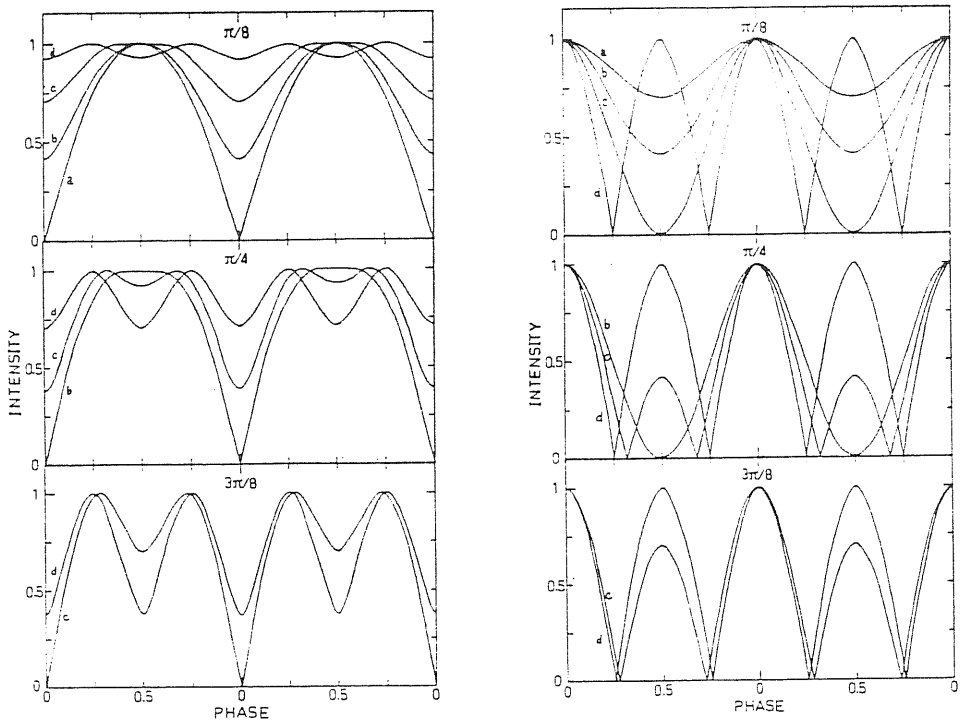

Figure 6.4: Pulse profiles calculated from a pencil beam *(left)* and a fan beam *(right)* with the beam patterns of Eqs. 6.12 and 6.13. The variations of the pulse profile are shown, for fixed α, as a function of the angle β: *(a)* means $\beta = \pi/8$, *(b)* $\beta = \pi/4$, *(c)* $\beta = 3\pi/8$ and *(d)* $\beta = \pi/2$.

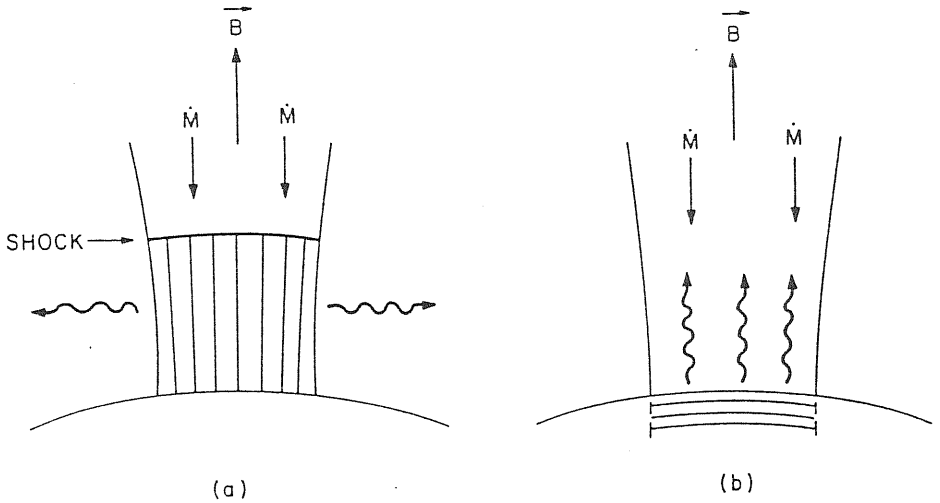

Figure 6.5: Possible longitudinal geometries of the emission region.

emitted *sideways*. In (b) plane parallel atmosphere, which does not stick out above the surface, arises if Coulomb and nuclear particle encounters produce deceleration. This produce a pencil beam, radiation escaping *upwards*.

But what we observe is that the pulse profiles are much more complex, are generally variable and energy dependent. Generally speaking, the variations in the pulse profiles seem stronger for wind-fed pulsars. In some occasions the pulsation even disappeared for a certain amount of time [25].

The appearance of the pulsation at higher energies is explained in terms of an accretion flux driven by the force lines of the magnetic field of the plasmapause to the magnetic polar caps for spherical accretion, in which the plasmapause radius increases with luminosity and becomes larger than the stellar radius for higher luminosities [14,17].

The dependence of the pulse profiles on energy is shown in Fig. 6.6 for 12 pulsars [42]. Generally, the profile is simpler at energies below 2 keV and above 10 keV than in the range 2–10 keV. This general feature is due to the fact that the modulation is relatively faint at higher energies, because of the radiative transfer and of circumstellar absorption, while at lower energies the absorption smears the fine structure of the profile. We therefore should say that at higher energies the profile is characterized mainly by the beam geometry; all the pulse profiles of SMC X-1, 4U 1538 – 52, Vela X-1 and GX 301 – 2 show a double peak but, while those of SMC X-1 has equal intensities, that of the other three show double dips of almost equal intensity. These profiles correspond to the two geometries described above, i.e. fan and pencil beam, respectively and, as the theory says, they correspond to different accretion rates (greater that of the fan beam) [41].

The asymmetric pulse profiles, characterized to have a shorter rise and a slower fall, observed for very luminous sources, are due to the asymmetric accretion columns which are deformed by rotation [41].

As the X-ray energy decreases, the pulse profiles change, because of the effects due both to the magnetic field and to the circumstellar absorption [18]. In the fan beam configuration we have that X-rays are emitted parallel to the magnetic axis, encounter the matter falling onto the magnetic polar caps and are so absorbed and scattered. Therefore the peak we see at higher energies is flattened and separated in two smaller peaks with a dip between.

If the X-ray energy is less than cyclotron energy, the Thomson scattering cross section for the X-rays which propagated along the direction of the magnetic field is reduced [14], because the motion of the electrons perpendicular to the magnetic field is suppressed. As a consequence, we have that we can observe radiation which comes from a deeper part of the accretion column, because the mean free path in this direction increases. Because the temperature inside the accretion column is greater than that at the surface, the intensity of the radiation in the direction of the magnetic field will be greater.

In the fan beam configuration, the direction for the high energy minimum intensity can be close to that of the column axis and therefore the low intensity in this direction increases. If this increase is superposed to the fan

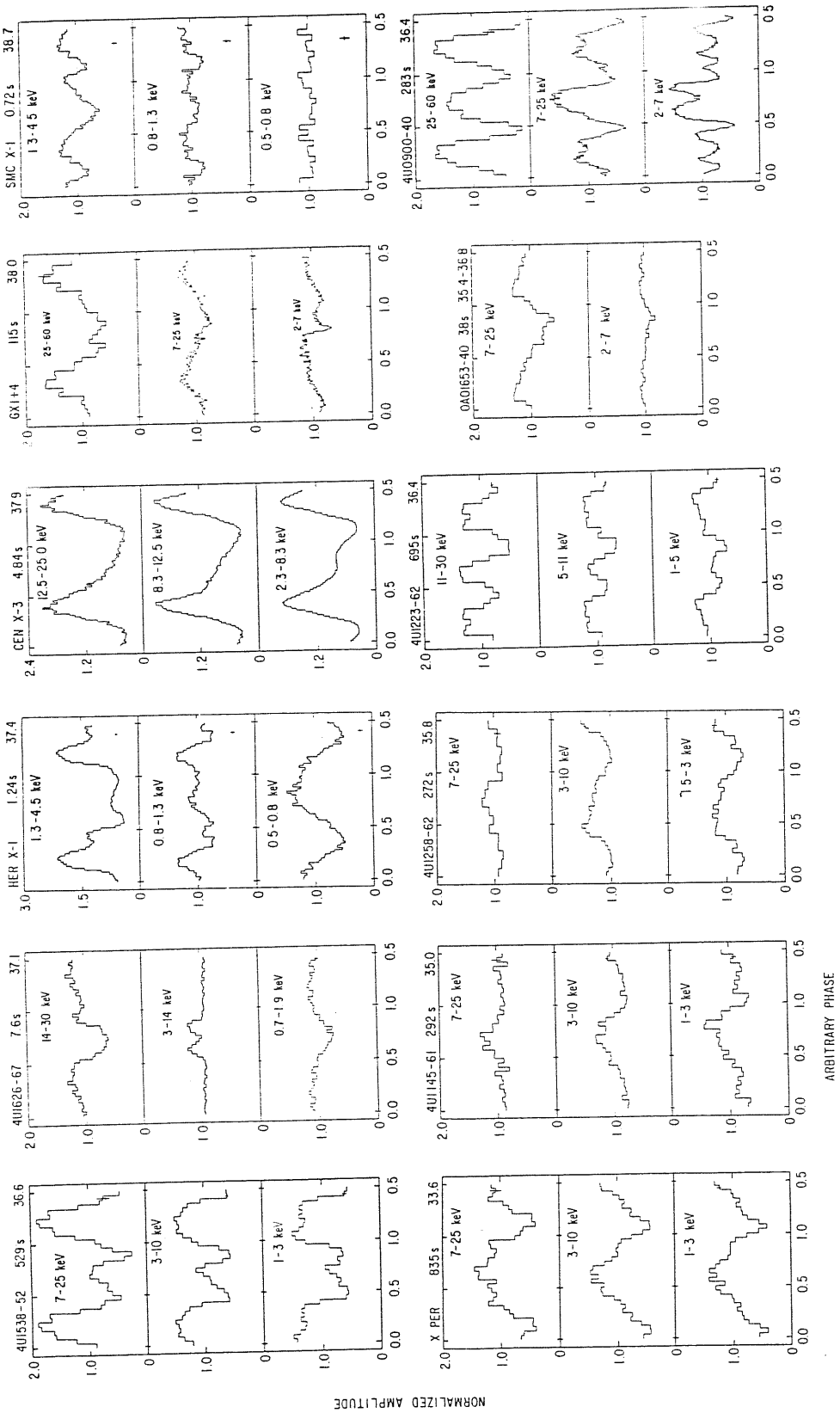

Figure 6.6: Average pulse profiles in different energy bands of 12 X-ray pulsars. The source name, pulse period and log of the X-ray luminosity, expressed in erg/sec, are indicated for each data set.

beam minimum, we observe a double peak, as we see in 4U 1626-67 [18].

6.3 Pulse periods

The pulse periods of X-ray binary pulsars are distributed over a wide range, unlikely of the pulse periods of single radio pulsars, which only range from 1^{ms} to $\sim 5^{s}$ (i.e. there are not the 'long-period' radio pulsars) [22]. Further, (almost) all radio pulsars show a spin-down [22], therefore they are born with pulse period much shorter and have been decelerated by emission of gravitational and/or electromagnetic waves. On the contrary, some X-ray pulsars show the phenomenon of spin-up [27,11], from which we may deduce that the actual period might be the result of a spin-up from many years.

In Table 6.2 we show the pulse periods of the known X-ray binary pulsars, together with their distance and X-ray luminosity. Nine pulsars have periods greater than 270^{s}, while the number of pulsars with periods in the range $10^{s} - 100^{s}$ is five, among which one pulsates only during the flaring state (4U 1700-37 [26]). Therefore the period distribution of the 26 pulsars seems to be uniform claimed from 69^{ms} to 835^{s}.

Although it seems to exist a tendency to a secular decrease of the period, the pulse period change rate is not constant and, further, varies in much complex manner. Some pulsars, as SMC X-1 [4] and GX 1+4 [12,32], show a constant decreasing of pulse period, while the majority of the others show erratic pulse period variations (for example, Vela X-1 show changes in the sign of $\dot{P}_p$ [27]).

In Fig. 6.7 long-term variations of the pulse period [15] are shown, from which it is possible to observe that there is a decrease (also if it is not constant) in the period for the disk-fed pulsars Her X-1, Cen X-3 and 4U 0352+30, while there are irregular variations for the wind-fed pulsars A0535+26, Vela X-1 and GX 301-2.

The variation rate of the pulse period depends on time length over which $\dot{P}_p$ is obtained. In fact, for Vela X-1 we have that the long term variations, computed over years of observations, are an order of magnitude less than the short term ones. This suggests that the variations on long time scales are small and possibly absent [11].

As we have seen in chapter 4, the pulse period variations are described in terms of accretion torque variations. From Eqs. 4.65 and 4.66 we have that

$$\frac{\dot{P}_p}{P_p} \sim (10^{-5} - 10^{-4})\, P_p L_{37} \quad \mathrm{yr}^{-1} \tag{6.14}$$

whose absolute value is in rough agreement with the observed values. But it remains to explain whether short-term variations and scattering of the observed values around the expected values can be explained in terms of variations in the parameters of these equations.

To date, the observations do not seem to favorite a strong dependence on luminosity, and the observed sign changes in $\dot{P}_p$ imply a substantial variation

Name	P_p (sec)	Distance (kpc)	$\mathcal{L}_x$ (10^{37} erg/sec) Max	Min
A0538-66	0.069	52	120	0.02
SMC X-1	0.7	65	58	0.5
Her X-1	1.24	4.5	2	0.02
4U 0115+63	3.61	5	3	$< 10^{-5}$
V0332+53	4.37	1.5-4	7.5	$< 10^{-4}$
Cen X-3	4.83	8	8	0.1
1E 2259+586	6.97	4.4	0.02	
4U 1626-67	7.68	< 6	0.75	
2S 1553-54	9.26	10	1	0.05
LMC X-4	13.50	55	150	60
2S 1417-62	17.6	1.4-6.6	0.1	0.04
OAO 1653-40	38.21	1.95	0.63	0.025
EXO 2030+375	41.83	4	6.4	<0.01
4U 1700-37	67.4	1.7	0.2	0.017
A0535+26	103.89	2.6	5	0.002
GX 1+4[a]	117.22	10	10	0.7
4U 1320-61[b]	191 ?			
GX 304-1	272.2	2.4	0.03	0.0012
VELA X-1	282.80	1.9	0.6	0.011
4U 1145-61	292	1.5	0.01	0.0028
1E 1145.1-6141	298	8.2	0.03	0.003
A1118-61	405	4	0.46	10^{-4}
4U 1907+09	437	2.4-4	1.7	0.07
4U 1538-52	529 5.5	0.4	0.04	
GX 301-2	698.3	1.8	1	0.08
4U 0352+30	835.98	3	0.002	0.0002

Table 6.2: Observational properties of X–ray binary pulsars.

[a] This value of the pulse period has been obtained from low enegy observations ($E < 20$ keV [33,12]); from high energy measurements [32,20] it seems to be twice this value.

[b] This source has been observed only during 1977. Is is also known as A1239-59.

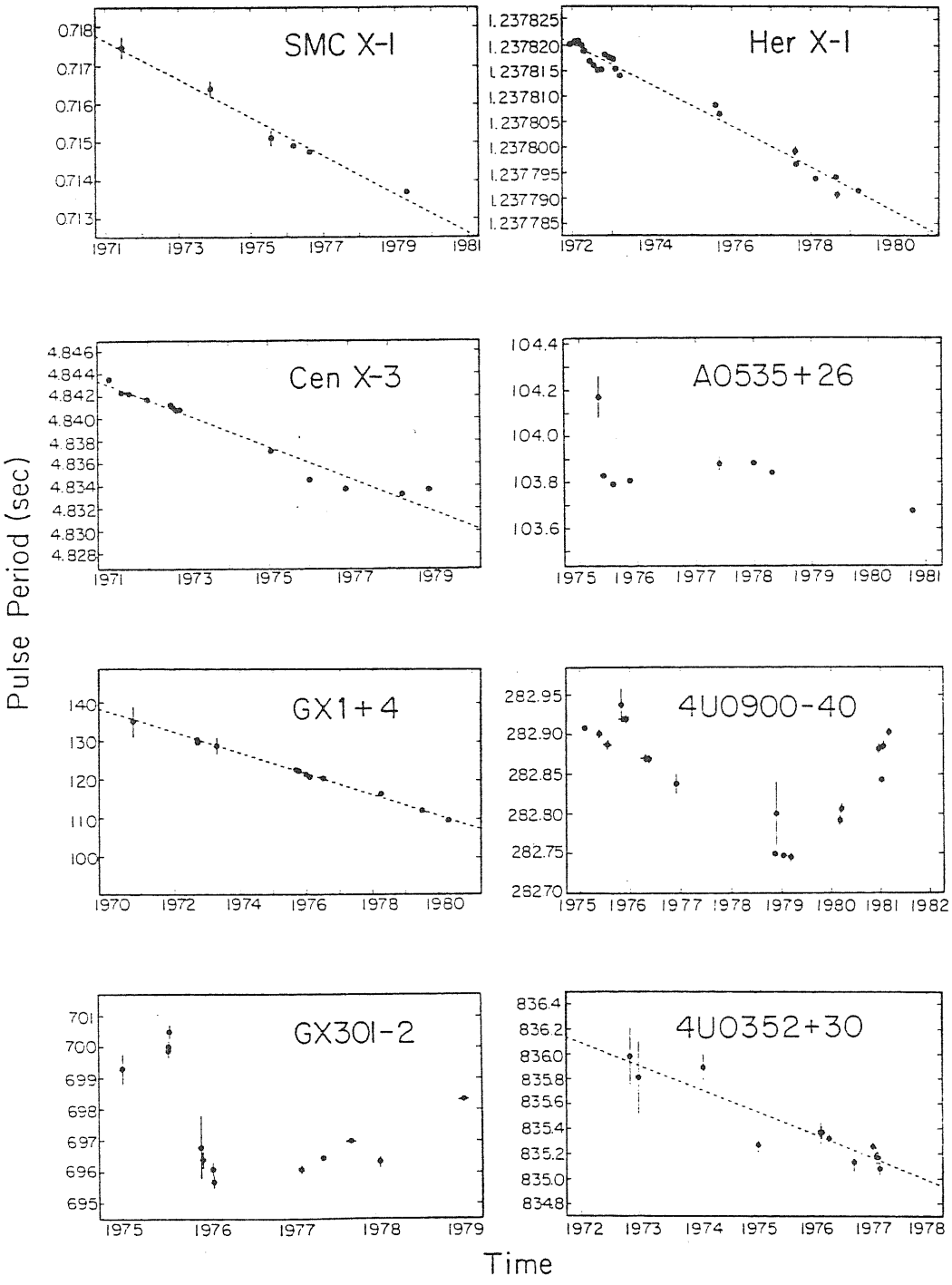

Figure 6.7: Pulse period histories for eight pulsars. The heavy dots are individual measurements of pulse periods. The dashed lines are linear fits to the data points.

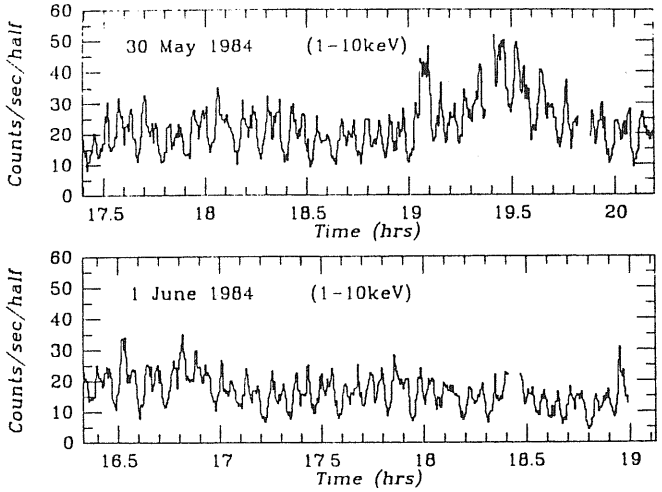

Figure 6.8: The 1.5-10 keV light curve of three observations of 4U 1907+09 obtained by EXOSAT. It is also present longer time scale variability.

in the parameter f of Eq. 4.66, which substantially depends on the angular momentum transfer mechanism.

In any case it is almost certain that the large observed period variations cannot be due to internal torques, which are considered the responsible of the radio pulsar glitches [1,2]. In the interior of a neutron star there is a coupling between interior superfluid and the outer crust (composed by a solid array of iron nuclei) through vortex lines pinned to large nuclei floating in the superfluid core. The force requested for pinning and unpinning the vortex lines is proportional to the difference between the crust and core angular velocities, and this difference is much greater than that observed in the fluctuations.

Therefore the neutron star behaves as a rigid rotator under the external torques which produce the fluctuations in the observed angular velocities [5].

6.3.1 Pulse periods: determination by means of the χ^2 method

Before to conclude about the neutron star pulse periods we will briefly discuss about the *statistical* method which permits to obtain the pulse period by the X-ray observations.

The more difficult subject to treat regards the errors in the measurements, because the method is a statistic one; this is not an adequate seat for this and we will skip about it.

The pulse period determination from X-ray observations may be summarized in the following points [23]:

1. The starting point is a run of count rate data vs. time (see Fig. 6.8 [8]). In this figure a periodicity is seen at naked eye (but in most cases this is not visible).

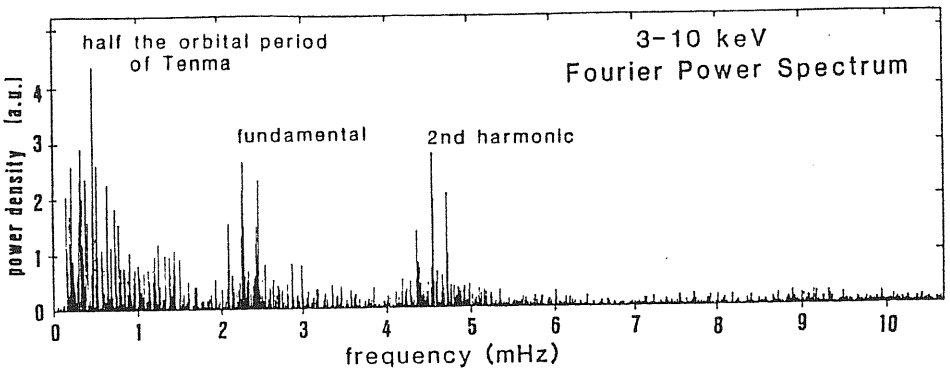

Figure 6.9: An example of the Fourier power spectrum corresponding to the 3-10 keV X-ray flux of the X–ray source 4U 1907+09 observed on August 30-31 by TEMNA. The total data span is $\sim 1.3 \cdot 10^5$ sec. The fundamental and the second harmonic of the $437^s.5$ pulsation are clearly seen. The sidebands are caused by the data sampling window.

By computing a Fourier transform on data set we obtain a first estimate of the pulse period [21]. It is important to remark the fact that it is very easy to confuse the true period with other spurious values, as shown in Fig. 6.9 [21], expecially in the low frequency range.

2. The data set is then folded modulo a series of trial periods around the period estimated from Fourier analysis, with step ΔP_p. For each trial period a χ^2 test is applied against the hypothesis of constant intensity (i.e. a stationary flux). The period which gives the maximum value for the χ^2 is then considered as the best value of the periodicity.

3. A pulse profile (*template*) is built, obtained by folding the data with the best period. The time origin T_0 of the data set is chosen arbitrarily.

4. Then a fit of the template based on the above pulse profile with the data of point 2. is made, leaving the amplitudes of the template to vary: the minimum value of χ^2 indicates the epoch of phase zero for which the best template agrees upon the data. This determines T_0.

5. Once obtained T_0 it is possible to determine the integer number of cycles between two epochs, assuming a constant period.

The same type of analysis is applicable for research of longer periods, for example the orbital period: of course, in this case, the run of data must extend for a longer time, because it must contain a sufficient number of periods. In Fig. 6.10 [30] examples are shown for some sources in which the peak at $41^d.5$ for GX 301-2 is clearly visible.

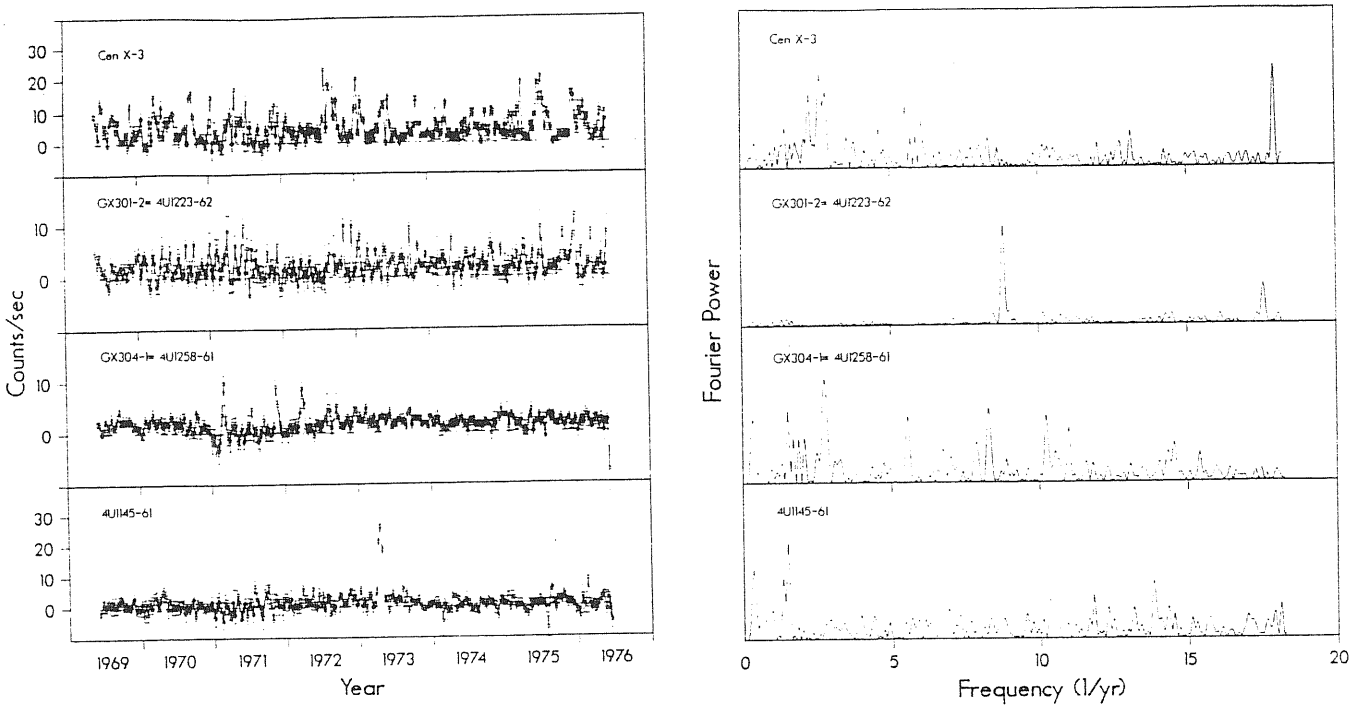

Figure 6.10: At left are shown the X-ray time histories of Cen X-3, GX 301-2, GX 304-2 and 4U 1145-61 as determined from Vela 5B. Each data set point represents a 10^d average. At right are shown the Fourier transforms of the same data sets.

6.4 Energy spectra

6.4.1 Continuous spectra

The energy spectra for 12 pulsars, averaged on pulse phase, are shown in Fig. 6.11 [42]. This spectra are well represented by a power law with photon index α, modified at energies higher than an high-energy cut-off E_c by the function $\exp[(E_c - E)/E_f]$, where E_f is called folding energy [42]:

$$F(E) = \begin{cases} AE^{-\alpha} & \text{for } E \leq E_c \\ & \text{photons/cm}^2 \text{ sec kev} \\ AE^{-\alpha}\exp[(E_c - E)/E_f] & \text{for } E \geq E_c \end{cases} \tag{6.15}$$

Due to the presence of a strong magnetic field, the interpretation of such a spectral shape is not simple. It resembles that of a Comptonized spectrum [14].

Unfortunately, it is not possible to build a model which correlates the spectral parameters among them and with the luminosity [13].

For low luminosities, i.e. for $\mathcal{L}_x \leq 10^{36}$ erg/sec, the Compton cooling is not enough efficient to maintain low the temperature of the infalling matter, and this implies a higher value for E_c and E_f. On the other hand, the optical depth of this plasma is rather small, because of a lower accretion rate, therefore the value of α is greater for lower luminosities.

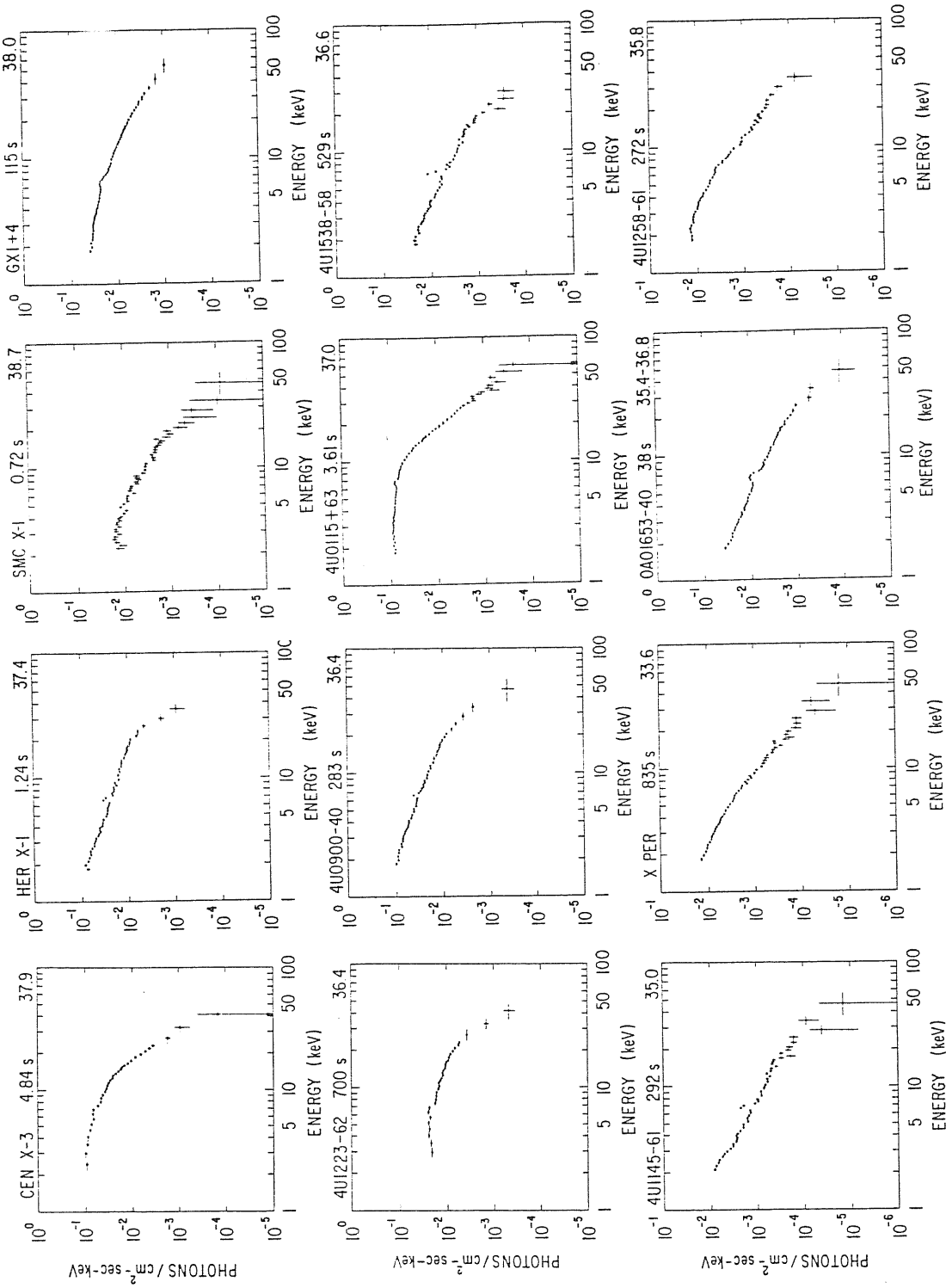

Figure 6.11: Average energy spectra of 12 X-ray pulsars. The source name, period and log of the luminosity in erg/sec are indicated for each spectrum.

Regarding luminous sources, i.e. $\mathcal{L}_x \geq 10^{37}$ erg/sec, we have difficult to represent the spectrum by means of Eq. 6.15, because for doing so we should have to need different values of α or a α increasing with energy.

The standard way to avoid the obstacle consists in using the so called 'two-component model' for the energy spectrum, which is nothing else that the representation of the spectrum by a law for $E < E^*$ and by another one for $E > E^*$. The choice of the type of law is done by a best-fit test on the data points, normally a χ^2 test.

Other laws which are fitted are [37,39]:

$$\frac{dN}{dE} = N_0\, A(N_H)\, E^{-\alpha} \quad \text{Power law} \tag{6.16}$$

$$\frac{dN}{dE} = N_0\, A(N_H)\, \frac{E^2}{e^{-E/kT} - 1} \quad \text{Blackbody} \tag{6.17}$$

$$\frac{dN}{dE} = N_0\, A(N_H)\, E^2\, e^{-E/kT} \quad \text{Wien} \tag{6.18}$$

$$\frac{dN}{dE} = N_0\, A(N_H)\, g(E)\, \frac{e^{-E/kT}}{\sqrt{kT}} \quad \text{Thermal bremsstrahlung} \tag{6.19}$$

where [39]

$$g(E) = 0.8 \left(\frac{E}{kT}\right)^{-0.4}. \tag{6.20}$$

$$\frac{dN}{dE} = N_0\, A(N_H)\, \frac{E^2}{e^{-E/kT} - 1} \sqrt{\frac{\kappa_{ff}}{\kappa_{ff} + \kappa_{es}}} \quad \text{Modified blackbody} \tag{6.21}$$

where

$$\begin{gathered} \kappa_{es} \simeq 0.4 \\ \kappa_{ff} = 2.63\, \rho\, (kT)^{-7/2} (E/kT)^{-3} (1 - e^{-E/kT}). \end{gathered} \tag{6.22}$$

The two terms κ_{es} and κ_{ff} are the electron scattering and free-free electron scattering opacity, respectively. The factor $A(N_H)$ takes into account the X-ray absorption, being N_H the column density measured in hydrogen atoms per cm^2.

This factor can be expressed both in the form [37]

$$A(N_H) = e^{-\sigma N_H} \tag{6.23}$$

where σ is the X-ray scattering cross section [6], or in the form [6]

$$A(N_H) = e^{(E_a/E)^{8/3}} \tag{6.24}$$

where E_a is called absorption energy. The two equations are linked by the relation

$$E_a = 2.6 \left(\frac{N_H}{5.5 \cdot 10^{22}\ H/\mathrm{cm}^2}\right)^{3/8}. \tag{6.25}$$

Name		Spect. type	Spect. index	E_c (keV)	E_f (keV)	N_H (10^{22} H/cm^2)
A0538-66		TB	6.7			2
		W	2.4			
SMC X-1		P	-0.2	17	10	50
Her X-1		P	0.95	20	7	
4U 0115+63		P	0.94	8	7	
V0332+53		P	0.6	15.7	11	
Cen X-3		P	1.30	14	12	3.5
		TB	7.7-8.7			
1E 2259+586		P	3.5			0.8
		TB	1.8			
4U 1626-67		P	0.65	25		
2S 1553-54						
LMC X-4	HE	P	-1.4	17	22	
	LE	P	-0.8			
2S 1417-62		P	-0.9			3.1
		TB	12			0.03
OAO 1653-40		P	-0.6	18	26	28
		TB	16			23
EXO 2030+375						
4U 1700-37	HE	TB	28		25	
	LE	P	-0.15	10	11-20	5-14
A0535+26	HE	EX	17.67-26.5			
	LE	P	2			
GX 1+4	HE	P	-1.3			0.79
	LE	TB	35			3.2
4U 1320-61	HE	P	1.8			3.8
	LE	TB	14.1			2.3
GX 304-1	HE	P	4.9	30		
	LE	TB	10	30		
VELA X-1		P	1.8	28.6	14.0	3.4
4U 1145-61		P	-0.6	16	19	2.6
1E 1145.1-6141						1.2

Table 6.3: Spectral parameters of X–ray binary pulsars.

Name		Spect. type	Spect. index	E_c (keV)	E_f (keV)	N_H (10^{22} H/cm^2)
A1118-61	HE	P	1.1	4		5.5
	LE	P/TB	2.7/3.5			<3.7
4U 1907+09	HE	P	1.2			1.5
	LE	P/TB	3.0/2.5			<0.8
4U 1538-52		P	1.2			3.2
GX 301-2	HE	P	0.78			60.6
	LE	P	1.27	6.46	7.36	>100
4U 0352+30		P	1.7	6.7	4	2.52

Table 6.3: Spectral parameters of X–ray binary pulsars.

In Table 6.3 are shown the spectral parameters of the known X-ray binary pulsars, where the captions for the spectral types (column 2) are: P for power law (Eq. 6.15), W for Wien law, TB for thermal bremsstrahlung, EX for exponential law. The symbols HE and LE mean spectra fitted for high energy ($E > 20$ keV) and low energy ($E < 20$ keV) photons, respectively.

Unfortunately, self-consistent and parametrized theoretical models are not available. This does not allow to fit theory with values of physical parameters, like B, $\dot{M}$, etc. Attempts to compare experimental spectra with models available are made in [9].

6.4.2 Cyclotron lines

The direct evidence of a strong magnetic field in a neutron star has come from the discovery of a cyclotron line in the X-ray spectrum of Her X-1 [38](see Fig. 6.12 [40]). In the falling part of the spectrum a prominent peak at 58 keV was observed with full width at half maximum (FWHM) of about 13 keV. The line feature may be also interpreted as an absorption dip at about 35 keV.

Since its discovery, it was immediately clear that it should be difficult to interpret this line as due to an atomic or nuclear process [19]: in a normal magnetic field the typical transition energy of an electron in the K-shell is of the order of some keV. Only with elements of high atomic number it is possible to obtain enough transition energy (for example the L_α line of Pt^{37+} has an energy of about 58 keV, when corrected for gravitational redshift). However, the elements heavier than Fe are present only in a very small percentages and a line which accounts for more than 1% of the total

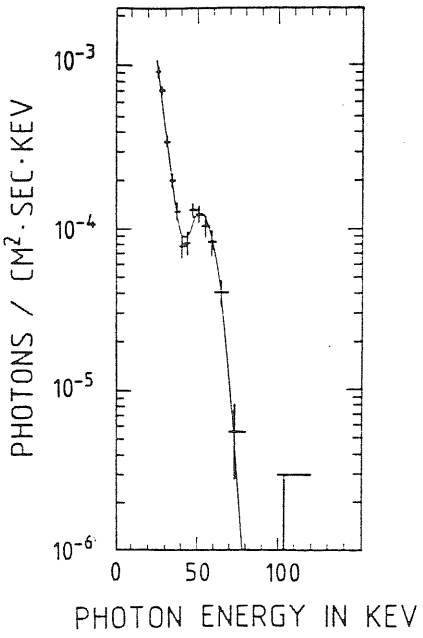

Figure 6.12: Energy spectrum of Her X-1, in which is clearly visible the cyclotron line at about 58 keV.

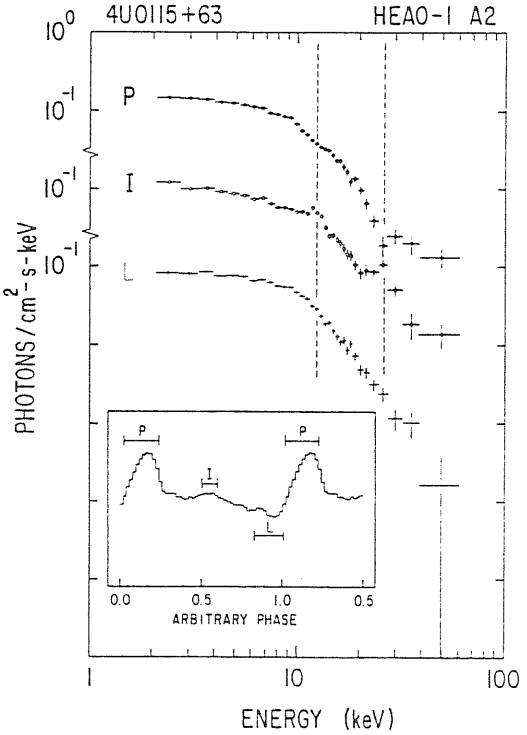

Figure 6.13: Cyclotron line features observed in the spectrum of the X–ray pulsar 4U 0115+63. The spectra at the pulse period (P), at the interpulse (I) and at the low (L) state show absorption, emission and no features, respectively.

X-ray luminosity cannot be produced by an element which is present only in traces.

It is also true that in a strong magnetic field, as we expect in a neutron star, the resonance line of hydrogen-like ions are shifted towards higher energies, but to shift the 7.3 keV resonance line of $Fe\ XXVI$ to the observed value, we need a magnetic field of $5 \cdot 10^{13}$G, which is not impossible but unlikely [19] (moreover it might be difficult to explain the intensity observed).

In case of nuclear transition, typical energies are of the order of MeV, and only the heavier nuclei, as Am^{241}, have excited state enough low to produce a resonant line at 58 keV.

Another example of cyclotron line is that observed in 4U 0115+63. Fig. 6.13 [42] shows the energy spectrum in three pulsation phases, including the peak, the low and the interpulse peak.

We can clearly see two lines, at 11.5 and 23 keV, in absorption at (P) but in emission in (I); they are not visible in (B).

These two lines can be identified with the fundamental and the first harmonic cyclotron lines for a magnetic field of strength of about 10^{12}G.

The above features may be understood in the following terms [14]: The emission in (B) represents that of the non-pulsating component, which results from the superposition of the X-rays emitted from a wide region over the neutron star. Although the magnetic field strength varies considerably in the emission region, the cyclotron lines are deleted, because of the superposition. On the contrary, during (I) and (P) the emission comes from the magnetic polar caps: the depth of the emission region is different therefore we observe a double peak.

6.4.3 Iron emission and absorption edge

Most of the X–ray pulsar spectra show an emission line between 6 and 7 keV. This line, exactly at 6.4 keV, is due to the iron fluorescence, produced by photons which strike the neutron star atmosphere and ionize the Fe atoms [19]. In fact, the line intensity is proportional to the intensity of the continuum for energies higher than 7 keV (which is the ionization energy of the K-shell electron) and the ratio between these two intensities is $\sim 1\%$.

But in some occasions the spectrum changes drastically; the absorption edge at about 7 keV is due to the K absorption by the iron of lower degree of ionization [36].

The absence of modulation in this line indicates that the matter responsible of this feature is not associated to the accretion columns [14]. The absence of correlation between the line intensity and the measure of the absorption, obtained from the low energy spectrum, indicates that the matter responsible of the emission of the line is not localized between the X-ray source and the observer, but is not even too much close to the source, because we observe a decrease in the line intensity of about 6% during the eclipses [34]. Therefore there is also a contribute from the stellar wind.

Four possible sources of the iron fluorescence have been investigated [28]

- Companion star atmosphere

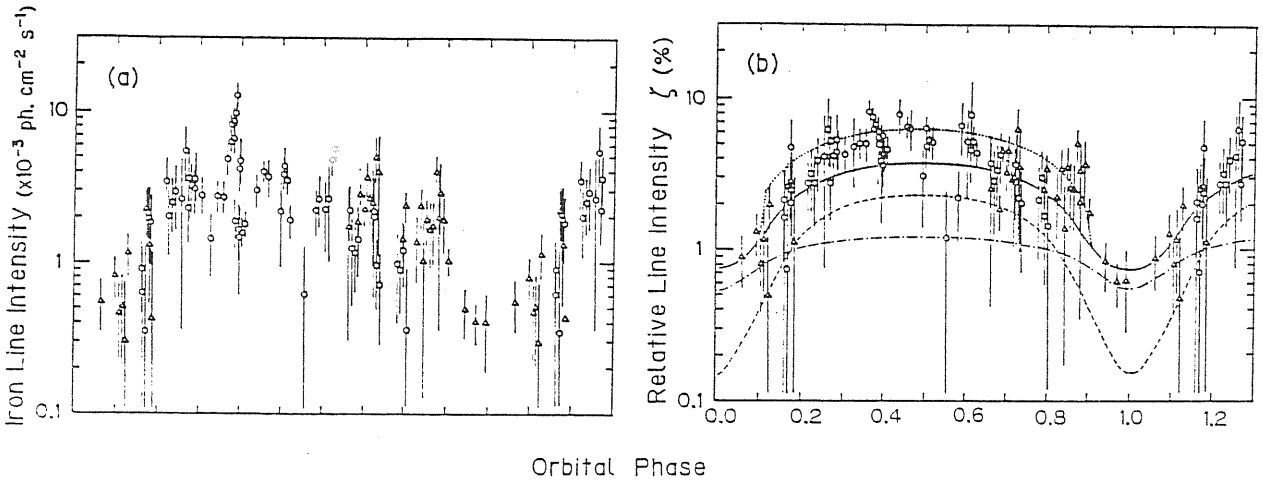

Figure 6.14: *(a)* The observed iron line intensity and *(b)* the relative intensity ζ as a function of the orbital phase. The thin dashed and dash-dotted curves represent the fractions of the relative line intensity attributed to the stellar atmosphere and to the stellar wind, respectively, and the thick-solid curve is their sum. The dotted curve indicates the intensity including the contribution of fluorescence in the proximity of the neutron star.

- Stellar wind
- Accretion disk
- Magnetosphere of the neutron star

A model which can explain the observed features considers as source of iron fluorescence the companion star atmosphere in interaction with the stellar wind [34]. The matter density at a distance r from the neutron star surface is due to the combination of a spherical atmosphere of scale-height H and a spherical stellar wind, therefore we will have

$$\rho(r) = \rho_0 \exp\left[-\frac{r - R_\star}{H}\right] + \frac{\dot{M}_\star}{4\pi\, r^2 v_w(r)} \tag{6.26}$$

where $R_\star$ is the radius of the companion, $\dot{M}_\star$ is the mass loss rate and $v_w(r)$ is the wind velocity. In a hydrostatic model H is given by

$$H = \frac{kT_{eff}}{\mu\, m_H g_{eff}} \quad g_{eff} = g\left(1 - \frac{\kappa L_\star}{4\pi\, c\, G\, M_\star}\right) \tag{6.27}$$

where T_{eff} and g_{eff} are the effective temperature and gravity, respectively, $L_\star$ and $M_\star$ are the luminosity and mass of the companion, m_H is the hydrogen mass, μ the average molecular weight, k the Boltzmann constant, G the gravitational constant and κ the companion opacity. Assuming a velocity law for the stellar wind of the form [7]

$$v_w(r) = v_\infty \left(1 - \frac{R_\star}{r}\right)^\beta \tag{6.28}$$

where v_∞ is the terminal velocity and $\beta = 1/2$ [7], we are able to determine the dependence of the Fe line intensity on the orbital phase, as is shown in Fig. 6.14 [34].

Bibliography

[1] ALPAR M.A. - ANDERSON P.W. - PINES D. - SHAHAM J. 1984. *Astrophysical Journal*, **276 p.325**.

[2] ALPAR M.A. - ANDERSON P.W. - PINES D. - SHAHAM J. 1984. *Astrophysical Journal*, **278 p.791**.

[3] AVNI Y. 1976. *Astrophysical Journal*, **209 p.574**.

[4] BONNET-BIDAUD J.M. - VAN DER KLIS M. 1981. *Astronomy & Astrophysics*, **97 p.134**.

[5] BOYNTON P.E. *et al.* 1984. *Astrophysical Journal*, **283 p.L53**.

[6] BROWN R.L. - GOULD R.J. 1970. *Physical Review*, **D1 p.2252**.

[7] CASTOR J.I. - ABBOTT D.C. - KLEIN R.I. 1975. *Astrophysical Journal*, **195 p.157**.

[8] COOK M.C. - PAGE C.G. 1987. *Montly Notices of R.a.S.*, **225 p.381**.

[9] DAL FIUME D. - FRONTERA F. - MORELLI E. 1988. *Astronomy & Astrophysics*, **331 p.313**.

[10] DEETER J.E. - BOYNTON P.E. - PRAVDO S.H. 1981. *Astrophysical Journal*, **247 p.1003**.

[11] DEETER J.E. - BOYNTON P.E. - SHIBAZAKI N. - HAYAKAWA S. - NAGASE F. - SATO N. 1987. *Astronomical Journal*, **93 p.877**.

[12] ELSNER R.F. *et al.* 1985. *Astrophysical Journal*, **297 p.288**.

[13] HARDING A.K. - MESZAROS P. - KIRK J.K. - GALLOWAY D.J. 1984. *Astrophysical Journal*, **278 p.369**.

[14] HAYAKAWA S. 1985. *Physics Reports*, **121 p.318**.

[15] JOSS P.C. - RAPPAPORT S.A. 1984. *Annual Review of Astronomy and Astrophysics*, **22 p.537**.

[16] KELLEY R.L. - RAPPAPORT S. - CLAK G.W. - PETRO L.D. 1983. *Astrophysical Journal*, **268 p.790**.

[17] KII T. - HAYAKAWA S. - NAGASE F. 1986. *Astrophysics and Space Science*, **118 p.375**.

[18] KII T. - HAYAKAWA S. - NAGASE F. - IKEGAMI T. - KAWAI N. 1986. *Pubbl. Astron. Soc. Japan*, **38 p.751**.

[19] KIRK J.G. - TRUMPER J.E. 1983. In *Accretion–Driven Stellar X–ray Sources*, LEWIN W.H.G. - VAN DEN HEUVEL E.P.J. Eds., Cambridge Un. Press.

[20] KOO J.W.C. - HAYMES R.C. 1980. *Astrophysical Journal*, **239 p.L57**.

[21] MAKISHIMA K. *et al.* 1984. *Pubbl. Astron. Soc. Japan*, **36 p.679**.

[22] MANCHESTER R.N. - TAYLOR J.H. 1977. *Pulsars*. Freeman Co.

[23] MARSHALL N. - RICKETTS M.J. 1980. *Montly Notices of R.a.S.*, **193 p.7P**.

[24] MESZAROS P. 1984. *Space Science Review*, **38 p.325**.

[25] MITANI K. - MATSUOKA M. - MAKISHIMA K. - INOUE H. 1984. *Astrophysics and Space Science*, **103 p.345**.

[26] MURAKAMI T. *et al.* 1984. *Pubbl. Astron. Soc. Japan*, **36 p.691**.

[27] NAGASE F. *et al.* 1984. *Astrophysical Journal*, **280 p.259**.

[28] NAGASE F. - HAYAKAWA S. - SATO N. - MASAI K. - INOUE H. 1986. *Pubbl. Astron. Soc. Japan*, **38 p.547**.

[29] PLAVEC M. 1968. *Adv. in Astron. and Astrophys.*, **6 p.201**.

[30] PRIEDHORSKY W.C. - TERRELL J. 1983. *Astrophysical Journal*, **273 p.709**.

[31] RAPPAPORT S. - JOSS P.C. 1983. In *Accretion–Driven Stellar X–ray Sources*, LEWIN W.H.G. - VAN DEN HEUVEL E.P.J. Eds., Cambridge Un. Press.

[32] REFLOC'H A. - CHANBON G. - NIEL M. - VEDRENNE G. - RAKHAMINOV C.Y. 1986. *Astrophysical Journal*, **310 p.773**.

[33] RICKETTS M.J. - HALL R. - PAGE C.G. - WHITFORD C.H. - POUNDS K.A. 1982. *Montly Notices of R.a.S.*, **201 p.759**.

[34] SATO N. - HAYAKAWA S. - NAGASE F. - MASAI K. - DOTANI T. - INOUE H. - MAKINO F. 1986. *Pubbl. Astron. Soc. Japan*, **38 p.731**.

[35] SCHREIRER E. - LEVINSON R. - GURSKY H. - KELLOGG E. - TANANBAUM H. - GIACCONI R. 1972. *Astrophysical Journal*, **172 p.L79**.

[36] TANAKA Y. 1983. In *Workshop on Non–thermal and Very High Temperature Phenomena in X–ray Astronomy*, , Roma.

[37] TREVES A. *et al.* 1988. *Astrophysical Journal*, **325 p.119**.

[38] TRUEMPER J. - PIETSCH W. - REPPIN C. - VOGES W. - STAUBERT R. - KENDZIORRA E. 1978. *Astrophysical Journal*, **219 p.L105**.

[39] TUCKER W.H. 1977. *Radiation Processes in Astrophysics*. The MIT Press.

[40] VOGES W. - PIETSCH W. - REPPIN C. - TRUEMPER J. - KENDZIORRA E. - STAUBERT R. 1982. *Astrophysical Journal*, **263 p.803**.

[41] WANG Y.M. - WELTER G.M. 1981. *Astronomy & Astrophysics*, **102 p.97**.

[42] WHITE N.E. - SWANK J.H. - HOLT S.S. 1983. *Astrophysical Journal*, **270 p.711**.

Chapter 7

PECULIAR X–RAY BINARY PULSARS

In this chapter we will give a detailed description of some X–ray binary pulsars that show peculiarities which make them prototypes of those classes we discussed in Chapter 2.

We have selected the following sources:

A0538-66	Her X-1	Vela X-1
A0535+26	1E 2259+586	GX 301-2

Among these objects, A0538-66 and A0535+26 are Be/XRBSs, Her X-1 and 1E 2259+586 are LMXRBs, Vela X-1 and GX 301-2 are HMXRBs.

We will try to give a panorama about the observational characteristics of each source, the possible models which may describe them, taking into account the problems open yet.

7.1 Be/X–ray binary pulsars: A0538-66

Normally we assume that the outbursts seen in Be/X–ray binary pulsars reflect the orbital period. The modulation along the orbit may be given by [66]:

1. Variation in the separation between the two components the binary system [61]. As the neutron star approaches the companion, in its orbital motion, the accretion rate from the denser, slower stellar wind increases.

2. The modulation is given by the passage of the neutron star in the dense equatorial envelope which surrounds the Be star [47]: during the passage there is an increase of the accretion rate (in this way the non corrispondence between the periastron passage and the maximum X–ray luminosity is explained. In this way is also explained the double maximum observed in some sources, which is due to the passage

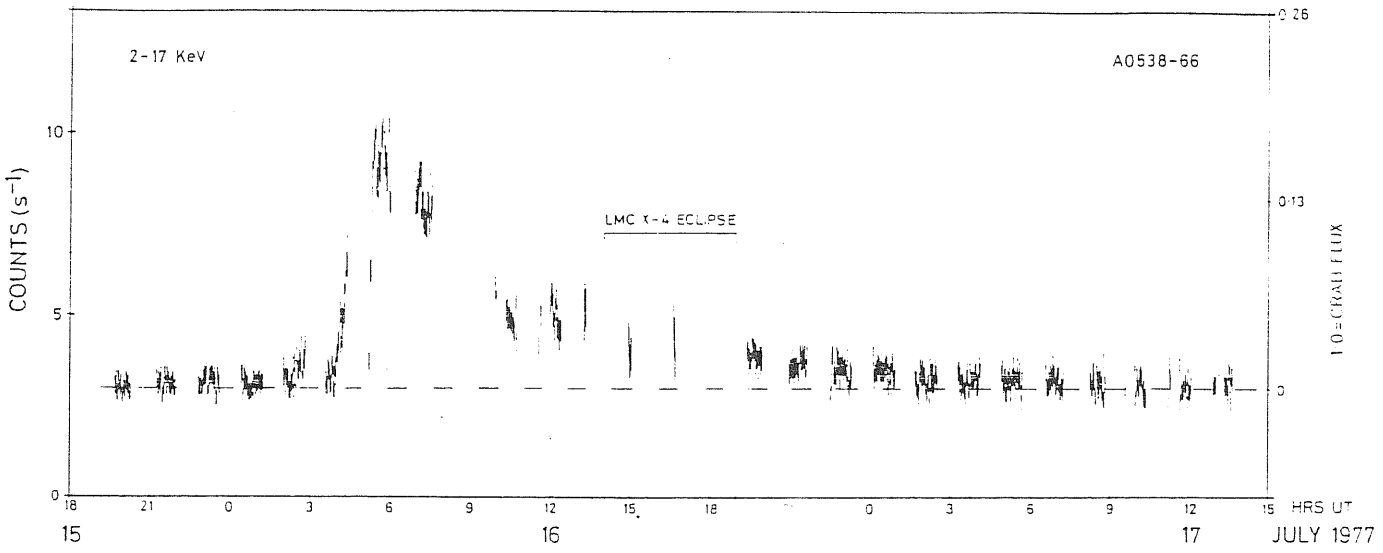

Figure 7.1: The X–ray flux from A0538-66, observed by the PCS on board *Ariel V*, plotted with a time resolution of 1 minute. The gaps are the result of data losses caused by operational constraints. The field of view was centered on LMC X-4, but also contained LMC X-1, LMC X-3 and LMC X-5. These sources, plus the contributions from the X–ray and particle background, are responsible for the steady flux.

through the two sides of the disk).

The (optical) spectral characteristic of Be stars are [87]: *(a)* an infrared excess in the normal photospheric continuum and [8] *(b)* strong H_α and H_β emission lines. Both these features originates in the circumstellar disk which forms because the high velocity of the Be star. The IR component forms from free–free transitions in the ionized plasma of the disk [5].

The peculiarity of A0538-66 resides in the fact that it shows typical characteristics of transient X-ray sources (i.e. flaring activity), but they occur on very short timescale. In Fig. 7.1 [91] is shown the behaviour of the X–ray flux observed by *Ariel V*, in which is clearly visible an outburst centered at 15.6 July 1977.

The X–ray spectrum observed by *Ariel V* during the 26 June outburst [91] is well fitted by both a thermal law plus a Gaunt factor [86], with $kT = 6.7 \pm 0.8$ keV ($\chi^2_{dof} = 1.2$) in the energy band 2–17 keV, and by a power law, with photon index $\alpha = +2.3 \pm 0.2$ ($\chi^2_{dof} = 1.6$) in the same energy band, with no evidence in either case for a low energy absorption turnover ($N_H < 2 \cdot 10^{22}$ H/cm^2, see Fig. 7.2 [91]).

This source has been observed later by the *Einstein* Observatory; the energy spectrum during two different observations (16 December 1980 and 3 February 1981) is well fitted by a power law with $\alpha = -1.6$ and -0.6 in the two observations, respectively (energy band 1.1–21 keV), plus a low

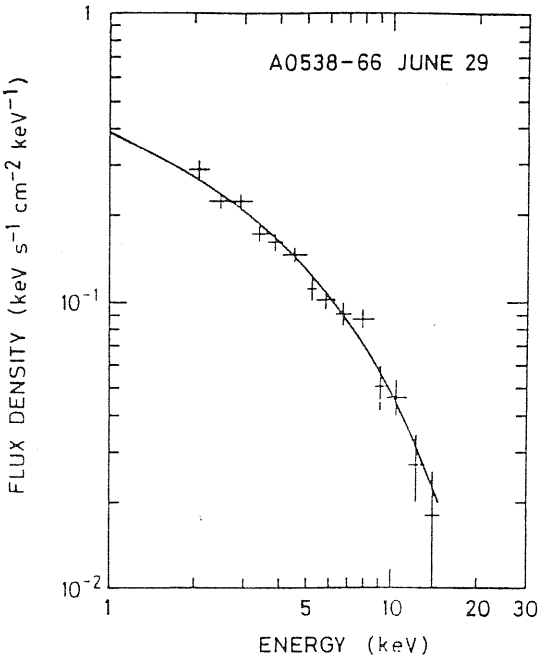

Figure 7.2: The spectrum of A0538-66 seen at the peak of activity during the first outburst.

energy absorption corresponding to a column density $N_H \simeq 2 \cdot 10^{23}$ H/cm^2.

While from *Ariel* observations there was no indication of pulsation, from *Einstein* data a persistent periodicity was found, at a mean heliocentric pulse period of 0.00692126 seconds in the December experiment. This pulsation was not detected in the following observation. As we can see from Fig. 7.3 [80], the pulse profile shows the characteristic asymmetrical double peak; the main peak is centered at pulse phase $\phi_p = 0.66$, while the secondary peak is centered at $\phi_p = 0.25$. The minimum is centered at $\phi_p = 0.1$.

The system parameters are shown in Table 7.1, while in Fig. 7.4 [28] are visible the possible ranges for the masses of the components the system, as derived from the observations.

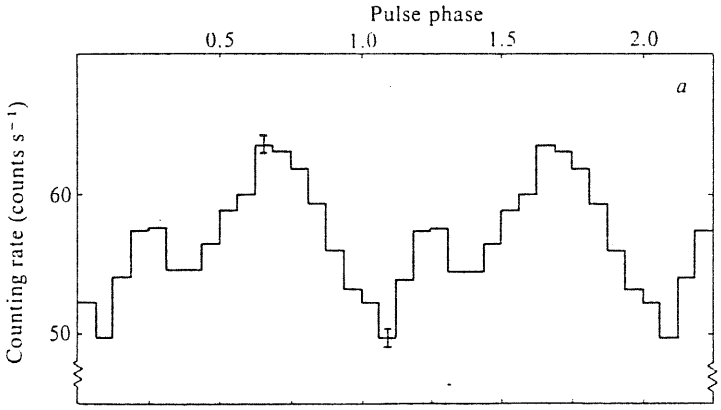

Figure 7.3: Averaged pulse profile of A0538-66 observed by *Einstein* on 16 December 1980.

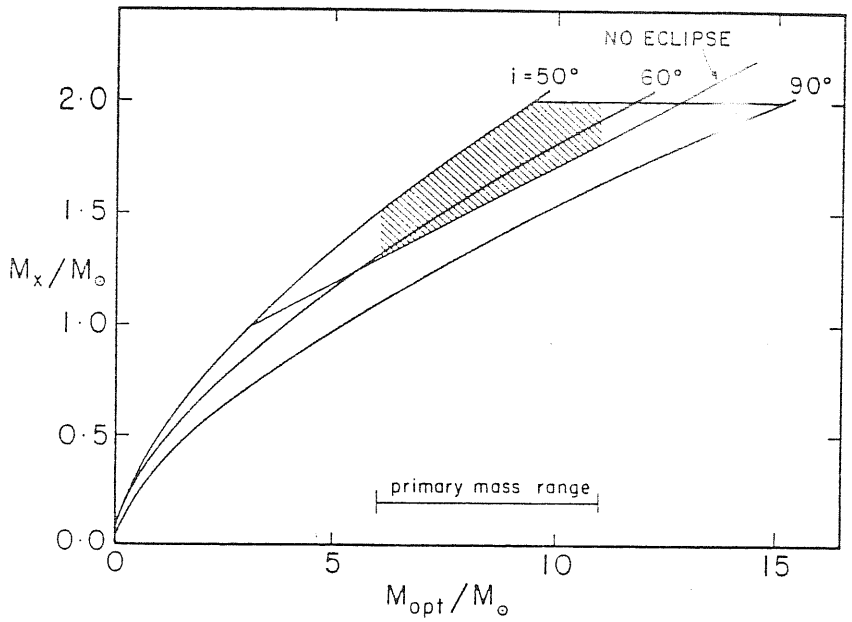

Figure 7.4: Mass diagram derived from orbital parameters. Hatched area is the most likely region of the plane for the two star to occupy. The probable upper limit for a neutron star is 2 $M_\odot$.

The short pulse period, the very high value of eccentricity and the great variability lead to the conclusion that this system has to be very young, i.e. its age would be less than 10^8 years.

The 69^{ms} pulsations give no doubt about the nature of the compact object that causes them. In fact, from the relation $\Omega_p \leq \sqrt{G\langle\rho\rangle}$ [79], where $\langle\rho\rangle$ is the mean density of the object and G is the gravitational constant, we obtain that the only compact object compatible with the observed value of Ω_p is a neutron star. Further, we have evidence of the presence of a strong magnetic field from the increase in the polarization during the outbursts, observed in optical [5].

The system A0538-66 is a typical Be/X–ray binary system, showing several periods of quiescence among periods of activity, in which a flaring activity is present, both in optical and in the X–ray band (coincident), with period between flares of $16^d.7$ ("OFF" and "ON" states, respectively).

The two states are characterized by [64]

1. *High–state*: the optical spectrum of the Be star shows 'P Cygni' profiles in the H_β , H_γ and HeII λ4686 emission lines.

2. *Low–state*: the optical spectrum is that of a 'normal' Be star, but shows 'inverse' P Cygni profiles in the emission lines.

The observation of inverse P Cygni profiles suggests the presence of circumstellar matter, probably with asymmetric distribution around the primary. During the observations a variation in the spectral type of the companion has been observed, which passed from $B7IIe$ to $B2IIIe$ [64], further variations in the color temperature were observed [8]. All these variations are explained in terms of variations in the intrinsic intensity of the X-rays.

$$V_0 = 308 \pm 3 \text{ Km/sec}$$
$$K = 44 \pm 7 \text{ Km/sec}$$
$$e = 0.82 \pm 0.04$$
$$\omega = 222^\circ \pm 21^\circ$$
$$i > 50^\circ$$
$$f(M) = 0.027\, M_\odot$$
$$d = 52 \text{ kpc}$$
$$T_0 = 2,445,722.386 \pm 0.215 \text{ JD}$$
$$P_p = 0^s.06921166 \pm 0^s.00000017$$
$$\dot{P}_p = (5.01 \pm 0.86) \cdot 10^{-10}$$

Table 7.1: Parameters of the Be/X–ray binary system A0538-66.

A model describes these variations in terms of an accreting neutron star buried in the dense atmosphere of its Be star companion [64]. In fact, when the neutron star is plunged in the atmosphere of the Be star during an outburst, these variations in absorption[1] may be explained in terms of variations in the ionization of the gas surrounding the X–ray source (see Chapter 4 for details). Of course, these regions of different ionization will have a complex structure but, assuming them as spherical 'clouds' composed by elements which absorb soft X–rays, i.e. Carbon, Nitrogen and Oxygen, we will have that the ionization radius r_{io}, beyond which the gas is completely ionized,[2] is given by [84,24]

$$r_{io} \approx (1.0 \cdot 10^{11} \text{ cm}) \sqrt{\frac{L_{37}}{N_{12}}} \tag{7.1}$$

where L_{37} is the X–ray luminosity in units of 10^{37} erg/sec and N_{12} is the proton density of the cloud, in units of 10^{12} particles/cm^3.

We may obtain an estimate for N_p from the observed value of the absorption column density N_H, from which we obtain $N_p \sim 10^{12}$ particles/cm^3; therefore, from Eq. 7.1

$$r_{io} \approx 5 \cdot 10^{11} \text{ cm}. \tag{7.2}$$

An emission model for A0538-66 is as follows [64]:

For $r < r_{io}$ the X–ray radiation pressure dominates on all the others, creating a 'cavity' in the atmosphere of the Be star which surrounds the neutron star. This will imply a non homogeneous distribution of the absorber matter, which yields a zone of enhanced absorption towards that part of the cavity turned to the companion star (see Fig. 7.5 [64]).

[1] That is, variation in intensity.

[2] In this way it defines the distance from the source beyond which the absorption occurs.

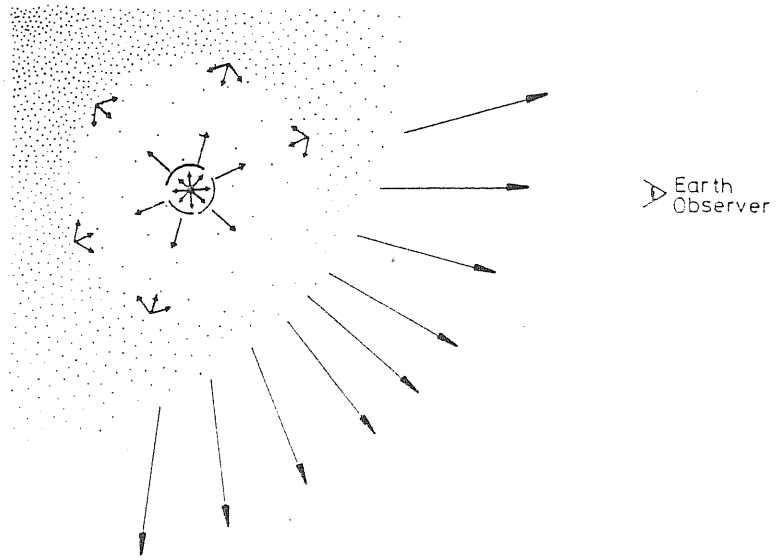

Figure 7.5: Schematic view of the proposed model for A0538-66. The source is submerged in the stellar atmosphere but its radiation pressure clears a cavity. Radiation from the accreting neutron star escaping via the incomplete Alfvén shell is absorbed or Compton reflected at the walls of the cavity, emerging only over some beam angle centered on the thinnest part of the absorber.

The opposite part will be a 'hole', which is not aligned with our line of sight. The radiation will be Compton reflected by the walls of the cavity, but will be able to escape from the hole (the thinner part of the absorber) towards our direction. In this way the typical power law spectrum will become a Wien thermal spectrum.

This model represents A0538-66 as a flashlight with a Compton reflector. The anisotropy of the emission which results cause the overstimate of the total X–ray luminosity.

The X–rays absorbed by the walls of the cavity will be reprocessed and they will be re-emitted in the optical and ultraviolet band.

The defect of this model consists in the fact that it provides the presence of the iron line in the X–ray spectrum, line which is due to fluorescence (see Chapter 6), but this line has not been observed.

Another model explains the variation in the X–ray luminosity as due to a variation in the centrifugal barrier [82] (see Chapter 4); in this way also the long quiescence intervals are explained very well.

Finally, we want to mention the model which explains the emission far from the periastron passage as due to accretion of matter which remains (temporarily ?) gravitationally bound to the compact object (for example a disk) during the precedent periastron passage [5]. In this way the super–Eddington luminosity is explained because the source emits only during a small fraction of its orbital cycle and, in any case, not in a steady way.

Regarding the evolutionary scheme of A0538-66 see section 3.2.3 [21].

We conclude with open questions about A0538-66:

$$V_0 \sin i = 254 \pm 12 \text{ Km/sec}$$
$$e = 0.494 \pm 0.002$$
$$\omega = 89°.2 \pm 0°.5$$
$$40° < i < 60°$$
$$f(M) =\leq 20\ M_\odot$$
$$d = 2.6 \pm 0.4 \text{ kpc}$$
$$T_0 = 2,444,521.4652 \text{ JD}$$
$$P_p = 103^s.6741 \pm 0^s.002$$
$$\dot{P}_p = -(8.428 \pm 0.045) \cdot 10^{-8}$$
$$\ddot{P}_p = +(6.36 \pm 0.10) \cdot 10^{-14} \text{ sec}^{-1}$$

Table 7.2: Parameters of the Be/X–ray binary pulsar A0535+26.

1. What is the mass transfer mechanism at periastron ? Is it stellar wind, tidal overflow [5] or passage of the neutron star through the envelope (disk ?) surrounding the Be star ?

2. Does some matter remain gravitationally bound to the neutron star during the periastron passage ? If it occurs, how and when is this matter lost ?

3. Is A0538-66 a young system we have the luck to observe in a special phase of its evolution ?

All these problems wait for an answer.

7.2 Be/X–ray binary pulsars: A0535+26

The X–ray source A0535+26 is the typical example of *recurrent transient*, in which, unlike other types of transients as EXO 2030+375 and V0332+53, the X–ray outburst activity is without doubt correlated to the orbital motion of the neutron star around the dense envelope of the Be star. This is demonstrated by the fact that we do not observe large variations in the optical and infrared flux during outbursts [30,49], and the times of periastron passages[3] (almost) always coincides with the maxima of the X–ray emission [67]. "Almost" means that two among the more intensive flares did not occur in phase with the 111^d cycle between flares (25 April 1975 [73] and 13 October 1980 [55]).

The observations demonstrated the presence of periodic modulations in the X–ray flux, with fast spin-up during outbursts, and secular spin-down during the quiescent phase [94]. In Fig. 7.6 [95] we can see a possible scenario

[3]This must be treated with caution because an orbital solution for A0535+26 is not known.

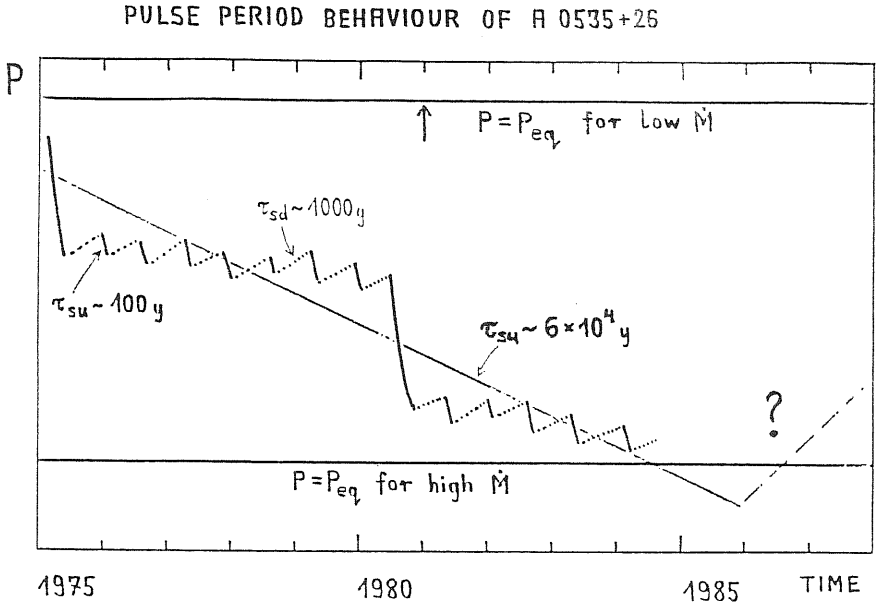

Figure 7.6: Theoretical pulse period variations, shown with the two periodicities discussed in the text.

to explain the observations, while in Fig. 7.7 [70] we show the observed history of pulse period changes.

The pulse shape, as we can see in Fig. 7.8 [3,18] is strongly energy dependent and (from Table 7.3 [22]) epoch dependent. At lower energies ($E < 20$ keV) the light curve presents a series of five non regularly spaced dips. The deep minimum in the light curve at lower energies becomes sharper at higher energies. The center of this minimum at lower energies is shifted in phase of about 5^s from the center of the minimum, at higher energies. This features are persistent.

At higher energy ($E > 20$ keV), the light curve presents a double peak, with two asymmetric peaks. The main peak lasts $40^s.7$ between pulse phase $\phi_p = 0.039$ and 0.43 and it is centered at $\phi_p = 0.17$. The secondary peak lasts $46^d.7$, between phases 0.57 and 1.02; it is centered at $\phi_p = 0.82$ and seems the result of the superposition of three sharper peaks. The interpulse region lasts $14^s.2$ and is centered at $\phi_p = 0.5$. Further, it is present a sharp dip at phase 0.03.

As we have seen in section 6.2, the pulse distance different by 0.5 between the two maxima of the light curve could imply that the two emission regions (polar magnetic caps) are non exactly located in opposite directions with respect to the center of the star. Further, the fact that the pulsed and average flux have the same shape implies that emission comes only from these two regions, modulated by the star rotation and with given angular radiation patterns.

The double peak structure is well visible up to 90 keV, while beyond this value the secondary peak is lost. Also at higher energies the center of the minimum does not show any shift.

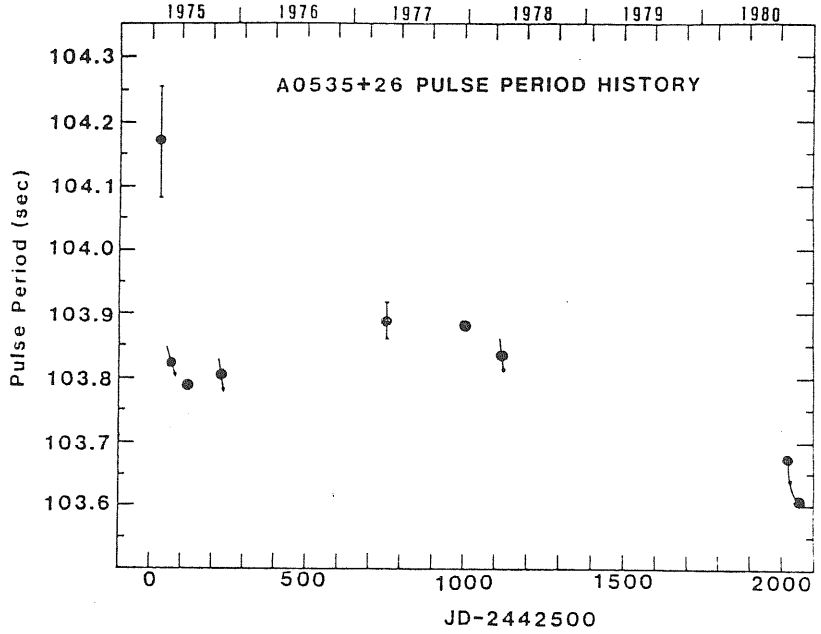

Figure 7.7: Pulse period history of A0535+26. Data points for outbursts other than that of December 1977. The open circle is a *SAS 3* observation on 27 December 1977.

The amplitude of the two peaks must be energy dependent, because any tentative to fit all the light curves with an average light curve (obtained leaving two free parameters: a phase–independent intensity level and a single amplitude of the modulated component for the two peaks[4]) gave a negative result [18].

From Fig. 7.8 [18] is clearly visible a transition in the pulse profile at about 35 keV: above 35 keV there is a variation in the relative intensity of the two peaks together with a variation in the symmetry of the main peak. Below 35 keV we can notice a variation in the structure itself of both the peaks.[5]

We can further notice that the pulsed fraction increases with energy, reaching 100% at about 100 keV.

It is important to remark that the pulse shape is stable only on average (as we have for the radio pulsars), while every pulse has a different shape (to obtain a stable shape it is necessary to average over 14 pulses). This variability is intrinsic in the X–ray source and can be treated as chaotic variability [78,4,88,69] (see Fig. 7.9 [18]).

From an analysis of the power spectrum density we obtain that the noise is intrinsic of the source and can be described in terms of *shot–noise*, with events which typically last 10^s and they occur, in average, one every 25^s. Simulations show that the shot shape might be assumed triangular [18].

[4] The modulated component is estimated by the sum of the intensity of the two peaks.

[5] This is a further confirmation that hard X–rays come from deeper layers of the accretion columns while low-energy photons are effected by the presence of matter surrounding the neutron star.

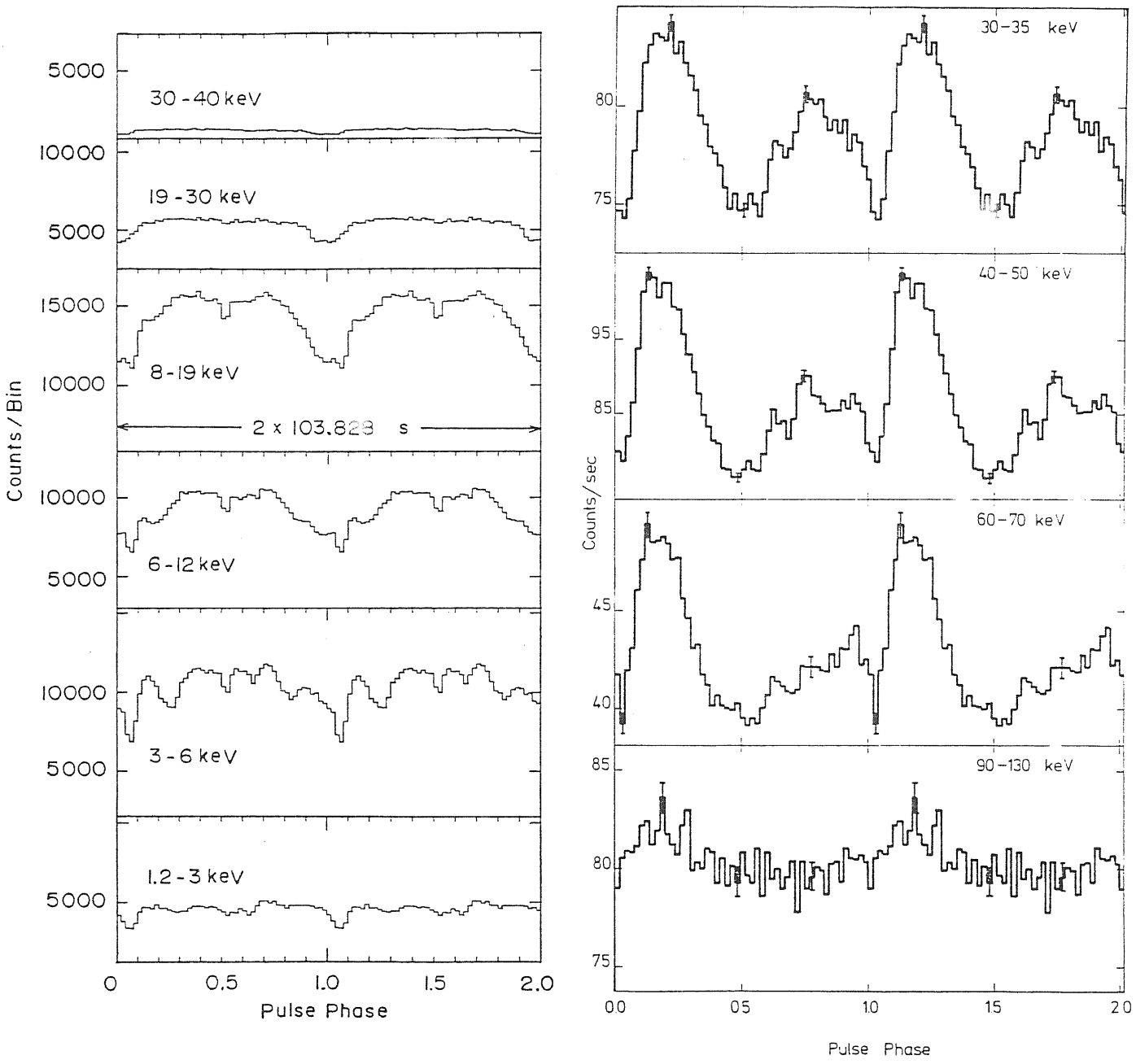

Figure 7.8: Time-averaged light curves of A0535+26 in different energy intervals. For low-energy data, the observation was made in the period 30 May—2 June 1975 by the *SAS 3* experiment, while the high-energy data are from a balloon experiment launched on 4 October 1980. In the former data no background and Crab subtraction has been performed.

Detection device	Period of observation	Energy range (keV)	Pulse information	Spectral information
Ariel V	23–29 Apr 1975	26–1200	None	Exponential: $kT = 3$ keV(LE) $kT = 8$ keV(HE)
Ariel V	28 Apr 1975	3–7	1 peak and 1 dip	None
Ariel V	19 May 1975	2–18	None	Power-law: $\alpha = -0.8$
Balloon	22 May 1975	25–400	1 peak and 1 strong dip	None
Ariel V	1 Jun 1975	2–18	None	Power-law: $\alpha = -1.1$
SAS 3	30 May 1975	1–50	Flat with a dip	None
Balloon	1 Jun 1975	18–150	Flat with a dip	Exponential: $kT = 17.6$ keV
Prognoz 6	22 Dec 1978		None	Power-law: $\alpha \sim -3$
Balloon	25 Sep 1980	20–800	2 peaks with 1 dip	Power-law: $\alpha = -3.42$; Exponential: $kT = 17.7$ keV
Balloon	4 Oct 1980	20–200	2 peaks	Wien law: $kT = 7.68$ keV Blackbody law: $kT = 7.73$ keV
Balloon	7 Oct 1980	45–75	1 peak with a strong peak	None
Hakucho	7–30 Oct 1980		2 peaks then flat with 1 dip	None
Balloon	21 Jul 1981		1 broad peak	Power-law: $\alpha = -1.2$

Table 7.3: Summary of observations of A0535+26.

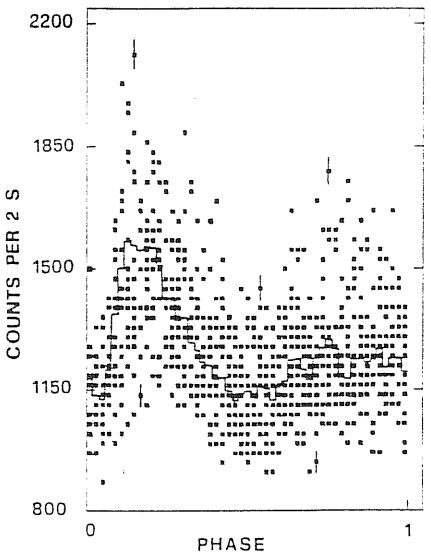

Figure 7.9: Scatter plot obtained from the superposition of individual pulses of A0535+26 in the 27–100 keV energy band. The solid line shows the time averaged light curve. One sigma statistical errors are shown for some data points.

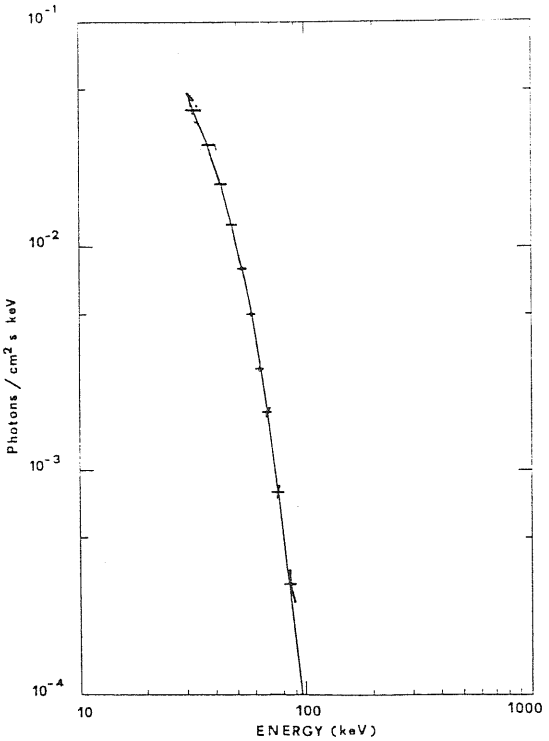

Figure 7.10: Pulse phase averaged photon spectrum of A0535+26 integrated on the total observation time.

The X–ray spectrum of A0535+26, as we can see in Table 7.3, can be fitted by several spectral laws. In Fig. 7.10 is shown the spectrum of the 4 October 1980 experiment [9]. The spectrum fits with a blackbody law

$$\frac{dN}{dE} = (2.34 \pm 0.05) \cdot 10^{-3}\, E^2 \left\{ \exp\left[\frac{E}{7.73 \pm 0.036} \right] - 1 \right\}^{-1} \quad \frac{\text{Photons}}{\text{sec}\cdot\text{cm}^2\cdot\text{keV}} \tag{7.3}$$

with $\chi^2_{dof} = 1.45$, and with a Wien law

$$\frac{dN}{dE} = (2.46 \pm 0.05) \cdot 10^{-3}\, E^2 \exp\left[- \frac{E}{7.68 \pm 0.035} \right] \quad \frac{\text{Photons}}{\text{sec}\cdot\text{cm}^2\cdot\text{keV}} \tag{7.4}$$

with $\chi^2_{dof} = 1.08$.

In this spectrum line features are not visible, even if a transient line feature at 77 keV [83] has been observed.

From observations about how the spectrum changes with pulse phase, and therefore how the spectrum varies according to the different emission regions, we can obtain informations about the anisotropy of the emitted radiation and, therefore, a quantitative measure of the effects of the magnetic field on the cross sections of the processes involved. In this way it is possible to obtain an estimate of the intensity of the magnetic field of A0535+26, without using line features, and in this case we obtain $B \sim 10^{13} G$ [9]. But as we have just said, a theory which is able to correlate among them all the parameters which enter in play in the description of the energy spectra of X–ray sources is not present.

A possible emission model of A0535+26 is shown in Fig. 7.11 [95]. In the quiescence phase the neutron star orbits far from the companion Be star and therefore the accretion rate is so small that the corotation radius R_c (see Eq. 4.16) is smaller than the magnetospheric radius R_m (see Eqs. 4.14 and 4.15). In this case, the stellar wind matter is not accreted and we have the so–called "propeller effect" [29,89]. As the neutron star approaches the Be star, the accretion rate increases until then $R_c > R_m$: in this phase the accretion might occur and this corresponds to the active phase of X–ray emission (flaring). However, A0535+26 has been observed also during the quiescence, making this model unlikely.

We have also a problem: how to explain the two big outbursts which did not occur in phase with the orbital cycle ?

A model [70] could explain this delay by the formation of a *transient* disk, due to matter which remained gravitationally bound to the neutron star during its passage through the dense atmosphere of the Be star. At the beginning, the matter flux is almost radial and it is quickly thermalized in a thick, prolate envelope. Then, as a result of a coupling of this envelope with the rotating magnetosphere, and of energy dissipation by turbolent viscosity, the envelope becomes flat (a disk).

Because before the collapse to a disk shape the envelope is optically thick to X–rays [70], the energy irradiated from the magnetic polar caps will emerge only when the disk is completely formed.

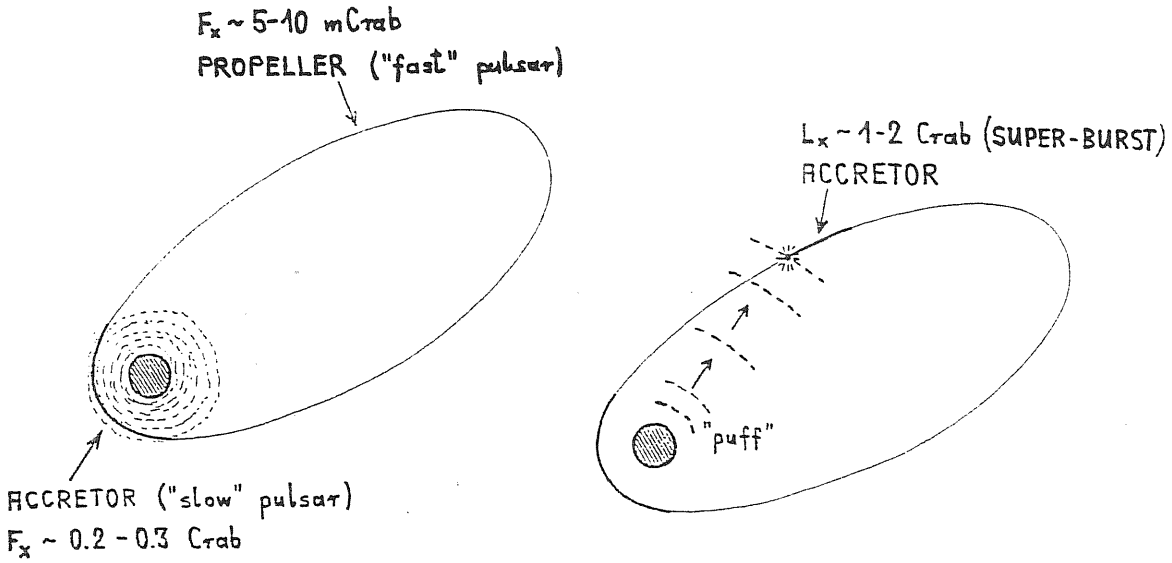

Figure 7.11: Proposed geometry of the system A0535+26 to explain the observed features. See text for details.

The timescale which determines the disk evolution is the magnetic timescale τ_m due to dissipation by magnetic coupling, defined as [70]

$$\tau_m \approx 25 \frac{\Sigma}{B^2 R_m r^2} \tag{7.5}$$

where Σ is the angular momentum of the disk and B is the magnetic field strength at $r = R_m$. In fact, we have that the hydrostatic dissipation and the turbolent viscosity give timescales much more smaller than τ_m [70].

Assuming that the majority of the disk angular momentum is transferred to the neutron star during the flares, we will have that

$$\Sigma = I \, \Delta\omega \tag{7.6}$$

where I is the moment of inertia of the neutron star and $\Delta\omega$ is the difference between the angular velocities before and after the flare.

For the April flare we obtain $\tau_m \sim 1^d$, which is just the observed value for the flux rise time. In this way is further explained why the delay is greater when the luminosity (and consequently the accreted mass) is greater.

The bigger problem regarding A0535+26 is about if the source is totally switched off during the quiescence phase, or if its luminosity is low but different from zero. For example, another X–ray transient, A1118-61, has been detected *also* in the 'OFF' state [53] (without pulsed emission), therefore making not valid the propeller effect here considered.

7.3 Low–mass X–ray pulsars: Her X-1

The X–ray binary system Her X-1 is certainly the most studied X–ray binary system. Its importance resides in the fact that, being its orbital parameters

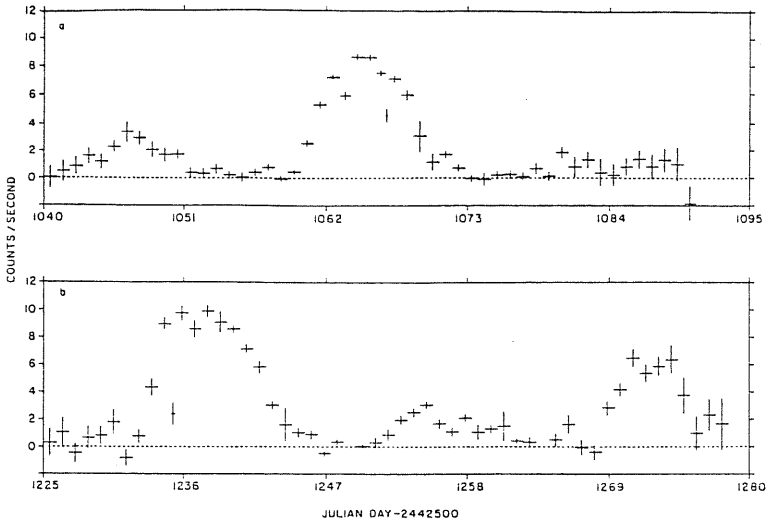

Figure 7.12: The 13–80 keV count rate due to Her X-1, with background subtracted, averaged in time bins of duration less than 1^d. The reduced Julian Day (Julian Date less 2,444,500.0) is given in the horizontal axes. The error bars indicate $\pm 1\sigma$ statistical errors. The two low points at RJD 1035.2 and RJD 1066.5 correspond to pre–eclipse dips.

known, because we can observe an X–ray eclipse (see Section 6.1 for the determination methods for orbital parameters), the detailed study of its evolution and of the physical processes which are at the base of the X-ray emission is possible. In fact, the cyclotron resonance line was observed for the first time in its spectrum [85], which permitted the determination of the magnetic field at the compact object surface. The value of $(3-5)\cdot 10^{12}G$ leaves no doubt about the nature of this object: a neutron star. In Her X-1 is further clearly visible the presence of an accretion disk; therefore the accretion process is by Roche-lobe overflow.

Now we will describe into details all the peculiarities of this object. First of all its flux variation: Her X-1 presents three types of variations, with three different timescales (see Fig. 7.12 [19]):

- Pulsation with period $P_p = 1^s.24$.
- Variations due to orbital motion, with period $P_o = 1^d.7$.
- A cycle of period $P_c = 35^d$.

While for the first two periodicities the cause is clear, for the third there are still big problems. All the models which try to explain the 35^d cycle introduce a *precessional* motion, but regarding the object which is preceding nothing is clear.

We can summarize the models on the base of the object which precedes (see Fig. 7.13 [66]):

1. Precession of the outer part of the tilted accretion disk, which precedes in the tidal field of the companion [35];

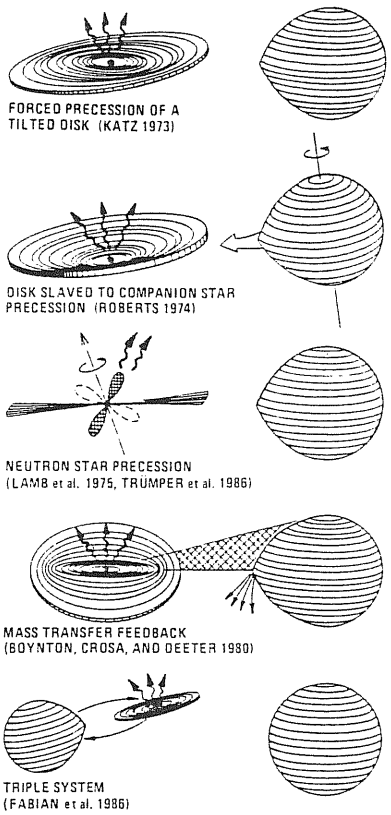

Figure 7.13: Precessional scenarios for Her X-1.

2. Precession of the optical companion in the tidal field of the compact object, followed then by the precession induced on the disk [72];

3. Precession of the neutron star due to a slightly oblateness [42,44];

4. Precession of the outer part of the accretion disk, due to the asymmetric matter accretion flux which arrives from the companion [2];

5. Triple system formed by the optical companion plus a binary system containing a preceding disk [14].

The fact that a lot of models have been proposed is due to the fact that anyone, alone, is able to explain all the observed phenomena.

Now, let we see which are the pulsation characteristics (see Table 7.4 for the system parameters). As it is possible to see from Fig. 7.14 [38], the light curves are characterized by having [63]

- Pulsation with 1 peak for $2 \leq E \leq 20$ keV;
- Pulsation with 2 peaks for $18 \leq E \leq 60$ keV;
- Pulsation with 1 peak for $66.6 \leq E \leq 88.5$ keV.

The transitions 1 peak $\rightarrow$ 2 peaks and 2 peaks $\rightarrow$ 1 peak occur in exceptional points of the energy spectrum; in fact they occur at $E \sim E_c \sim 25$ keV

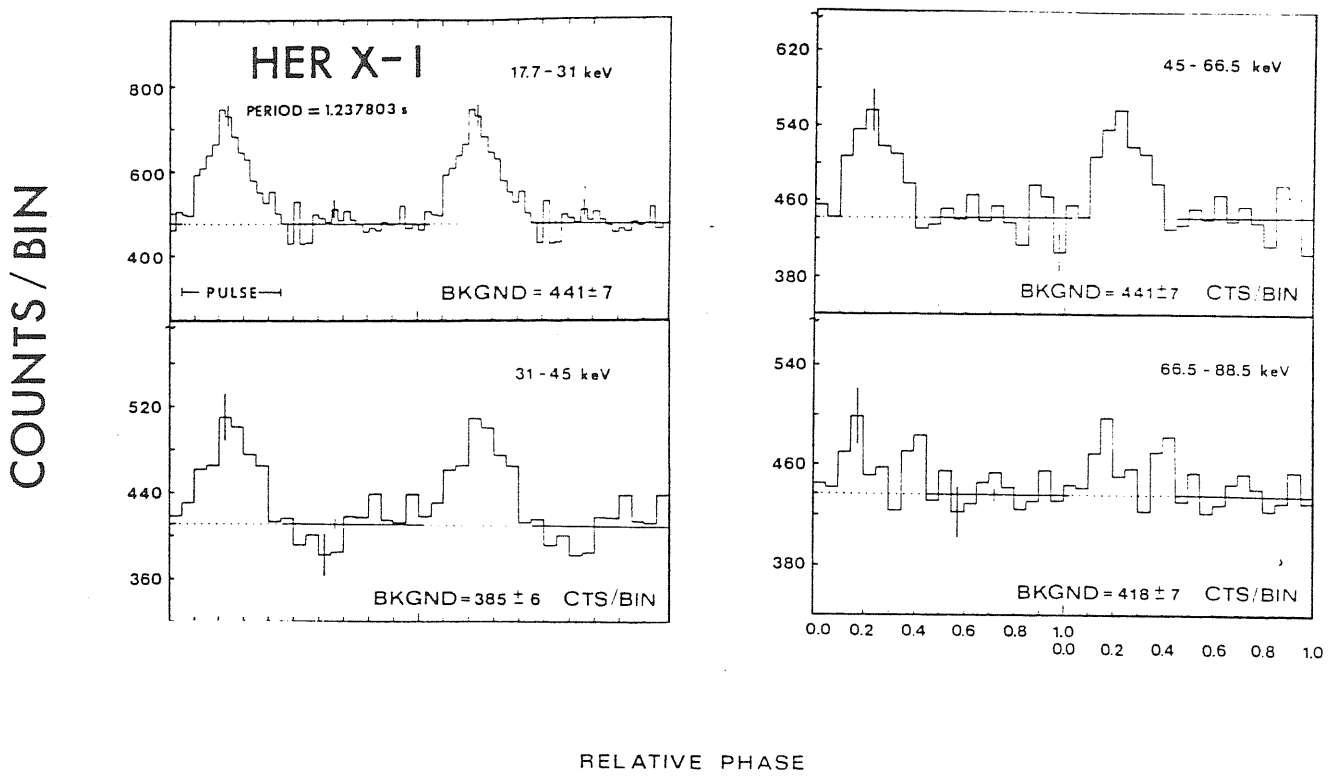

Figure 7.14: Her X-1 pulse profiles for four different energy intervals. Horizontal lines represents average count rates outside the pulses (phases 0.45–0.05). Background values given are total off–source counts. Error bars indicated are $\pm 1\sigma$ statistical deviations.

$a_x \sin i = 13.206 \pm 0.006$ lt-s
$e < 0.0003$
$i = 87° \pm 3°$
$d = 4.5$ kpc
$T_e = 0^d.24 \pm 0^d.01$
$M_c = 2.18 \pm 0.11\ M_\odot$
$M_x = 1.30 \pm 0.14\ M_\odot$
$T_0 = 2,444,521.4652$ JD
$P_p = 1^s.2377991 \pm 0^d.0000004$
$\dot{P}_p/P_p = -(2.9 \pm 0.2) \cdot 10^{-6}$ yr^{-1}
$P_o = 1^d.7001644 \pm 0^d.0000003$

Table 7.4: Parameters of the Low–mass X–ray binary pulsar Her X-1.

and at $E \sim E_{line} \sim 58$ keV, respectively. The pulsation is present during all the 35^d cycle and does not show any dependence of the phase on energy [31].

It is interesting to remark that the pulsation is present also in the optical companion, HZ Her, with the same period and in phase [32]. The spectral type of this object is A for the surface turning towards the X–ray source, and F for the other [10].

In the context of a model which describes the system by synchronous rotation of regions which emit in optical, the observed Doppler shifts show that the optical pulsations come from at least three different, distinct regions [51]:

1. The limb of the companion star of the X–ray pulsar;
2. The outer part of the accretion disk/accretion flux along the line of sight;
3. The terminal part of the accretion flux closer to Her X-1, which is illuminated by the X–rays.

The first two regions are zones in which a reprocessing of the X–ray pulsation occurs, while the third is due to the primary emission from the neutron star.

The spectra coming from these regions are different, because from region (3) the spectrum is thermal while from (1) and (2) is not [65]. This means that in the total spectrum we have to see a 'soft' excess, and in fact in Fig. 7.15 [65] this soft excess is clearly visible, which luminosity is about a tenth of the total one.

About the disk structure, one of the models describes it in the following terms [63]:

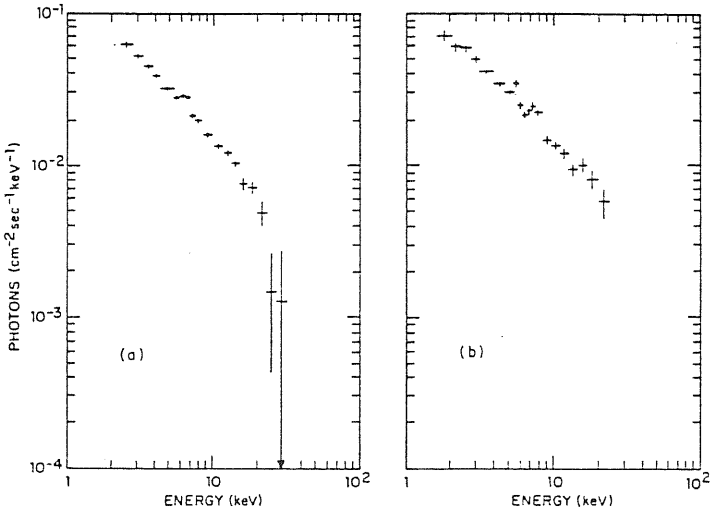

Figure 7.15: Hercules X-1 incident energy spectra, in which are clearly visible the lines due to the iron fluorescence at 6.4 keV.

The disk is optically thick, geometrically thin, and consists of a series of rings tilted with respect to the orbital plane and twisted each others;

In the final part of the disk there is the Alfvén shell, where the accreted matter suffers a drastic change, because in this region matter is not more confined in a thin strip (the disk is concave);

Around the disk an optically thin corona is present (but it is geometrically thicker than the disk);

The accretion flux between the inner Lagrangian point and the disk is not steady (this is the most important point; we will discuss it later).

Solving the hydrodynamical equations for the disk we obtain a configuration as that shown in Fig. 7.16 [63], in which the outer part of the disk assumes a 'fuzzy band' shape. In this way are well evident how the 'ON' and 'OFF' states originate.

About the precession, we have two possibilities [66]: if the precession is *external* to the disk then the models (1), (2) and (3) of page 104 do not work well; the only model which give results in agreement with the observations, at least qualitatively, is (4). In this model, which is a modification of (1), the asymmetric accretion flux forms when the shadow of the disk passes over the inner Lagrangian point. Therefore we have a decrease and then an (almost) complete disappearance of the X–ray radiation when the shadow comes. In this way the radiation pressure disappears and the accreted matter acquires not only a radial component of the velocity, but also a perpendicular component, due to the shadow motion perpendicular to the orbital plane.

This vertical velocity would be greater than the sound speed in the medium v_s, therefore the maximum tilt of the disk edge can be $\theta_{max} = (v_c/\omega r_n)$, where ωr_n is the orbital velocity with respect to the compact object [66].

If, on the other hand, the source of precession is *internal* to the disk, then there is the problem of how the precession is transferred throughout

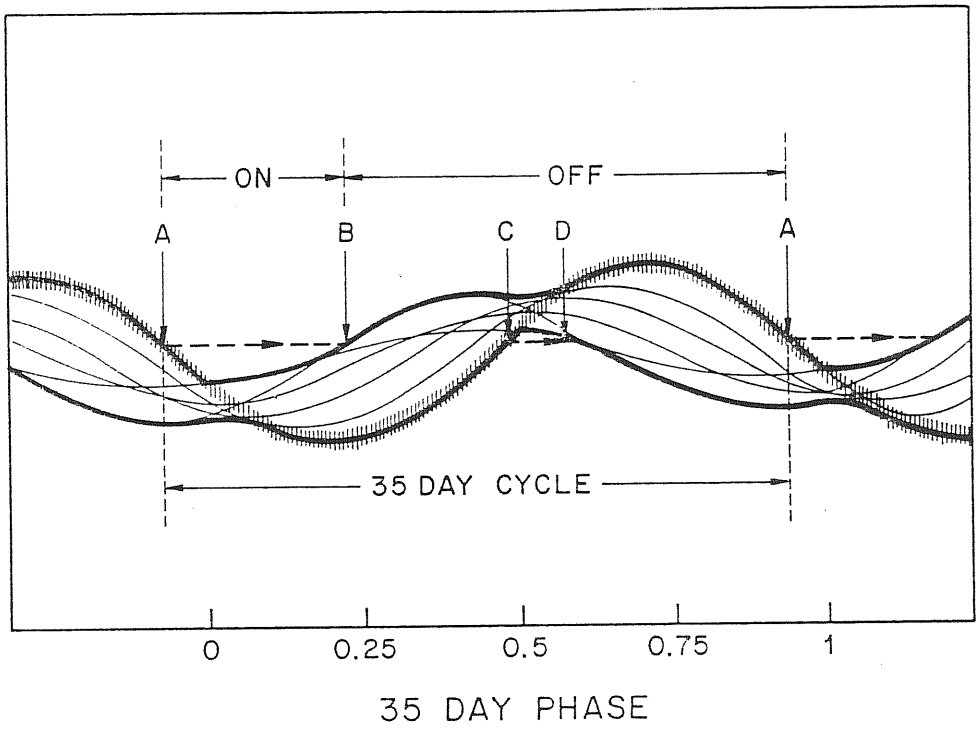

Figure 7.16: Panoramic view of the disk as seen from the neutron star. The outermost disk ring is identifiable by a 'fuzzy band'; its inclination angle is arbitrary in the model, but is here—for clarity—shown unrealistically large. The dotted line shows the position of the Earth at different moments in the 35^d cycle; its height above the orbital plane is chosen to give the best agreement with observations. Easily identifiable features are the 'ON' state (A–B), the 'OFF' state (B–A) and the 'short ON' state (C–D). Low energy absorption is expected when the outermost ring crosses the dotted line (points A and C).

the disk [66].

We want to remark, further, that the three periodicities we discussed above, are due to geometrical effects: it is not the radiation mechanism which varies, but the direction of the radiation region (in the case of P_p) and some shield effect (in the case of P_o and P_c).

But a non–pulsating, irregular part in the X–ray flux exists, which is clearly visible in all three periodicities. In fact we have the so–called 'absorption dips' [60], due to obscuration caused by the accretion disk; a second type of variability is when the radiation is not obscured by the disk or by the companion. Finally, a third type of variability (also this in intensity) is in the 35^d cycle. This cycle is not a stable cycle: we can observe variation of the order of a day.

About this latter case there are two explored possibilities [59]:

1. The quality of the clock which produces the periodicity is good and the observed fluctuations may be described in terms of white *phase* noise.

2. The intrinsic quality of the clock is not good and the fluctuation may be described in terms of white *period* noise.

From an analysis using deterministic chaos [78,4] methods the following results were obtained [59]:

- The time variability during the eclipses, as that of the background, are purely stochastic and do not show any chaotic component.

- The time variability obtained observing the source when it is not obscured by the accretion disk or the companion, shows a strong chaotic component. From this analysis we obtain that there are good chances to be able to describe it by a simple model (the minimum number of parameters we need to describe the system is $\sim 2-3$).

- Also the time variability obtained observing the source during the absorption dips shows a strong chaotic component, but this time the minimum number of parameters we need to completely describe the system is very high ($\sim 8-10$) so it is not possible to describe it by a simple model. This may be ascribed to turbolent dynamics, which obscures the radiation coming from the X–ray source.

Finally, it is important to remark that Her X-1 pulsates also in the γ–ray band [71,43] (energy of the order of TeV). In fact we have that [43]

$$P_p^\gamma = 1^s.23593 \pm 0^s.00018 \tag{7.7}$$

which is $(0.16 \pm 0.02)\%$ greater that that associated to the X–ray pulsation. This pulsation is visible only when the source is in the 'ON' state [43].

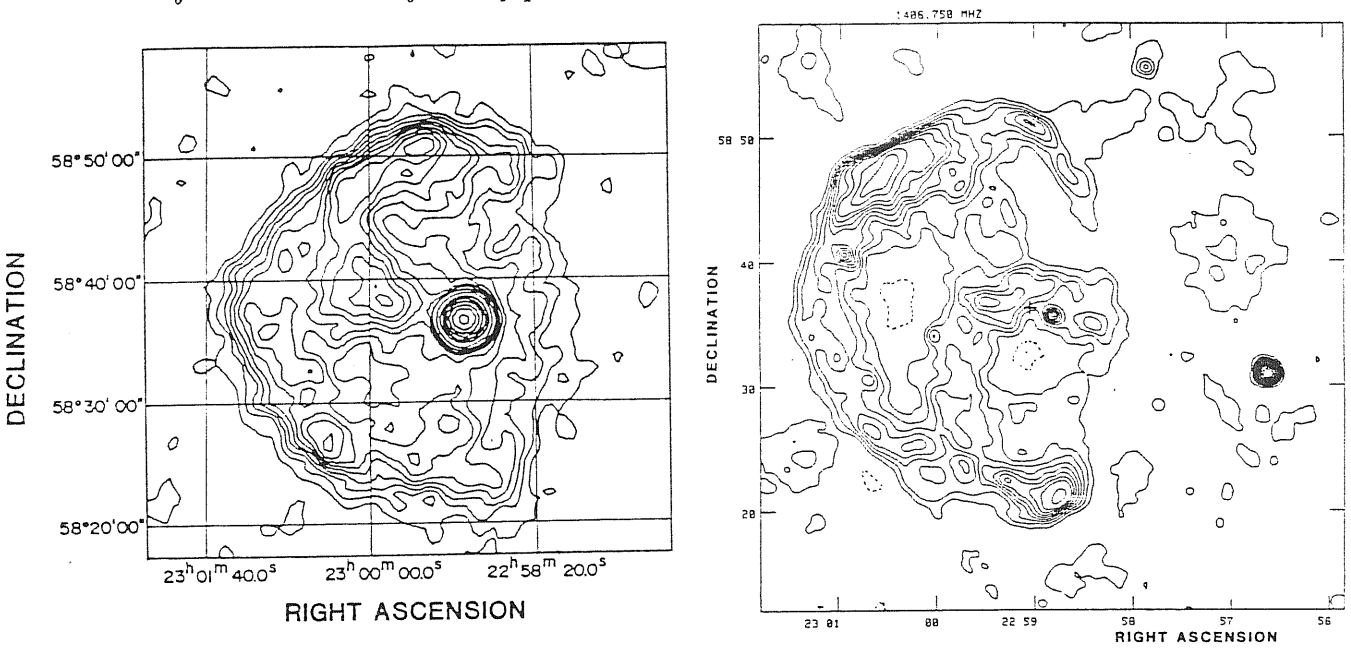

Figure 7.17: *(a)* X–ray image of G109.1-1.0 obtained with the *Einstein* IPC detector, July 1980. Relative contour levels are 20, 30, 40, 52, 67, 83, 100, 118, 142, 200, 332, 470, 664, 940, 1328, 1878 and the map peak corresponds to a level of 2134.
(b) VLA 20 cm map of G109.1-1.0 at a resolution of 1 arcmin, corrected for the primary beam of the array antennas. The peak flux is 0.60 Jy/Beam. Relative contour levels at $0.30 \cdot 10^{-2}$ (-2, 2, 3, 4, 5, 6, 7, 8, 10, 12, 14, 16, 20, 24, 28, 32, 36, 40).

7.4 Low–mass X–ray pulsars: 1E 2259+586

The X–ray source 1E 2259+586 is certainly an extraordinary object. First of all, it is the only X–ray binary pulsar associated with a supernova remnant. From Fig. 7.17a [20] we may observe a semicircular structure with at its center a point–like source, and a large scale jet which links the outer part of the diffuse emission to the pulsar. Comparison with radio image of Fig. 7.17b [20] makes immediately the following features stand out:

- The structure of the X–ray and radio emission is similar, but there are differences in the emission distributions in the supernova remnant.
- The structure of the jet is present in the X–ray image but it is not present in the radio image.
- The radio emission presents two arcs which intersects each others.
- A pointlike radio counterpart of the X–ray source does not exist.
- The peaks in the X–ray and radio emission do not coincide.
- The $C^{12}O$ emission suggests an interaction between the supernova remnant and a background molecular cloud (also observed in radio).

$0.16 \leq a_x \sin i \leq 0.21$ lt-s
$200° \leq \omega \leq 280°$
$0.15 \leq e \leq 0.55$
$d = 3.6 \pm 0.4$ kpc
$f(M) = 0.0080 \pm 0.0002\, M_\odot$
$1.0 \leq M_x \leq 1.4\, M_\odot$
$M_c \geq 0.2\, M_\odot$
$T_0 = 2,445,620.0$ JD
$P_p = 6^s.978720 \pm 0^s.000006$
$\dot{P}_p/P_p = +(3.3 \pm 0.2) \cdot 10^{-6}$ yr^{-1}

Table 7.5: Parameters of the Low–mass X–ray pulsar 1E 2259+586.

– The radio spectrum is constant along the supernova remnant and has the typical frequency dependance $S \propto \nu^{-\alpha}$, with $\alpha = 0.45$.

The association of 1E 2259+586 with a supernova remnant allows us to obtain, by means of the relation between radio surface brightness and distance [7], the distance, which result (see Table 7.5) $d = 3.6$ kpc. At this distance, its luminosity is $\mathcal{L}_x = 2 \cdot 10^{35}$ erg/sec. This value of X–ray luminosity makes implausible the hypothesis that 1E 2259+586 is a isolated object: in fact, if the observed energy were completely due to the conversion of kinetic rotational energy into electromagnetic energy, we will have

$$\mathcal{L}_x \approx \frac{1}{2} I\, \Omega_p \left(\frac{d\Omega_p}{dt}\right) \simeq 10^{32} \text{ erg/sec} \tag{7.8}$$

where I is the moment of inertia of the neutron star and Ω_p is the pulse frequency. This value is calculated for the observed value of $\dot{P}_p$ and is at least three orders of magnitude smaller than the observed X–ray luminosity. Further, any radio counterpart of 1E 2259+586 has been observed [26], and the pulse period is relatively long, with respect to other isolated (radio) pulsars [48].

All these facts favour the hypothesis that 1E 2258+586 is a binary system. There is another model [15], which considers this object as a single one. It is accreting matter from the surrounding molecular cloud, observed in radio. This model has several problems, the most important of which regards the way in which matter is accreted.

Because of the small inferred absolute magnitude of the optical counterpart ($M_b > 23$) [15], the companion must be a low-mass star and therefore the accretion should occur by means of Roche-lobe overflow via accretion disk.

From the observations of the optical counterpart we have two possible candidates, with one which shows pulsations in the infrared band [51]. The frequency of this pulsation is however 285.6 mHz, different from the 286.6

mHz observed in the X–ray band. This difference is interpreted as due to interaction of the X–ray radiation with an orbital companion. From the fact that $\mathcal{L}_x/\mathcal{L}_{opt} \geq 100$, we can deduce that this companion of the neutron star cannot be a massive, main–sequence star.

From the theory of supernova remnants we can obtain the age of the object [23], which results to be $T \approx 10^4$ years. Because the timescale needed to create a close binary system is much greater than T (it is of the order of 10^8 years), the pre–supernova configuration has to be in turn a close system. This suggests that the neutron star was born by a collapse induced by accretion onto a white dwarf [77] (see Section 3.3). It is also important to remark here that in a supernova explosion at least the binding energy of the neutron star has to be relaxed, therefore the original system had to be also closer.

As we have seen in section 4.2.1, the torque experienced by a pulsar depends on the adimensional function $n(\omega_s)$, where ω_s is the 'fastness parameter'. Putting the values of the parameters of 1E 2259+586 in the expression of ω_s we obtain $\omega_s \approx 0.44$ (which corresponds to $n(\omega_s) \approx -0.51$). This value is very close to the critical value ω_c and this suggests the hypothesis that the neutron star is spinning at a pulse period close to that for which $\dot{P}_p = 0$ [40]. As we have seen, this corresponds to the case in which $R_c = R_m$, where R_c is the corotation radius and R_m is the magnetospheric radius (see Eqs. 4.16 and 4.14, respectively).

Equalling these two quantities, we can obtain the surface magnetic field of the neutron star (we remark, for spherical accretion) [40]:

$$B = (4.9 \cdot 10^{11} G) \left(\frac{M_x}{M_\odot}\right)^{1/3} R_6^{-5/6} \tag{7.9}$$

where $R_6 \equiv R_\star/(10^6 \text{ cm})$ is the neutron star radius in units of 10^6 cm. This value of the magnetic field is surprising low, both for the young age of the neutron star (we normally assume that a neutron star is born with a strong magnetic field, which then decays) and with respect to the magnetic fields observed in other X–ray binary pulsars (which are $\geq 10^{12} G$).

The observation made by the *Einstein* satellite [15] demonstrated that the pulsar spectrum is significantly harder than the spectrum of the surrounding diffuse emission. In fact, both may be fitted with thermal bremsstrahlung laws, with $kT = 0.41 \pm 0.1$ keV and $N_H \approx 6 \cdot 10^{22}$ H/cm^2 for the diffuse emission, and $kT \geq 10$ keV and $N_H \approx 8 \cdot 10^{22}$ H/cm^2 for the emission from the neutron star.

Also the EXOSAT observations found a very soft pulsed spectrum [6] [23]. It is well fitted by a power–law with photon index $\alpha = +4.9^{+3.1}_{-1.5}$ and absorption given by $N_H = 24^{+45}_{-24} \cdot 10^{22}$ H/cm^2 ($\chi^2_{dof} = 0.39$) in the energy band 1.4–4.7 keV.

The spectrum fits also with a thermal bremsstrahlung law, with $kT = 1.0^{+0.6}_{-0.4}$ keV and $N_H = 8^{+16}_{-6} \cdot 10^{22}$ H/cm^2 ($\chi^2_{dof} = 0.30$).

[6] Because of the geometry of the detector, it was not possible to divide the contributions from the neutron star from that of the supernova remnant, therefore the only achievable information is the pulsed spectrum.

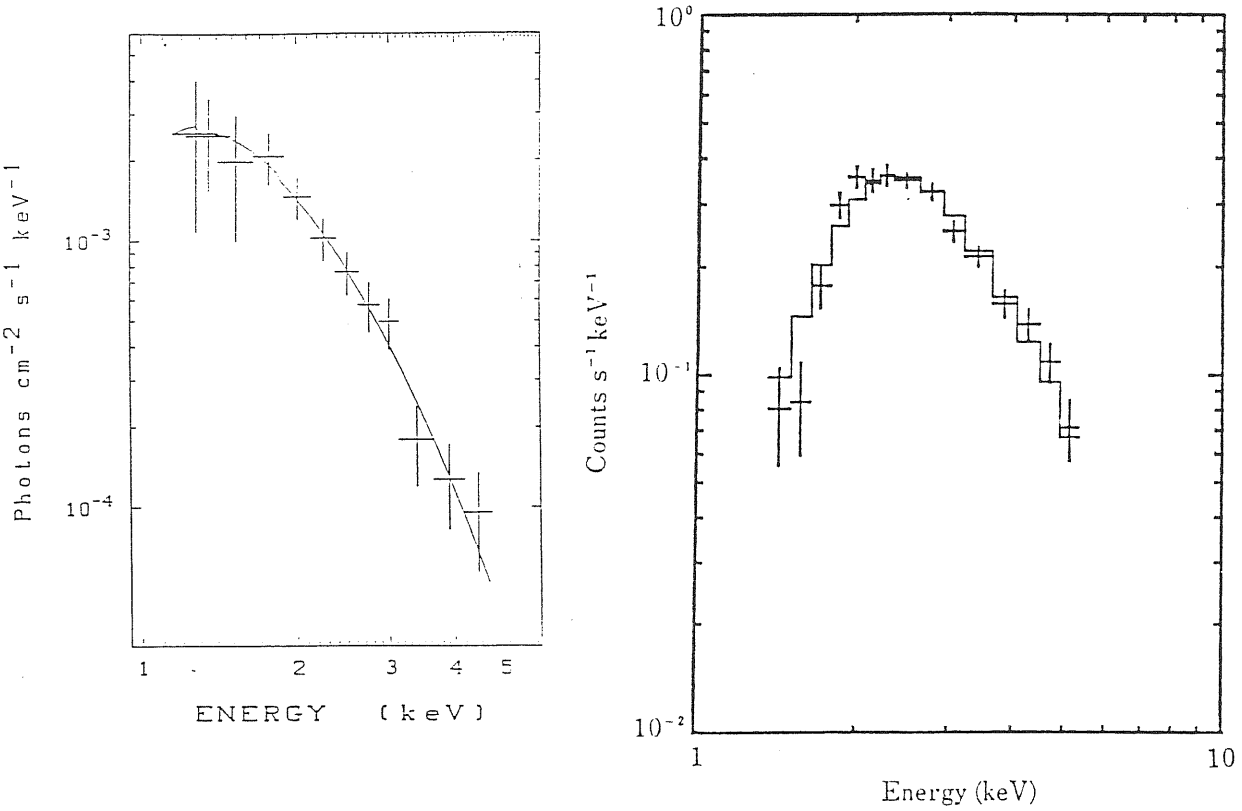

Figure 7.18: *(a)* The combined LE and ME pulsed spectrum of 1E 2259+586 as seen by EXOSAT.
(b) The X–ray spectrum of 1E 2259+586 convolved with the detector response, as seen by TEMNA. The solid line is the best fit power–law model.

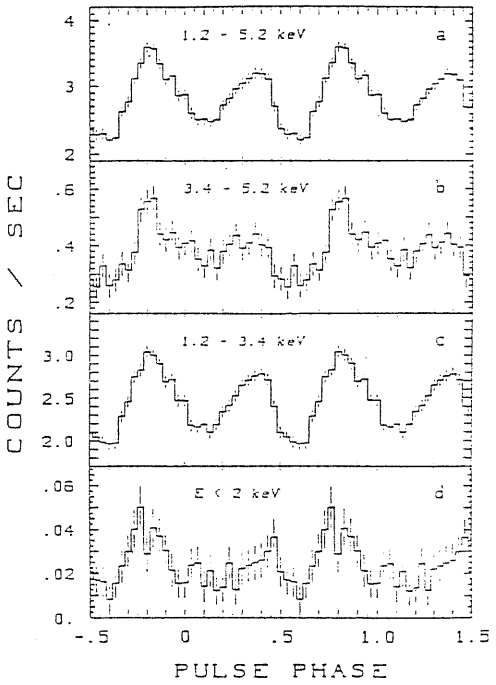

Figure 7.19: The energy dependent pulse profiles of 1E 2259+586 as seen by EXOSAT. Two pulse cycles are shown for extra clarity. The profile has been background subtracted and aspect corrected. Error bars are $\pm$ 1σ and the integration time is about 21^h.

In Fig. 7.18 are shown the energy spectra as given by EXOSAT [23] (a) and TEMNA [40] (b), where the latter is fitted by a power–law, with photon index $\alpha = 3.7 \pm 0.3$ ($\chi^2_{dof} = 1.56$).

The pulse profiles, shown in Fig. 7.19 [23], have the characteristic double peak and, for energies higher than 3.4 keV, the main peak presents a strong, sharp component which is not present for lower energies. It seems that the separation between the pulse and the interpulse increases with the decrease of energy, because of a motion of the interpulse [23] in phase.

About short timescale variability ($\tau < 1^d$) we do not observe significant statistical variations, although the overall intensity varies by a few percent [23].

7.5 High–mass X–ray pulsars: Vela X-1

The optical counterpart of the massive X–ray binary system Vela X-1 is the supergiant HD 77581 [27], of spectral type $B0.5Iab$, a variable star both on short and long timescale. The system, when observed in the X–ray band, presents flaring activity, deep dips and an eclipse, that lasts $1^d.72$ every $8^d.9$ [45,16]. The presence of an eclipse allows the determination of the orbital parameters, which are shown in Table 7.6. The X–ray pulsation is not present in optical (upper limit 0.004 magnitudes [13,75]).

There are several observations that demonstrate the presence of both a strong stellar wind and a dense atmosphere around the primary star and the neutron star [13]:

$a \sin i = 112.70 \pm 0.47$ lt-sec
$a_x \sin i = 111.4 \pm 3.3$ lt-sec
$a_c \sin i = 7.79 \pm 0.74$ lt-sec
$e = 0.0881 \pm 0.0036$
$i = 73°–90°$
$\omega = 152°.8 \pm 2°.2$
$\dot{\omega} = +\,6°.9 \pm 3°.4$ yr^{-1}
$f(M) = 19.12 \pm 0.24\ M_\odot$
$M_c = 23.0^{+3.5}_{-1.5}\ M_\odot$
$M_x = 1.85^{+0.35}_{0.30}\ M_\odot$
$T_0 = 2,443,654.0$ JD
$P_o = 8^d.96443 \pm 0^d.00022$
$\dot{P}_o/P_o = +\,(2.7 \pm 2.6) \cdot 10^{-5}$ yr^{-1}
$P_p = 282^s.787 \pm 0^s.004$
$\dot{P}_p/P_p = -\,(2.3 \pm 0.8) \cdot 10^{-4}$ yr^{-1}
$T_e = 1^d.72 \pm 0^d.04$
$d = 1.9 \pm 0.2$ kpc

Table 7.6: Parameters of the massive X–ray pulsar Vela X-1.

1. From observations in the optical we note the presence of a strong emission profile in the H_α line and a weak "P Cygni" profile in the H_β line.

2. There is also X–ray emission during eclipses, which corresponds to 3.2%, 2.0% and 0.9% of the non-eclipsed emission in the energy bands 2–6 keV, 6–10 keV and 10–20 keV, respectively.

3. The times of transit to the ingress and egress from the eclipse are smaller when observed at higher energy.

4. We observe a gradual decrease in the X–ray intensity observed soon after the ingress in eclipse, at all energy bands.

All these facts take to the conclusion that a strong stellar wind (points 1. and 4.) and a dense atmosphere surrounds the neutron star (points 2., 3. and 4.).

A characteristic of Vela X-1 is to show an excess in the X–ray flux, variable in time, in the low energy band (1–4 keV) [75]. This excess is interpreted as due to inhomogeneities in the stellar wind matter [75,57]. In fact, the possible causes of this excess may be:

1. reprocessing of hard X–ray radiation by an absorbing object which partially obscure the neutron star [25];

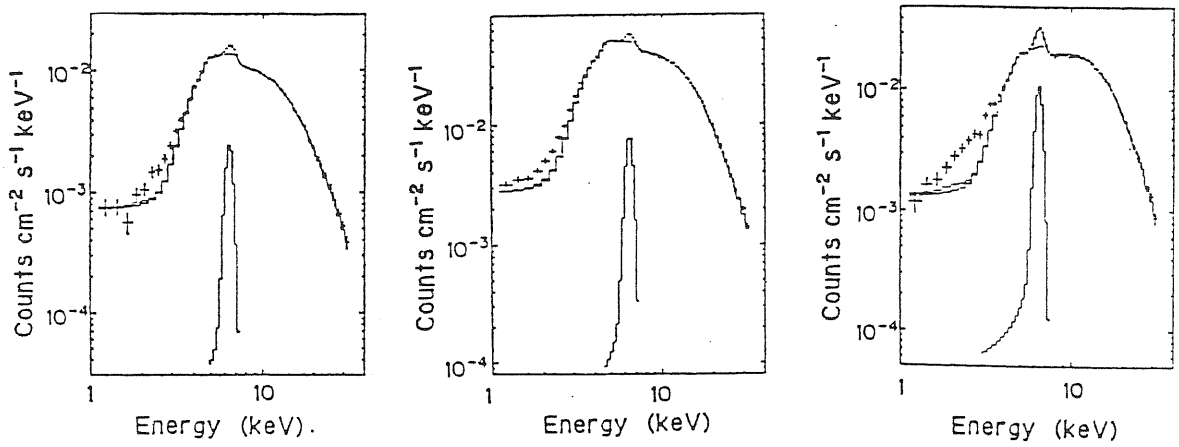

Figure 7.20: Examples of energy spectra with soft excess features observed for Vela X-1. The histograms in the figures indicates the contributions of the iron emission line.

2. different abundances of heavy elements which "yield" soft X–rays, as Oxygen, Sulphur, Magnesium, Iron etc. [34];

3. the effect of ionization on the stellar wind [50];

4. the presence of a region which emits soft X–rays [34].

Because the X–ray flux of the soft excess shows pulsations in phase with that present in hard X–rays [57], the fourth mechanism does not work. The third mechanism is not able to reproduce the observed spectra while the second mechanism should require different atomic abundances for different spectra, which is unlikely. So we are left with the likely first mechanism, in which the inhomogeneous matter might act as clouds which surround the neutron star (see Section 4.1.2) and that intersect our line of sight (this should be the observed dips). In Fig. 7.20 [57] we can see some examples of observed soft excess.

However, it is necessary to introduce, besides this large–scale inhomogeneity, a small–scale inhomogeneity, to explain the time variable soft excess on timescale of ten hours [57]. This timescale corresponds to that necessary to the source for crossing a clumpy region. From this we obtain a length scale of the inhomogeneity region of $\sim 10^{11}$–10^{12} cm.

We have just discussed about the formation mechanism of blobs of matter (see Section 4.2.1), due to the interaction between matter stopped at the magnetopause and the magnetosphere.

Another possibility of formation of disomogeneity is the ionization front (see Section 4.1.1), associated to thermal instabilities [24,33]. In fact, in radiatively ionized regions, the formation of $HeII$ occurs much more easily than in dense matter. Once that $HeII$ is stopped, recombination is sped up by more effective absorption of X–rays. Therefore dense blobs can be formed in the $HeII$ front [57].

Finally, there is the possibility that blobs form because of the radiation pressure of the optical companion [46,41].

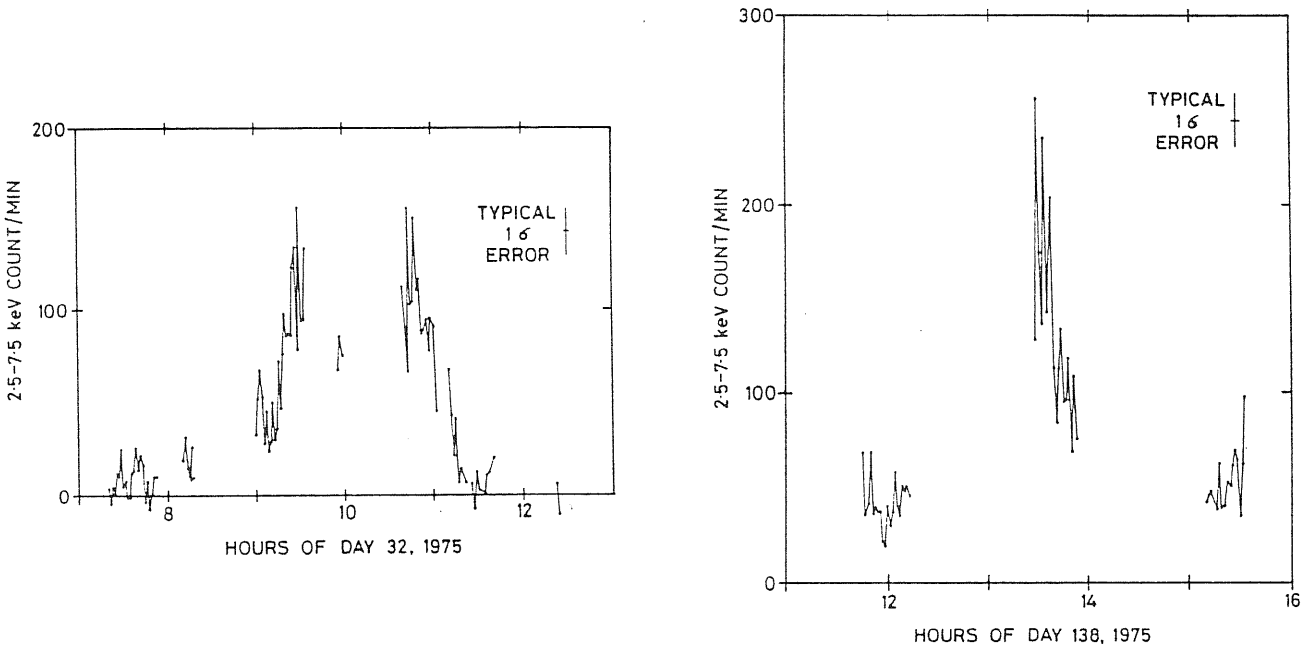

Figure 7.21: Two flaring intervals from Vela X-1, one on February 1977 *(left)* and the other on May 1977 *(right)*.

To obtain the partial obscuration of the X–ray source by blobs, as we observe, we have two limiting cases [57]:

– There are always blobs which fluctuate statistically around our line of sight;

– The obscuration is caused by blobs which cross our line of sight only in limited time intervals.

In the former case we would have to observe always the soft excess; in the latter this excess should be due to an average over a time interval. In both cases, it is not possible to distinguish them because our spectra are averaged in time.

It is important to remark, here, that some authors interpret the gradual decrease of X–ray intensity at the ingress in eclipse as due to an accretion wake [17], due to the motion of the neutron star in the dense atmosphere of HD 77581 (the same occurs for 4U 1700-37 [54]).

The $8^d.9$ modulation is interpreted as orbital motion but, besides a periodic modulation, Vela X-1 presents a non periodic modulation [6], in which the source strongly varies on timescale which ranges from second to month. In Fig. 7.21 [6] two flares observed by *Copernicus* are shown.

In this case the small timescale may be attributed to the 283^s modulation.

The X–ray energy spectrum of Vela X-1 fits well, at lower energies ($E <$

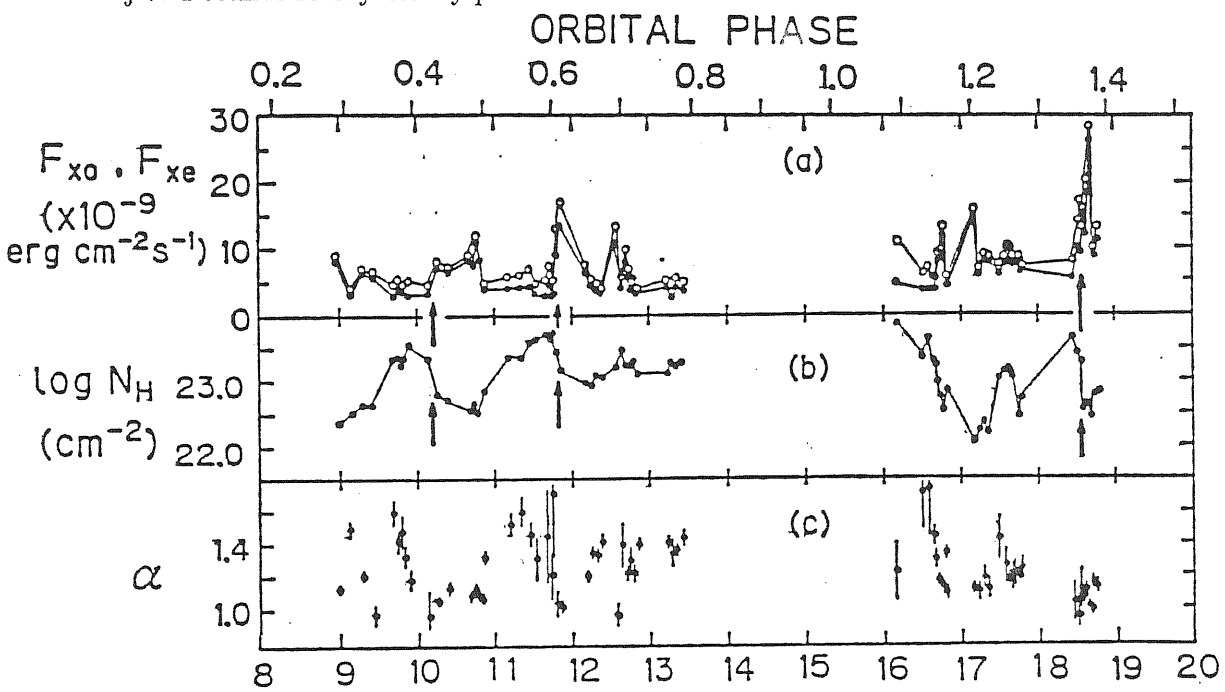

Figure 7.22: Light curves of X–ray flux and spectral parameters for continuum observed for Vela X-1 in March 1983. *(a)* Energy flux in 2–30 keV in units of 10^{-9} erg cm^{-2} sec^{-1} (solid circles: observed flux F_{xo}, open circles: flux corrected for absorption F_{xe}. *(b)* absorption measure $\log N_H$ in units of H/cm^2. *(c)* photon power index α. The upper abscissa indicates the orbital phase of Vela X-1.

20 keV), with a power–law with exponential cut–off, of the form [57]

$$\frac{dN}{dE} = \begin{cases} A(N_H)\left(\dfrac{E}{E_0}\right)^{-\alpha} & \text{for } E \le E_c \\ & \text{Photons/cm}^2 \text{ sec keV} \\ A(N_H)\left(\dfrac{E}{E_0}\right)^{-\alpha} \exp\left[\dfrac{-(E-E_c)}{E_f}\right] & \text{for } E > E_c \end{cases} \tag{7.10}$$

with $E_0 = 10$ keV, while the Iron emission line is described in terms of a single Gaussian distribution function [57]

$$\left.\frac{dN}{dE}\right|_{line} = \frac{I_l}{\sqrt{2\pi}\Sigma_l} \exp\left[-\frac{(E-E_l)^2}{2\Sigma_l^2}\right] \tag{7.11}$$

where I_l, E_l and Σ_l are the line intensity, energy and intrinsic broadening (related to the FWHM Γ_l by $\Gamma_l = 2.355\Sigma_l$), respectively.

The spectrum parameters are shown in Table 7.7 [57], as a function of the orbital phase. We can see that while the cut–off energy is stable, the folding energy scatters over a wide range of values. During flares the spectrum becomes harder ($\alpha \approx 1$) than that of the normal state [57], as can be seen from Fig. 7.22 [57].

For energies higher than 26 keV the energy spectrum fits also well with a thermal bremsstrahlung law [57,81], with $kT = 10.3^{+0.3}_{-0.4}$ keV [57]. The value

Orbital phase ϕ_o	0.20	0.37	0.65	0.70
Power index α	1.12 ± 0.02	1.06 ± 0.02	1.30 ± 0.03	1.15 ± 0.05
Column density N_H (10^{22} H/cm^2)	1.14 ± 0.12	4.64 ± 0.12	10.5 ± 0.4	18.7 ± 0.8
Cut–off energy E_c (keV)	16 ± 1	16 ± 1	17 ± 4	13 ± 2
Folding energy E_f (keV)	32 ± 7	39 ± 4	89 ± 52	80 ± 23
Iron line energy E_l (keV)	6.38 ± 0.14	6.44 ± 0.04	6.41 ± 0.08	6.41 ± 0.08
Iron line intensity I_l (10^{-3} Ph.cm^{-2}sec^{-1})	3.8 ± 1.4	9.2 ± 0.9	2.2 ± 0.5	2.7 ± 0.7
Reduced χ^2_{dof} (78 dof)	0.67	1.20	1.36	1.00

Table 7.7: Parameters for Vela X-1 spectra observed by TEMNA in March 1983.[a]

[a] Quoted errors are all single parameter 90 % confidence limits.

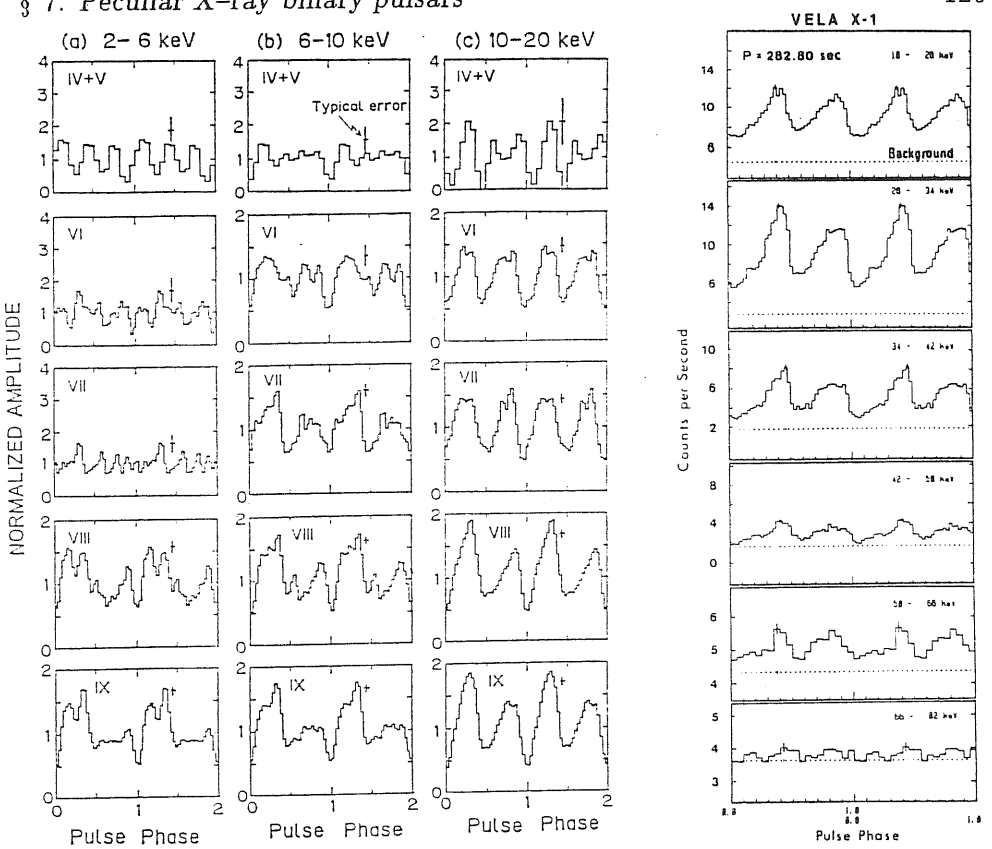

Figure 7.23: Time–averaged pulse profiles for the 283^s pulsation of Vela X-1. *(left)* Evolution of pulse profiles along the eclipse at low energies. *(right)* High energy pulse profiles; the dashed lines indicate the off–source background rate.

of N_H increases gradually with the orbital phase, with occasional increases on 1^d timescale close to the lower conjunction of the neutron star in the binary phase.

Let us remark here that the X–ray intensity increase occurs when N_H is decreasing, several hours after its peak.

The pulse period history of Vela X-1 is very complex, because this source shows both spin–up and spin–down episodes, in which the erratic variations have timescales which can arrive at half the orbital period [56,12]. This variations are explained as variation in the accretion torque which the neutron star feels because of the inhomogeneity of the accretion matter (the observation of spin–down rules out the possibility of disk accretion).

About the pulse profile, it strongly varies with energy [1] (therefore the spectrum varies with the pulse phase). We observe a complex structure at lower energies, but at increasing energy the characteristic double peak appears, with asymmetry between the two (see Fig. 7.23 [75,81]). At energies higher than $\sim$ 50 keV the secondary peak disappears.

As in A0535+26, also for Vela X-1 there are variations from pulse to pulse, and in Fig. 7.24 [81] the scattered plot around the mean light curve is shown (for a discussion of these variations see A0535+26).

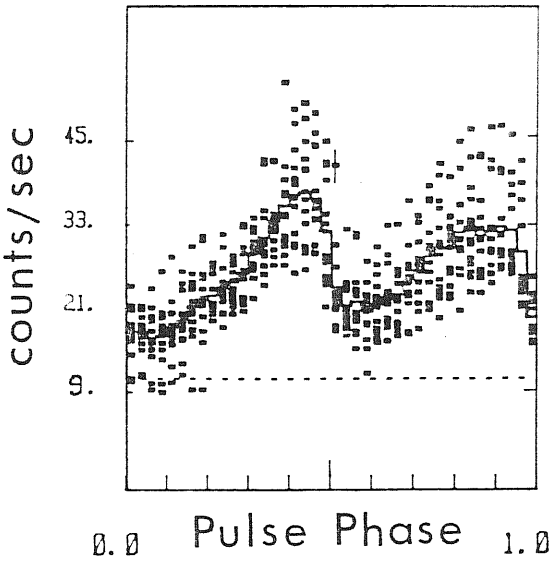

Figure 7.24: Superposition of all 15 pulses observed for energies 18–50 keV. The solid curve is the average of all the data, the dashed line is the off–source background. A typical $\pm 1\ \sigma$ is indicated for one data point.

For Vela X-1 an analysis was performed to search for apsidal motion [11]. In fact the classical apsidal motion (advance) is quite different from the relativistic one (which is, normally, much more smaller), because it is due to tidal and/or rotational distorsion of one or both the components the binary system. The advance rate depends on the mass distribution, so its measurement allows us to check star models [39].

The apsidal advance is great when the radius of at least one of the components the system is an appreciable fraction of the orbital separation, therefore Vela X-1 is a good candidate for the success of this measure. In fact the orbital parameters in Table 7.6 were obtained with this method.

Finally, we remark that also for Vela X-1, as for Her X-1, a pulsation has been observed in the γ–ray band [58] ($E_\gamma > 1.5$ TeV). The pulse period is $P_p^\gamma = 282^s.805$, and the pulsation was observed also during a γ–ray burst. Instead, there is not evidence for the $8^d.9$ pulsation [58].

The luminosity of Vela X-1 in this energy band is $\mathcal{L}_\gamma = (2.4 \pm 1.1) \cdot 10^{34}$ erg/sec [58].

7.6 High–mass X–ray pulsars: GX 301-2

The X–ray binary system GX 301-2 is very similar to Vela X-1, because for both there are direct proofs of the existence of a strong stellar wind (from the observation of P Cygni profiles in the lines of the optical spectrum [62]). The fact which renders the observations of GX 301-2 more difficult than that of Vela X-1 is the absence of an eclipse and the longer orbital period [92,90,74], which asks for longer observation time to monitor source pulsation.

From the observational parameters, shown in Table 7.8, we can immediately see that the system is too large for a Roche-lobe overflow to occur

$$a_x \sin i = 371.2 \pm 3.3 \text{ lt-sec}$$
$$e = 0.472 \pm 0.011$$
$$\omega = -50^\circ.1 \pm 2^\circ.6$$
$$i \leq 78^\circ$$
$$P_o = 41^d.508 \pm 0^d.007$$
$$P_p = 696^s.665 \pm 0^s.017$$
$$\dot{P}_p = -(2.44 \pm 0.19) \cdot 10^{-7}$$
$$\ddot{P}_p = +(7.4 \pm 0.8) \cdot 10^{-14} \text{ sec}^{-1}$$
$$f(M) = 31.9 \pm 0.8\ M_\odot$$
$$M_c \geq 35\ M_\odot$$
$$d = 1.8 \pm 0.4 \text{ kpc}$$

Table 7.8: Parameters of the massive X–ray pulsar GX 301-2.

[37], also at the periastron passage, therefore the system will be a wind–fed system.

The optical counterpart of GX 301-2 is the supergiant Wray 977, of spectral type $B1.5\,Ia$, the mass of which, spectroscopically determined, is $30 \pm 5\ M_\odot$ [62].

The main characteristic (and at the same time the more difficult problem to solve) of GX 301-2 is that the system presents an outburst activity in the low energy X–ray band ($E < 20$ keV), lasting about four days [93], which occurs $1^d.8 \pm 0^d.4$ *before* the periastron passage [93,68]. This anticipation is very difficult to understand in terms of the standard theory which estimates the flaring activity as due to an increase in the accretion rate approaching the periastron [61] (and therefore the maximum in the emission at the passage of the neutron star to the closest distance from the optical companion).

The active state is very variable, with minima which are 25 times the quiescence state, and variations of a factor two in less than half an hour [93,74]. This phase of activity may be described [74] both in terms of a sum of a smoothly varying component, which increases by a factor four with respect to the average, together with a flaring activity which may cause a further increase of five times on timescale of hours; and completely in terms of a flaring activity which occurs randomly, with an increase in intensity of more than an order of magnitude on timescale of hours.

The temporal variability of GX 301-2 may be described in terms of three regions which emit at different intensities [74]:

1. The *high* activity region, near the periastron, which is centered at $\phi_{orb} = 0.98$ and lasts for about the 10% of the binary period.

2. The *low* activity region, which lasts for 10–20% of the orbital period

Epoch		α	E_c (keV)	E_f (keV)	χ^2_{dof}
1:	*High*	0.49 ± 0.18	21.3 ± 0.5	8.2 ± 0.3	2[illegible]0
	Mean	1.32 ± 0.22	25.2 ± 1.5	8.0 ± 1.1	21.5
	Low	1.05 ± 0.40	24.6 ± 2.0	3.0 ± 1.9	5.6
2:	*High*	0.68 ± 0.23	22.5 ± 0.8	7.4 ± 0.6	6.1
	Mean	1.46 ± 0.15	25.3 ± 1.2	7.4 ± 0.9	8.0
	Low	0.46 ± 1.04	25.7 ± 3.3	2.7 ± 4.2	20.9

Table 7.9: Spectral parameters of the massive X–ray pulsar GX 301-2.

and is centered at $\phi_{orb} \sim 0.2$.

3. The *average* activity region, which includes a second, smaller minimum, which constitutes the average emission level.

The energy spectrum in region 1 does not show variations in mean intensity and spectral shape for $E > 21$ keV [74], in two observations (early and mid-1978); for lower energies a variation ($\sim +19\%$) in the mean intensity has been observed, which can be attributed or to a difference in the X–ray production or to a variation in the photoelectric absorption in the circumstellar matter [74,93].

The spectra fit with a power law with two cut–offs [93,74]: the spectrum varies with orbital phase, in accordance with the three regions of activity. The spectral parameters are shown in Table 7.9 with the numbers one and two referring to the two observations, made by the $HEAO$–1 $A2$ experiment. The "high" state spectrum can be fitted both with an emission line ($\chi^2_{dof} = 1.10$) and an absorption line ($\chi^2_{dof} = 1.00$) [74].

The line parameters are [74]:

$$\left.\begin{array}{l} E_l = 30.5 \pm 0.5 \quad \text{keV} \\ I_l = (1.0 \pm 0.3) \cdot 10^{-2} \quad \text{Phot/cm}^2\text{sec} \end{array}\right\} \quad \text{Emission line} \qquad (7.12)$$

$$\left.\begin{array}{l} E_l = 23.8 \pm 0.3 \quad \text{keV} \\ EW_l = 1.3 \pm 0.3 \quad \text{keV} \end{array}\right\} \quad \text{Absorption line} \qquad (7.13)$$

The energy of the emission line is very close to the iodine K–edge energy, which is 33.17 keV.

In Fig. 7.25 [74] are shown the energy spectra of the three regions, from which we can see that the spectral shape is generally constant in time (the

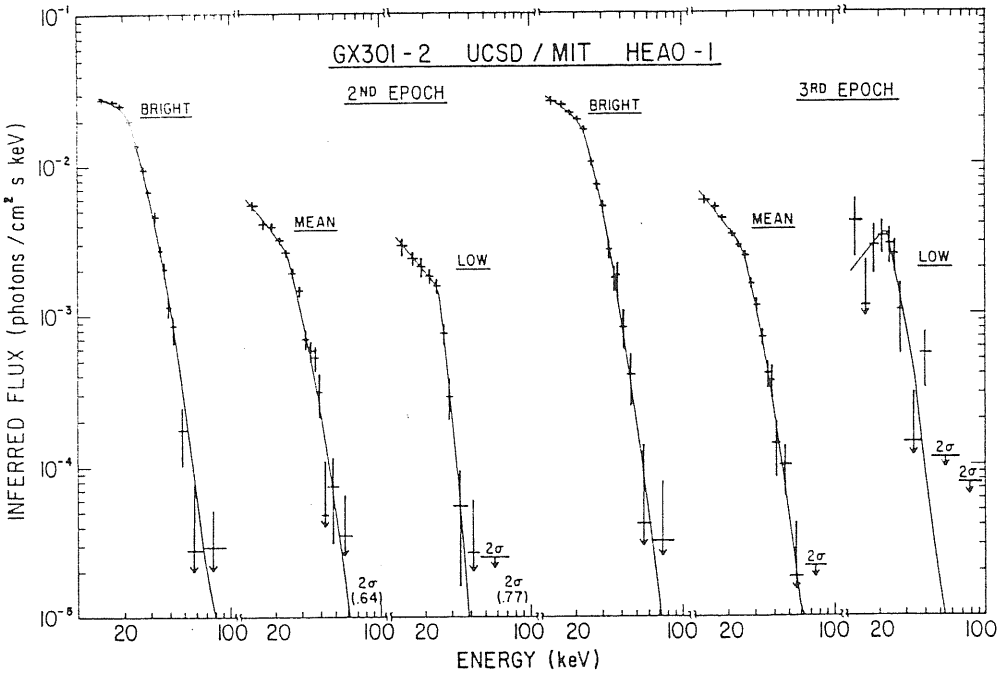

Figure 7.25: The "high" ($0.9 < \phi_{orb} < 1.0$), "mean" ($0.0 < \phi_{orb} < 0.1$ and $0.3 < \phi_{orb} 0.8$) and "low" ($0.1 < \phi_{orb} < 0.3$) spectra of GX 301-2 for both *HEAO 1* observing epochs. The solid lines are the best fit spectra, as described in the text.

two epochs are separated by six months). The X–ray flux drops by a factor two, and the continuum possibly temporarily steepens. Because the spectra of lower and higher activity are similar, the emission process responsible of the flaring activity is probably the same than that responsible of the average flux.

The energy spectrum at lower energy ($E < 20$ keV) presents (see Fig. 7.26 [93]) very well visible the line due to the iron fluorescence at 6.46 ± 0.01 keV, while the absorption is much higher in the quiescence phase ($N_H \geq 10^{24}$ H/cm^2) than in the flaring phase ($N_H = (6.06 \pm 0.16) \cdot 10^{23}$ H/cm^2) [93].

As we can see from Fig. 7.27 [93], the pulse profile is strongly energy dependent, and it shows the characteristic double peak. It is interesting to note that in three occasions, corresponding to January 27.27, 28.78 and 29.28 the pulsation disappeared [93].

The pulse period history is very complex, as that of Vela X-1, showing both spin–up and spin–down episodes [52,36]. The tentative model of the source based on the following assumptions [74]:

- The stellar wind is not influenced either by the X–ray emission or by the gravitational field of the neutron star.
- There is not any accumulation of matter close to the neutron star.

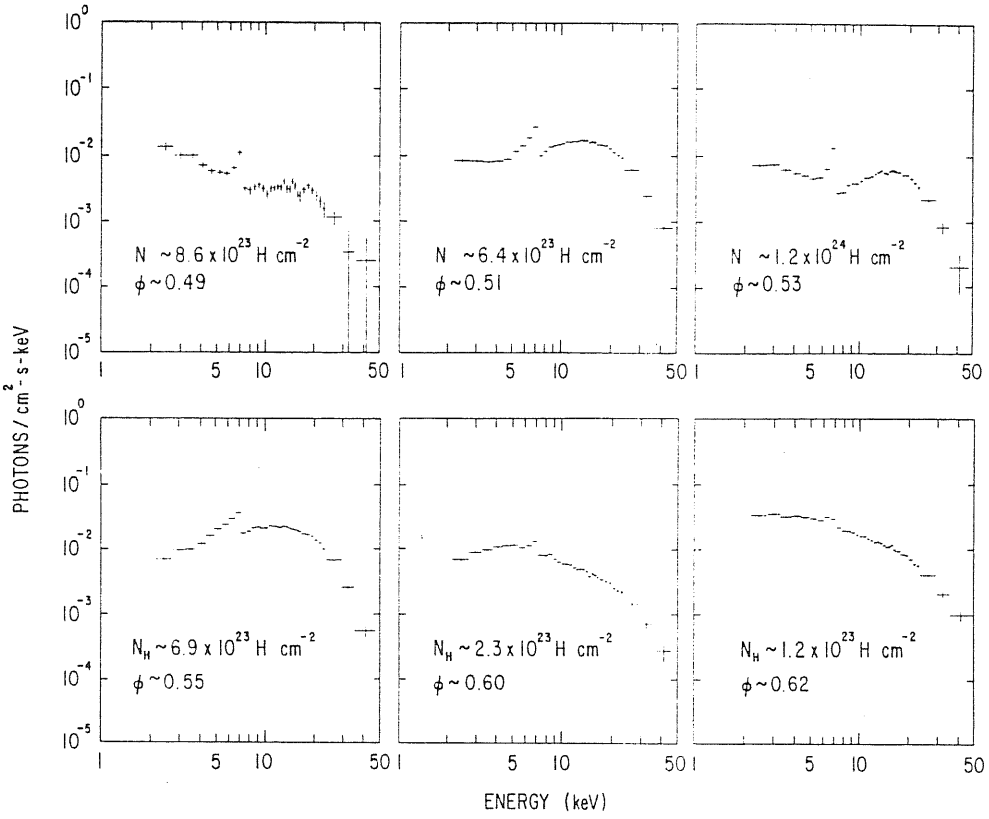

Figure 7.26: Incident spectra from *OSO 8* observations. The X–ray photometric phases are indicated, which corresponds 0.49, 0.51, 0.53, 0.55, 0.58, 0.60 and 0.62 ϕ_{orb} respectively.

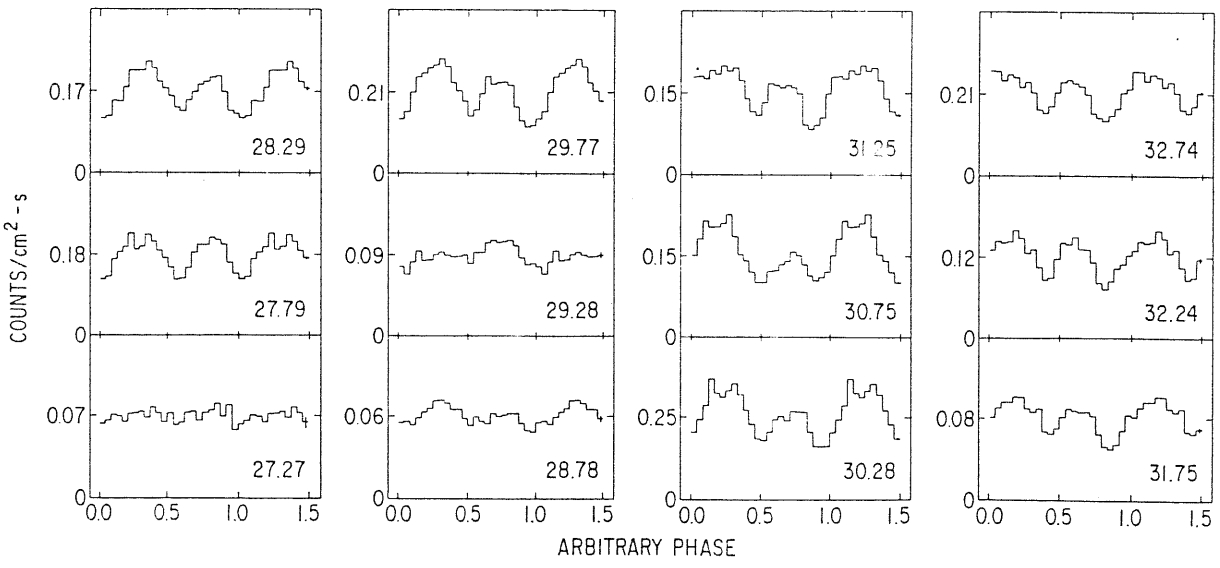

Figure 7.27: The *OSO 8* pulse profiles from half–day averages for indicated 1976 day numbers. The average count rate for each interval can be obtained from the ordinate.

- The X–ray absorption is due to Compton scattering and photoelectric absorption.
- The velocity law for the wind has the form of Eq. 6.35

did not give any positive result. Therefore at least one of the above points does not work; in particular, we have to take into account for the interaction between stellar wind and X–ray flux, and for the accumulation of matter at the magnetopause (see Section 4.1.2) [74].

The problem of the delay between the periastron passage and the X–ray maximum is explained by some authors as due to the presence of a small magnetic field in the optical companion [93], of the order of 10^2 G. In this way there is a constraint for the stellar wind to corotate around the primary before to leave it. A velocity gradient is produced, which gives spin–up or spin–down episodes according to the magnetic field cycle of the supergiant (analogous to the 11 year cycle of the Sun).

On the other hands, other authors invoke the presence of an accretion wake [76] (as seen in 4U 1700-37 [54]), due to the interaction between the accelerating wind from the optical star and the hot, ionized material surrounding the X–ray source. The proof of the existence of the accretion wake should be given by the variation of the absorption, which increases at $\phi_{orb} = 0.05$ [93].

It is interesting to remark that the time of X–ray maxima occur when the neutron star is approximately along the line of sight to the companion star [74,76].

Bibliography

[1] BAUTZ M. - HOWE S. - GORECKI A. - LANG F. - LEVINE A. - PRIMINI F. - LEWIN W.H.G. 1983. *Astrophysical Journal*, **266 p.794**.

[2] BOYNTON P.E. - CROSA L.M. - DEETER J.E. 1980. *Astrophysical Journal*, **237 p.169**.

[3] BRADT H. *et al.* 1976. *Astrophysical Journal*, **204 p.L67**.

[4] BUCHLER J.R. - PERDANG J.M. - SPIEGEL E.A. Eds. 1985. *Chaos in Astrophysics, NATO ASI Series n.*161. Reidel Pub. Co.

[5] CHARLES P.A. *et al.* 1983. *Montly Notices of R.a.S.*, **202 p.657**.

[6] CHARLES P.A. - MASON K.O. - WHITE N.E. - CULHANE J.L. - SANFORD P.W. - MOFFAT A. 1978. *Montly Notices of R.a.S.*, **183 p.813**.

[7] CLARK D.H. - CASWELL F.L. 1976. *Montly Notices of R.a.S.*, **174 p.267**.

[8] CORBET R.H.D. - MASON K.O. - CORDOVA F.A. - BRANDUARDI-RAYMOND G. - PARMAR A.N. 1985. *Montly Notices of R.a.S.*, **212 p.565**.

[9] DAL FIUME D. - FRONTERA F. - MORELLI E. 1988. *Astrophysical Journal*, **331 p.313**.

[10] DAVIDSEN A. - HENRY J.P. - MIDDLEDITCH J. - SMITH H.E. 1972. *Astrophysical Journal*, **177 p.L97**.

[11] DEETER J.E. - BOYNTON P.E. - LAMB F.K. - ZYLSTRA G. 1987. *Astrophysical Journal*, **314 p.634**.

[12] DEETER J.E. - BOYNTON P.E. - SHIBAZAKI N. - HAYAKAWA S. - NAGASE F. - SATO N. 1987. *Astronomical Journal*, **93 p.877**.

[13] DUPREE A.K. *et al.* 1980. *Astrophysical Journal*, **238 p.969**.

[14] FABIAN A.C. - EGGLETON P.P. - HUT P. - PRINGLE J.E. 1986. *Astrophysical Journal*, **305 p.333**.

[15] FALHMAN G.G. - HICKSON P. - RICHER H.B. - GREGORY P.C. - MIDDLEDITCH J. 1982. *Astrophysical Journal*, **261 p.L1**.

[16] FORMAN W. *et al.* 1973. *Astrophysical Journal*, **182 p.L103**.

[17] FRANSSON C. - FABIAN A.C. 1980. *Astronomy & Astrophysics*, **87 p.102**.

[18] FRONTERA F. - DAL FIUME D. - MORELLI E. - SPADA G. 1985. *Astrophysical Journal*, **298 p.585**.

[19] GORECKI A. *et al.* 1982. *Astrophysical Journal*, **256 p.234**.

[20] GREGORY P.C. - BRAUN R. - FAHLMAN G.G. - GULL S.F. 1982. In *Supernova Remnants and their X–ray Emission, IAU Symposium n.101*, DANZIGER J. - GORENSTEIN P. Eds., Reidel Pub. Co. ,p.437.

[21] HABETS G.M.H.J. 1987. *Astronomy & Astrophysics*, **184 p.209**.

[22] HAMEURY J.M. *et al.* 1983. *Astrophysical Journal*, **270 p.144**.

[23] HANSON C.G. - DENNERL K. - COE M.J. - DAVIES S.R. 1988. *Astronomy & Astrophysics*, **195 p.114**.

[24] HATCHETT S. - BUFF J. - McCRAY R. 1976. *Astrophysical Journal*, **206 p.847**.

[25] HOLT S.S. *et al.* 1980. *Astrophysical Journal*, **241 p.L13**.

[26] HUGHES V.A. - HARTEN R.H. - COSTAIN C. - NELSON L. - VINER M.R. 1982. In *Supernova Remnants and their X–ray Emission, IAU Symposium n.101*, DANZIGER J. - GORENSTEIN P. Eds., Reidel Pub. Co. ,p.455.

[27] HUTCHINGS J.B. 1974. *Astrophysical Journal*, **192 p.685**.

[28] HUTCHINGS J.B. *et al.* 1985. *Pubbl. Astron. Soc. Pacific*, **97 p.418**.

[29] ILLARIONOV A.F. - SUNYAEV R.A. 1975. *Astronomy & Astrophysics*, **39 p.185**.

[30] JANOT-PACHECO E. - MOTCH C. - MOUCHET M. 1987. *Astronomy & Astrophysics*, **177 p.91**.

[31] JOSS P.C. - FECHNER W.B. - FORMAN W. - JONES C. 1978. *Astrophysical Journal*, **225 p.994**.

[32] JOSS P.C. - LI F. - NELSON J. - MIDDLEDITCH J. 1980. *Astrophysical Journal*, **235 p.592**.

[33] KALLMAN T.R. - McCRAY R. 1982. *Astrophysical Journal Suppl.*, **50 p.263**.

[34] KALLMAN T.R. - WHITE N.E. 1982. *Astrophysical Journal*, **261 p.L35**.

[35] KATZ J.I. 1973. *Nature Phys.Sci.*, **246 p.87**.

[36] KAWAI N. - MAKISHIMA K. - MATSUOKA M. - MITANI K. - MURAKAMI T. - NAGASE F. 1985. *Pubbl. Astron. Soc. Japan*, **37 p.647**.

[37] KELLEY R. - RAPPAPORT S. - PETRE R. 1980. *Astrophysical Journal*, **238 p.699**.

[38] KENDZIORRA E. - STAUBERT R. - PIETSCH W. - REPPIN C. - SACCO B. - TRUEMPER J. 1977. *Astrophysical Journal*, **217 p.L93**.

[39] KOPAL Z. 1978. *Dynamics of Close Binary Systems.* Reidel Pub. Co.

[40] KOYAMA K. - HOSHI R. - NAGASE F. 1987. *Pubbl. Astron. Soc. Japan*, **39 p.801**.

[41] KROLIK J.H. - RAYMOND J.C. 1986. *Astrophysical Journal*, **298 p.660**.

[42] LAMB D.Q. - LAMB F.K. - PINES D. - SHAHAM J. 1975. *Astrophysical Journal*, **198 p.L21**.

[43] LAMB R.C. *et al.* 1988. *Astrophysical Journal*, **328 p.L13**.

[44] LANDAU L. - LIFSHITZ E. 1958. *FIELD THEORY.* Pergamon Press.

[45] LI F.K. - RAPPAPORT S. - CLARK G.W. - JERNIGAN J.G. 1979. *Astrophysical Journal*, **228 p.893**.

[46] LUCY L.B. - WHITE N.E. 1980. *Astrophysical Journal*, **241 p.300**.

[47] MAKISHIMA K. *et al.* 1984. *Pubbl. Astron. Soc. Japan*, **36 p.679**.

[48] MANCHESTER R.N. - TAYLOR J.H. 1977. *Pulsars.* Freeman Co.

[49] MASLENNIKOV K.L. 1986. *Soviet Astronomy*, **12 p.191.**

[50] McCRAY R. - KALLMAN T.R. - CASTOR J.I. - OLSON G.L. 1984. *Astrophysical Journal*, **282 p.245.**

[51] MIDDLEDITCH J. - PENNYPACKER C.R. - BURNS M.S. 1983. *Astrophysical Journal*, **274 p.313.**

[52] MITANI K. - MATSUOKA M. - MAKISHIMA K. - INOUE H. 1984. *Astrophysics and Space Science*, **103 p.345.**

[53] MOTCH C. - JANOT-PACHECO E. - PAKULL M.W. - MOUCHET M. 1988. *Astronomy & Astrophysics*, **201 p.63.**

[54] MURAKAMI T. *et al.* 1984. *Pubbl. Astron. Soc. Japan*, **36 p.691.**

[55] NAGASE F. *et al.* 1982. *Astrophysical Journal*, **263 p.814.**

[56] NAGASE F. *et al.* 1984. *Astrophysical Journal*, **280 p.259.**

[57] NAGASE F. - HAYAKAWA S. - SATO N. - MASAI K. - INOUE H. 1986. *Pubbl. Astron. Soc. Japan*, **38 p.547.**

[58] NORTH A.R. - RAUBENHEIMER B.C. - DE JAGER O.C. - VAN TONDER A.J. - VAN URK G. 1987. *Nature*, **326 p.567.**

[59] ÖGELMAN H. 1987. *Astronomy & Astrophysics*, **172 p.79.**

[60] ÖGELMAN H. - TRUEMPER J. 1988. *Max–Planck Preprint.*

[61] OKUDA T. - SAKASHITA S. 1977. *Astrophysics and Space Science*, **47 p.385.**

[62] PARKES G.E. - MASON K.O. - MURDIN P.G. - CULHANE J.L. 1980. *Montly Notices of R.a.S.*, **191 p.547.**

[63] PETTERSON J.A. 1977. *Astrophysical Journal*, **218 p.783.**

[64] PONMAN T.J. - SKINNER G.K. - BEDFORD D.K. 1984. *Montly Notices of R.a.S.*, **207 p.621.**

[65] PRAVDO S.H - BECKER R.H. - BOLDT E.A. - SERLEMITSOS P.J. - SWANK J.H. 1977. *Astrophysical Journal*, **215 p.L61.**

[66] PRIEDHORSKY W.C. - HOLT S.S. 1987. *Space Science Review*, **45 p.291.**

[67] PRIEDHORSKY W.C. - TERREL J. 1983. *Nature*, **303 p.681.**

[68] PRIEDHORSKY W.C. - TERRELL J. 1983. *Astrophysical Journal*, **273 p.709.**

[69] PROCACCIA I. 1988. *Nature*, **333 p.618**.

[70] REFLOC'H A. - CHANBON G. - NIEL M. - VEDRENNE G. - RAKHAMINOV C.Y. 1986. *Astrophysical Journal*, **310 p.773**.

[71] RESVANIS L.K. *et al.* 1988. *Astrophysical Journal*, **328 p.L9**.

[72] ROBERTS W.J. 1974. *Astrophysical Journal*, **187 p.575**.

[73] ROSENBERG F.D. - EYLES C.J. - SKINNER G.K. - WILLMORE A.P. 1975. *Nature*, **256 p.628**.

[74] ROTHSCHILD R.E. - SOONG Y. 1987. *Astrophysical Journal*, **315 p.154**.

[75] SATO N. - HAYAKAWA S. - NAGASE F. - MASAI K. - DOTANI T. - INOUE H. - MAKINO F. 1986. *Pubbl. Astron. Soc. Japan*, **38 p.731**.

[76] SATO N. - NAGASE F. - KAWAI N. - KELLEY R.L. - RAPPAPORT S. - WHITE N.E. 1986. *Astrophysical Journal*, **304 p.241**.

[77] SAVONIJE G.J. - DE KOOL M. - VAN DEN HEUVEL E.P.J. 1986. *Astronomy & Astrophysics*, **155 p.51**.

[78] SCHUSTER H.G. 1988. *Deterministic Chaos. An introduction.* VCH Verlagsgesellschaft.

[79] SHAPIRO S.L. - TEUKOLSKY S.A. 1983. *Black Holes, White Dwarfs and Neutron Stars. The Physics of Compact Objects.* John Wiley & Sons, Inc.

[80] SKINNER G.K. *et al.* 1982. *Nature*, **297 p.568**.

[81] STAUBERT R. - KENDZIORRA E. - PIETSCH W. - REPPIN C. - TRUEMPER J. - VOGES W. 1980. *Astrophysical Journal*, **239 p.1010**.

[82] STELLA L. - WHITE N.E. - ROSNER R. 1986. *Astrophysical Journal*, **308 p.669**.

[83] STRICKMAN M.S. - KURFESS J.D. - JOHNSON W.N. 1982. *Astrophysical Journal*, **253 p.L23**.

[84] TARTER C.B. - TUCKER W.H. - SALPETER E.E. 1969. *Astrophysical Journal*, **156 p.943**.

[85] TRUEMPER J. - PIETSCH W. - REPPIN C. - VOGES W. - STAUBERT R. - KENDZIORRA E. 1978. *Astrophysical Journal*, **219 p.L105**.

[86] TUCKER W.H. 1977. *Radiation Processes in Astrophysics.* The MIT Press.

[87] UNDERHILL A. - DOAZAN V. 1982. *B Stars with and without Emission Lines.* NASA SP-456.

[88] VOGES W. - ATMANSPACHER H. - SCHEINGRABER H. 1987. *Astrophysical Journal*, **320 p.794**.

[89] WANG Y.M. - ROBERTSON J.A. 1984. *Max–Planck Preprint*, **146**.

[90] WATSON M.G. - WARWICK R.S. - CORBET R.H.D. 1982. *Montly Notices of R.a.S.*, **199 p.915**.

[91] WHITE N.E. - CARPENTER G.F. 1978. *Montly Notices of R.a.S.*, **183 p.11P**.

[92] WHITE N.E. - MASON K.O. - SANFORD P.W. 1978. *Montly Notices of R.a.S.*, **184 p.67P**.

[93] WHITE N.E. - SWANK J.H. 1984. *Astrophysical Journal*, **287 p.856**.

[94] ZIOLKOWSKI J. 1985. In *Multifrequency Behaviour of Accreting Sources*, GIOVANNELLI F. Ed., CNR Frascati.

[95] ZIOLKOWSKI J. 1988. Seminar helded in SISSA.

Chapter 8

SUMMARY AND CONCLUSIONS

The basic model used to interpret the pulsed emission in X–ray sources is, as we have seen, as follows: matter is lost from the normal star via a stellar wind or via a matter flux through the inner Lagrangian point (see Fig. 1.1 and Chapter 4). At the distance $r = R_m$, where R_m is the magnetospheric (Alfvén) radius (see Eq. 4.14) this matter is stopped by the magnetic pressure due to the neutron star magnetic field, and then it somehow threads the field lines. How it occurs is one of the key features determining the structure of the emitting region since, from this point on, matter probably is channeled down more or less rigidly along the lines of force to the neutron star surface, where it will yield most of its X–ray radiation.

The transverse structure of the emitting region (i.e. in the θ, ϕ variables of a spherical coordinate system) depends critically on the way in which matter attaches to the field lines at $r = R_m$. It is not clear, at this time, if the "threading" region is small or not with respect to R_m; this is important because it determines whether the accretion column is a thin-walled hollow funnel or whether it is a more or less completely filled cylinder (see Fig. 8.1 [10]). Also the role of great scale instabilities is not clear: variations in the accretion rate can give departures from the cylindrical symmetry and/or the formation of slabs in which only segments of the funnel are present (see Fig. 8.1 [10]).

The vertical structure (z or radial) of the emitting region is another main problem (i.e. the intrinsic beaming pattern). In fact, aside from large scale inhomogeneities, the larger uncertainties regard the fact if collisionless shocks above the neutron star surface are formed or not (there is also the complication due to the presence of a strong magnetic field). In case of presence of shocks, the stand-off distance is a fraction of the stellar radius [3], so the emitting post-shock region is a cylinder sticking up above the neutron star surface: the emission occurs predominantly from the sides of the accretion column, in a "fan" beam pattern (see Fig. 6.5).

In absence of shocks and for $\mathcal{L}_x \leq 10^{37}$ erg/sec, the deceleration occurs via multiple Coulomb encounters or nuclear collisions with atmospheric par-

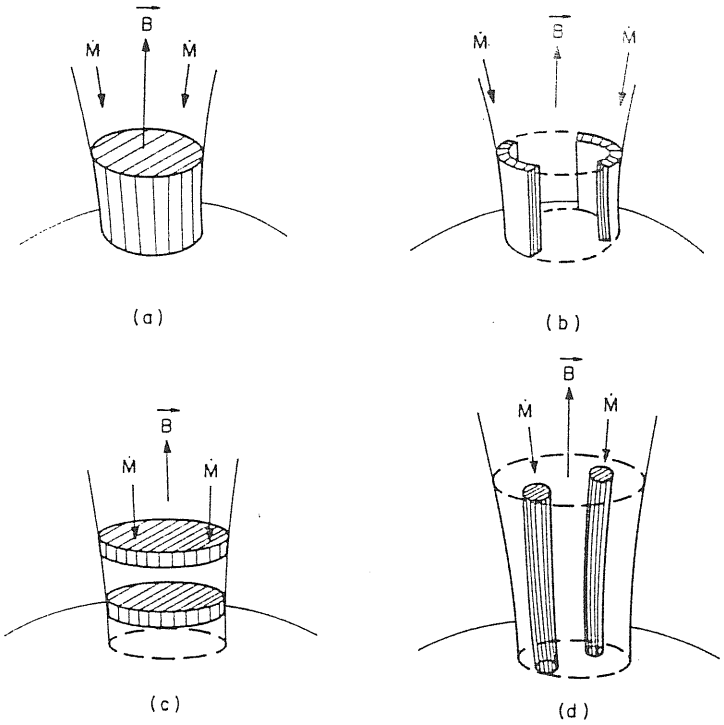

Figure 8.1: Possible transverse geometries of the emission region at the polar cap. *(a)* Filled funnel. *(b)* Hollow sectional funnel. *(c)* Pancaked (slab) *(d)* Spaghetti [5].

ticles [11], occurring in the denser part of the atmosphere. Then the emitting region is a plane, parallel section of the polar cap, which does not significantly sticks up, emitting upwards in a "pencil" beam.

In case of absence of shocks but with $\mathcal{L}_x \geq 10^{37}$ erg/sec, radiation pressure can decelerate matter in a diffuse quasi-shock structure [1] and can influence the transverse structure of the flow.

A second main problem is related to the radiative transfer in the atmosphere of the neutron star. In fact, even for simple, homogeneous models for atmosphere, the dependence on direction, frequency and polarization of cross sections (see Chapter 5) makes the transfer problem difficult [11,14,15,7]. The simpler way to attack this problem is, in principle, a Monte Carlo approach. The results confirm the suspicions that the direction and width of the beaming is energy dependent, and give indications of phase dependent spectral effects [22,17].

All these informations are available, in principle, from the study of the pulse profiles and their dependence on the pulse phase [21,12,8]. The problem arises from the observation of asymmetrical pulse profiles (see Section 6.2) which cannot be reproduced by means of simple models: probably there are effects due to the strong gravitational field at the neutron star surface [16,18,13] and/or the axes of the accretion column is not parallel to the magnetic field axes, so that we have an asymmetry in the intrinsic beaming pattern.

An open problem regards the observed energy spectra. Although average

spectra are roughly explained, it is not so for spectra at high ($E > 20$ keV) and low ($E < 20$ keV) energy (see Section 6.4). A "two-component" model is not satisfactory because it describes separately low and high energy spectra and it resembles the situation at the beginning of this century when the blackbody spectrum was described by means of different laws for high and low frequency (the Rayleigh-Jeans spectrum at low frequency). The "Planck law" which is hidden under the observed energy spectra at this moment is not known.

Another "bug" in the theory consists in the fact that all spectrum models are not parametrized: i.e., spectra obtained from the theory are calculated for some given physical parameters: plasma temperature, density, etc. and some given geometry [6]. The variations of spectra with respect to the physical parameters are not given, so that comparison with observations is very difficult. A first approach to this problem is given in [2].

The noise we observe in the X–ray light curves (sums of count rates data vs. time) might, formally, give us informations about the particular models which can describe X–ray emission by means of a deterministic chaos analysis: unfortunately, this approach has been successfully applied only to two sources: Her X-1 [20] and A0535+26 [4] (see Sections 7.2 and 7.3).

In conclusion, the problem looks very difficult to manage, essentially because we have not the theory which describe the process of conversion of the kinetic energy of accreted matter in X–ray emission, and how this radiation interact with so strong magnetic fields. A new progress occurred recently with the discovery that the major source of photons, in a strong magnetic field, is not the bremsstrahlung process but a process of resonant emission of two photons (see Section 5.3) [8,9,7], and with the introduction of effects of reflection of the emitted X–rays by the atmosphere of the companion star [19].

About our research program, it will begin by analyzing 4U 1907+09 and Vela X-1 data records obtained from the EXOSAT Observatory archive, which will be carried out at the TESRE Institute of CNR in Bologna. A deterministic chaos analysis on these data will be performed, to obtain informations about the models which might describe the emission mechanisms in these sources; then a theoretical study will be done on the beaming geometries, to extract all the possible informations on the details of the accretion mechanisms which occurs in these sources. Our goal is to obtain a parametrized theory of energy spectra, in such a way to have the possibility to go back and to achieve the physical parameters of the X–ray sources from the observed values.

Bibliography

[1] BASKO M.M. - SUNYAEV R.A. 1976. *Montly Notices of R.a.S.*, **175 p.395.**

[2] DAL FIUME D. - FRONTERA F. - MORELLI E. 1988. *Astrophysical Journal*, **331 p.313.**

[3] FRANK J. - KING A.R. - RAINE D.J. 1985. *Accretion Processes in Astrophysics.* Cambridge Un. Press.

[4] FRONTERA F. - DAL FIUME D. - MORELLI E. - SPADA G. 1985. *Astrophysical Journal*, **298 p.585**.

[5] HAMEURY J.M. *et al.* 1983. *Astrophysical Journal*, **270 p.144**.

[6] HARDING A.K. - MESZAROS P. - KIRK J.K. - GALLOWAY D.J. 1984. *Astrophysical Journal*, **278 p.369**.

[7] KIRK J.G. - MELROSE D.B. 1986. *Astronomy & Astrophysics*, **156 p.277**.

[8] KIRK J.G. - NAGEL W. - STOREY M. 1986. *Astronomy & Astrophysics*, **169 p.259**.

[9] MELROSE D.B. - KIRK J.G. 1986. *Astronomy & Astrophysics*, **156 p.268**.

[10] MESZAROS P. 1984. *Space Science Review*, **38 p.325**.

[11] MESZAROS P. - HARDING A.K. - KIRK J.G. - GALLOWAY D.J. 1983. *Astrophysical Journal*, **266 p.L33**.

[12] MESZAROS P. - NAGEL W. 1985. *Astrophysical Journal*, **299 p.138**.

[13] MESZAROS P. - RIFFERT H. 1988. *Astrophysical Journal*, **327 p.712**.

[14] NAGEL W. 1981. *Astrophysical Journal*, **251 p.278**.

[15] NAGEL W. 1981. *Astrophysical Journal*, **251 p.288**.

[16] PECHENICK K.R. - FTACLAS C. - COHEN J.M. 1983. *Astrophysical Journal*, **274 p.846**.

[17] PRAVDO S.H. - BUSSARD R.W. 1981. *Astrophysical Journal*, **246 p.L115**.

[18] RIFFERT H. - MESZAROS P. 1988. *Astrophysical Journal*, **325 p.207**.

[19] TITARCHUK L.G. 1987. *Astrophysics*, **26 p.57**.

[20] VOGES W. - ATMANSPACHER H. - SCHEINGRABER H. 1987. *Astrophysical Journal*, **320 p.794**.

[21] WANG Y.M. - WELTER G.L. 1981. *Astronomy & Astrophysics*, **102 p.97**.

[22] YAHEL R.Z. 1980. *Astronomy & Astrophysics*, **90 p.26**.

Chapter 9

BIBLIOGRAPHY ON X–RAY PULSARS

In this chapter we will give an updated, essential bibliography about all X–ray binary pulsars which were treated in this work.

Other two pulsed X–ray sources have been discovered by the GINGA group (N.R. Robba, *private communication*), but we have not, to date, other data but their position and pulse period:

$$2136{+}57 \qquad P_p = 66^s.25$$

$$\text{V}1722\text{-}36 \qquad P_p = 413^s.9\ .$$

9.1 Bibliography on A0538-66

[1] CHARLES P.A. *et al.*. 1983. *Extreme variability in the Be-type, periodic recurrent X–ray transient A0538-66: a highly eccentric interacting binary. Montly Notices of R.a.S.*, **202 p.657**.

[2] CORBET R.H.D. - MASON K.O. - CORDOVA F.A. - BRANDUARDI-RAYMOND G. - PARMAR A.N. 1985. *Optical spectroscopy and photometry of the periodic X–ray transient A0538-66 during an outburst and an OFF state. Montly Notices of R.a.S.*, **212 p.565**.

[3] HABETS G.M.H.J. 1987. *An evolutionary scenario for the formation of highly eccentric Be/X–ray binaries. Astronomy & Astrophysics*, **184 p.209**.

[4] HUTCHINGS J.B. *et al.*. 1985. *The optical orbit of the X–ray pulsar binary 0535-668 (= A0538-66). Pubbl. Astron. Soc. Pacific*, **97 p.418**.

[5] PONMAN T.J. - SKINNER G.K. - BEDFORD D.K. 1984. *A0538-66 in outburst: a buried neutron star ? Montly Notices of R.a.S.*, **207 p.621**.

[6] SKINNER G.K. *et al.*. 1982. *Discovery of 69 ms periodic X–ray pulsations in A0538-66. Nature*, **297 p.568**.

[7] WHITE N.E. - CARPENTER G.F. 1978. *The recurrent X–ray transient A0538-66. Montly Notices of R.a.S.*, **183 p.11P**.

9.2 Bibliography on SMC X–1

[1] BONNET-BIDAUD J.M. - VAN DER KLIS M. 1981. *Long term X–ray observations of SMC X-1 including a turn-on. Astronomy & Astrophysics*, **97 p.134**.

[2] CLARK G.W. - DOXSEY R. - LI F. - JERNIGAN J.G. - VAN PARADIJS J. 1978. *On 2 newly X–ray sources in the SMC and the high luminosities of the magellanic X–ray sources. Astrophysical Journal*, **221 p.L37**.

[3] DAVISON P.J.N. 1977. *Spin-up in SMC X-1. Montly Notices of R.a.S.*, **179 p.15P**.

[4] GRUBER D.E. - ROTHSCHILD R.E. 1984. *SMC X-1 variability observed from HEAO-1. Astrophysical Journal*, **283 p.546**.

[5] HUTCHINGS J.B. - CRAMPTON D. - COWLEY A.P. - OSMER P.S. 1977. *The spectroscopic orbit and masses of Sk 160/SMC X-1. Astrophysical Journal*, **217 p.186**.

[6] KHRUZINA T.S. - CHEREPASHCHUK A.M. *Parameters of the X–ray binary system Sk 160 = 4U 0115-73 (SMC X-1).* 1987. *Soviet Astronomy*, **31 p.180**.

[7] LUCKE R. - YENTIS D. - FRIEDMAN H. - FRITZ G. - SHULMAN S. 1976. *Discovery of X–ray pulsations in SMC X-1. Astrophysical Journal*, **206 p.L25**.

[8] MARSHALL F.E. - WHITE N.E. - BECKER R.H. 1983. *A two-component X–ray spectrum from SMC X-1. Astrophysical Journal*, **266 p.814**.

[9] PRIMINI F. - RAPPAPORT S. - JOSS P.C. 1977. *Pulse profile and refined orbital elements for SMC X-1. Astronomical Journal*, **217 p.543**.

[10] VAN PARADIJS J. - ZUIDERWIJK E. 1977. *Evidence for an accretion disk in SMC X-1. Astronomy & Astrophysics*, **61 p.L19**.

9.3 Bibliography on HER X–1

[1] DAY C.S.R. - TENNANT A.F. - FABIAN A.C. 1988. *Observations of three high-state eclipse egresses of Hercules X-1. Montly Notices of R.a.S.*, **231 p.69**.

[2] DEETER J.E. - BOYNTON P.E. - PRAVDO S.H. 1981. *Pulse-timing observations of Hercules X-1. Astrophysical Journal*, **247 p.1003**.

[3] DOWTHWAITE J.C. *et al.*. 1984. *Hercules X-1. A 1000 GeV γ–ray pulsar. Nature*, **309 p.691**.

[4] EICHLER D. - VESTRAND W.T. 1985. *Implications of ultra-high-energy emission from Hercules X-1. Nature*, **318 p.345**.

[5] GORECKI A. *et al.*. 1982. *HEAO-1 observations of the long-term variability of Hercules X-1. Astrophysical Journal*, **256 p.234**.

[6] JOSS P.C. - FECHNER W.B. - FORMAN W. - JONES C. 1978. *Properties of the 2-6 keV pulse profile of Hercules X-1. Astrophysical Journal*, **225 p.994**.

[7] JOSS P.C. - LI F. - NELSON J. - MIDDLEDITCH J. 1980. *Coordinated observations of optical and X–ray pulsations from Hercules X-1. Astrophysical Journal*, **235 p.592**.

[8] KENDZIORRA E. - STAUBERT R. - PIETSCH W. - REPPIN C. - SACCO B. - TRUEMPER J. 1977. *Hercules X-1: the 1.24 second pulsation in hard X–rays. Astrophysical Journal*, **217 p.L93**.

[9] KONDO Y. - VAN FLANDERN T.C. - WOLFF C.L. 1983. *On the clock mechanism and the implausibility of the 35 day precessing disk in Her X-1. Astrophysical Journal*, **273 p.716**.

[10] LAMB R.C. *et al.*. 1988. *TeV γ–rays from Hercules X-1 pulsed at an anomalous frequency. Astrophysical Journal*, **328 p.L13**.

[11] LIPUNOV V.M. *On the equilibrium of Hercules X-1.* 1987. *Soviet Astronomy*, **31 p.167**.

[12] MAURER G.S. *et al.*. 1979. *The high-energy pulsed X–ray spectrum of Hercules X-1 as observed with OSO 8. Astrophysical Journal*, **231 p.906**.

[13] MEYER F. - MEYER-HOFMEISTER E. 1984. *HZ Her/Her X-1: an alternative model for the 35 day cycle ? Astronomy & Astrophysics*, **140 p.L35**.

[14] MIDDLEDITCH J. - NELSON J. 1976. *Studies of optical pulsations from HZ Her/Her X-1: a determination of the mass of the neutron star. Astrophysical Journal*, **208 p.567.**

[15] MIDDLEDITCH J. - PUETTER R.C. - PENNYPACKER C.R. 1985. *Optical and infrared pulsations from the HZ Her binary system during the 1983 prolonged X-ray low state. Astrophysical Journal*, **292 p.267.**

[16] ÖGELMAN H. 1987. *The 35 day cycle of Her X-1: quality of the clock mechanism. Astronomy & Astrophysics*, **172 p.79.**

[17] ÖGELMANN H. - TRUEMPER J. 1988. *EXOSAT observations of Hercules X-1. Max-Planck Preprint.*

[18] PETTERSON J.A. 1977. *The 35 day cycle of the X-ray binary Hercules X-1. Astrophysical Journal*, **218 p.783.**

[19] PRAVDO S.H - BECKER R.H. - BOLDT E.A. - SERLEMITSOS P.J. - SWANK J.H. 1977. *X-ray spectra of Her X-1. I. Iron line fluorescence from a subrelativistic shell. Astrophysical Journal*, **215 p.L61.**

[20] PRAVDO S.H. - BOLDT E.N. - HOLT S.S. - SERLEMITSOS P.J. 1977. *X-ray spectra of Her X-1. II. The pulse. Astrophysical Journal*, **216 p.L23.**

[21] PRAVDO S.H. - BUSSARD R.W. - BECKER R.H. - BOLDT E.A. - HOLT S.S. - SERLERMITSOS. 1978. *X-ray spectra of Her X-1. III. Pulse phase dependence in the high-energy continuum. Astrophysical Journal*, **225 p.988.**

[22] RESVANIS L.K. *et al.*. 1988. *VHE γ-rays from Hercules X-1. Astrophysical Journal*, **328 p.L9.**

[23] SHEFFER E.K. *The neutron star in Hercules X-1 system does not precess with a 35-day period.* 1987. *Soviet Astronomy Letters*, **13 p.82.**

[24] SUTANTYO W. - VAN DER LINDEN T.J. - VAN DEN HEUVEL E.P.J. 1985. *On the evolution of Her X-1.* In *The Evolution of Galactic X-ray Binaries, NATO ASI Series N.*167, TRUEMPER J. - LEWIN W.H.G. - BRINKMANN W., Eds., p.261.

[25] SUTANTYO W. - VAN DER LINDEN T.J. - VAN DEN HEUVEL E.P.J. 1986. *The evolutionary history of Hercules X-1. Astronomy & Astrophysics*, **169 p.133.**

[26] THOMAS H.C. - SCHMIDT H.U. - SCHOEMBS R. 1985. *Eclipse of a bright spot in the disk of Her X-1.* In *The Evolution of Galactic X-ray Binaries, NATO ASI Series N.*167, TRUEMPER J. - LEWIN W.H.G. - BRINKMANN W., Eds., p.221.

[27] TRUEMPER J. - KAHABKA P. - ÖGELMAN H. - PIETSCH W. - VOGES W. 1985. *EXOSAT observations of the 35-day cycle of Her X-1: evidence for neutron star precession.* In *The Evolution of Galactic X-ray Binaries, NATO ASI Series N.*167, TRUEMPER J. - LEWIN W.H.G. - BRINKMANN W., Eds., p.239.

[28] TRUEMPER J. - KAHABKA P. - ÖGELMAN H. - PIETSCH W. - VOGES W. 1986. *EXOSAT observations of the 35 day cycle of Her X-1: evidence for neutron star precession. Astrophysical Journal*, **300 p.L63.**

[29] TRUEMPER J. - PIETSCH W. - REPPIN C. - VOGES W. - STAUBERT R. - KENDZIORRA E. 1978. *Evidence for strong cyclotron line emission in the hard X-ray spectrum of Hercules X-1. Astrophysical Journal*, **219 p.L105.**

[30] VOGES W. - ATMANSPACHER H. - SCHEINGRABER H. 1987. *Deterministic chaos in accreting systems: analysis of the X-ray variability of Her X-1. Astrophysical Journal*, **320 p.794.**

[31] VOGES W. - PIETSCH W. - REPPIN C. - TRUEMPER J. - KENDZIORRA E. - STAUBERT R. 1982. *Cyclotron lines in the hard X-ray spectrum of Hercules X-1. Astrophysical Journal*, **263 p.803.**

[32] VRTILEK S.D. - HALPERN J.P. 1985. *Temporal and spectral study of a newly discovered spiking phenomenon in the pre-eclipse and anomalous dip states of Hercules X-1. Astrophysical Journal*, **296 p.606.**

[33] YAHEL R.Z. 1980. *Spectra and pulse formation mechanism in X-ray pulsars: application to Her X-1. Astronomy & Astrophysics*, **90 p.26.**

9.4 Bibliography on 4U 0115+63

[1] CHADWICK P.M. *et al.*. 1985. *4U 0115+63: an energetic γ-ray binary pulsar. Astronomy & Astrophysics*, **151 p.L1.**

[2] COMINSKY L. - CLARK G.W. - LI F. - MAYER W. - RAPPAPORT S. 1978. *Discovery of 3.6 second pulsations from 4U 0115+63. Nature*, **273 p.367.**

[3] HUTCHINGS J.B. - CRAMPTON D. 1981. *The optical counterpart of 4U 0115+63. Astrophysical Journal*, **247 p.222.**

[4] JOHNSTON M. - BRADT H. - DOXSEY R. - GURSKY H. - SCHWARTZ D. - SCHWARTZ J. 1978. *Position and pulse profile of the X-ray transient 4U 0115+63. Astrophysical Journal*, **223 p.L71.**

[5] KELLEY R.L. - RAPPAPORT S. - BRODHEIM M.J. - COMINSKY L. 1981. *A search for apsidal motion in 4U 0115+63. Astrophysical Journal*, **251 p.630.**

[6] KRISS G.A. - COMINSKY L.R. - REMILLAND R.A. - WILLIAMS G. - THORSTENSEN J.R. 1983. *The 1980 outburst of 4U 0115+63 (V635 Cassiopeiae). Astrophysical Journal*, **266 p.806.**

[7] LAMB R.C. - WEEKES T.C. 1986. *TeV γ-ray sources: Cas γ-1 = 4U 0115+63. Astrophysical Letters*, **25 p.73.**

[8] RAPPAPORT S. - CLARK G.W. - COMINSKY L. - JOSS P.C. - LI F. 1978. *Orbital elements of 4U 0115+63 and the nature of the hard X-ray transients. Astrophysical Journal*, **224 p.L1.**

[9] RICKETTS M.J. - HALL R. - PAGE C.G. - POUNDS K.A. 1981. *Observation of an outburst from the X-ray pulsator 4U 0115+63. Space Science Review*, **30 p.399.**

[10] ROSE L.A. *et al.*. 1979. *Observations of the transient X-ray source 4U 0115+63. Astrophysical Journal*, **231 p.919.**

[11] SHARMA D.P. - RADHA M.S. - NAGARAJA B.V. 1983. *Rocket X-ray observations of 4U 0115+63. Astrophysics and Space Science*, **92 p.317.**

9.5 Bibliography on V0332+53

[1] COE M.J. - LONGMORE A.J. - PAYNE B.J. - HANSON C.G. 1987. *A near-IR study of the X-ray transient V0332+53. Montly Notices of R.a.S.*, **226 p.455.**

[2] CORBET R.H.D. - CHARLES P.A. - VAN DER KLIS M. 1986. *The optical and X-ray decline of V0332+53 (X0331+53, BQ Cam). Astronomy & Astrophysics*, **162 p.117.**

[3] HONEYCUTT R.K. - SCHLEGEL E.M. 1985. *Spectrophotometry of the probable optical counterpart of the X-ray source V0332+53. Pubbl. Astron. Soc. Pacific*, **97 p.300.**

[4] IYE M. - KODAIRA K. 1985. *H_α variability in the X-ray transient source V0332+53. Pubbl. Astron. Soc. Pacific*, **97 p.1186.**

[5] KODAIRA K. *et al.*. 1985. *Optical observations of X0331+53. Pubbl. Astron. Soc. Japan*, **37 p.97.**

[6] STELLA L. *et al.*. 1985. *The discovery of 4.4 second X-ray pulsations from the rapidly variable transient V0332+53. Astrophysical Journal*, **288 p.L45.**

[7] STOCKE J. - SILVA D. - BLACK J.H. - KODAIRA K. 1985. *High-resolution spectroscopy of the optical candidate for the X-ray transient X0331+53. Pubbl. Astron. Soc. Pacific*, **97 p.126.**

[8] TERREL J. - PRIEDHORSKY W.C. 1984. *The 1973 X-ray transient V0332+53. Astrophysical Journal*, **285 p.L15.**

9.6 Bibliography on CEN X–3

[1] AVNI Y. - BAHCALL J.N. 1974. *Mass limits for the Cen X-3 system. Astrophysical Journal*, **192 p.L139**.

[2] CHESTER T.J. 1978. *Centaurus X-3: the periodicity of the extended lows. Astrophysical Journal*, **219 p.L77**.

[3] CLARK G.W. - MINATO J.R. - MI G. 1988. *The atmospheric structure of the O-type supergiant Krzeminski's star and the mass of its neutron star companion. Astrophysical Journal*, **324 p.974**.

[4] FABBIANO G. - SCHREIRER E.J. 1977. *Further studies of the pulsation period and orbital elements of Centaurus X-3. Astrophysical Journal*, **214 p.235**.

[5] GRUBER D.E. 1988. *The very low frequency power spectrum of Centaurus X-3. Astrophysical Journal*, **328 p.265**.

[6] HOWE S.K. - PRIMINI F.A. - BAUTZ M.W. - LANG F.L. - LEVINE A.M. - LEWIN W.H.G. 1983. *HEAO-1 high-energy X—ray observations of Centaurus X-3. Astrophysical Journal*, **272 p.678**.

[7] HUTCHINGS J.B. - COWLEY A.P. - CRAMPTON D. - VAN PARADIJS J. - WHITE N.E. 1979. *Centaurus X-3. Astrophysical Journal*, **229 p.1079**.

[8] KELLEY R.L. - RAPPAPORT S. - CLAK G.W. - PETRO L.D. 1983. *Orbital period changes in Centaurus X-3. Astrophysical Journal*, **268 p.790**.

[9] KRZEMINSKI W. 1974. *The identification and UBV photometry of the visible component of the Cen X-3 binary. Astrophysical Journal*, **192 p.L135**.

[10] LIEU R. - VENKATESAN D. - MITANI K. 1984. *A study of the spectra and pulse profiles of Centaurus X-3 from HAKUCHO. Astrophysical Journal*, **282 p.709**.

[11] MURAKAMI T. *et al.*. 1983. *Observation of Centaurus X-3 by HAKUCHO. Astrophysical Journal*, **264 p.563**.

[12] SCHREIRER E. - LEVINSON R. - GURSKY H. - KELLOGG E. - TANANBAUM H. - GIACCONI R. 1972. *Evidence for the binary nature of Centaurus X-3 from UHURU X–ray observations. Astrophysical Journal*, **172 p.L79**.

[13] VAN DER KLIS M. - BONNET-BIDAUD J.M. - ROBBA N.R. 1980. *Characteristics of the Cen X-3 neutron star from correlated spin-up and X–ray luminosity measurements. Astronomy & Astrophysics*, **88 p.8**.

9.7 Bibliography on 1E 2259+586

[1] CLARK D.H. - CASWELL F.L. 1976. *A study of galactic supernova remnants, based on Molonglo-Parkes observational data. Montly Notices of R.a.S.*, **174 p.267**.

[2] FAHLMAN G.G. - GREGORY P.C. 1981. *An X–ray pulsar in SNR G109.1-1.0. Nature*, **293 p.202**.

[3] FAHLMAN G.G. - GREGORY P.C. 1982. *The pulsation period and possible orbit of 1E 2259+586.* In *Supernova Remnants and their X–ray Emission, IAU Symposium n.*101, DANZIGER J. - GORENSTEIN P. Eds, p.445.

[4] FALHMAN G.G. - HICKSON P. - RICHER H.B. - GREGORY P.C. - MIDDLEDITCH J. 1982. *A possible optical counterpart to the X–ray pulsar 1E 2259+586. Astrophysical Journal*, **261 p.L1**.

[5] GREGORY P.C. - BRAUN R. - FAHLMAN G.G. - GULL S.F. 1982. *Comparision of radio and X–ray observations of SNR G109.1-1.0.* In *Supernova Remnants and their X–ray Emission, IAU Symposium n.*101, DANZIGER J. - GORENSTEIN P. Eds, p.437.

[6] GREGORY P.C. - FAHLMAN G.G. 1980. *An extraordinary new celestial X–ray source. Nature*, **287 p.805**.

[7] GREGORY P.C. - FAHLMAN G.G. 1982. *Precessing jet model for the supernova remnant G109.1-1.0.* In *Supernova Remnants and their X-ray Emission, IAU Symposium n.*101, DANZIGER J. - GORENSTEIN P. Eds, p.429.

[8] HANSON C.G. - DENNERL K. - COE M.J. - DAVIES S.R. 1988. *A 23 hours EXOSAT observation of the X-ray pulsar 1E 2259+586 and the associated supernova. Astronomy & Astrophysics*, **195 p.114.**

[9] HUGHES V.A. - HARTEN R.H. - COSTAIN C. - NELSON L. - VINER M.R. 1982. *Radio observations of the supernova remnant CTB109 (G109.1-1.0).* In *Supernova Remnants and their X-ray Emission, IAU Symposium n.*101, DANZIGER J. - GORENSTEIN P. Eds, p.455.

[10] HUGHES V.A. - HARTEN R.H. - VAN DEN BERGH S. 1981. *A new supernova remnant G109.2-1.0. Astrophysical Journal*, **246 p.L127.**

[11] KOYAMA K. - HOSHI R. - NAGASE F. 1987. *X-ray observatins of the extraordinary pulsar 1E 2259+586. Pubbl. Astron. Soc. Japan*, **39 p.801.**

[12] LIPUNOV V.M. - POSTNOV K.A. 1985. *The binary X-ray pulsar 1E 2259+586: a descendant of AM Her type system ? Astronomy & Astrophysics*, **144 p.L13.**

[13] MARGON B. - ANDERSON S.F. 1983. *Digital imagery of the X-ray pulsar 1E 2259+586. Astrophysical Letters*, **23 p.211.**

[14] MIDDLEDITCH J. - PENNYPACKER C.R. - BURNS M.S. 1983. *Infrared and optical pulsations from HZ Her and a possible 3.5 sec infrared pulsations from 1E 2259+586. Astrophysical Journal*, **274 p.313.**

[15] SAVONIJE G.J. - DE KOOL M. - VAN DEN HEUVEL E.P.J. 1986. *The minimum orbital period for ultra-compact binaries with helium burning secondaries. Astronomy & Astrophysics*, **155 p.51.**

9.8 Bibliography on 4U 1626-67

[1] ELSNER R.F. *et al.*. 1983. *X-ray observations of 4U 1626-67 by the MC on the* Einstein *(HEAO-2) observatory. Astrophysical Journal*, **266 p.769.**

[2] GRINDLAY J.E. 1978. *Photometric study of the X-ray pulsar 4U 1626-67. Astrophysical Journal*, **225 p.1001.**

[3] ILOVAISKY S.A. - MOTCH C. - CHEVALIER C. 1978. *Discovery of optical pulsations from 4U 1626-67. Astronomy & Astrophysics*, **70 p.L19.**

[4] JOSS P.C. - AVNI Y. - RAPPAPORT S. 1977. *Accreting neutron stars in highly compact binary systems and the nature of 3U 1626-67. Astrophysical Journal*, **221 p.645.**

[5] KII T. - HAYAKAWA S. - NAGASE F. 1986. *TENMA observation of the X-ray pulsar 4U 1626-67. Astrophysics and Space Science*, **118 p.375.**

[6] KII T. - HAYAKAWA S. - NAGASE F. - IKEGAMI T. - KAWAI N. 1986. *Anisotropic X-ray transfer in a strongly magnetized plasma of the X-ray pulsar 4U 1626-67. Pubbl. Astron. Soc. Japan*, **38 p.751.**

[7] LEVINE A. - MA C.P. - McCLINTOCK J. - RAPPAPORT S. - VAN DEN KLIS M. - VERBUNT F. 1988. *4U 1626-67: the binary pulsar with the smallest known mass function. Astrophysical Journal*, **327 p.732.**

[8] LI F.K. - JOSS P.C. - McCLINTOCK J.E. - RAPPAPORT S. - WRITE E.L. 1980. *4U 1626-67 and the character of highly compact binary X-ray sources. Astrophysical Journal*, **240 p.628.**

[9] McCLINTOCK J.E. - CANIZARES C.R. - BRADT H.V. - DOXSEY R.E. - JERNIGAN J.G. 1977. *Optical candidates for two X-ray bursters and X-ray pulsar. Nature*, **270 p.320.**

[10] McCLINTOCK J.E. - CANIZARES C.R. - LI F.K. - GRINDLAY J.E. 1980. *Simultaneous X–ray optical and optical observations of the 7.7 second X–ray 4U 1626-67. Astrophysical Journal*, **235 p.L81.**

[11] MIDDLEDITCH J. - MASON K.O. - NELSON J.E. - WHITE N.E. 1981. *4U 1626-67: a prograde spinning X–ray pulsar in a 2500 sec binary system. Astrophysical Journal*, **244 p.1001.**

[12] PETTERSON B.A. - WALLACE P. - ELLIOTT H. - HILL P.W. - MANCHESTER R.N. 1980. *Optical observations of 4U 1626-67. Montly Notices of R.a.S.*, **190 p.33P.**

[13] PRAVDO S.H. *et al.*. 1979. *HEAO-1 observations of the X–ray pulsar 4U 1626-67. Astrophysical Journal*, **231 p.912.**

[14] RAPPAPORT S. - MARKERT T. - LI F.K. - CLARK G.W. - JERNIGAN J.G. - McCLINTOCK J. 1977. *Discovey of a 7.68 second X–ray periodicity in 4U 1626-67. Astrophysical Journal*, **217 p.L29.**

9.9 Bibliography on 2S 1553-54

[1] KELLEY R.L. - RAPPAPORT S. - AYASLI S. 1983. *Discovery of 9.3 sec X–ray pulsation from 2S 1553-54 and a determination of the orbit. Astrophysical Journal*, **274 p.765.**

9.10 Bibliography on LMC X–4

[1] CHEVALIER C. - ILOVAISKY S.A. 1977. *The binary nature of the LMC X-4 optical candidate. Astronomy & Astrophysics*, **59 p.L9.**

[2] HUTCHINGS J.B. - CRAMPTON D. - COWLEY A.P. 1978. *Spectroscopic observations and orbit of LMC X-4. Astrophysical Journal*, **225 p.548.**

[3] ILOVAISKY S.A. - CHEVALIER C. - MOTCH C. - PAKULL M. - VAN PARADIJS J. - LUB J. 1984. *LMC X-4: the optical 30-day cycle and its implications. Astronomy & Astrophysics*, **140 p.251.**

[4] KELLEY R.L. - JERNIGAN J.G. - LEVINE A. - PETRO L.D. - RAPPAPORT S. 1983. *Discovery of 13.5 sec X–ray pulsations from LMC X-4 and an orbital determination. Astrophysical Journal*, **264 p.586.**

[5] LANG F.L. *et al.*. 1981. *Discovery of a 30.5 day periodicity in LMC X-4. Astrophysical Journal*, **246 p.L21.**

[6] LI F.K. - RAPPAPORT S. - EPSTEIN A. 1978. *Observations of X–ray eclipses from LMC X-4. Nature*, **271 p.37.**

[7] PAKULL M. *et al.*. 1985. *LMC X-4, A0538-66 and surrounding X–ray sources observed with EXOSAT. Space Science Review*, **40 p.379.**

[8] PIETSCH W. - PAKULL M. - VOGES W. - STAUBERT R. 1985. *LMC X-4: 13.5 pulsations and X–ray flare observed by EXOSAT. Space Science Review*, **40 p.371.**

[9] SKINNER G.K. *et al.*. 1980. *Observations of outbursts from the recurrent X–ray transient A0538-66 and LMC X-4. Astrophysical Journal*, **240 p.619.**

[10] WHITE N.E. 1978. *Discovery of eclipsing nature of LMC X-4. Nature*, **271 p.38.**

9.11 Bibliography on 2S 1417-62

[1] APPARAO K.M.V. - NARANAN S. - KELLEY R.L. - BRADT H.V. 1980. *2S 1417-624: a variable galactic X–ray source near CG 312-1. Astronomy & Astrophysics*, **89 p.249.**

[2] GRINDLAY J.E. - PETRO L.D. - McCLINTOCK J.E. 1984. *Optical identification of 2S 1417-62. Astrophysical Journal*, **276 p.621**.

[3] KELLEY R.L. *et al.*. 1981. *Discovery of X-ray pulsations from 2S 1417-624. Astrophysical Journal*, **243 p.251**.

9.12 Bibliography on OAO 1653-40

[1] ARMSTRONG J.T. *et al.*. 1980. *Precise positions and optical search for the 38 second X-ray pulsar near OAO1653-40 and upper limit on X-ray emission from V861 Scorpii. Astrophysical Journal*, **236 p.L131**.

[2] BYRNE P.F. *et al.*. 1981. *High energy X-ray observations of the 38 second pulsar. Astrophysical Journal*, **246 p.951**.

[3] PARMAR A.N. *et al.*. 1980. *X-ray observations of the OAO 1653-40 field. Montly Notices of R.a.S.*, **193 p.49P**.

[4] WHITE N.E. - PRAVDO S.H. 1979. *The discovery of 38.22 second X-ray pulsations from the vicinity of OAO 1653-40. Astrophysical Journal*, **233 p.L121**.

9.13 Bibliography on EXO 2030+375

[1] COE M.J. - LONGMORE A. - PAYNE B.J. - HANSON C.G. 1988. *The optical/IR counterpart of the newly discovered X-ray source EXO 2030+375. Montly Notices of R.a.S.*, **232 p.865**.

[2] JANOT-PACHECO E. - MOTCH C. - PAKULL M.W. 1988. *Optical spectroscopy of the Be star associated with the X-ray transient EXO 2030+375. Besancon Preprint.*

[3] MOTCH C. - JANOT-PACHECO E. 1987. *The optical counterpart of the X-ray transient EXO 2030+375. Astronomy & Astrophysics*, **182 p.L55**.

[4] PARMAR A.N. - WHITE N.E. - STELLA L. - IZZO C. - FERRI P. 1988. *The transient 42 second X-ray pulsar EXO 2030+375: the discovery of the pulse period variations. EXOSAT Preprint*, **60**.

[5] PARMAR A.N. - WHITE N.E. - STELLA L. 1988. *The transient 42 second X-ray pulsar EXO 2030+375: the luminosity dependence of the pulse profile. EXOSAT Preprint*, **61**.

9.14 Bibliography on 4U 1700-37

[1] BALOG N.I. - GONCHARSKII A.V. - KHRUZINA T.S. - CHEREPASHCHUK A.M. 1983. *Parameters of the X-ray binary system HD 153919 = 4U 1700-37. Soviet Astronomy*, **27 p.310**.

[2] BRANDUARDI G. - MASON K.O. - SANFORD P.W. 1978. *Further Copernicus X-ray observations of 3U 1700-37. Montly Notices of R.a.S.*, **185 p.137**.

[3] CHEREPASHCHUK A.M. - KHRUZINA T.S. 1981. *Optical eclipses and precession effects in the X-ray binary system HD 153919 = 4U 1700-37. Soviet Astronomy*, **25 p.697**.

[4] CONTI P.S. - COWLEY A.P. 1975. *Spectroscopic observations of the X-ray binary HD 153919 = 3U 1700-37. Astrophysical Journal*, **200 p.133**.

[5] DOLAN J.F. *et al.*. 1980. *The high-energy X-ray spectrum of 4U 1700-37 observed from OSO 8. Astrophysical Journal*, **238 p.238**.

[6] DOLL H. - BRINKMANN W. 1987. *Temporal variability of the massive X-ray binary 4U 1700-37. Astronomy & Astrophysics*, **173 p.86**.

[7] FAHLMAN G.G. - CARLBERG R.G. - WALKER G.A. 1977. *Spectrum variations of the X-ray binary HD 153919 = 3U 1700-37. Astrophysical Journal*, **217 p.L35.**

[8] GOSSET E. 1985. *The short time-scale light variability of HD 153919 revisited. Astrophysics and Space Science*, **108 p.323.**

[9] GOTTWALD M. - WHITE N.E. - STELLA L. 1986. *A search for X-ray periodicities from 4U 1700-37. Montly Notices of R.a.S.*, **222 p.21P.**

[10] HUTCHINGS J.B. 1974. *Analysis of the blue spectrum of the X-ray binary HD 153919. Astrophysical Journal*, **192 p.677.**

[11] JONES C. - FORMAN W. - TANANBAUM H. - SCHREIRER E. - GURSKY H. - KELLOGG E. 1973. *Evidence for the binary nature of 2U 1700-37. Astrophysical Journal*, **181 p.L43.**

[12] MASON K.O. - BRANDUARDI G. - SANFORD P. 1976. *The X-ray behavior of 3U 1700-37. Astrophysical Journal*, **203 p.L29.**

[13] MURAKAMI T. *et al.*. 1984. *A possible 67 second X-ray pulsation period from 4U 1700-37. Pubbl. Astron. Soc. Japan*, **36 p.691.**

[14] PIETSCH W. - VOGES W. - REPPIN C. - TRUEMPER J. - KENDZIORRA E. - STAUBERT R. 1980. *High-energy X-ray observation of the X-ray binary 4U 1700-37. Astrophysical Journal*, **237 p.964.**

[15] VAN PARADIJS J. - VAN AMERONGEN S. - VAN DER WOERD H. - TJEMKES S. - MENZIES J.W. 1984. *Optical photometry of massive X-ray binaries: 4U 1700-37/HD 153919 = V884 Sco. Astronomy & Astrophysics*, **55 p.7.**

[16] WHITE N.E. - KALLMAN T.R. - SWANK J.H. 1983. *The X-ray absorption spectrum of 4U 1700-37 and its implications for the stellar wind of the companion HD 153919. Astrophysical Journal*, **269 p.264.**

9.15 Bibliography on A0535+26

[1] AAB O.E. - BYCHKOVA L.V. - KOPYLOV I.M. - KUMAIGORODSKAYA R.N. 1982. *The H_α emission line in the star HDE 245770 = A0535+26. Soviet Astronomy Letters*, **8 p.191.**

[2] BRADT H. *et al.*. 1976. *The transient periodic X-ray source in Taurus, A0535+26. Astrophysical Journal*, **204 p.L67.**

[3] COE M.J. - CARPENTER G.F. - ENGEL A.R. - QUENBY J.J. 1975. *Hard X-ray measurements of nova A0535+26 in Taurus. Nature*, **256 p.630.**

[4] DAL FIUME D. - FRONTERA F. - MORELLI E. 1988. *The X-ray pulsar A0535+26 in hard X-rays: average spectrum, pulse phase spectroscopy and spectral time variability. Astrophysical Journal*, **331 p.313.**

[5] FRONTERA F. - DAL FIUME D. - MORELLI E. - SPADA G. 1985. *The X-ray pulsar A0535+26: pulse profile and its time variability in hard X-rays. Astrophysical Journal*, **298 p.585.**

[6] GOLINSKAYA I.M. *et al.*. 1985. *Fast X-ray and IR variability of A0535+26. Astrophysics and Space Science*, **115 p.393.**

[7] HAMEURY J.M. *et al.*. 1983. *Hard X-ray observations of the Crab nebula and A0535+26 with a high-energy resolution spectrometer. Astrophysical Journal*, **270 p.144.**

[8] HUTCHINGS J.B. 1984. *Spectroscopic orbit for HDE 245770 = A0535+26. Pubbl. Astron. Soc. Pacific*, **96 p.312.**

[9] JANOT-PACHECO E. - MOTCH C. - MOUCHET M. 1987. *An optical study of the Be/X-ray transient HDE 245770/A0535+26. Astronomy & Astrophysics*, **177 p.91.**

[10] KALUZIENSKI L.J. - HOLT S.S. - BOLDT E.A. - SERLEMITSOS P.J. 1975. *Decay of X-ray source A0535+26. Nature*, **256 p.633.**

[11] LARIANOV V.M. 1988. *Radiation parameters of the X-ray binary A0535+26 = HD 245770 based on polarization and photometric data. Astrophysics*, **27 p.345.**

[12] LI F.K. - RAPPAPORT S. - CLARK G.W. - JERNIGAN J.G. 1979. *A0535+26: refined position measurement and new pulse period data. Astrophysical Journal*, **228 p.893.**

[13] MASLENNIKOV K.L. 1986. *An optical flare in HDE 245770 near its predicted X-ray maximum. Soviet Astronomy*, **12 p.191.**

[14] NAGASE F. *et al.*. 1982. *Observation of an outburst of the transient X-ray pulsar A0535+26 in 1980. Astrophysical Journal*, **263 p.814.**

[15] PRIEDHORSKY W.C. - TERREL J. 1983. *111 day periodicity of the X-ray transient A0535+26. Nature*, **303 p.681.**

[16] REFLOC'H A. - CHANBON G. - NIEL M. - VEDRENNE G. - RAKHAMINOV C.Y. 1986. *Hard X-ray pulse profile and period evolution of A0535+26 and GX 1+4 as observed by the franco-soviet SIGNE satellite experiments. Astrophysical Journal*, **310 p.773.**

[17] RICKER G.R. *et al.*. 1976. *High-energy X-ray observations of the transient source A0535+26 from a balloon-borne telescope. Astrophysical Journal*, **204 p.L73.**

[18] RICKETTS M.J. - TURNER M.J.L. - PAGE C.G. - POUNDS K.A. 1975. *Observations of A0535+26 with the Leicester Sky Survey experiment. Nature*, **256 p.631.**

[19] ROSENBERG F.D. - EYLES C.J. - SKINNER G.K. - WILLMORE A.P. 1975. *Observations of a transient X-ray source with a period of 104 seconds. Nature*, **256 p.628.**

[20] VIOLES F. *et al.*. 1982. *A0535+26: a hard X-ray observation of the 1977 december flare-up with the PROGNOZ 6 Signe II experiment. Astrophysical Journal*, **263 p.320.**

9.16 Bibliography on GX 1+4

[1] BECKER R.H. *et al.*. 1976. *Spectral variability in the X-ray pulsar GX 1+4. Astrophysical Journal*, **207 p.L167.**

[2] DAVIDSEN A. - MALINA R. - BAWYER S. 1977. *The optical counterpart of GX 1+4: a symbiotic star. Astrophysical Journal*, **211 p.866.**

[3] DOTY J.P. - HOFFMAN J.A. - LEWIN W.H.G. 1981. *SAS 3 observations of GX 1+4. Astrophysical Journal*, **243 p.257.**

[4] ELSNER R.F. *et al.*. 1985. *X-ray observations of GX 1+4 with the MPC on board on Einstein observatory. Astrophysical Journal*, **297 p.288.**

[5] KOO J.W.C. - HAYMES R.C. 1980. *The hard X-ray periodicity of GX 1+4. Astrophysical Journal*, **239 p.L57.**

[6] RICKETTS M.J. - HALL R. - PAGE C.G. - WHITFORD C.H. - POUNDS K.A. 1982. *GX 1+4: pulse period measurement and detection of phase-variable iron line emission. Montly Notices of R.a.S.*, **201 p.759.**

[7] STRICKMAN M.S. - JOHNSON W.N. - KURFESS J.D. 1980. *The hard X-ray pulse profile of GX 1+4. Astrophysical Journal*, **240 p.L21.**

[8] WHITE N.E. - MASON K.O. - HUCKLE H.E. - CHARLES P.A. - SANFORD P.W. 1976. *Periodic modulation of three galactic X-ray sources. Astrophysical Journal*, **209 p.L119.**

9.17 Bibliography on 4U 1320-61 (A1239-59)

[1] CARPENTER G.F. - EYLES C.J. - SKINNER G.K. - WILSON A.M. - WILLMORE A.P. 1977. *New cosmic X-ray sources observed by the RMC experiment on ARIEL V. Montly Notices of R.a.S.*, **179 p.27P.**

[2] HUCKLE H.E. *et al.*. 1977. *Discovery of two periodic X-ray pulsators. Montly Notices of R.a.S.*, **180 p.21P.**

[3] SEWARD F.D. - PAGE C.G. - TURNER M.F.L. - POUNDS K.A. 1976. *X-ray sources in the southern Milkly Way. Montly Notices of R.a.S.*, **177 p.13P.**

9.18 Bibliography on GX 304-1

[1] CORBET R.H.D. *et al.*. 1986. *Long-term and periodic variability of 4U 1258-61 (GX 304-1). Montly Notices of R.a.S.*, **221 p.961.**

[2] GLASS I.S. 1979. *Infrared observations of galactic X-ray sources. Montly Notices of R.a.S.*, **187 p.807.**

[3] MASON K.O. - MURDIN P.G. - PARKES G.E. - VISVANATHAN N. 1978. *The optical counterpart of GX 304-1. Montly Notices of R.a.S.*, **184 p.45P.**

[4] McCLINTOCK J.E. - RAPPAPORT S.A. - NUGENT J.J. - LI F.K. 1977. *Discovery of a 272 second periodic variation in the X-ray source GX 304-1. Astrophysical Journal*, **216 p.L15.**

[5] MENZIES J. 1981. *Photoelectric photometry of GX 304-1 (4U 1258-61). Montly Notices of R.a.S.*, **195 p.67P.**

[6] PARKES G.E. - MURDIN P.G. - MASON K.O. 1980. *The shell spectrum of the optical counterpart of GX 304-1 (4U 1258-61). Montly Notices of R.a.S.*, **190 p.537.**

[7] PIETSCH W. - COLLMAR W. - GOTTWALD M. - KAHABKA P. - ÖGELMAN H. 1986. *EXOSAT observations of GX 304-1 in X-ray off state. Astronomy & Astrophysics*, **163 p.93.**

[8] THOMAS R.M. - MORTON D.C. - MURDIN P.G. 1979. *O I λ7773 absorption in optical counterparts of X-ray sources. Montly Notices of R.a.S.*, **188 p.19.**

9.19 Bibliography on Vela X–1

[1] BAUTZ M. - HOWE S. - GORECKI A. - LANG F. - LEVINE A. - PRIMINI F. - LEWIN W.H.G. 1983. *High-energy X-ray observations of Vela X-1. Astrophysical Journal*, **266 p.794.**

[2] BOYNTON P.E. - DEETER J.E. - LAMB F.K. - ZYLSTRA G. 1986. *Vela X-1 pulse timing. I. Determination of the neutron star orbit. Astrophysical Journal*, **307 p.545.**

[3] CHARLES P.A. - MASON K.O. - WHITE N.E. - CULHANE J.L. - SANFORD P.W. - MOFFAT A. 1978. *X-ray and optical observations of 3U 0900-40 (Vela X-1). Montly Notices of R.a.S.*, **183 p.813.**

[4] DEETER J.E. - BOYNTON P.E. - LAMB F.K. - ZYLSTRA G. 1987. *Apsidal advance in Vela X-1. Astrophysical Journal*, **314 p.634.**

[5] DEETER J.E. - BOYNTON P.E. - SHIBAZAKI N. - HAYAKAWA S. - NAGASE F. - SATO N. 1987. *Pulse-timing study of Vela X-1 based on HAKUCHO and TENMA data: 1980 - 1984. Astronomical Journal*, **93 p.877.**

[6] DUPREE A.K. *et al.*. 1980. *Simultaneous ultraviolet, optical and X-ray observations of the X-ray source Vela X-1. Astrophysical Journal*, **238 p.969.**

[7] HUTCHINGS J.B. 1974. *The X-ray binary HD 77581. Astrophysical Journal*, **192 p.685.**

[8] KALLMAN T.R. - WHITE N.E. 1982. *The anomalous X-ray absorption spectrum of Vela X-1. Astrophysical Journal*, **261 p.L35.**

[9] KHRUZINA T.S. - CHEREPASHCHUK A.M. 1986. *Parameters of the X-ray binary system Vela X-1. Soviet Astronomy*, **30 p.422.**

[10] McCLINTOCK J.E. *et al.*. 1976. *Discovery of a 283 second periodic variation in the X-ray source 3U 0900-40. Astrophysical Journal*, **206 p.L99.**

[11] NAGASE F. *et al.*. 1984. *Secular variation and short-term fluctuations of the pulse period of Vela X-1. Astrophysical Journal*, **280 p.259.**

[12] NAGASE F. - HAYAKAWA S. - SATO N. - MASAI K. - INOUE H. 1986. *Circumstellar matter in the Vela X-1/HD 77581 system. Pubbl. Astron. Soc. Japan*, **38 p.547.**

[13] NORTH A.R. - RAUBENHEIMER B.C. - DE JAGER O.C. - VAN TONDER A.J. - VAN URK G. 1987. *Pulsed TeV γ-rays from Vela X-1. Nature*, **326 p.567.**

[14] RAPPAPORT S. - JOSS P.C. - McCLINTOCK J.E. 1976. *The 3U 0900-40 binary system: orbital elements and masses. Astrophysical Journal*, **206 p.L103.**

[15] SATO N. - HAYAKAWA S. - NAGASE F. 1986. *X-ray emissions from Vela X-1 during its eclipsing period. Astrophysics and Space Science*, **119 p.81.**

[16] SATO N. - HAYAKAWA S. - NAGASE F. - MASAI K. - DOTANI T. - INOUE H. - MAKINO F. 1986. *X-ray probing of the circumstellar matter in the Vela X-1 system from observations over an eclipse phase. Pubbl. Astron. Soc. Japan*, **38 p.731.**

[17] STAUBERT R. - KENDZIORRA E. - PIETSCH W. - REPPIN C. - TRUEMPER J. - VOGES W. 1980. *Hard X-ray pulses from 4U 0900-40. Astrophysical Journal*, **239 p.1010.**

[18] TAAM R.E. - FRYXELL B.A. 1988. *On nonsteady accretion in stellar wind-fed X-ray sources. Astrophysical Journal*, **327 p.L73.**

[19] ULMER M.P. - BAITY W.A. - WHEATON W.A. - PETERSON L.E. 1972. *Observations of Vela X-1 by the UCSD X-ray telescope on OSO 7. Astrophysical Journal*, **178 p.L121.**

[20] VAN DER KLIS M. - BONNET-BIDAUD J.M. 1984. *The orbital parameters and X-ray pulsation of Vela X-1 (4U 0900-40). Astronomy & Astrophysics*, **135 p.155.**

9.20 Bibliography on 4U 1145-61

[1] COOK M.C. - WARWICK R.S. 1987. *A pulse timing study of the X-ray pulsar 4U 1145-619. Montly Notices of R.a.S.*, **225 p.369.**

[2] COOK M.C. - WARWICK R.S. 1987. *Spectral variability of 4U 1145-619 during X-ray outburst. Montly Notices of R.a.S.*, **227 p.661.**

[3] HUTCHINGS J.B. - CRAMPTON D. - COWLEY A.P. 1981. *The X-ray pulsars 2S 1145-619 and 1E 1145.1-6141: optical identifications and a nearby supernova remnant. Astronomical Journal*, **86 p.871.**

[4] LAMB R.C. - MARKERT T.H. - HARTMAN R.C. - THOMPSON D.J. - BIGNAMI G.F. 1980. *Two X-ray pulsars: 2S 1145-61 and 1E 1145-6141. Astrophysical Journal*, **239 p.651.**

[5] WARWICK R.S. - WATSON M.G. - WILLINGALE R. 1985. *EXOSAT observations of the X-ray pulsar 4U 1145-619. Space Science Review*, **40 p.429.**

[6] WATSON M.G. - WARWICK R.S. - RICKETTS M.J. 1981. *2S 1145-619: an X-ray pulsator in an eccentric binary system ? Montly Notices of R.a.S.*, **195 p.197.**

[7] WHITE N.E. - PARKES G.E. - SANFORD P.W. 1978. *Two X-ray periodicities from the vicinity of 4U 1145-61. Nature*, **274 p.664.**

[8] WHITE N.E. - PRAVDO S.H. - BECKER R.H. - BOLDT E.A. - HOLT S.S. - SERLEMITSOS P. 1980. *The X-ray pulsars 4U 1145-61 and 1E 1145.1-6141. Astrophysical Journal*, **239 p.655.**

9.21 Bibliography on 1E 1145.1-6141

[1] DENSHAM R.H. - CHARLES P.A. 1982. *Optical photometry and spectroscopy of the X-ray pulsar 1E 1145.1-6141. Montly Notices of R.a.S.*, **201 p.171.**

[2] HUTCHINGS J.B. - CRAMPTON D. - COWLEY A.P. - THOMPSON I.B. 1987. *Orbital parameters of the X-ray pulsar 1E 1145-6141. Pubbl. Astron. Soc. Pacific*, **99 p.420.**

[3] ILOVAISKY S.A. - CHEVALIER C. - MOTCH C. 1982. *The nature of the 1E 1145.1-6141 optical counterpart. Astronomy & Astrophysics*, **114 p.L7.**

9.22 Bibliography on A1118-61

[1] CARPENTER G.F. - COE M.J. - ENGEL A.R. - QUENBY J.J. 1975. *Hard X-ray observations near ARIEL 1118-61. Nature*, **256 p.292.**

[2] COE M.J. - PAYNE B.J. 1985. *The first UV studies of the optical candidate for the X-ray source 1118-61. Astrophysics and Space Science*, **109 p.175.**

[3] IVES J.C. - SANFORD P.W. - BELL BURNELL S.J. 1975. *Observations of a transient X-ray source with a regular periodicity of 6.75 minutes. Nature*, **254 p.578.**

[4] JANOT-PACHECO E. - ILOVAISKY S.A. - CHEVALIER C. 1981. *A photometric and spectroscopic study of He3-640 (? = A1118-61). Astronomy & Astrophysics*, **99 p.274.**

[5] MOTCH C. - JANOT-PACHECO E. - PAKULL M.W. - MOUCHET M. 1988. *Coordinated X-ray and optical observations of the pulsating X-ray transient A1118-61. Astronomy & Astrophysics*, **201 p.63.**

9.23 Bibliography on 4U 1907+09

[1] COOK M.C. - PAGE C.G. 1987. *The X-ray properties of 3A 1907+09. Montly Notices of R.a.S.*, **225 p.381.**

[2] IYE M. 1986. *High-resolution spectrum of the peculiar optical counterpart of the X-ray binary 4U 1907+09. Pubbl. Astron. Soc. Japan*, **38 p.463.**

[3] MAKISHIMA K. *et al.*. 1984. *Discovery of a 437.5 second X-ray pulsation from 4U 1907+09. Pubbl. Astron. Soc. Japan*, **36 p.679.**

[4] MARSHALL N. - RICKETTS M.J. 1980. *Determination of a binary period for the variable X-ray source A1907+09. Montly Notices of R.a.S.*, **193 p.7P.**

[5] SCHWARTZ D.A. - GRIFFITHS R.E. - THORSTENSEN J.R. - CHARLES P.A. - BOWYER S. 1980. *Optical identification of 4U 1907+09 using the HEAO-1 scanning modulation collimator position. Astronomical Journal*, **85 p.549.**

9.24 Bibliography on 4U 1538-52

[1] BECKER R.H. *et al.*. 1977. *A1540-53, an eclipsing X-ray binary pulsator. Astrophysical Journal*, **216 p.L11.**

[2] COWLEY A.P. - CRAMPTON D. - HUTCHINGS J.B. - LILLER W. - SANDULEAK N. 1977. *Optical candidates for 3U 1538-52. Astrophysical Journal*, **218 p.L3.**

[3] CRAMPTON D. - HUTCHINGS J.B. - COWLEY A.P. 1978. *Optical spectroscopy and system parameters for 4U 1538-52. Astrophysical Journal*, **255 p.L63.**

[4] DAVISON P.J.N. 1977. *A regular pulsation in the X-ray flux from A1540-53. Montly Notices of R.a.S.*, **179 p.35P.**

[5] DAVISON P.J.N. - WATSON M.G. - PYE J.P. 1977. *The binary X-ray pulsar 3U 1538-52. Montly Notices of R.a.S.*, **181 p.73P.**

[6] MAKISHIMA K. - KOYAMA K. - HAYAKAWA S. - NAGASE F. 1987. *Spectra and pulse period of the binary X-ray pulsar 4U 1538-52. Astrophysical Journal*, **314 p.619.**

[7] PARKES G.E. - MURDIN P.G. - MASON K.O. 1978. *The optical counterpart of the binary X-ray pulsar 4U 1538-52. Montly Notices of R.a.S.*, **184 p.73P.**

[8] SCHWARTZ D.A - GURSKY H. - SCHWARZ J. - BRADT H. - DOXSEY R. 1978. *Location of pulsating binary X-ray source 4U 1538-52 with the HEAO-1 SMC. Nature*, **275 p.517.**

9.25 Bibliography on GX 301-2

[1] KAWAI N. - MAKISHIMA K. - MATSUOKA M. - MITANI K. - MURAKAMI T. - NAGASE F. 1985. *HAKUCHO observation of the pulse period of GX 301-2 and confirmation of the orbital parameters. Pubbl. Astron. Soc. Japan*, **37 p.647.**

[2] KELLEY R. - RAPPAPORT S. - PETRE R. 1980. *A determination of the orbit of GX 301-2. Astrophysical Journal*, **238 p.699.**

[3] LEAHY D.A. *et al.*1988. *Detection of an X-ray intensity dip from GX 301-2. Pubbl. Astron. Soc. Japan*, **40 p.197.**

[4] MAKINO F. - LEAHY D.A. - KAWAI N. 1985. *Observation of X-ray spectrum of GX 301-2. Space Science Review*, **40 p.421.**

[5] MITANI K. - MATSUOKA M. - MAKISHIMA K. - INOUE H. 1984. *Variations of the pulse profile and the X-ray intensity of GX 301-2 (4U 1223-62). Astrophysics and Space Science*, **103 p.345.**

[6] PARKES G.E. - MASON K.O. - MURDIN P.G. - CULHANE J.L. 1980. *A spectral study of Wray 977, the optical counterpart of the binary X-ray pulsar 4U 1223-62. Montly Notices of R.a.S.*, **191 p.547.**

[7] ROTHSCHILD R.E. - SOONG Y. 1987. *Two binary cycles of GX 301-2. Astrophysical Journal*, **315 p.154.**

[8] SATO N. - NAGASE F. - KAWAI N. - KELLEY R.L. - RAPPAPORT S. - WHITE N.E. 1986. *Orbital elements of the binary X-ray pulsar GX 301-2. Astrophysical Journal*, **304 p.241.**

[9] WATSON M.G. - WARWICK R.S. - CORBET R.H.D. 1982. *The orbital period of 2S 1223-624 (GX 301-2). Montly Notices of R.a.S.*, **199 p.915.**

[10] WHITE N.E. - MASON K.O. - SANFORD P.W. 1978. *The binary X-ray pulsar 3U 1223-62. Montly Notices of R.a.S.*, **184 p.67P.**

[11] WHITE N.E. - SWANK J.H. 1984. *The 41.5 day binary x-ray pulsar 4U 1223-62 (GX 301-2). Astrophysical Journal*, **287 p.856.**

9.26 Bibliography on 4U 0352+30

[1] BECKER R.H. *et al.*. 1979. *X-ray spectra of X Persei. Astrophysical Journal*, **227 p.L21.**

[2] HUTCHINGS J.B. - COWLEY A.P. - CRAMPTON D. - REDMAN R.O. 1974. *Evidence for the existence of a massive companion to X Persei (= 2U 0352+30 ?). Astrophysical Journal*, **191 p.L101.**

[3] HUTCHINGS J.B. - CRAMPTON D. - REDMAN R.O. 1975. *Spectroscopic investigation of X Persei (= 2U 0352+30 ?). Montly Notices of R.a.S.*, **170 p.313.**

[4] KEMP J.C. - BARBOUR M.S. 1983. *X Persei: optical polarization variation on the 580 day binary-like period. Astrophysical Journal*, **264 p.237.**

[5] LATYSHEVA I.D. - LYUTYI V.M. 1987. *The 13.9 minute optical periodicity of X Persei. Soviet Astronomy Letters*, **13 p.127.**

[6] MARGON B. - BOWYER S. - PENEGOR G. 1976. *Simultaneous photometry of X Persei and 3U 0352+30. Montly Notices of R.a.S.*, **176 p.217.**

[7] MURAKAMI T. - IKEGAMI T. - INOUE H. - MAKISHIMA K. 1987. *Pulse period of X Persei. Pubbl. Astron. Soc. Japan*, **39 p.253.**

[8] SANWAL B.B. - RAUTELA B.S. - JOSHI S.C. 1985. *Spectroscopic study of X Persei. Astrophysics and Space Science*, **110 p.301.**

[9] WEISSKOPF M.C. *et al.*. 1984. *X-ray observations of X Persei. Astrophysical Journal*, **278 p.711.**

[10] WHITE N.E. - MASON K.O. - SANFORD P.W. 1977. *Evidence for a 581-day modulation in the pulse period of 3U 0352+30. Nature*, **267 p.229.**

[11] WHITE N.E. - MASON K.O. - SANFORD P.W. - MURDIN P. 1976. *The X-ray behaviour of 3U 0352+30 (X Per). Montly Notices of R.a.S.*, **176 p.201.**

[12] WHITE N.E. - SWANK J.H. - HOLT S.S. - PARMAR A.N. 1982. *A comparision of the X-ray properties of X Persei and γ Cassiopeiae. Astrophysical Journal*, **263 p.277.**

9.27 Bibliography on X–ray sources

[1] APPARAO K.M.V. 1985. *X-ray emission from Be star binaries. Astrophysical Journal*, **292 p.257.**

[2] APPARAO K.M.V. - BRADT H.V. - DOWER R.G. - DOXSEY R.E. - JERNIGAN J.G. - LI F. 1978. *Positions of galactic X-ray sources:* $320° < l^{II} < 340°$. *Nature*, **271 p.225.**

[3] BAHCALL J.N. 1978. *Masses of neutron stars and black holes in X-ray binaries. Annual Review of Astronomy and Astrophysics*, **16 p.241.**

[4] BLUMENTHAL G.R. - TUCKER W.H. 1974. *Compact X-ray sources. Annual Review of Astronomy and Astrophysics*, **12 p.23.**

[5] BRADT H.V.D. - McCLINTOCK J.E. 1983. *The optical counterparts of compact galactic X-ray sources. Annual Review of Astronomy and Astrophysics*, **21 p.13.**

[6] CHESTER T.J. 1979. *Continuum optical pulsation from the companions of the binary X-ray pulsars. Astrophysical Journal*, **227 p.569.**

[7] CONTI P.S. 1978. *Stellar parameters of five early type companions of X-ray sources. Astronomy & Astrophysics*, **63 p.225.**

[8] CORBET R.H.D. 1986. *The three types of high-mass X-ray pulsator. Montly Notices of R.a.S.*, **220 p.1047.**

[9] DACHS J. - HANUSCHIK R. - ROHE D. 1986. *Geometry of rotating envelopes around Be stars derived from comparative analysis of H_α emission line profiles. Astronomy & Astrophysics*, **159 p.276.**

[10] DOWER R.G. - APPARAO K.M.V. - BRADT H.V. - DOXSEY R.E. - JERNIGAN J.G. - KULIK J. 1978. *Positions of galactic X-ray sources:* $55° < l^{II} < 320°$. *Nature*, **273 p.364.**

[11] FEAST M.W. - STOY R.H. - THACKERAY A.D. - WESSELINK A.F. 1961. *Spectral classification and photometry of southern B stars. Montly Notices of R.a.S.*, **122 p.239.**

[12] FORMAN W. - JONES C. - TANANBAUM H. 1976. *UHURU observations of the galactic plane in 1970, 1971 and 1972. Astrophysical Journal*, **206 p.L29.**

[13] HAYAKAWA S. 1985. *X-rays from accreting neutron stars. Physics Reports*, **121 p.318**.

[14] HOLT S.S. - KALUZIENSKI L.J. - BOLDT E.A. - SERLEMITSOS. 1979. *Long-term studies with the ARIEL5 ASM. I. Her X-1, Vela X-1 and Cen X-3. Astrophysical Journal*, **277 p.563**.

[15] HOLT S.S. - McCRAY R. 1982. *Spectra of cosmic X-ray sources. Annual Review of Astronomy and Astrophysics*, **20 p.323**.

[16] HUTCHINGS J.B. 1978. *Evidence for noncircular orbits in X-ray binaries. Astrophysical Journal*, **226 p.264**.

[17] JONES C. 1977. *Energy spectra of 43 galactic X-ray sources observed by UHURU. Astrophysical Journal*, **214 p.856**.

[18] JOSS P.C. - RAPPAPORT S.A. 1984. *Neutron stars in interacting binary systems. Annual Review of Astronomy and Astrophysics*, **22 p.537**.

[19] MARASCHI L. - TREVES A. - VAN DEN HEUVEL E.P.J. 1976. *B-emission stars and X-ray sources. Nature*, **259 p.292**.

[20] MAURER G.S. - JOHNSON W.N. - KURFESS J.D. - STRICKMAN M.S. 1982. *Balloon observations of galactic high-energy X-ray sources. Astrophysical Journal*, **254 p.271**.

[21] NAGASE F. *et al.*. 1984. *Pulse-period changes of X-ray pulsars measured with HAKUCHO and TEMNA. Pubbl. Astron. Soc. Japan*, **36 p.667**.

[22] NARANAN S. *et al.*. 1985. *On fast X-ray rotators with long-term periodicities. Astrophysical Journal*, **290 p.487**.

[23] PAYNE B.J. - COE M.J. 1987. *The UV variability of binary X-ray pulsars: observations of Vela X-1, A0535+26 and 4U 1145-619. Montly Notices of R.a.S.*, **225 p.985**.

[24] PRIEDHORSKY W.C. - HOLT S.S. 1987. *Long-term cycles in cosmic X-ray sources. Space Science Review*, **45 p.291**.

[25] PRIEDHORSKY W.C. - TERRELL J. 1983. *Long-term X-ray observations of Cen X-3, GX 301-2, GX 304-1 and 4U 1145-61. Astrophysical Journal*, **273 p.709**.

[26] PYLYSER E. - SAVONIJE G.J. 1988. *Evolution of low-mass close binary systems with a compact mass accreting component. Astronomy & Astrophysics*, **191 p.57**.

[27] RAPPAPORT S. - JOSS P.C. 1977. *Accretion torques in X-ray pulsars. Nature*, **266 p.683**.

[28] SAVONIJE G.J. 1979. *Roche-lobe overflow and massive X-ray binary systems. Astronomy & Astrophysics*, **71 p.352**.

[29] SCHULZ N.S. - HASINGER G. - TRUEMPER J. 1988. *Spectral classification of LMXRB energy spectra with color-color diagrams. Max-Planck Preprint*, **111**.

[30] STELLA L. - WHITE N.E. - ROSNER R. 1986. *Intermittent stellar wind accretion and long-term activity of population I binary systems. Astrophysical Journal*, **308 p.669**.

[31] TJEMKES S.A. - ZUIDERWIJK E.J. - VAN PARADIJS J. 1986. *Optical light curves of massive X-ray binaries. Astronomy & Astrophysics*, **154 p.77**.

[32] VAN PARADIJS J. 1981. *Average properties of low-mass X-ray binaries. Astronomy & Astrophysics*, **103 p.140**.

[33] VAN PARADIJS J. - VAN AMERONGEN S. - DAMEN E. - VAN DER WOERD H. 1986. *Five-color photometry of early-type stars in the direction of the galactic X-ray sources. Astronomy & Astrophysics*, **63 p.71**.

[34] VERBUNT F. 1988. *The evolution of low-mass X-ray binaries. Max-Planck Preprint*, **118**.

[35] WATERS L.B.F. - TAYLOR A.R. - VAN DEN HEUVEL E.P.J. - HABETS G.M.H.J. - PERSI P. 1988. *Evidence for low-velocity winds in Be/X-ray binaries. Astronomy & Astrophysics*, **198 p.200.**

[36] WHITE N.E. - SWANK J.H. - HOLT S.S. 1983. *Accretion powered X-ray pulsars. Astrophysical Journal*, **270 p.711.**